UNIVERSITA' DEGLI STUDI DI MILANO

Facoltà di Farmacia

Dottorato di Ricerca in Chimica del Farmaco

HIGH RESOLUTION MASS SPECTROMETRIC STRATEGIES IN DRUG DISCOVERY FOR THE INVESTIGATION OF COVALENT AND NON COVALENT INTERACTIONS

Coordinatore: Chiar.mo Prof. Ermanno VALOTI

Docente Guida: Prof. Giancarlo ALDINI

Candidato

Dr. Danilo DE MADDIS

Matr. n. R09058

XXVI Ciclo (A.A. 2010/2011-2012/2013)

Index

1. Introduction and aim of the work.

The Ph.d thesis here described concerns the set-up and application of analytical methods for studying compounds effective as inhibitors of the advanced glycation end-products (AGEs) and advanced lipoxidation end-products (ALEs), as well as antagonists of the receptors of AGEs (RAGE).

AGEs and ALEs represent a quite complex and heterogeneous class of compounds that are formed by different mechanisms, by heterogeneous precursors and can be formed either exogenously or endogenously as detailed in the chapter 2.2. of the present thesis.

AGEs represent a class of covalently modified proteins generated by oxidative and non-oxidative pathways, involving sugars or their degradation products. The term ALEs includes a variety of covalent adducts which are generated by the non-enzymatic reaction of reactive carbonyl species (RCS), produced by lipid peroxidation and lipid metabolism, with the nucleophilic residues of macromolecules, especially proteins.

AGEs and ALEs share some common properties, for example, both consist of non-enzymatic, covalently modified proteins and oxidative stress is often (although not always) involved in the mechanism of their formation. Moreover some AGEs and ALEs have the same structure, since they arise from common precursors, as in the case of carboxymethyllysine (CML) which is generated by glyoxal, which in turn is formed by both lipid and sugar oxidative degradation pathways [1].

Besides being considered as reliable biomarkers of oxidative damage, as well as predictors and prognostic factors, more recently, AGEs and ALEs have also been recognized as important pathogenetic factors of some oxidative based diseases, as supported by the following facts: 1) a strict correlation between the amount of AGEs/ALEs in tissues and fluids and disease states has been found, in both animal and human subjects; 2) a substantial amount of literature is now available reporting the molecular and cellular pathogenic mechanisms for the AGEs/ALEs involvement in the onset and progression of different oxidative-based diseases including diabetes [2], chronic renal failure [3], cardiovascular diseases [4] and neurological disorders [5]. The AGEs/ALEs damaging effect is mediated by different mechanisms, including the dysfunction of the proteins undergoing the oxidative modification, protein polymerization, signal transduction, immunoresponse and RAGE activation. Some of the biological effects are due to the loss of function of the target proteins undergoing the covalent modification, such as in the case of extracellular matrix proteins that lose their elastic and mechanical functions when modified as AGEs/ALEs and in particular, when cross-links are involved [6]. Other examples of a direct damaging effect of AGEs/ALEs can be ascribed to the covalent modification of enzymes and receptors that lose their activity due to the covalent modification involving the catalytic or binding site, or following a conformational change of the protein structure. Moreover AGEs and ALEs can be immunogenic.

Hence AGEs/ALEs are now considered as promising drug targets and a substantial effort is dedicated to delve the molecular strategies aimed at preventing, reducing or removing these protein oxidation products.

The different molecular approaches thus far reported can be grouped by considering at which level of the damaging AGEs/ALEs cascade they are effective and in particular if they act by inhibiting the AGEs/ALEs formation, accelerating their catabolism or blocking their biological effects as summarized in Fig.1 and detailed in the chapter 2.4.

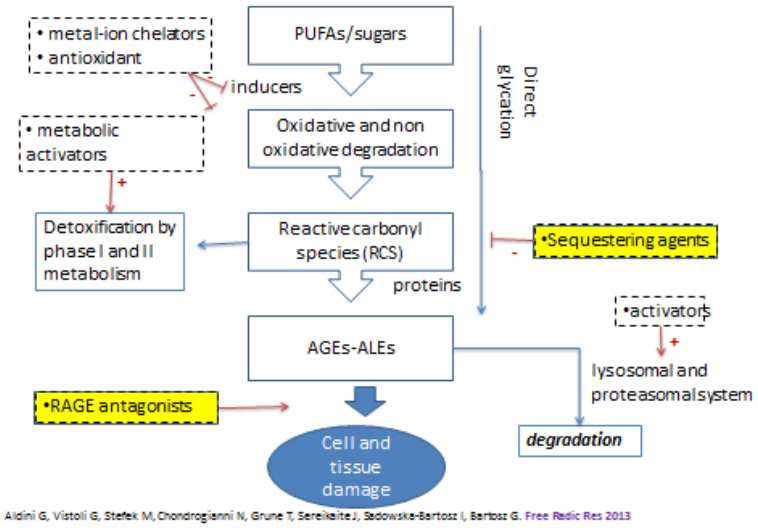

Fig 1. Molecular strategies to inhibit AGEs/ALEs formation and damaging response.

The first level of action, the inhibition of AGEs/ALEs formation, also consists of different approaches, which target the different inducers (ROS, metal ions) and intermediate products (mainly reactive carbonyl species, RCS) involved in the AGEs/ALEs formation. Antioxidants, radical scavengers, metal-ion chelators and reactive carbonyl compounds quenchers (RCS sequestering agents) represent the most promising approaches so far reported for inhibiting AGEs/ALEs formation. In some cases, as found both for natural or synthetic compounds, the inhibition of AGEs/ALEs formation does not proceed through a single specific mechanism but implicates multiple mechanisms, involving at least two of the following ones: antioxidant, radical-scavenging, metal ion chelation and RCS trapping. The second level of intervention consists of accelerating the catabolism of already formed AGEs/ALEs and this can be achieved by potentiating the endogenous proteolytic system or by using xenobiotics able to catalytically degrade AGEs/ALEs.

The third level of intervention, which is also the most innovative, consists of blocking the biological response of AGEs/ALEs by inhibiting the activation of the RAGE receptors through different classes of antagonists. It should be noted that such an approach permits the blocking of the damaging effect induced not only by endogenously formed AGEs/ALEs but also by exogenously derived AGEs/ALEs.

In view of a drug discovery program aim to search bioactive compounds, the first step of the research program was to set up analytical methods based on high resolution MS strategies able to test the efficacy and selectivity of compounds effective as sequestering agents of RCS and also acting as RAGE antagonists. The methods so far reported in the literature to test RCS sequestering compounds consist to measure the consumption of the aldehydes when incubated with the test compounds by a direct spectrophotometric analysis and depending on the aldehyde, the derivatization reaction should also be considered. The main limitations of such approach is that it cannot be applied to mixtures or extracts, it cannot be applied to a high throughput screening and in several cases the experimental conditions such as the acid condition of the derivatization process can dissociate the adducts between the aldehydes and the sequestering agents.

Therefore, based on the limits above reported, the initial aim of this research project was focused to set-up and then apply suitable analytical methods able to screen novel RCS sequestering agents.

An HPLC method was firstly set-up in order to measure the consumption of RCS (reactivity) and of endogenous carbonyls such as pyridoxal (selectivity) when incubated in presence of the tested compounds. The method was optimized in order to use a mobile phase buffered at pH 7.4 in order to avoid the acid catalyzed degradation of the formed adducts.

The work was then addressed to set-up a rapid and accurate method for testing the ability of RCS sequestering agents to inhibit protein carbonylation.

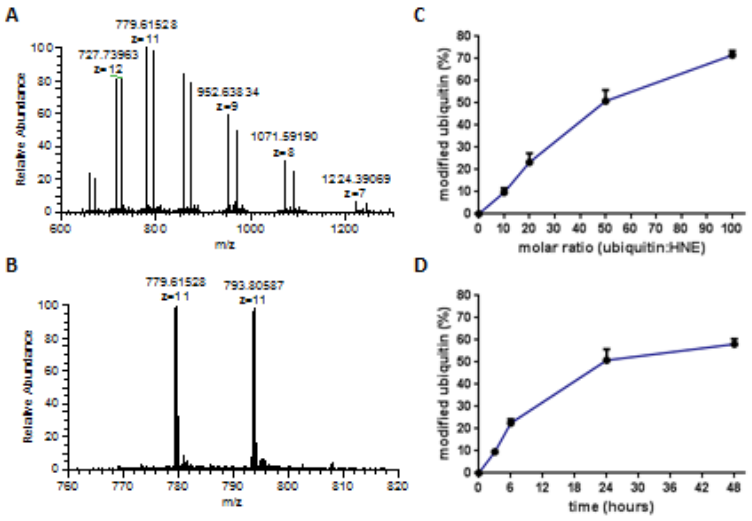

Fig 2. HNE-induced modification on ubiquitin: intact protein analysis. A) Multi-charged spectrum for HNE-modified ubiquitin, upon 24 h incubation with HNE (1:50 ubiquitin:Hmolar ratio). B) Zoom on the m/z region of the $[M+11H]^{11+}$ peaks corresponding to non-modified and HNE-modified ubiquitin. C) Quantification of the percentage of modified ubiquitin upon incubation with increasing concentration of HNE (equal to 0.1, 0.2, 0.5 and 1 mM, corresponding to 10, 20, 50, 100-fold excess over ubiquitin concentration, equal to 10 µM). D) Quantification of the percentage of modified ubiquitin upon incubation with HNE for 3, 6, 24 and 48 hours (1:50 ubiquitin:HNE molar ratio).

To set-up the method, HNE, which is one of the most abundant and reactive lipid-derived RCS, was used as RCS, and ubiquitin [8] as a model of protein substrate. Going into details, ubiquitin was selected as a protein target since it is commercially available at high purity and at a reasonable cost and because its molecular weight is suitable for intact protein analysis using a high resolution mass spectrometer such as the Orbitrap. Despite lacking cysteine residues, ubiquitin exposes a set of reactive lysines and a highly reactive histidine, which make this protein a suitable benchmark to test protein carbonylation and its inhibition. The method was firstly validated by using known RCS sequestering agents and the results well correlate with those obtained by HPLC analysis. The method was found suitable to test mixtures or extracts and to be used for HTS applications.

In the second part of the work, the methods set-up were then applied in view to search effective and selective RCS sequestering agents.

Reactivity towards RCS was evaluated by testing the ability of the tested compound to quench 4-hydroxy-nonenal (HNE) chosen as a model of alfa,beta-unsaturated aldehydes, glyoxal (GO) and methylglyoxal (MGO) as di-carbonyl derivatives. Selectivity was tested by measuring the consumption of pyridoxal as an endogenous aldehyde. The method was firstly validated by testing the reactivity and selectivity of known RCS scavenger compounds such as edaravone (EDA), hydralazine (HY), aminoguanidine (AG), and pyridoxamine (PYR). Even though they are very effective as RCS detoxifying agents, their usage is limited due to their lack of selectivity because they react with physiological aldehydes such as pyridoxal and by a promiscuous activity: ED is a neuroprotective compound, HY an antihypertensive drug and AG a NOS inhibitor. The HPLC method was then applied to study the reactivity and selectivity of carnosine (CAR) and derivatives such as anserine, n-acetyl carnosine and of carnosine analogues designed to be stable to carnosinase, a specific metal-ion dependent homodimeric dipeptidase (carnosinase, CN1 EC.3.4.13.20),.

The screening permitted to identify carnosinol, a carnosine peptidomimetic characterized by the replacement of the carboxyl group with a hydroxyl group, as a selective and reactive RCS sequestering agent, characterized by a suitable PK profile since resistant to serum carnosinase and recognized by HPEPT1 (patent application: WO2011080139).

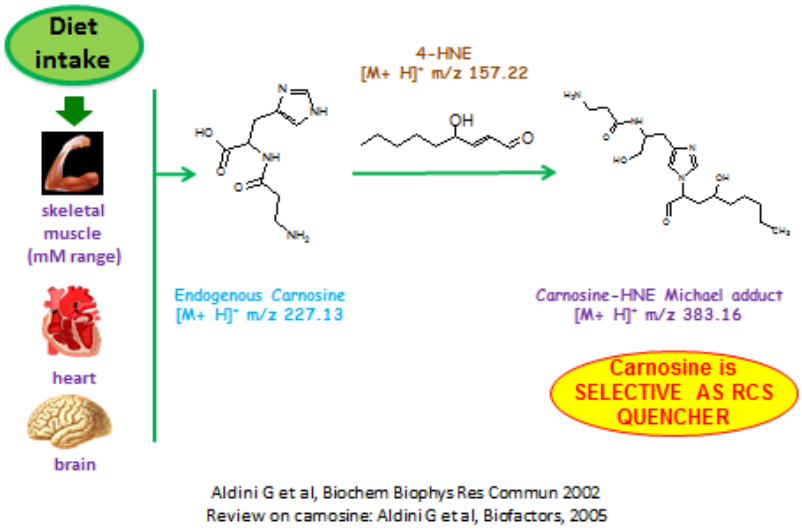

Fig 3. Metabolic description pathway of the Carnosine derivation.

Beside evaluating the reactivity and the selectivity, the approach was then implemented by an ESI-MS approach aimed to fully characterize the covalent adducts between RCS and the sequestering agents. The investigation of the mechanisms of carbonyl quenching have so ensued a broad understanding of the biochemical mechanisms in vitro as well as in vivo that occur between cytotoxic RCS and the "sweepers" detoxifying agents.

The method was then applied to test the RCS sequestering activity of proteinogenic histidine-containing dipeptides with the C-terminus capped by a methyl ester or by a primary amido group so as to study dipeptides which should be still recognized by peptide transporters and resistant to proteolysis. Moreover, the study considered diastereoisomeric pairs of dipeptides produced by alternating the absolute configuration of the histidine residue thus revealing the effect of configuration on the quenching activity.

AGEs and most probably ALEs are ligands and activators of the receptor RAGE whose activation is involved in a NF-kB pathway, leading to NADPH oxidase activation, oxidative stress and a condition of inflammatory and pro-fibrotic response.

Since the damaging AGEs-RAGE axis has been associated to the onset and/or progression of many chronic and degenerative oxidative based disease and in many metabolic disorders, it has been recently hypothesized that the AGE-RAGE axis represents a promising drug target. One approach to counteract the AGEs-RAGE axis is represented by the design of RAGE antagonists. It should be considered that a drug design approach aimed to screen RAGE antagonists firstly requires a reliable analytical method able to test the binding affinity of small molecules and the set-up of such a method represents the final aim of the present research program that is based on the following steps:

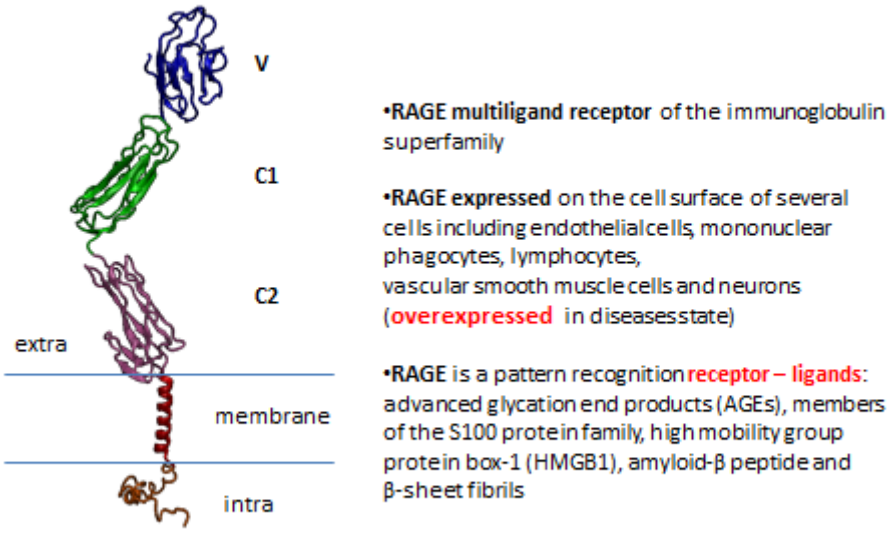

Fig 4. Receptor for Advances Glyco/oxidation End Products(RAGE).

- RAGE expression as recombinant protein in E. coli strain ORIGAMI B (DE3) with recombinant plasmid pET-15b VC1;
- Application of the automated loop injection High Resolution Mass Spectrometry (MS) method, based on the High Resolution Mass Spectrometry method developed to study the Ubiquitin-RCS interaction, to inquire in vitro non-covalent binding relationship between low molecular weight AGEs and recombinant RAGE.

The receptor for advanced glycation end products (RAGE) is a type I transmembrane glycoprotein of the immunoglobulin superfamily of cell surface receptors. RAGE extracellular portion is involved in ligand binding and contains one "V" –type followed by two "C"-type immunoglobulin-like domains (V-C1-C2 structure). V-C1 domains form an integrated unit whereas C2 domain is attached to V-C1 by a flexible linker but is a fully independent unit.

As a general strategy, we decided to express the V-C1 portion of the extracellular domain of human RAGE (sRAGE) as protein target since it is water soluble and involved in the molecular recognition and engagement of the AGEs ligands.

Therefore, V, V-C1 and s-RAGE expression was focused on the recombinant protein expression carried out by the protein studies obtained through the E. coli expression system.

Despite a greater facility to handling the microorganism, E. coli in contrast to eukaryotic expression system, is not capable to perform post-translational modifications, including glycosylation, which are instead present in the human RAGE.

Regardless for the lack of this peculiarity, numerous studies reported in literature, indicate that, post-translational modifications have not significantly effect on the RAGE properties regarding for instance the bind activity toward certain ligands and so that, the bacterial E. coli expression system represent one of the most used host for the heterologous proteins expression.
A great advantage by using E.coli is its peculiarity of secreting the protein of interest in the medium that it can be easily purified in one-step. This advantage have avoided the use of tags, such as the Poly-His, that could affect the property of sRAGE during high throughput screening of libraries of compounds and making unnecessary the removal step by specific protease treatments.

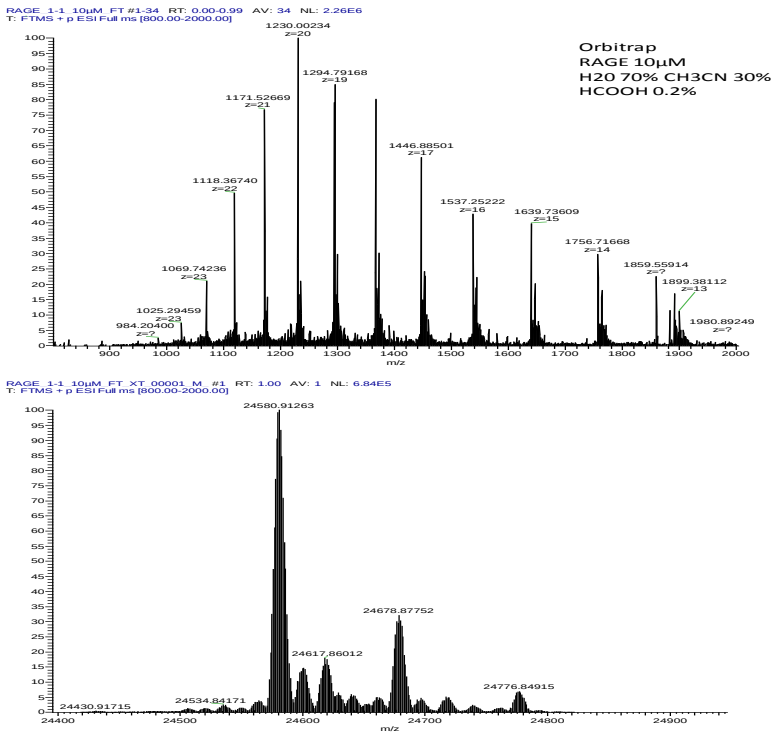

Fig 5. ESI-MS spectrum of recombinant sRAGE.

The high resolution mass spectrometric (ESI-MS) approach in top-down and bottom-up approach was then used in order to verify the identity of the protein. Fig. 5, upper panel, shows the multi-charged ESI-MS spectrum of the recombinant protein and in lower panel is displayed the corresponding deconvoluted MS spectrum showing the MW of 24580 Da which is consistent with the theoretical one.

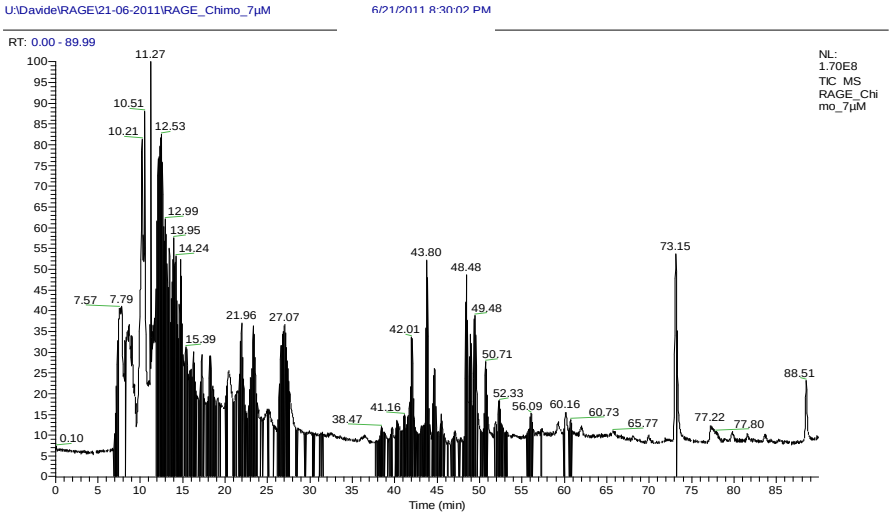

GSHMAQNITARIGEPLVLKCKGAPKKPPQRLEWKLNTGRTEAWKVLSPQGGGPWDSVAR VLPNGSLFLPAVGIQDEGIFRCQAMNRNGKETKSNYRVRVYQIPGKPEIVDSASELTAGVP NKVGTCVSEGSYPAGTLSWHLDGKPLVPNEKGVSVKEQTRRHPETGLFTLQSELMVTPAR GGDPRPTFSCSFSPGLPRHRALRTAPIQPRVWEPV-PLEEVQLVVE.

Fig 6. LC-ESI-MS chromatogram of peptides arising from sRAGE digestion by trypsin.

The primary sequence was then identified by a bottom-up approach (Fig. 6) consisting to enzymatically digest the protein, separate the peptides by reversed phase capillary column. Eluted peptides were then sequenced by MS/MS analyses. The primary structure of the protein is reported in Fig. 6 corresponding to the predicted sequence on the bases of the designed nucleotide sequence of sRAGE.

After having characterized the protein, a MS approach to study the non covalent binding of RAGE with ligands was set-up. The ligand-binding properties of RAGE was studied by a native MS method that is suitable to study the non covalent interactions between ligands and recombinant V-C1. The advantages of native MS over other methods is that it does not require labeled target or ligands, it is characterized by high sensitivity, low sample consumption, fully automatation and that ligands can be screened as mixture.

The experiments consist in maintaining the concentration of VC1 constant and increasing the ligand concentration. The ligands used are well known low molecular weight sRAGE ligands such as carboxymethyl lysine (CML) and carboxyethyl lysine (CEL) derived peptide [9].
Unmodified peptides were also used as controls. Validation of the method was obtained by comparing the Kd values obtained by native MS analysis in respect to the Kd values determined from fluorescence titration experiments. The native MS method was found accurate and suitable to test libraries in order to understand the structure requirements for RAGE recognition as well as for searching antagonists.

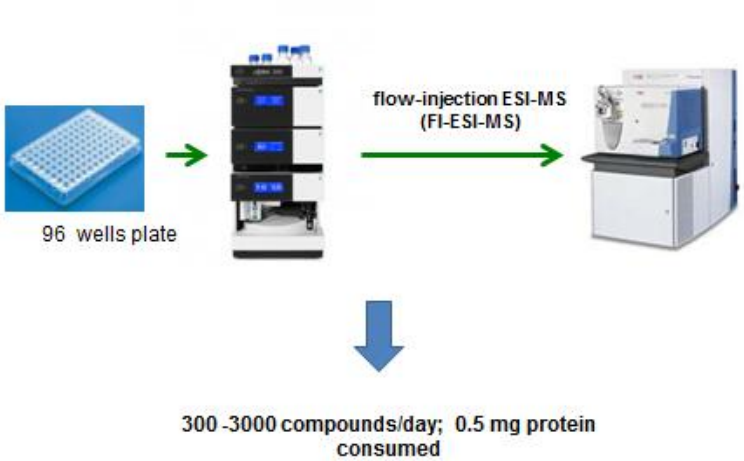

Fig 7. Automatization method flow scheme.

1.1. References.

[1] Baynes JW. (2003). "Chemical modification of proteins by lipids in diabetes". *Clin Chem Lab Med*;41: 1159 – 1165.

[2] Yamagishi S, Maeda S, Matsui T, Ueda S, Fukami K, Okuda S. (2012). "Role of advanced glycation end products (AGEs) and oxidative stress in vascular complications in diabetes". *Biochim Biophys Acta*;1820:663 – 671.

[3] Iacobini C, Menini S, Ricci C, Scipioni A, Sansoni V, Mazzitelli G. et al. (2009). "Advanced lipoxidation end-products mediate lipid-induced glomerular injury: role of receptormediated mechanisms". *J Pathol*;218:360 – 369.

[4] Del Turco S, Basta G. (2012). "An update on advanced glycation endproducts and atherosclerosis". *Biofactors*;38:266 – 274.

[5] Li JL, Liu DN, Sun L, Lu Y, Zhang Z. (2012). "Advanced glycation end products and neurodegenerative diseases: Mechanisms and perspective. *J Neurol Sci*;317:1 – 5.

[6] Ciulla MM, Paliotti R, Carini M, Aldini G. (2011). "Fibrosis, enzymatic and non-enzymatic cross-links in hypertensive heart disease". *Cardiovasc Hematol Disord Drug Targets.*

[7] Vistoli G, De Maddis D, Straniero V, Pedretti A, Pallavicini M, Valoti E, Carini M, Testa B, Aldini G. (2013). "Exploring the space of histidine containing dipeptides in search of novel efficient RCS sequestering agents". *Eur J Med Chem.*;66:153 – 60.

[8] Liang X, Chen Y, Zhuang J, Zhang M, Xiong W, Guo H, Jiang F, Hu P, Guo D, and Shi W. (2012). "Advanced oxidation protein products as prognostic biomarkers for recovery from acute kidney injury after coronary artery bypass grafting". *Biomarkers*;17:507 - 12.

[9] Xue J, Rai V, Singer D, Chabierski S, Xie J, Reverdatto S, Burz DS, Schmidt AM, Hoffmann R, Shekhtman A. (2011). "Advanced glycation end product recognition by the receptor for AGEs". *Cell Press*.;19(5):722 - 32.

2. Background.

2.1. Oxidative stress

Oxidative stress is often defined as an imbalance of pro-oxidants and antioxidants in favor of the latter, through an impairment of the basal red-ox balance in favor of the oxidation reactions. This physiopathological imbalance could be triggered by several factors. The starting factors are mainly grouped in endogenous and/or exogenous particles. In both cases the disequilibrium condition is reached as a result of an increase of the concentration of pro-oxidant species, or the depletion of the endogenous antioxidant.

Chemically, oxidative stress is associate with increased production of oxidizing species or a significant decrease in the effectiveness of antioxidant defenses, such as glutathione[1].

The effects of oxidative stress depend upon the size of these changes, with a cell being able to overcome small perturbations and regain its original state. The extent and the reversibility of the molecular damages and the adaptation capability of the biological system involved, are the main factors which leads up to a restore of the physiological condition. However, more severe oxidative stress can cause cell death and even moderate oxidation can trigger apoptosis, while more intense stresses may cause necrosis [2].

The direct consequence of the oxidative stress is a widespread oxidation of the biological substrates (DNA, protein, lipids and sugars)through non-physiological reaction mechanism.

A massive increase of the basal levels of oxidative stress has been associated in the genesis and/or progression of many chronic and degenerative disease and in many metabolic disorders.

Oxidative stress is suspected to be important as above reported in neurodegerative diseases including Lou Gehrig's disease (ALS), Parkinson's disease (PD), Alzheimer's disease (AD), and Huntington's disease, amyotrophic lateral sclerosis (ALS) [3].

Indirect evidence via monitoring biomarkers such as reactive oxygen species (ROS) ,and reactive nitrogen species production, antioxidant defense indicates oxidative damage may be involved in the pathogenesis of these diseases,[4;5], while cumulative oxidative stress with disrupted mitochondrial respiration and mitochondrial damage are related with AD, PD, and other neurodegenerative diseases[6].

Oxidative stress is thought to be linked to certain cardiovascular diseases (CVD), since oxidation of LDL in the vascular endothelium is a precursor of plaque formation [7]. Oxidative stress also plays a role in the ischemic cascade due to oxygen reperfusion injury following hypoxia. This cascade includes both strokes and heart attacks[8].

Oxidative stress also contributes to both tissue and organs injury playing important roles in the pathophysiology of type 2 diabetes mellitus (T2DM) and as well in the related diseases[9].

Furthermore, is it well known the close correlation of oxidative stress and ageing, and it seems likely to be involved in several age-related development of cancer. The reactive species produced in

oxidative stress can cause direct damage to the DNA and are therefore mutagenic, and it also suppress apoptosis and promote proliferation, invasiveness and metastasis[10].

Up to now it is unclear however, whether the oxidative stress is causal in disease progression or the result of the cell death associated with cell dying by necrosis. For instance, if the disease can be linked to a prolonged disturbance of redox regulation then oxidative stress can be determined as causal. In such instances, pharmacological interventions would be optimal when the corresponding redox imbalance are still reversible. This, however, requires detailed knowledge on the biochemical mechanisms involved.

2.1.a. Reactive Oxygen species(ROS).

Reactive oxygen species (ROS) represent the main molecular inducers and mediators of oxidative stress. ROS are reactive compounds generated in cells by both enzymatic and non-enzymatic sources[11], and have been implicated in a magnitude of physiological processes including ageing and immune function, as well as in disease initiation or progression. Oxidative stress occurs when the rate of ROS generation during normal/aerobic metabolism exceeds the detoxification abilities of the cell, and it has been implicated in many chronic and degenerative diseases[12].

Besides to act as injurious by-product of cellular metabolism, recent evidences indicate that ROS are also essential participants in cell signaling and regulation. Although this role for ROS is a relatively novel concept in vertebrates, there is a strong evidence of a physiological role for ROS in several non mammalian systems[13]. The apparent paradox in the roles of ROS as essential biomolecules in the regulation of cell functions and as a toxic by-product of metabolism may be addressed, at least in part, to differences in the concentration of ROS produced[14]. This is analogous to the effect of nitric oxide(NO), which has both regulatory functions and cytotoxic effect depending on the enzymatic source and relative amount of NO generated[15]. NO functions as a signaling molecule mediating vasodilation when produced in low concentrations by the constitutive isoform on nitric oxide synthase(NOS) in vascular endothelial cells[16] and as a source of highly toxic oxidants utilized for microbicidal killing when produced in high concentration by inducible NOS in macrophages[17]. Indeed, all phagocytic cells have a well-characterized O2-.generating plasma membrane oxidase capable of producing the large amounts of ROS required for its function in host defense[18].

2.1.b. Chemistry of Endogenous Reactive Oxygen Species.

Reactive oxygen species (ROS) are chemically reactive molecules containing oxygen. ROS are formed as a natural byproduct of the normal metabolism of oxygen but very often they are also generated by exogenous sources such as ionization radiation or xenobiotic[19].

Endogenously ROS are produced intracellulary through multiple mechanisms, the major sources being mitochondria, peroxisomes, endoplasmic reticulum, and the NADPH oxidase (NOX) complex in the membranes[20].

For instance, in aerobic organisms the energy needed to fuel biological functions is produced in the mitochondria via the electron transport chain which require ROS as physiological intermediates.

Mitochondria convert energy for the cell into an usable form, adenosine triphosphate (ATP) via oxidative phosphorylation, involving the transport of protons across the inner mitochondrial membrane by means of the electron transport chain. The different intermediates and ATP are carried out athwart a series of oxidation-reduction reactions in which the driving force is obtained from a great potential reduction. Ordinarily, during these redox passages, most of the amount of oxygen is reduced to water; however, up to 2% of electrons passing through the chain oxygen is instead incompletely reduced to give the superoxide radical(.O2-). This intermediate is not highly reactive, but can inactivate specific enzymes or acting as trigger of lipid peroxidation in its protonate form H02-[21].

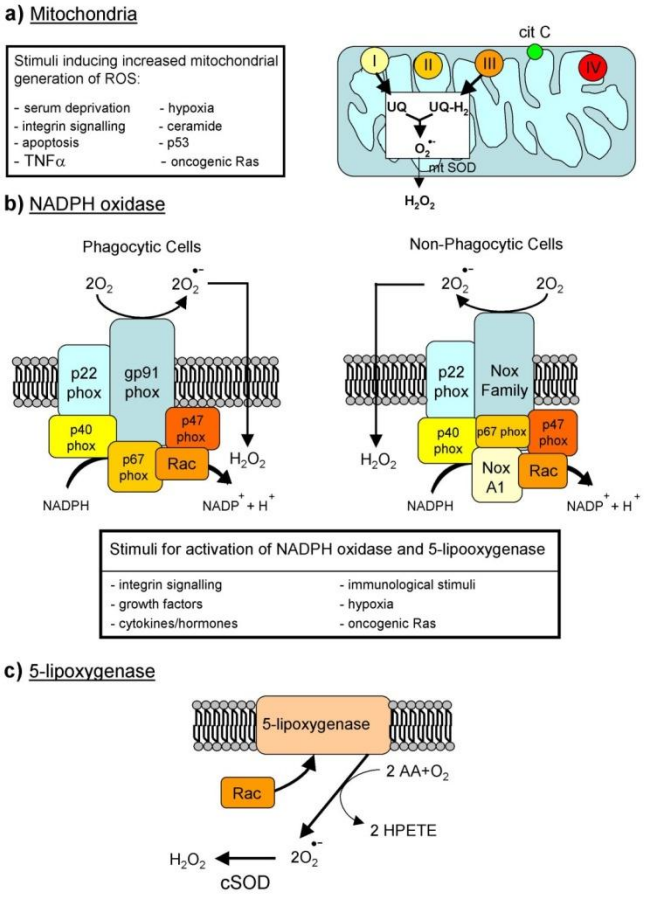

Fig 1. Major cellular sources of ROS in living cell(Major cellular sources of ROS in living non-photosynthetic cells. From a review by Novo and Parola, 2008)

As above reported several physiological ROS classified as oxygen ions and peroxides can be generated to act in many cellular functions in order to allow a correct cellular signaling or to maintain a finely balanced homeostasis. Furthermore, the different classes of ROS are generated ubiquitously at different concentrations depending of the cell type:
Some relevant ROS include:

- The superoxide anion (•O2-), formed through one-electron reduction of O_2:
O_2 + e- > •O2-

- Hydrogen peroxide (H_2O_2), which has no unpaired electrons, and thus it is not a radical as reported by Halliwell and coworker in 1991
It is formed by several metabolic reactions, for instance the dismutation reaction of •O2- catalyzed by superoxide dismutase, and which has as intermediate the hydroperoxyl radical:
•O2- + H^+ > HO_2.
2HO_2. > H_2O_2 + O_2

- The hydroxyl radical (•OH) that can be formed from either the superoxide anion through the Haber-Weiss reaction or from H_2O_2:
$^{\bullet}O_2^-$ -+ H_2O_2 > O_2 + HO^- + $•OH^-$

The reactions leading to hydroxyl radicals(•OH), from Hydrogen peroxide (H_2O_2) and superoxide (•O2-) are very slow, but can be catalyzed catalyze by iron. The first step involves the reduction of ferric ion in ferrous
Fe^{3+} + $^{\bullet}O_2^-$ > Fe^{2+} + O_2

The second step is the Fenton reaction:
Fe^{2+} + H_2O_2 > Fe^{3+} + OH^- + •OH

Net reaction:
•O2- + H_2O_2 > Fe^{3+} + OH^- + O_2

The reaction is named by Fritz Haber and his student Joseph Joshua Weiss[22].

2.1.c. Endogenous defenses toward ROS.

Enzymatic antioxidants, i.e. superoxide dismutase (SOD), catalase (CAT) and glutathione peroxidase (GPX) and glutatihione S-transferase, (GSH), together with antioxidant, radical scavengers and metal-ion chelators represent the first defense-line toward ROS[23].
SOD represent the most powerful and immediate line of defense against oxidative stress at all cells exposed to oxygen. Going into details SOD are a class of enzymes that catalyze the dismutation of peroxide into oxygen and hydrogen peroxide. In all the mammals, three form of superoxide dismutase are present. SOD1, located primally in the cytoplasm, SOD2 in the mitochondria and SOD3 at extracellular level. SOD1 and SOD3 contain copper and zinc ions, while SOD2 has manganese ion in its reactive center.

$M^{(n+1)} – SOD + O_2^- > Mn^+ - SOD + O_2$

$- M^{(n+)} – SOD + O_2- + 2H^+ > m^{(n+1)} – SOD + H_2O_2$

Catalase is another enzyme particularly effective. It is concentrated in peroxisome, located next to mitochondria, and reacts with the hydrogen peroxide to catalyze the formation of water and oxygen.

$2\ H_2O_2 > 2\ H_2O + O_2$

Glutathione peroxidase reduces hydrogen peroxide by transferring the energy of the reactive peroxides to a very small sulfur-containing protein called glutathione. The metal center (selenium) in this enzymes act as reactive center, carrying electrons from the peroxide to the glutathione.

$2GSH + H_2O_2 > GS-SG + 2H_2O$

A further class of ubiquitous enzyme called Peroxiredoxins are able to degrade H_2O_2 in its basic non-cytotoxic components, within mitochondria, cytosol, and nucleus.

2.2. Advanced glycoxidation and lipoxidation end products (AGEs and ALEs): an overview of their mechanisms of formation.

2.2.a. Protein Carbonylation and Carbonyl Stress.

As previously described ROS can cause specific protein modifications that may lead to a change in the activity or function of the oxidized protein. Several major forms of oxidative modifications can occur on amino acid residue side chains including carbonylation.

Carbonylation of proteins is irreversible and irreparable and may alter the conformation of the polypeptide chain, determining the partial or total inactivation of proteins[24;25].

Hence the protein carbonylation induces widespread cellular dysfunctions which can also reflected at the tissue level. The major alterations can be a loss of functional activity, dysfunction of the protein folding processes, accumulation of misfolded proteins, inhibition of the ubiquitin-dependent proteosomal function, direct inactivation of proteasome, accumulation of oxidized proteins and induction of apoptosis and necrosis[26].

The carbonyl derivatives, grouped in aldehydes and ketones, can act through direct oxidation of proteins binding the amino acid side-chains of Pro, Arg, Lys, and Thr. Protein carbonyl derivatives can also be generated through oxidative cleavage of proteins, via the a-amidation pathway or through oxidation of glutamine side chains, leading to the formation of a peptide in which the N-terminal amino acid is blocked by an a-ketoacyl derivative. In addition, carbonyl groups may be introduced into proteins by secondary reaction of the nucleophilic side chains of Cys, His, and Lys residues with reactive carbonyl species (RCS) produced during lipid peroxidation (mainly α,β-unsaturated aldehydes), or generated as a consequence of the reaction of reducing sugars, such as glyoxal (GO) and methylglyoxal (MGO), or their oxidation products (ketoamines, ketoaldehydes, deoxyosones) with Lys residues of proteins (glycation and glycoxidation reactions) [27;28;29].

Most of the biological effects of intermediate RCS are attributed to their capacity to react with the nucleophilic sites of proteins, forming Advanced Lipoxidation End Products (ALEs) and Advanced Glycation End-Products (AGEs).

Glycation is a spontaneous reaction recognized as the initial step of a very complex process, the Maillard cascade, which involves the formation of several end-stage products responsible for protein modification and is catalyzed by oxidative stress and ROS[30;31].

Protein modification by lipoxidation-derived RCS is little known, although a large body of evidence indicates their involvement in physiological ageing as well as in the onset and/or progression of several cardiovascular(e.g., atherosclerosis, long-term complications of diabetes) and neurodegenerative diseases[32;33;34].

.Accumulation in serum of RCS-derived from lipids and carbohydrates and the subsequent protein carbonylation have first been defined as ‘‘carbonyl stress’’ by Miyata et al[35].

The increased protein carbonylation by lipids and carbohydrates in chronic diseases is the result of carbonyl overload on metabolic pathways involved in detoxification of RCS[36;37;38].

This leads to a general increase in steady-state levels of RCS formed by both oxidative and non-oxidative reactions. In fact, in both diabetes and uremia, not only glycoxidation and lipoxidation products are increased, but also the products of reaction of proteins with dicarbonyl compounds formed by non-oxidative mechanisms[39].

2.2.b. ALEs: an introduction.

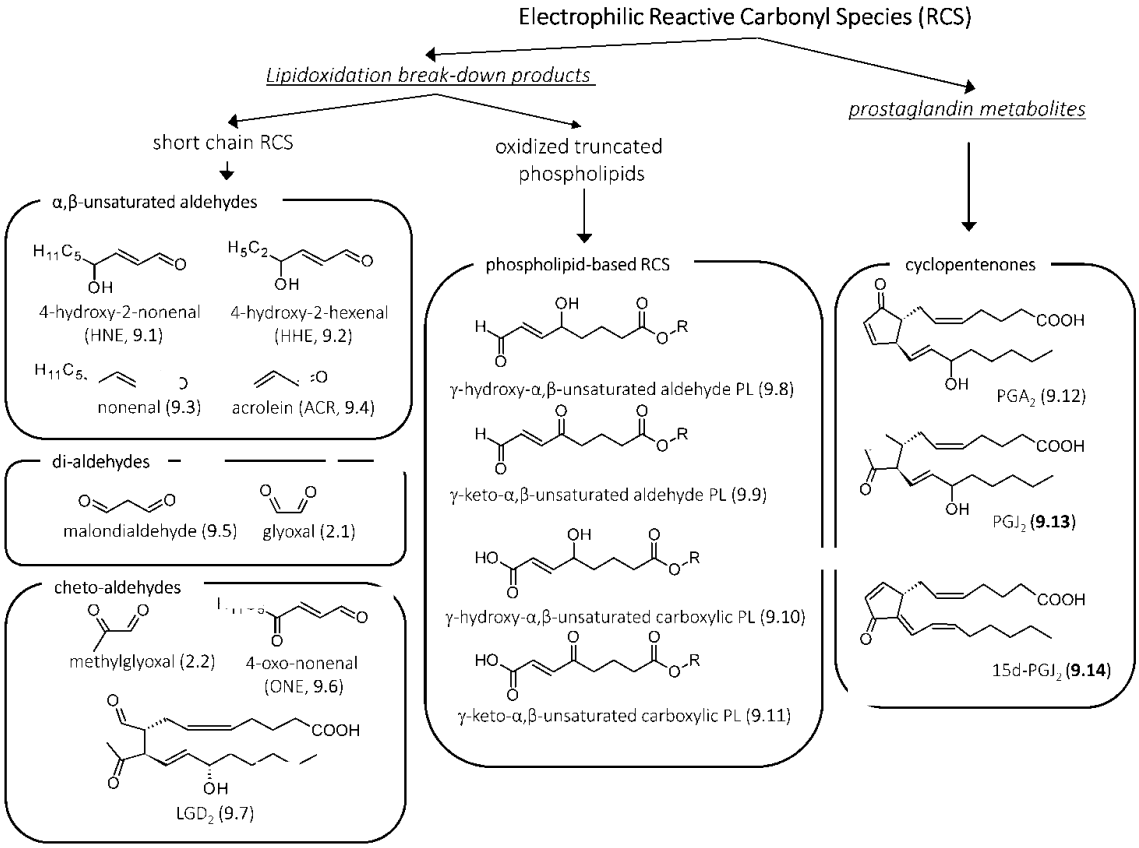

Fig 2 . Structure of the most reactive carbonyl species (RCSs) arising from lipoxidation break-down and prostaglandin metabolism.

The term ALEs (Advanced Lipoxidation End products) includes a variety of adducts and cross-links which are generated by the non-enzymatic reaction of RCS produced by lipid peroxidation and the lipid metabolism with the nucleophilic sites of macromolecules such as proteins, DNA, and aminophospholipids, leading to their irreversible modification[40]. The most studied ALEs are those arising from the reaction of RCS break-down products of the lipid peroxidation cascade with the nucleophilic residues of proteins, mainly Cys, Lys, His, and Arg residues.

As schematized in Fig 2, the RCS arising from the lipid peroxidation cascade are quite heterogeneous and can be divided into three main classes, namely :

(1) the α,β-unsaturated aldehydes, including hydroxylated, such as 4-hydroxy-2-nonenal (HNE) and 4-hydroxy hexenal (HHE), and nonhydroxylated derivatives, nonenal and acrolein (ACR);

(2) di-aldehyde, including the well-known lipid peroxidation by product malondialdehyde (MDA) and glyoxal (GO);

3) cheto-aldehyde such as methylglyoxal (MGO), 4-oxo-nonenal (ONE), and the isoketals also called levuglandins (LGD2, as exemplified in Figure x) which are gammaketoaldehydes formed via the isoprostane pathway of arachidonic acid peroxidation.

The RCS acting as precursor of ALEs, besides including the short-chain carbonyl derivatives generated by the break-down of nonenzymatic lipoxidation-derived hydroperoxides, also include the oxidized truncated phospholipids, where the electrophilic moiety remains covalently linked to the phospholipid[41].
Examples of phospholipids-based RCS, as reported in Fig.2, include γ-hydroxy-α,β-unsaturated aldehyde, γ-keto-α,β-unsaturated aldehyde phospholipid,γ-hydroxy-α,β-unsaturated carboxylic phospholipid and γ-keto-α,β-unsaturated carboxylic phospholipid[42]. As in the case of short-chain RCS, also the oxidized phospholipids containing electrophilic moieties are able to covalently react with the nucleophilic sites of proteins forming Michael adducts or Schiff bases. Although the ALEs formed by short-chain RCS have been much more studied in respect to those generated by oxidized phospholipid, some protein and peptide targets of oxidized phospholipid have already been identified, such as cathepsin B and angiotensin II[43].
It should be noted that although the chemical reactions of RCS in free form or bound to phospholipid are practically the same and mainly based on the formation of Michael adduct or Schiff base as below described, the protein targets might be different since the two classes of compounds have a quite different lipophilicity and consequently a different cellular distribution.
The above-mentioned RCS are generated by a common lipid-peroxidation cascade, which can involve free polyunsatured fatty acids (PUFAs) or phospholipids. An additional class of RCS able to form protein adducts is represented by electrophilic prostaglandin metabolites, which are characterized by an α,β-unsaturated carbonyl moiety (cyclopentenone). Among these RCS, it is worth mentioning Prostaglandin 2 (PGA2) generated from the dehydration of Prostaglandin E2 (PGE2) and 15-deoxy- Δ 12,14 -prostaglandin J2 (15d-PGJ2) which is generated as a consequence

of dehydration of PGD2, a principal COX-2 product formed in various cells and tissues during the inflammatory processes[44,45].

It should be stressed that some RCS such as glyoxal and methylglyoxal are generated by the oxidative pathways involving both lipids and sugars, thus the corresponding reaction products with proteins can be named both as ALEs and AGEs or as EAGLEs (either advanced glycation or lipoxidation endproducts).

2.2.c. α,β-unsaturated carbonyls.

2.2.c.1. Exogenous and endogenous sources.

Regarding the endogenous sources of α,β-unsaturated carbonyls, lipid peroxidation represent the major mechanism by which they can be generated *in vivo*[46;47].

Lipid peroxidation is initiated by the generation of free radicals close to cellular membranes, which represent rich source of PUFAs. Hence, the levels of α,β-unsaturated carbonyls is strictly related to radical formation and spontaneously but is one hundred times faster when catalyzed by glutathione-S-transferases (GSTs) [48].

Other metabolic reactions can involve the carbonyl function that can be either reduced into alcohol or oxidized into acid, involving alcohol dehydrogenase or aldo/keto reductase (AKR) and aldehyde dehydrogenase, respectively[49].

While HNE (Fig.2), (which is the most abundant and toxicα,β-unsaturated aldehyde and generated through the β-cleavage of hydroperoxides from ω-6 PUFAs containing ω -six chains, such as linoleic acid and arachidonic acid [50] is almost exclusively formed endogenously, acrolein (ACR) is ubiquitously present in foods and in the environment, which might help understanding of the mostly cytotoxic effect of ACR on the one hand and cytotoxic and regulatory effect on the other[51;52].

Acrolein is generated by heat-induced dehydration and decomposition reactions of sugars, lipids, and amino acids during food cooking[53;54], but, nonetheless, smoking of tobacco products represent the major source of the total human exposure to ACR [54] as demonstrated by the level of its main metabolite, namely 3-hydroxypropyl mercapturic acid, in urine of smokers, which is about twice than that of non-smokers[55].

ACR is the strongest electrophilic α,β-unsaturated aldehydes, showing the highest reactivity with thiols and amines reacting more than 100 times faster with GSH than HNE. The thiol adducts of ACR formed by the same mechanism of reaction of HNE but without the cyclization rearrangement are considerably more stable than those formed by other α,β-unsaturated aldehydes with dissociation constants 10-10,000 times lower[56].

2.2.c.2. ALEs formed by α,β-unsaturated carbonyls.

Most of the lipid-derived RCS are characterized by a carbonyl group (a keto or an aldehyde function) which is conjugated to a double bond and which regulates the electrophilic reactivity toward the nucleophilic moieties.

In particular, the carbonyl group acts as an electronwithdrawing group, which decreases the electron-richness of the conjugated alkene group. The combination of polarizable mobile electrons and the electron-withdrawing capacity of the carbonyl group thus creates an area of electron deficiency at the alkene β-carbon atom of the α,β-unsaturated carbonyl derivatives[57].

Hence, the β-carbon atom shows an electrophilic character, which in the case of γ-hydroxylated derivatives, such as HNE and HHE is further enhanced by the inductive effect of the vicinal hydroxyl group. It covalently reacts with the nucleophilic (electron-rich species) side chains on amino acid residues of proteins, such as the thiol group of cysteine, the imidazolic nitrogen of histidine, and the epsilon amino group of Lys, forming the corresponding Michael adduct. However, although the Michael adducts formed with Cys and His are stable in isolation, Michael adducts to Lys ε -amino groups are formed reversibly and can be isolated only following reductive trapping with NaBH4[58;59].

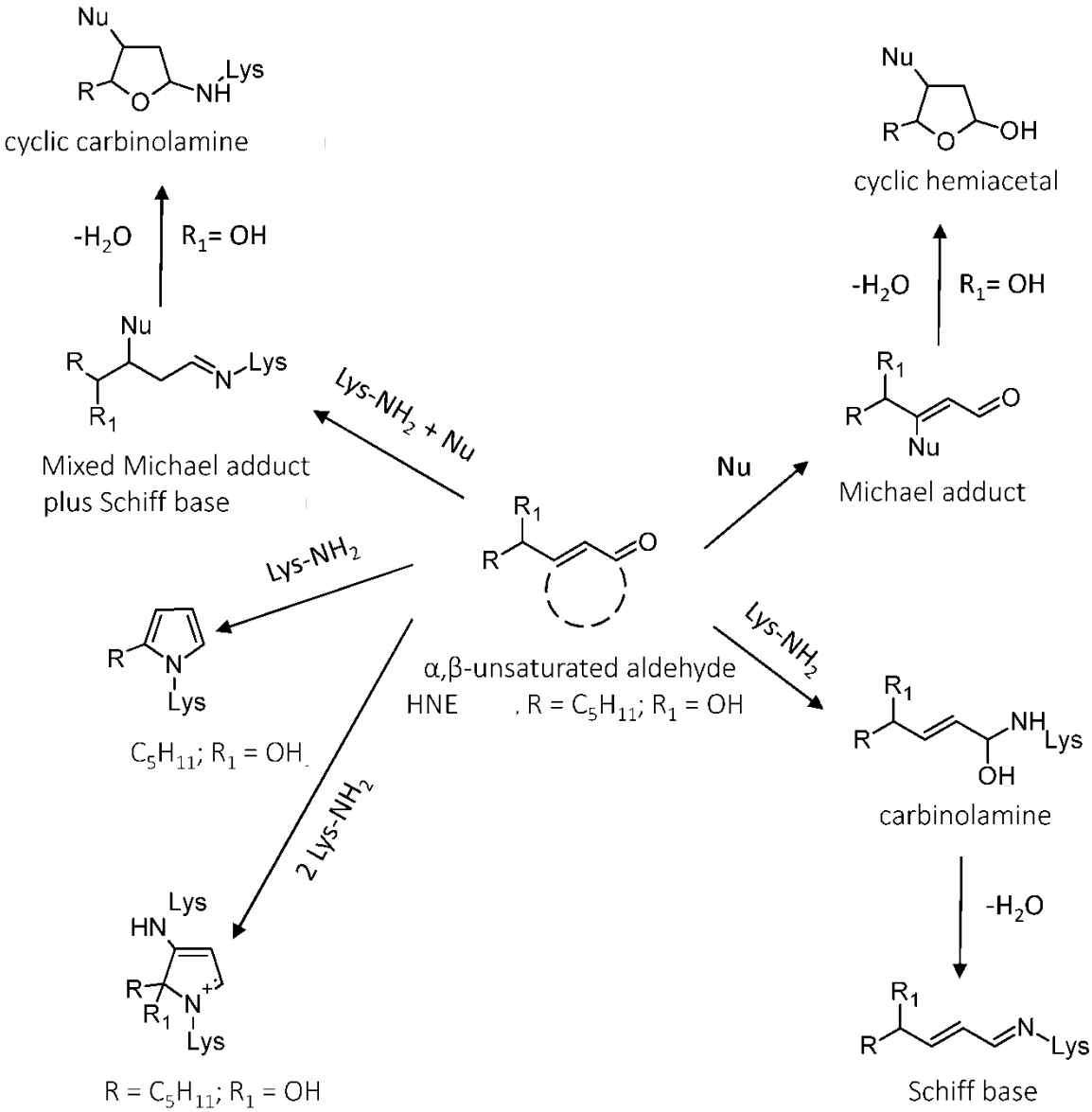

Fig 3. General reaction mechanisms of ALEs formation for hydroxylated and nonhydroxylated α,β-unsaturated aldehydes with specific focus to HNE-derived ALEs.

If the resulting Michael adduct contains an γ-hydroxyaldehyde, it can further react intra-molecularly forming cyclic hemiacetals (Fig 3). Another general reaction involving α,β-unsaturated aldehydes consists of the reaction of the aldehydic carbonyl group with the primary amino group of Lys or with the terminal amino group, forming the corresponding Schiff base. In more detail, the reaction starts with the formation of a carbinolamine intermediate that rearranges and loses water to yield a Schiff base.

The Schiff base is a reversible adduct which undergoes a hydrolytic cleavage and hence it is more stable when the reaction involves the Lys residues embedded in lipophilic and anhydrous

protein pockets. The right side of the figure 10 summarizes the general reaction mechanisms for hydroxylate and nonhydroxylated α,β-unsaturated aldehydes.

The Michael adducts and Schiff bases are the early reaction products of α,β-unsaturated carbonyl that for most of the RCS further react and rearrange forming additional reaction products such as cross-links and which are specific for each RCS.

For example, the upper left side of Fig 3 shows that HNE besides forming Michael adduct reaction products with His, Cys, and Lys residues as well as Schiff bases with Lys residues, also forms other different ALEs, such as the HNE-derived 2-pentylpyrroles and the fluorescent four-electron oxidation product, 2-hydroxy-2-pentyl-1,2-dihydropyrrol-3-one iminium[60].

HNE, since possessing both an aldehyde and an electrophilic carbon, can form cross-links, involving condensation with Lys at carbonyl carbon atom (Schiff base) and the Michael adduct at β -carbon atom with nucleophilic residues. As shown in the bottom left side of the figure 3 this adduct can then dehydrate yielding the cyclic carbinolamine[61].

The 4-keto derivative of HNE, 4-oxo-nonenal (ONE, figure 3), has been demonstrated to be a direct product of lipid oxidation[62], arising independently and not from oxidation of HNE, and more reactive that HNE (it reacts with protein nucleophiles through conjugate addition at a rate 6 – 31 times faster than does HNE) [63].

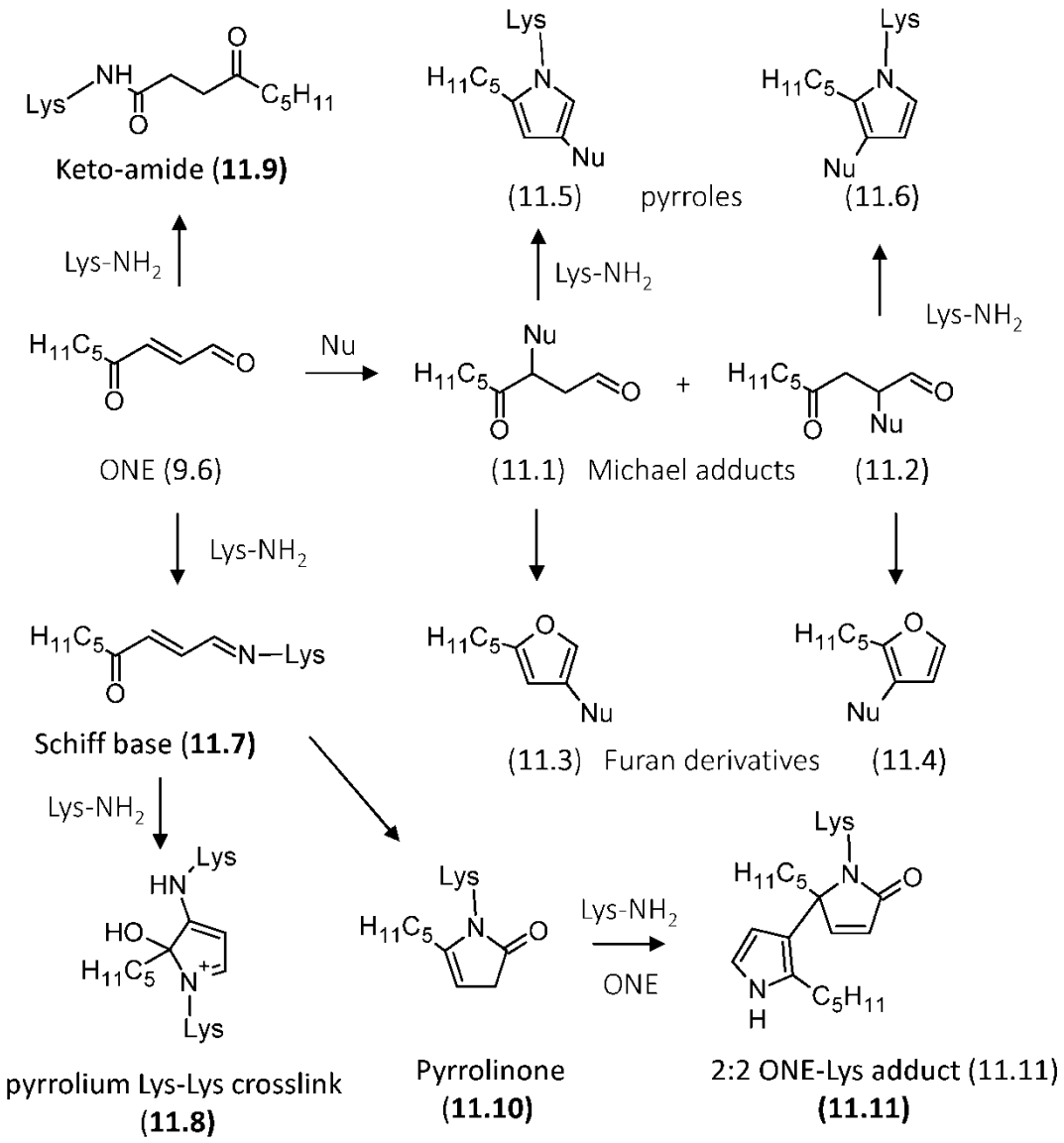

Fig 4. Reaction mechanisms of formation for the ONE-based adducts with nucleophilic sites.

As depicted in Fig 4, ONE forms simple 4-ketoaldehyde Michael adducts by the reaction of C2 and C3 with His, Lys, and Cys that can exist as such or undergo ring-closure to furans forming the furan derivatives.

ONE reacts also with the amino group of Lys forming the corresponding Schiff base, which then reacts with a second amine moiety at C3, followed by tautomerization and then a second two-electron autoxidation to give the fluorophore pyrrolium Lys – Lys cross link which is also formed by HNE. More recently Zhu and Sayre[64] reported that apparent long-lived Lys adducts with the mass expected of a Michael adduct are actually the isomeric 4-ketoamide which together with Lys-derived pyrrolinone and Lys–His imidazolylpyrrole cross-links are all major products that form on proteins from ONE.

Notably, Lys-derived pyrrolinone which is inequilibrium with its corresponding hydroxy pyrrole tautomer, can dimerize generating the 2:2 ONE-Lys adduct.

It should be noted that unlike HNE and other α , β -unsaturated aldehydes, ONE reacts also with Arg residues to give stable covalent adducts. Preference for the reaction of amino acid nucleophiles with ONE was determined to have the following order: Cys >>His >>Lys >Arg[64].

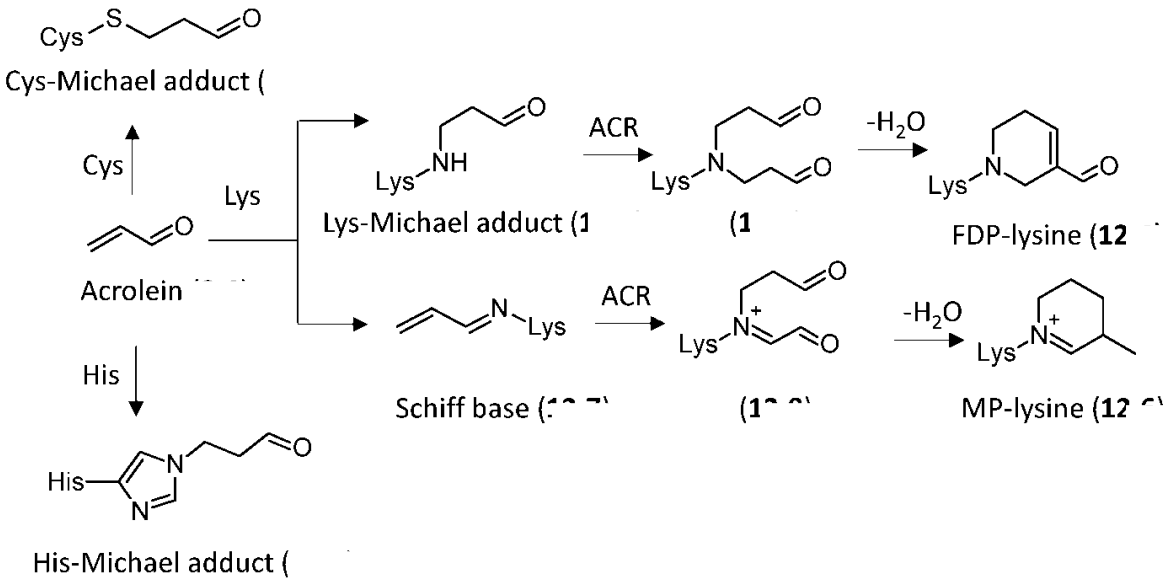

Fig 5. Reaction mechanism of formation for the acrolein-based adducts with nucleophilic sites.

Another well-studied α,β-unsaturated aldehyde is represented by ACR (Fig 5) which has several sources other than peroxidation of PUFAs including the metabolism of amino acids, polyamines and drugs as well as the environment and food[65].

Among the α,β-unsaturated aldehydes, ACR is by far the strongest electrophile and therefore shows the highest reactivity with protein nucleophiles, the order of reactivity (Cys >His> Lys) being the same as that established for HNE. As illustrated in Fig 5 and among these sites, the preferential formation of Michael-type adducts on cysteine residues is believed to be the predominant way for ACR to exert its reactivity in biological systems.

Besides a simple Michael adduct, ACR forms additional ALEs as studied by Uchida et al.

In particular they identified an ACR – lysine adduct, N ε -(3-formyl-3,4-dehydropiperidino) lysine (FDP-lysine). The mechanism proposed for FDP-Lys formation involves Michael addition of the Lys amino group to the ACR β-carbon atom to give a secondary amine with retention of the aldehyde group (Lys-Michael adduct). This intermediate reacts with another ACR molecule via a

Michael addition forming an unstable derivative that, after aldol condensation and dehydration, gives the FDP-Lys adduct[66].

Later Uchida et al. identified another ACR-dependent ALE, the Nε-(3-methylpyridinium)-lysine (MP-lysine), resulting from the initial Schiff base formation of ACR with theε-amino group of lysine, which further reacts with a second ACR molecule via a Michael addition to generate an imine derivative. The subsequent conversion of this imine derivative to the final product (MP-lysine) requires two oxidation steps and intramolecular cyclization, but its detailed mechanism has not yet been clarified[67].

More recently the same research group, by using a reductive amination-based method, analyzed the ACR-specific adducts with a carbonyl function and found that ACR modifcation of the protein produced a number of carbonylated amino acids, including an ACR _ histidine adduct.

On the basis of the chemical and spectroscopic evidence, this adduct was identified as N τ -(3-propanal) histidine which appeared to be one of the major adducts generated in the oxidized LDL[68].

2.2.d. Di-carbonyls.

2.2.d.1. Exogenous and endogenous sources.

In this section the attention is focused on those of malodialdeyde (MDA) and isoketals.
The former has endogenous sources almost identical to those of α,β -unsaturated carbonyls since its main *in vivo* source is represented by peroxidation of poly unsaturated fatty acids with two or more methylene interrupted double bonds[69].
Isoketals, also called LGs and isolevuglandins (isoLGs), are formed by the rearrangement of endoperoxide intermediates generated through the cyclooxygenase and free radical-induced oxidation of arachidonates[70].
While isoketals are generated almost only endogenously, malondialdeyde can be present in foods arising from lipid peroxidation induced by heating. Indeed, it has been found in heated edible oils such as sun flower and palm oils and is contained at high levels in many rancid foods[71].

2.2.d.2. ALEs formed by di-carbonyls.

Different ALEs are generated by the reaction of dicarbonyls (di-aldehydes and cheto-aldehydes) with proteins.
Some of these RCS, such as GO and MGO, besides being generated by a lipid oxidation/metabolism, are also formed by different enzymatic and nonenzymatic pathways involving sugars and their reactivity and formation of AGEs adducts will be discussed under the AGEs section.
It should firstly be noted that the ability of the dicarbonyls to form stable and irreversible ALEs in relatively short periods is due to the presence of both the electron-withdrawing carbonyl groups, the chemical reactivity of which is further enhanced by the activation of one carbonyl group on the other. Indeed, the presence of only one carbonyl function can only give reversible Schiff bases that to be analytically detected require stabilization by a chemical reduction (reductive amination) using, for example, sodium borohydride.
The reaction of the lipid-derived di-carbonyls usually involves the formation of a carbinolamine as a first step, followed by different rearrangement reactions leading to, in most cases, heterocylic cross-links as in the cases of glyoxal and methylglyoxal. Isoketals is another example of di-carbonyls forming irreversible ALEs, which include heterocyclic cross-links.

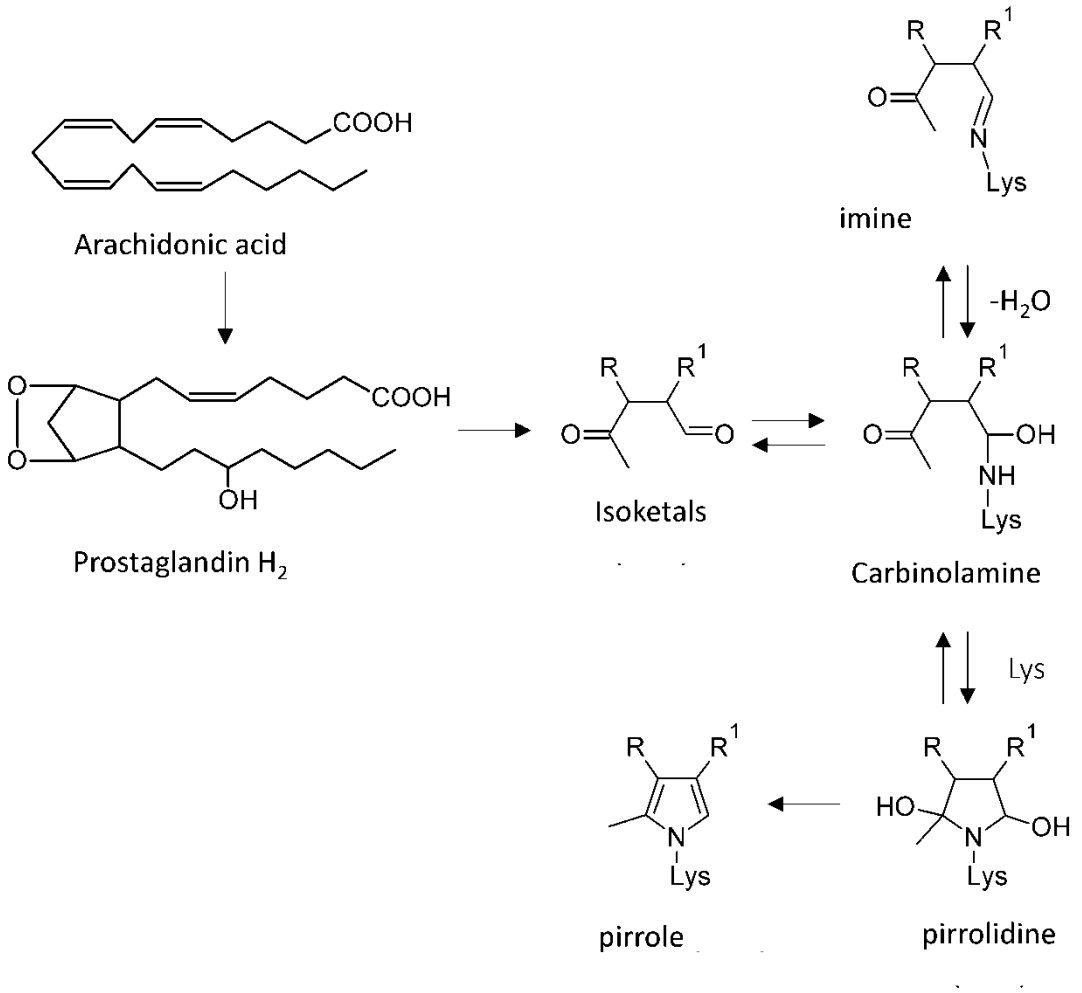

Fig 6. Reaction mechanism of formation for the isoketal-based adducts with nucleophilic sites.

Isoketals are highly reactive γ-ketoaldehydes formed by free radical-mediated lipid peroxidation of H2-isoprostanes.

Unlike the F2-isoprostanes, the biological effect of these products is due to their ability to modify proteins rather than through activation of specific receptors[72].

Fig 6 reports the reaction of isoketals with the amino group of Lys which is based on the formation of a carbinolamine intermediate that is in equilibrium with the corresponding reversible Schiff base or the remaining carbonyl of hemiaminal can undergo an intramolecular nucleophilic attack by the ε-amino group of a second Lys residue to yield a highly unstable pyrrolidine adduct which undergoes a rapid dehydration to form a pyrrole adduct[73].

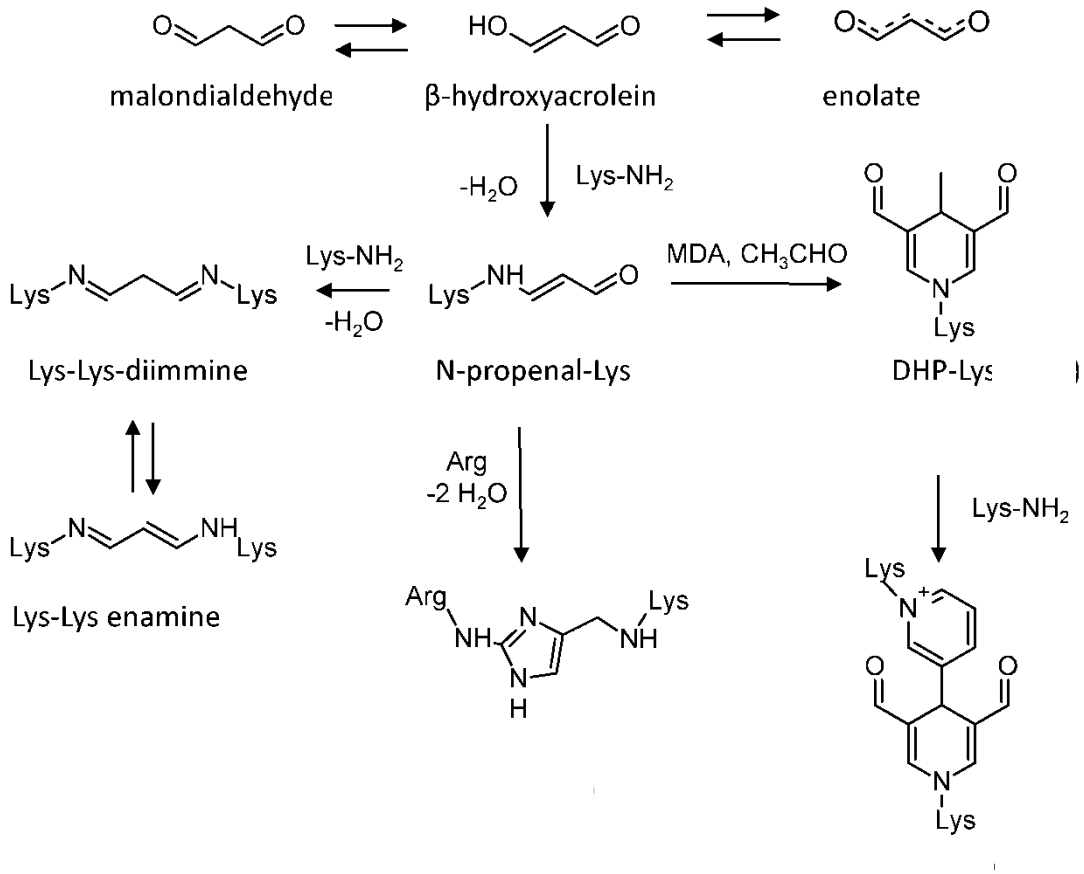

Fig 7. Reaction mechanisms of formation for the MDA-based adduct with nucleophilic sites.

Malondialdehyde is often the most abundant individual aldehyde resulting from lipid peroxidation and occurs in biological materials in various covalently bound forms[74].

As shown in Fig 7 and compared with other RCS, MDA is relatively less reactive at neutral pH and this is explained by considering that it enolizes rapidly and then loses a proton at neutral pH forming the enolate salt which is stabilized by a conjugated π -bond system. The reactivity of MDA is due to the nondissociated enolate (the β-hydroxyacrolein) which is able to react with the ε -amino group of Lys forming the semistable N ε -(2-propenal)lysine (N-propenal-Lys). N-propenal-Lys can further react with another molecule of MDA and a molecule of acetaldehyde (derived from MDA breakdown) to form a stable fluorescent product containing a dihydropyridine moiety (DHP-Lys) or with an additional Lys residue to form a Lys – Lys-diimine which would exist as its resonance-stabilized enamine[75].

Thealdehyde side chains on the stable dihydropyridine ringcan further react with Lys residues to form a reversible cross-link[76].

MDA protein adducts and, in particular, N-propenal-Lys and the dihydropyridine cross-links have been more recently characterized by MS approaches and using insulin and albumin as target

proteins[77;78]. Beside Lys, MDA reacts with other nucleophilic residues such as Arg, as shown in the bottom side of the Fig 7, forming the stable N δ-(2-pirimidyl)-Lornitine[79] and recently the cross-linking of MDA involving Lys and Arg residues, 2-ornithinyl-4-methyl-1,3-imidazole has been elucidated by NMR and MS and identified in diabetic patients[80].

2.2.d.3. AGEs: an introduction.

The browning process, that occurs during food heating, is a well-known phenomenon which characterizes several cooked dishes and is caused by the so-called Maillard reaction, a nonenzymatic process firstly described by Maillard in 1912 (Louis Camille Maillard, 1878 – 1936) [81].

It generates yellowish-brown colored products and involves a complex series of degradative reactions between sugars and proteins, whose chemical mechanisms were first described by Hodge 40 years later[82].

For many years, studies on the Maillard reaction were focused on foods and food-like systems where it occurs during heating, processing, and storage, and plays key roles in determining color, flavor, and nutritional quality.

Other studies concerned the effects of the Maillard reaction when it occurs in paper, textile, soil, and biopharmaceutical products.

Even though the first glycated protein was discovered by Kunkel and Wallenius in 1955 (a glycated HbA1C hemoglobin) [83] increasing attention has been shifted to the human body only in the last three decades, namely since the pathological role of *in vivo* posttranslational protein glycation has become clearly evident in all its detrimental consequences. *In vivo*, the process can occur in tissue and body fluids, is usually associated with hyperglycemic pathophysiological conditions, and involves the generation of irreversible protein adducts and cross-links known as AGEs.

In vivo , several disorders appear to be exacerbated by such damaging protein adducts, especially when they involve long-lived proteins. A paradigmatic example is offered by collagen[84], the glycation of which induces vascular thickening with detrimental consequences including decreased elasticity, hypertension, and endothelial dysfunctions, and induces marked accelerating effects on disorders such as atherosclerosis, nephropathy, and retinal pathologies[85;86].

Moreover, glycation can also affect short lived peptides causing detrimental changes in their biological functions as demonstrated by the accumulation of glycated insulin in the pancreatic β - cells of diabetic animal models[87].

2.2.d.4 Maillard reaction.

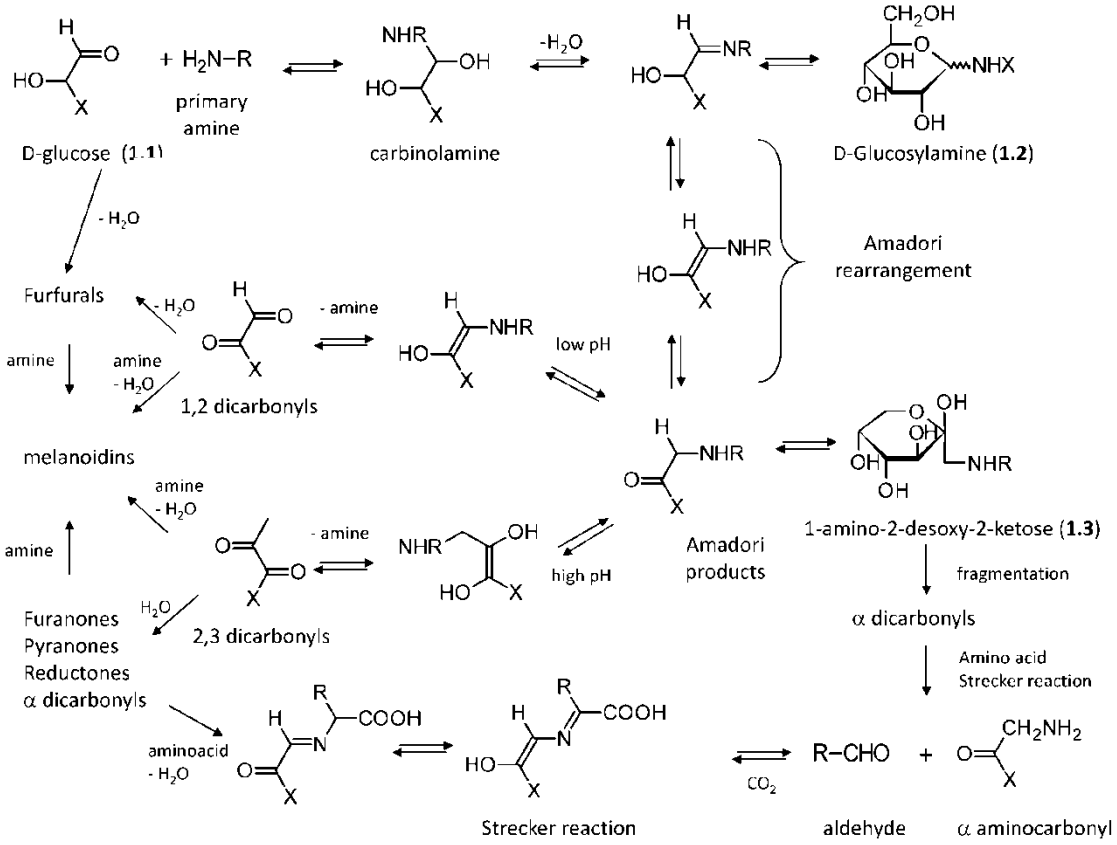

Fig 8. Major steps in the Maillard reaction of reducing sugars following the well-known Hodge scheme.

As shown in Fig 8 and following the well-known Hodge's scheme[88], the first step in the Maillard reaction involves condensation between a carbonyl group from a reducing sugar (e.g. D-glucose) and a primary amino group belonging, for example, to the lysine side chain or to the protein N-terminus. The condensation yields a carbinolamine intermediate, which dehydrates to give an unstable imine adduct which can, in turn, cyclize to generate N-substituted D-glucosylamine (D-Glucosylamine) [89].

At physiological pH and room temperature, the imine derivative spontaneously undergoes the acid-catalyzed Amadori rearrangement (Mario Amadori, 1886 – 1941) and gives the corresponding N-substituted 1-amino-2-desoxy-2-ketose, which can cyclize yielding very stable derivatives called Amadori products which are more stable compared to that of the N-substituted

D-glucosylamine[90] even though all these products can react with amino acids to produce brown melanoidins[91].

Formation of the Amadori products is favored at alkaline pH values and in the presence of phosphate ions. Despite being relatively stable, the Amadori products can react following two major routes. At low pH values, they undergo enolization yielding 1,2-dicarbonyls, which then dehydrate to give furfural derivatives[92].

At higher pH values, enolization produces 2,3-dicarbonyls which then dehydrate to give reductones[93].

These conjugated enediols have a moderate reducing power and can contribute to antioxidant activity. In the presence of amino acids they can generate brown melanoidins.

The cyclization of 2,3 dicarbonyl intermediates can also give furanones and pyranones which include important flavor compounds with very low aroma threshold values[94].

By following different pathways, Amadori products can generate α-dicarbonyls mainly through oxidative fission[95] or retro-aldol fragmentation[96], the former being markedly catalyzed by the presence of transition metal ions. Sugar fragmentation can also occur via a free radical-based mechanism according to the so-called Namiki pathway[97].

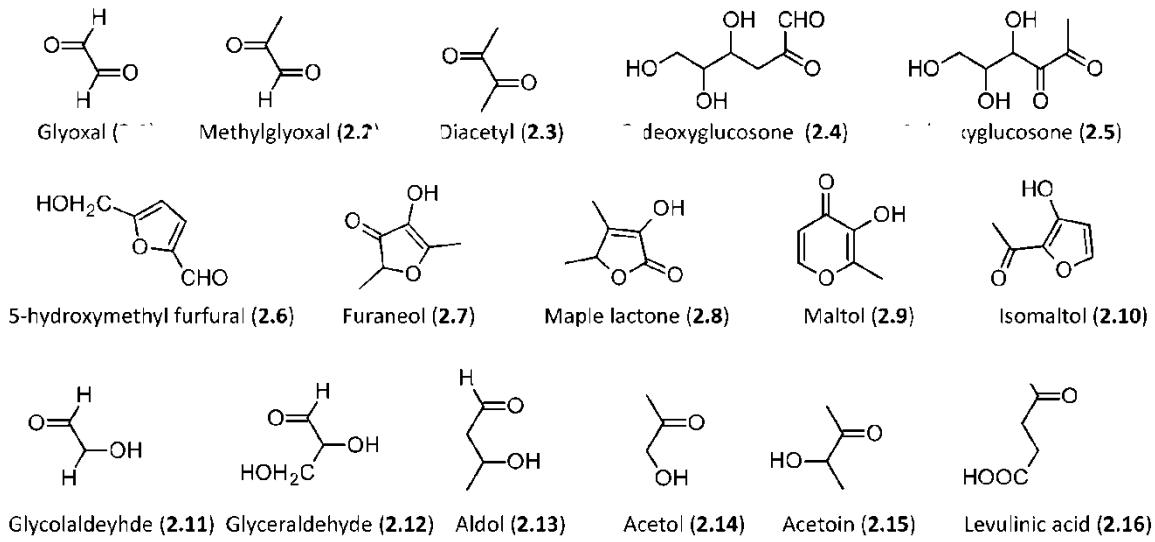

Fig 9. Relevant molecules involved in Maillard reaction. The first row includes α-dicarbonyls, the second row collect cyclization producrs, and the third row shows carbonyl derivatives generated by sugar fragmentation.

Di-carbonyl compounds are very reactive products and their critical relevance in AGEs generation will be discussed in-depth in this introduction.

Besides di-carbonyls, sugar fragmentation can also generate hydroxyl aldehydes and the corresponding oxidized acid analogues as depicted in Fig 9. Di-carbonyl compounds can react with amino acids through the so-called Strecker degradation, in which the amino acid is transformed into the corresponding aldehyde liberating CO2 and the remaining α-aminocarbonyl compound, which can then condense to yield pyrazine derivatives, typical aroma components in heated foods[98].

The relationship between sugar structure and susceptibility to Maillard reaction has been extensively studied both *in vivo* and in foodstuffs[99].

Although in all sugars the cyclic form is thermodynamically favored, the reactivity of monosaccharides is directly related to the abundance of their open chain form[100].

This easily explains why glucose, due to the stability of its pyranose ring, is the least reactive sugar, while fructose whose furanosic cyclic form is somewhat less stable is about 7.5-fold more reactive than glucose[101].

Notably, the Maillard reaction can also involve fructose metabolites, such as fructose-6-phosphate or glyceraldehyde-3-phosphate, which show an extraordinary reactivity up to 200-fold compared to that of glucose. The resulting critical role of fructose in protein glycation leads to the term " fructosylation ", and the fructose effects are further exacerbated by its widespread diffusion[102].

Despite its low reactivity, even glucose, which is present in millimolar concentration in several tissues, markedly contributes to protein glycation also because it can be converted into fructose via the Polyol pathway[103]. Besides the abundance of open chain forms, other factors governing susceptibility to the Maillard reaction include the sugar length and the intrinsic reactivity of the functional groups. Thus,

aldoses are more reactive than ketoses, because aldehydes are more accessible and more electrophilic than ketones[103].

Figure 9 illustrates some relevant players involved in the above-described Maillard reaction. The first row collects the major α -dicarbonyls including both short-chain derivatives (e.g. glyoxal and methylglyoxal) and longer polyol dicarbonyls (e.g. glucosone analogues such as 3-deoxyglucosone and 1-deoxyglucosone).

The second row shows the main cyclization products. Beside the already-mentioned 5-hydroxymethyl furfural, it is worth mentioning furaneol (2,5-dimethyl-4-hydroxy-3(2H)-furanone) [104], which represents an illustrative example of reductones.

Cyclization of 2,3-dicarbonyls can also afford flavored and colored furanones (e.g. Maple furanone, 5-Ethyl-3-hydroxy-4-methyl-2(5H)-furanone) [105], pyranones (maltol, 3-Hydroxy-2-methyl-4-pyrone) [106], and isomaltol (1-(3-hydroxy-2-furanyl)-ethanone) [107].

The last row includes examples of hydroxyl carbonyl compounds arising from sugar fragmentation. They include aldehydes (glycolaldehyde, glyceraldehyde, aldol), ketones (aceton, acetoin), and oxidized derivatives as in the case of levulinic acid which arises from the acid-catalyzed ring opening of the 5-hydroxymethylfurfural[108].

Notably, the chemical reactivity of these last compounds decreases from left to right.

2.2.d.5. AGEs and their reactive precursors.

AGE formation involves complex sequential and parallel reactions, whose precise mechanism is still debated even though at least two main pathways by which AGE can be generated are well established[109]. The first route involves irreversible rearrangements of the Amadori products following both oxidative and nonoxidative pathways. The second route involves condensation between the side-chain of lysine, cysteine and arginine residues, and di-carbonyls, which can be generated by enolization of Amadori products as well as by the direct degradation of aldoses and ketoses.

Through multiple mechanisms, a large variety of AGE structures can be generated, some of which conserve completely the sugar carbon skeleton even though condensed to form aromatic rings, as in the case of crossline, while other AGEs involve oxidative degradation with loss of sugar carbon atoms. The analysis of the valence of carbon atoms shows that oxidative reactions are not necessarily required in AGE formation and, in some cases, non-oxidative pathways can be involved depending also on the considered precursors. For this reason, the term glycation is preferable to glycoxidation, which would not be broadly applied to all AGEs.

Although the following sections are clearly focused on endogenously formed AGEs, the dietary intake of food derived AGEs may significantly contribute to the total body AGEs load[110;111].

Several AGEs have so far been identified in heated foods, and indeed preclinical and clinical studies have demonstrated that an elevated intake of thermally processed foods might induce diabetogenic and nephrotoxic effects, low-grade inflammation, enhance oxidative stress, and promote atherosclerosis[112].

Besides the AGEs which are also endogenously generated (e.g., carboxymethyllysine, pyrraline, pentosidine) [113;114], some adducts are typically found only in heated foods since they derive by thermal degradation of AGEs. A well-known example is represented by furosine(N6-(2-(2-Furanyl-2-oxoethyl))-L-lysine), which arises from the heating of fuctosyl lysine in weakly acid conditions[115].

Finally, di-carbonyls and AGEs can react with specific residues producing several nitrogen-, sulphur-, and oxygen-containing heterocyclic derivatives, which are potent aroma compounds. They include alkylpyrazines, oxazoles, oxazolines, tetrahydropyridine, pyrroline, thiazoles, thiazolines, and pyrazinones, which are generated at high temperature via Strecker degradation followed by decarboxylation and rearrangement reactions[116].

2.2.e. Glyoxal.

2.2.e.1. Exogenous and endogenous sources.

Glyoxal is the smallest dialdehyde and appears as a yellow liquid, which forms hydrates in water solution. The hydrates tend spontaneously to condense to yield oligomeric species, the exact structures of which remain unclear[117].

Sources of glyoxal can involve both exogenous and endogenous pathways. The former include dietary and environmental sources, while the latter include various metabolic and oxidative reactions all of which are able to induce cellular damage[118].

Environmental sources include all products arising from combustion processes such as cigarette smoke and vehicle exhaust, while detectable amounts of glyoxal are also found in soil, groundwater, seawater, and sediment[119].

With regard to endogenous production mechanisms, glyoxal can be essentially generated starting from sugars and lipids (plus their metabolites) [120]. Sugars can produce glyoxal through two major pathways. The first includes direct autoxidation reactions, which appear to be promoted by the presence of phosphates and transition metal ions, although the direct conversion of sugars in glyoxal can also involve retroaldol fragmentation[121;122].

The second pathway involves the Maillard reaction and occurs via Amadori products, which can be transformed into glyoxal by enolization as described above.

Although sugars are often seen as the main source, glyoxal can also arise from lipid peroxidation. Indeed, the nonenzymatic peroxidation of polyunsaturated fatty acids, such as linoleic and linolenic acids, generates peroxide intermediates, which then degrade to yield a variety of oxidative products including glyoxal[123]. Lastly, ascorbate can also spontaneously hydrolyze into glyoxal through an unknown mechanism[124]. Concerning the metabolic fate of glyoxal, the large majority is enzymatically converted in glycolate by GSH dependent glyoxalase system, which comprises two isozymes differing for tissue and subcellular localization[125]. When GSH is depleted, as happens in many oxidative-based disorders, other enzymes including aldehyde reductase, aldose reductase, carbonyl reductase, aldehyde dehydrogenase, and 2-oxoaldehyde dehydrogenase can contribute to the glyoxal metabolism[126].

Finally, several lines of evidence have revealed that glyoxal catabolism could be involved in oxalate formation as suggested, for example, by studies on diabetics showing that they have increased levels of both plasma glyoxal and urinary oxalate[127].

2.2.e.2. Glyoxal-derived AGE.

The remarkable activity of glyoxal is clearly evidenced by the observation that more than 90% of glyoxal present in biological matrices is covalently bound to Cys, Lys, and Arg residues thus having a key role in protein glycation[128;129].

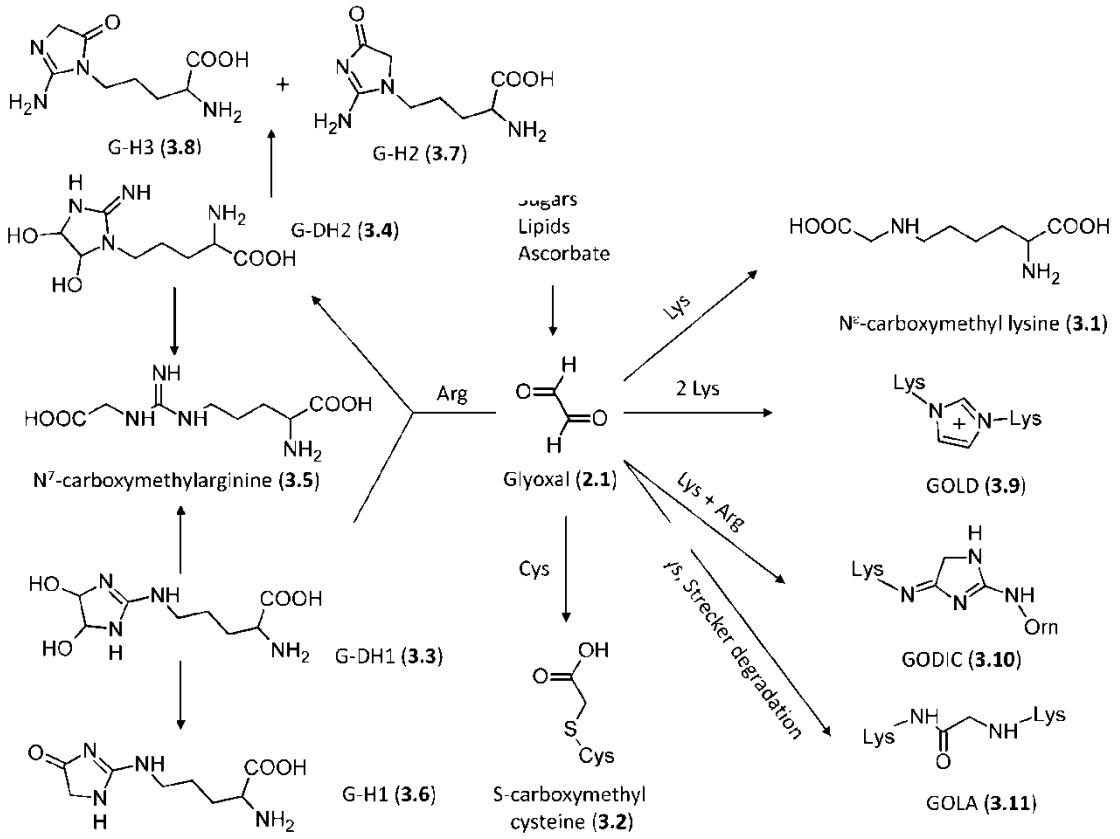

Fig 10. Schematized pathways for Glyoxal derived AGEs formation.

As depicted by Figure 10, glyoxal can react with the lysine side chain to yield N^{ε}-(carboxymethyl)lysine(CML) through an aldimine intermediate, and with the cysteine thiol group to give an irreversible end product, S-(carboxymethyl)cysteine(CMC), the formation of which involves a Cannizzaro-like rearrangement of the corresponding thioacetal intermediate[130]. Notably, the single modified CMC amino acid has long been known as a mucolytic agent, and has attracted recent interest in the long-term treatment of chronic obstructive pulmonary disease (COPD) for its capacity to decrease the adhesion of bacteria to the upper respiratory tract[131].

Fig 10 shows that the *in vivo* reactions between the arginine side chain and glyoxal are clearly more complex[132], since they involve the formation of two possible dihydroxyimidazolidine intermediates: G-DH1, N^{δ}-(3,4-dihydroxy-1-imidazolidin-2-yl) (ornithine) and its isomer G-DH2,

(5-(4,5-dihydroxy-2-imino-1-imidazolidinyl) (norvaline). Both intermediates can (1) open to give the N^7-(carboxymethyl) arginine(CMA)adduct [133] or (2) dehydrate to yield three different imidazolone derivatives, that is, N^{δ}-(5-hydro-4-imidazolon-2-yl) ornithine, G-H1, and its isomers 5-(2-amino-5-hydro-4-imidazolon-1-yl) norvaline G-H2and5-(2-amino-4-hydro-5-imidazolon-1-yl) norvaline, G-H3. Among the possible arginine adducts, the dihydroxyimidazolidines, despite acting as intermediates, are the most abundant followed by the imidazolones and CMA[133].

While considering that each protein residue possesses a specific reactivity depending on its microenvironment, comparison of the possible adducts of lysine and arginine residues shows that the latter are usually more abundant thus emphasizing the greater susceptibility of arginine residues in producing AGEs[134].

Due to its dicarbonyl structure, glyoxal can also react with two lysine or arginine residues yielding imidazol cross-linked adducts. As represented in Fig 10, glyoxal can react with two lysine residues giving the corresponding glyoxal–lysine dimer (GOLD, 6-{1-[(5S)-5-ammonio-6-oxido-6-oxohexyl]imidazolium-3-yl}-L-norleucine) whose mechanism of formation is common to the corresponding methylglyoxal containing dimer and involves an initial bis lysyl diimine intermediate, which reacts with a second glyoxal molecule through a Cannizzaro-type reaction, and, after dehydration, condenses to give the final imidazolium dimer[135].

The cross-linking reaction between arginine, lysine, and glyoxal gives the GODIC product (N6-(2-{[(4S)-4-ammonio-5-oxido-5-oxopentyl]amino}-3,5-dihydro-4H-imidazol-4-ylidene)-L-lysine).

Lastly, two lysine residues can react with glyoxal via Strecker degradation to yield the amide adduct, *GOLA* (N6-(2-{[(5S)-5-ammonio-6-oxido-6-oxohexyl] amino}-2-oxoethyl)-L-lysine) which can be derived also through oxidative fragmentation of the Amadori products and which appears to be favored with increased glyoxal concentrations[136;137].

2.2.e.3. Exogenous and endogenous sources.

Methylglyoxal, also called pyruvaldehyde or 2-oxopropanal (CH_3- CO–CHO or $C_3H_4O_2$), is a yellow liquid ubiquitous in living cells and therefore almost all foods contain methylglyoxal, the concentration of which is increased by processes such as cooking, fermentation, and prolonged storage[138].

In foods and beverages, the main sources of methylglyoxal are represented by sugars and lipids[139].

Sugars can generate methylglyoxal through retro-aldol reaction or auto-oxidative fragmentation and, although these processes are greatly favored by alkaline conditions, they can also occur during caramelization by the heating of mono-, oligo-, and polysaccharides[140;141].

Besides heating processes, also prolonged storage can degrade sugars to generate methylglyoxal through a process which is especially favored in foods with a high content of simple carbohydrates[142].

Regarding environmental sources and similarly, combustion processes can generate methylglyoxal, as in the case of cigarette smoke, which indeed is one of the major sources of air contamination by this toxic dicarbonyl compound[143].

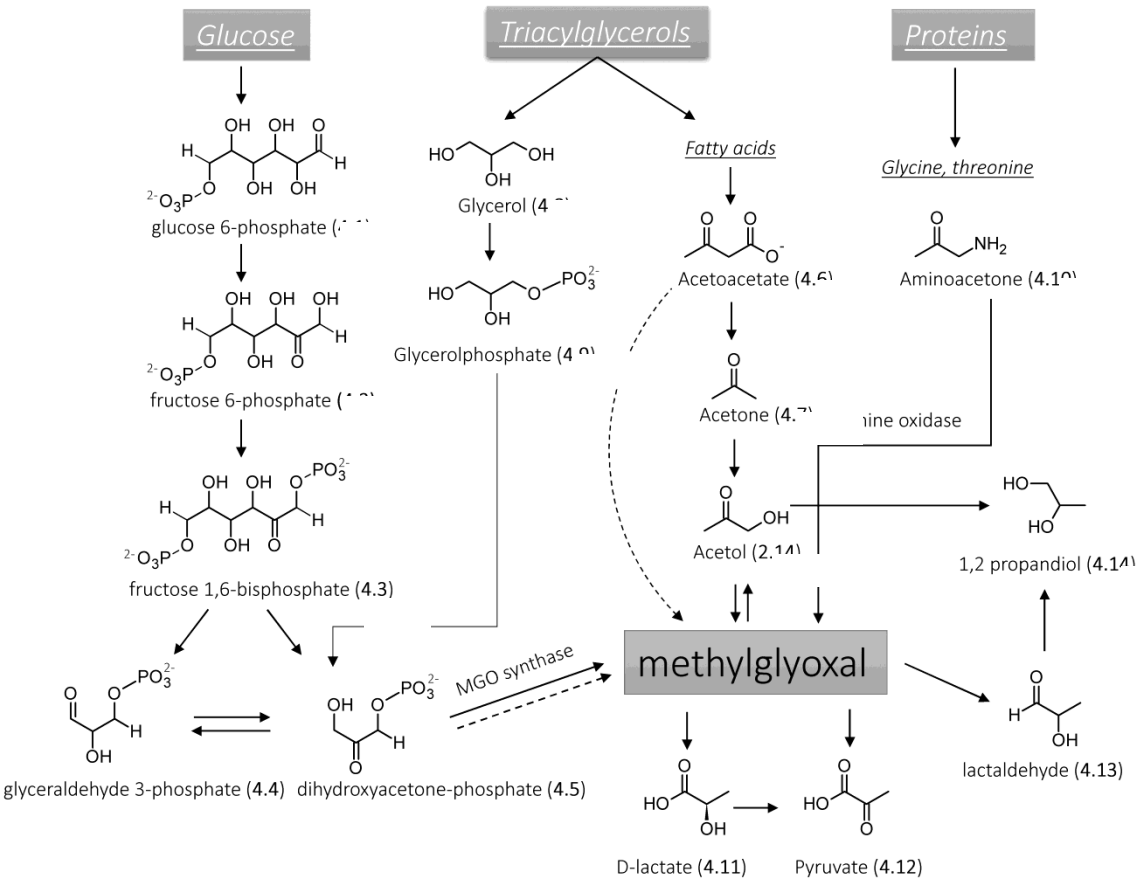

Fig 11. Schematized pathways for MGO formation and catabolism (dotted line indicate nonenzymatic MGO formation).

Endogenous sources of methylglyoxal involve manypathways that can be subdivided into enzymatic or nonenzymatic reactions[144;145]. As represented by Fig 11, the former includes reactions catalyzed by methylglyoxal synthase, cytochrome P450 2E1, myeloperoxidase, and amino oxidase, whereas the latter include the spontaneous decomposition of dihydroxyacetone-phosphate, the Maillard reaction, the oxidation of acetol, and lipid peroxidation[146]. In more detail, the main route leading to methylglyoxal involves the enzymatic or nonenzymatic degradation of the triose phosphate intermediates originating from the glycolytic processes[147]. The intermediates include glyceraldehyde 3-phosphate and dihydroxyacetone-phosphate, which are in equilibrium due to the activity of triosephosphate isomerase[148].

Thus, dihydroxyacetone-phosphate can yield methylglyoxal by both spontaneous nonenzymatic elimination of the phosphate group and by the effect of methylglyoxal synthase, an mammalian enzyme system[146;147].

Similarly to what was observed during food cooking, methylglyoxal can also derive via the Maillard reaction *in vivo* under physiological conditions.

Lipids can take part in the methylglyoxal generation through the acetone metabolism[149]. In detail, acetonederives from acetoacetate by myeloperoxidase activity and is converted to methylglyoxal by the cytochrome P450 2E1 via acetol as intermediate[150].

Particular pathophysiological conditions, such as ketosisand diabetic ketoacidosis, significantly increase methylglyoxal generation from acetone[151].

Yet again, glycerol resulting from triacylglycerol hydrolysis can be transformed into methylglyoxal through the glycerolphosphate intermediate which is produced by a specific glycerol kinase[152].

Threonine and glycine can also generate methylglyoxal through the aminoacetone intermediate[153]. This metabolic pathway is mediated by semi carbazide sensitive amine oxidase (SSAO) and appears to be exacerbated in low coenzyme A states[154;155].

Different enzymes contribute to methylglyoxal detoxification among which the glyoxalase system, aldose reductase (ALR), betaine aldehyde dehydrogenase, and2-oxoaldehyde dehydrogenase play a key role[156;157;158].

The above-described glyoxalase system catalyzes the biotransformation of methylglyoxal to D-lactate, which in turn is converted into pyruvate by D-lactate dehydrogenase. Aldose reductase (ALR2,AKR1B1) catalyzes the NADPH-dependent reduction of methylglyoxal into lactalde hyde or into acetol when GSH is depleted[159].

Nonspecific aldehyde dehydrogenases can recognize substrates only in their anhydrate forms and thus they cannot detoxify methylglyoxal and other α-oxoaldehydes, which are completely hydrated under physiological conditions[160]. However, methylglyoxalis substrate for betaine aldehyde dehydrogenase (ALDH9or E3) which indeed contributes to its detoxification[161].

Moreover, the missing activity of nonspecific aldehyde dehydrogenases is counterbalanced by the specific2-oxoaldehyde dehydrogenase (2-ODH) which catalyzes the NAD/NADPH-dependent oxidation of methylglyoxal into pyruvate. The enzyme also requires an activator: Vicinal aminoalcohols, aminothioles, and glycine were found to act as activators even though the physiological activator is still unknown[162].

2.2.e.4. Methylglyoxal-derived AGEs.

It has long been known that methylglyoxal is able to induce irreversible modifications in proteins under physiological conditions[163;164].

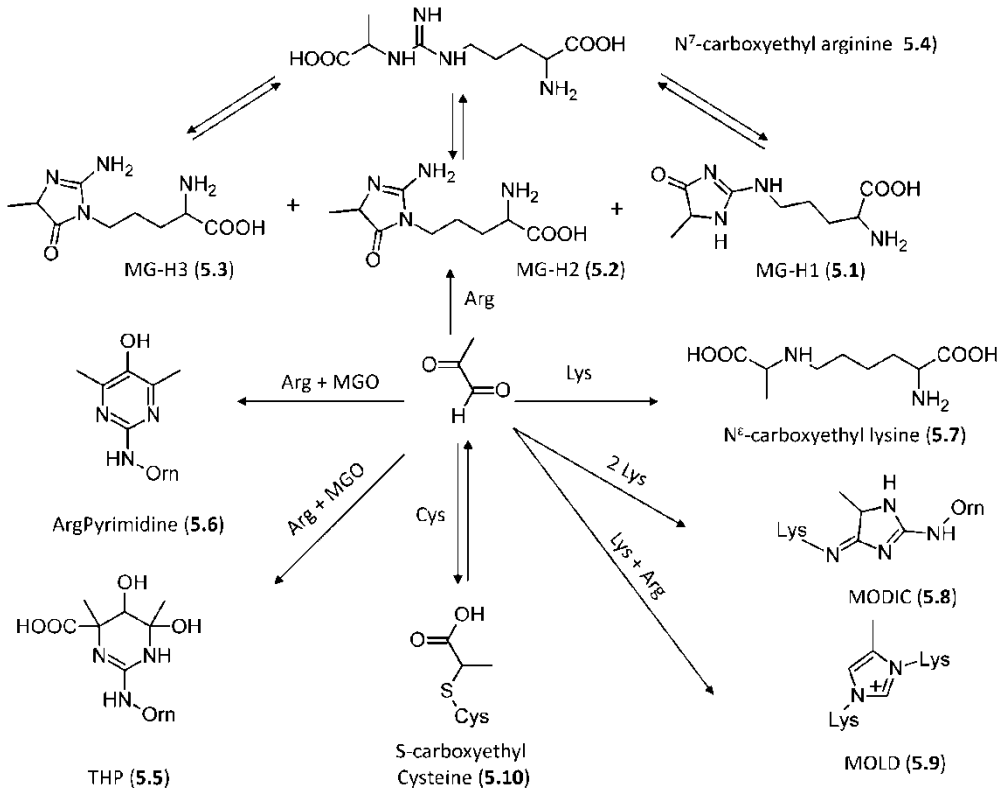

Fig 12. Major pathways for formation of the methylglyoxal-derived AGEs in vivo.

The formed adducts can be grouped into fluorescent and non fluorescent products. Specifically and as schematize by Fig 12, methylglyoxal reacts primarily with arginine residues yielding cyclic imidazolone adducts[165], whose formation mechanism involves firstly the condensation between a carbonyl group and the N^7 guanidino atom to give the corresponding carbinolamine which then cyclizes to form the diol intermediates and to yield the final adducts through two successive dehydrations[166].

Depending on the nitrogen atoms involved in the cyclization and on environmental pH value, three different adducts are possible, as represented in Figure x, namely N_δ-(5-methyl-4-imidazolon-2-yl)-

Lornithine (MG-H1), 2-amino-5-(2-amino-5-hydro-5-methyl-4-imidazolon-1-yl)pentanoic acid (MG-H2), 2-amino-5-(2-amino-4-hydro-4-methyl-5-imidazolon-1-yl)pentanoic acid (MG-H3).

These three imidazolone adducts are in equilibrium since they can open giving the carboxyethylarginine**(**CEA**)** adduct which in turn re-cyclizes allowing mutual interconversion between the imidazolone adducts[167].

Besides the mentioned ring opening, the imidazolone adducts can undergo other reactions as depicted by Figure 12. In more detail, they can add a second methylglyoxal molecule yielding either THP(N^{δ}-(4-carboxy-4,6-dimethyl-5,6-dihydroxy-1,4,5,6-tetrahydropyrimidine-2-yl)-L-ornithine) through an open intermediate [168] and a final re-cyclization reaction or argpyrimidine, (N^{δ}-(5-hydroxy-4,6-dimethylpyrimidine-2-yl)-l-ornithine), a fluorescent derivative via decarboxylation and dehydration[169].

Methylglyoxal can react with lysine residues generating the carboxylethyllysine(CEL) adduct through a mechanism, which involves an aldimine intermediate and brings to mind the already mentioned pathway for the formation of the nor-analogue carboxymethyl lysine[170].

As already seen for glyoxal, the aldimine intermediate can react with the arginine guanidine group yielding a cyclic intermediate that, after dehydration and rearrangement, produces the final cross-link imidazol MODIC adduct (2-ammonio-6-({2–[4-ammonio-5-oxido-5-oxopently)amino]-4-methyl-4,5-dihydro-1H-imidazol-5-ylidene}amino)hexanoate) with an overall mechanism almost identical to that described for GODIC formation[171;172].

Yet again, similarly to what was described for glyoxal, methylglyoxal can react with two lysine residues forming an initial diimine intermediate, which then adds a second methylglyoxal molecule and, via an intermolecular Cannizzaro-type reaction, yields the final imidazolium MOLD adduct (6{1-[(5S)-5-ammonio-6-oxido-6-oxohexyl]-4-methyl- imidazolium-3-yl}-L-norleucine) [173].

This cross-link reaction occurs more efficiently with methylglyoxal compared to glyoxal and this difference is in agreement with the proposed mechanism since the required fragmentation reaction is more favorable for methylglyoxal, due to increased relative stability of the leaving group[174].

Lastly, methylglyoxal can react with cysteine residues giving reversible hemithioacetal [166] and with tryptophan residues yielding βcarboline derivatives, a particularly common reaction during prolonged food storage[175;176].

2.3. The receptor for AGEs (RAGE) and its involvement in the inflammation.

Studies of the last decades have demonstrated that the oxidative stress of cells exposed to products of glycoxidation is partially due to the stimulation of specific receptors present on cell surface, namely RAGE.

Several lines of evidence have shown a key role of RAGE in many pathologic pathways and that it is involved in the inflammatory events involved in different pathological conditions such as atherosclerosis[177], severe diabetes complications[178], chronic inflammation[179], neurodegenerative disorders such as muscular dystrophy, alzheimer's , parkinson's[180].

In healthy animals and humans, the constitutive expression of RAGE in physiological conditions is very low in most cell types including smooth muscle cells, endothelial, and neurons and tissues. On the contrary, in different disease states but also during embryonic development, elevated levels of expression are observed afterwards the receptor engagement. Such changes in RAGE expression elicit concurrent increases in the expression of RAGE ligands, which themselves are also disease-associated[181].

As before mentioned the receptor expression in increased also during embryonic development suggesting that RAGE signaling has an important role during this growth phase[182;183].

Moreover, several lines of evidence suggest that RAGE is also involved in tissue homeostasis and regeneration/repair upon acute injury, and in resolution of inflammation highlighting the fact that the activation of the receptor not only has negative implications[184;185].

However AGEs accumulation and RAGE overexpression are enhanced in the presence of hyperglycemia and oxidative stress, typical characteristics of diabetes.

The final effect of RAGE axis hyper-activation includes endothelial dysfunction, activation of coagulation, and increase in activity of the renin-angiotensin system as a result ofthe trigger of an intracellular pathway ended by the release of many signal transduction that culminates in gene expression[186].

RAGE activation and the release of second messengers leads the onset of numerous diseases-correlated characterized primarily by inflammationsuch as diabetes and atherosclerosis that in turn lead to overexpression of RAGE[187].

RAGE-overexpressing diabetic in mice show in fact progressive glomerulosclerosis with renal dysfunction, compared with diabetic mice lacking of the RAGE transgene. Diabetic homozygous RAGE null mice fail to develop significantly increased mesangial matrix expansion or thickening of the glomerular basement membrane.

Taken together, these findings suggest that the activation of AGE–RAGE axis contributes to the expression of VEGF and enhanced attraction/activation of inflammatory cells in the diabetic glomerulus, thereby setting the stage for mesangial activation and TGF-beta production[188].

RAGE has also a pro-adipogenic function in senescent pre adipocytes by suppressing p53 function, which may contribute to aging-dependent adiposity by glycated, proteins derived from the diet and/or chronically dysregulated metabolic conditions such as hyperglycemia[189].

The receptor for advanced glycation end products (RAGE) is a multiligand transmembrane receptor member of the immunoglobulin (Ig) superfamily of cell surface receptors acting as a pattern recognition receptor, able to recognize a common pattern within its different ligands[190;191].

AGEs represent the first ligand of RAGE to be identified which derive from non-enzymatic glycation of proteins and lipids as above described[192].

RAGE is a pattern recognition receptor not only for ligands such as Advanced Glycation Endproducts (AGE) but also for members of S100 proteins family[193], the β-amyloid peptide and its fibrillar protein aggregates[194] and the high mobility group protein box-1 (HMGB1) [180].

RAGE ligands do not seem to share much similarity, nonetheless, all of them have a net negative charge at neutral pH: S100 proteins are very acidic, AGE modified proteins accumulate negative surface charge during their transformation by glycation and oxidation, amyloid β-peptide has a net negative charge, and amyloid fibrils expose a regular pattern of negative charges on their surface, while HMGB1 contains a highly acidic domain.

The second common feature is the tendency of most RAGE ligands to oligomerize[195]. The hydrophobic regions of the not-charged and lipophilic AGEs also contribute to the RAGE engagement. AGEs are negatively charged as the result of the Maillard formation reaction, by which reducing sugars or aldehydes. Modify arginines and lysines to produce glycated proteins, adding a net negative charge on the proteins at physiological pH. AGE binding to the V region of RAGE is initially facilitated by the ionic attraction between the positive charges of RAGE and the negative charges of AGE. The binding complex is then stabilized with hydrophobic interaction after conformational changes. However, it is not still well understood, which, among the different AGEs products so far identified, act as a binder of RAGE, nor whether ALEs, such as HNE or MDA protein adducts also bind RAGEs. In fact, with the exception of CML and CEL generated in a peptide or protein environment, most of the studies so far reported on RAGE activation by AGEs are based on not structurally resolved AGEs which are usually generated by incubating proteins (very often albumin) with glucose or fructose or with GO/MG resulting in the formation of a different set of glycoxidation products, spanning from either early glycation to cross-linking products, depending on the incubation times[196].

2.3.a. Structure of the receptor for Advanced Glycation Endproducts (RAGE).

RAGE is a type I transmembrane with a variable weight ranging between 45 and 55 kDa depending on the different states of glycosylation. Originally, the first isoform of RAGE have been isolated from the endothelium of lung cattle and this to mean that the protein is highly conserved and highly expressed in all mammals, including humans.

The Receptor for Advanced Glycation End Products is a transmembrane glycoprotein belonging to the receptor protein-activation immunoglobulins superfamily[197].

RAGE is encoded by a single gene (AGER) extended in humans for 3080 bp and located on chromosome 6, within the class III of the histocompatibility major complex and positioned in the proximity of the junction area with the class II.

Several transcription factors controlled the gene transcription of AGER gene, including the multipurpose factors as SP-1, AP-2, NF-kB and NF-IL6.

At different stage of development is possible to come up against different levels expression of RAGE that could be constitutive or inducible depending on the cell type and on the stage of development. In fact, while RAGE is constitutively expressed during the embryonic development, during the earliest stages of childhood its expression is inhibited with the exception of the lung in which AGER keeps the constitutive expression.

Furthermore, in other cell types, the constitutive expression RAGE is detectable only at very low levels in physiological conditions as for example in lymphocytes, endothelial cells, smooth muscle cells, phagocytesmononuclear cells, neurons, cardiac myocytes, hepatocytes, bipolar ganglion cells of the retina. The receptor expression can be triggered as a response to high levels of own ligands and/or following the activation of its transcription factor by specific signals inducing upregulation.

The Human-RAGE mature form is composed of 404 amino acids characterizing three different functional portions:

1) starting from the N-terminus it is possible to distinguish, in addition to the signal peptide of 22 amino acids, an extensive extracellular domain required for the ligand recognition and for the binding activity. The extracellular portion is in turn formed by three subdomains with a highly conserved sequence structurally similar to those of Immunoglobulin G and for this reason named according to the same nomenclature.

The first subdomain, domain V (variable), is appointed by the acronym of the letter V which indicates the own hypervariability, and also of two consequential C domains (constants) defined C1 and C2.

2) The single transmembrane portion is formed by an α-helix followed by a cytoplasmic domain characterized by extreme acidity essential for the signal transduction and distinguished by the loss of homologous to any tyrosine or serine / threonine kinases motif.

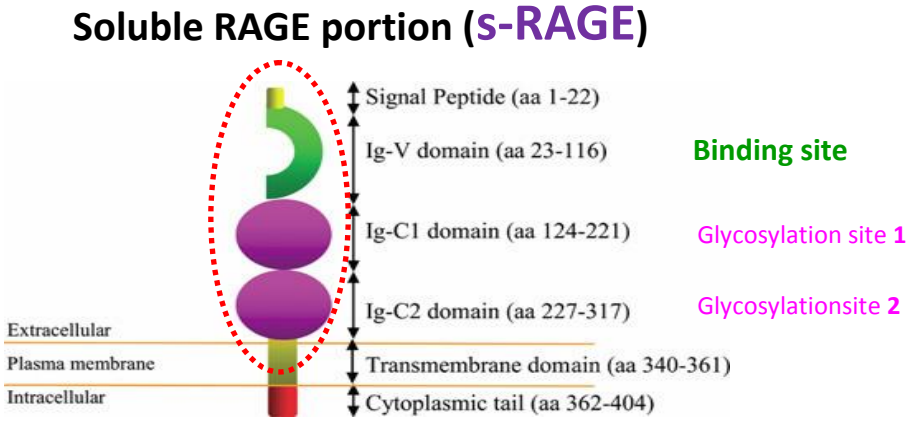

Fig 13. Schematic representation of the RAGE protein[198].

More recently it has been found that at the level of V domain there are two potential N-glycosylation sites located in correspondence of the asparagine residues 25 and 81.

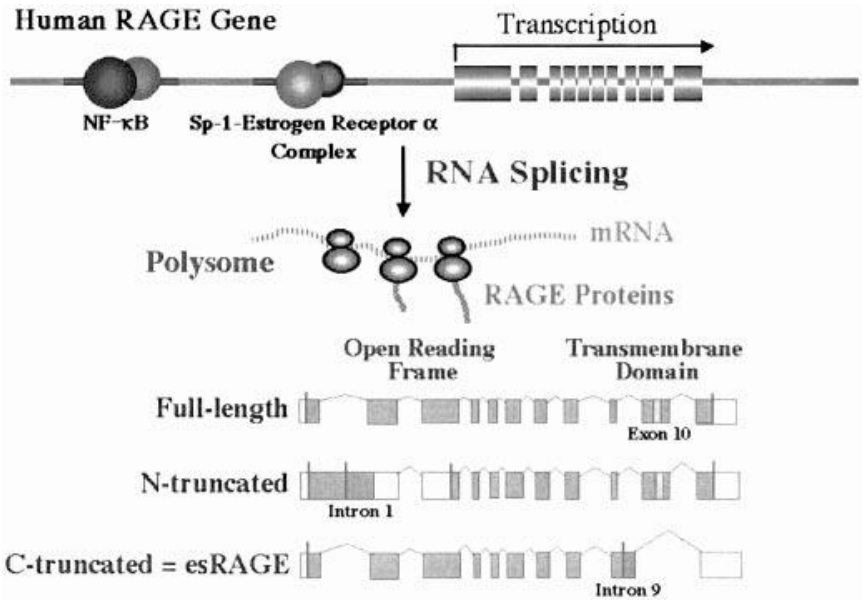

Fig 14. Regulation of human RAGE gene expression and the splice variants[199].

Three major variants were identified: the known full-length membrane bound form, a novel N-terminally truncated membrane-bound form, and a novel C-terminally truncated soluble form. The first main product is the full-length form anchored to the membrane, ant the other forms are represented by the soluble forms lacking of the transmembrane domain (TMD). The production of sRAGE (soluble RAGE portion) can be achieved either by proteolytic cutting (for instance through ADAM10 membrane metalloproteinases)

or through the alternative splicing phenomenon and in this case the corresponding product of the enzymatic activity takes the name of esRAGE (endogenous secretory RAGE).

The soluble isoforms include the extracellular domains but not the cytoplasmic and transmembrane portions. An additional product resulting to alternative splicing, appointed as DN-RAGE (dominant negative RAGE), is characterized by the lack of the intracellular region and hence, even if being expressed on the membrane, is not able to transduce an effective intracellular signal (Figure 14).

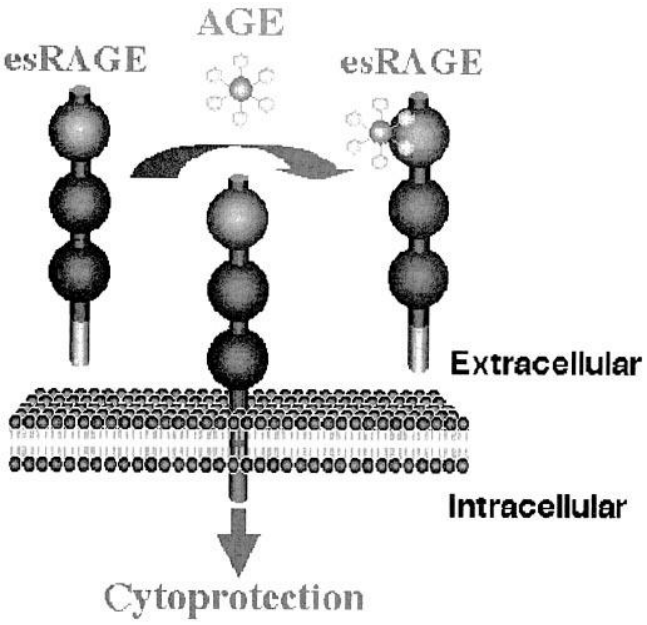

Fig 15. esRAGE[199].

2.3.b. The RAGE structure.

The circular dichroism and NMR were used to characterize the secondary and tertiary sRAGE structure[200]. Going into the details the soluble isoform of RAGE is mainly composed by β-sheet and random coil subunits. In particular, the V-domain, whose folding is homologous to that of the V-type domain of immunoglobulins, is composed of seven β-strands linked by six hairpin loops, which after assembly, form two complete β-sheets structures.

The disulfide bridge formation between the cysteine 38 and cysteine 99 allows the connection of the two β-sheets acquiescing the β-sandwich structure formation (Fig 16).

The secondary structure elements were labeled in agreement with the immunoglobulins nomenclature in use.

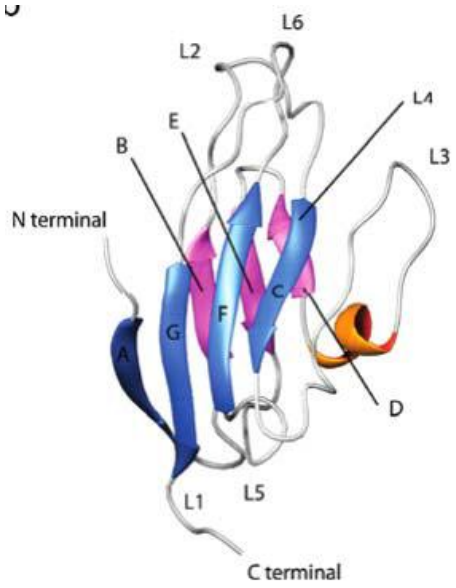

Fig 16. Computational representation of V domain . The α-helix is colored orange. The β-sheets are colored in blue (β-sheet 1) and purple (β-sheet 2) and named, by convention, A, B, C, D, E, F and G while the six loops are called L1, L2, L3, L4, L5 and L6 starting at the N-terminus[201].

Compared to the traditional structure of immunoglobulins, however, recent evidence from molecular modeling analysis have highlighted at the V domain level , two main differences with respect to the reference structure. The first one is represented by an α-helix structure located after L3 (reported in orange in Fig 16) included between Trp72-Ala76 residues and also by two β-strand lost, called C 'and C". In replacement of these structures take place another region characterize by a not defined secondary structure, but forming a long extended loop called L3. All these information permit to extensively describe the structural characteristics of soluble RAGE and are essential to

carry out a massive structure comprehension as well as to better understand the relationships between the three domains V, C1 and C2[201].
In addition to the above results, more detailed experiment based on proteolysis digestions and heteronuclear-NMR, permitted to conclude that the C2 domain shows the characteristics of an independent and well-folded stable domain, while V and C1 domains do not behave as independent domains, forming, instead, a single structural unit.
In particular the C1 domain appears to be the most unstable domain that in the absence of the V domain increase its instability, while the latter, albeit in limited manner, is more stable and even if isolated is better structured. The instability of the C1 domain mentioned above is due to three residues located within the domain which (Tyr150, Arg179, Phe186) that usually interact with V domain and when exposed to an aqueous solvent, make C1 particularly unstable. Actually, the structural configuration of the VC1 region which joins the domains V and C1 is supported by hydrogen-hydrogen bond and hydrophobic interactions bonds and hydrophobic interactions[202;203].
In more details, the aminoacid Gln119 located into the V domain forms a hydrogen bond with the C1 subunit through the residual Tyr150 that in turn interacts with Glu94[204] Regarding the hydrophobic interactions between C1 and V, several aminoacids belonging to the lateral chain are involved, such as the Pro215 of C1 tied whit Tyr118 of V and also through Tyr150 of C1 and Ile91 of V[204].
Consequently, compared to isolated forms, these two regions strongly are anchored to each other thus to be more resistant to the trypsin digestions and also more structurally homogeneous. The studies conducted by Dattilo[205] permitted to establish the dividend points of the various domains. The V-domain starts with the asparagine 25 and ends with the tyrosine 118 (important to notice that the heterologous expression of this region just involves the stretch from alanine 23 to proline 121), while the C1 domain starts from glycine 122 to tyrosine 222.
It can be assumed that the linker between V and C1 domains consist of only one tripeptide (Gln119-Pro121), because Tyr118 forms a single hydrogen bond which is involved in the β-strand of the V-domain and in addiction the Gly122 forms an equivalent type of bond with a β-strand of C1 domain. Instead, the link jointing C1 domain with C2 result to be longer with respect to the link between C1 and V, being formed by 14 residues (Ala123-Glu236). The greater length of this region is in agreement with the experimental observations which show high possibility of flexibility between C1 and C2. This observation further confirm confirms the complete independence of C1 and V with respect of C2.

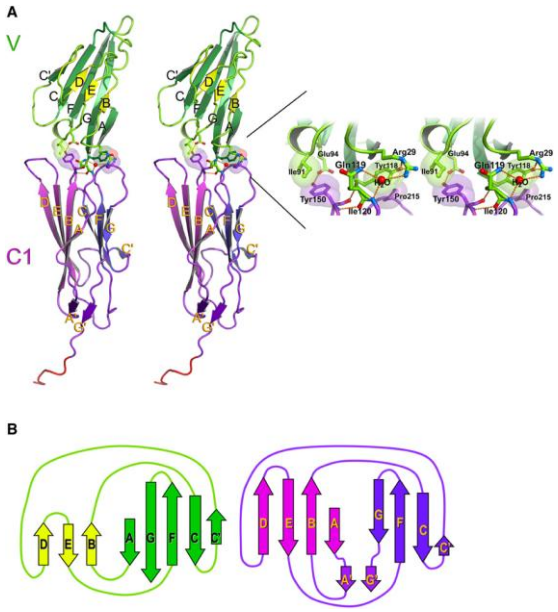

Fig 17. *Structure of the Tandem VC1 Domains of RAGE (A) Stereo ribbon diagram VC1 with the V domain in green and the C1 domain in magenta. The two Ig domains adopt a fixed orientation that is stabilized by hydrogen bonds and hydrophobic contacts.*
(B) Topology diagram of VC1 with the strands colored as in (A). The structure of the V domain shows it belongs to the I-set of Ig domains, whereas C1 remains in the C1 set. Note that a unique parallel b sheet is formed by strands A0 and G0 , which stabilizes the C terminus of the C1 domain[204].

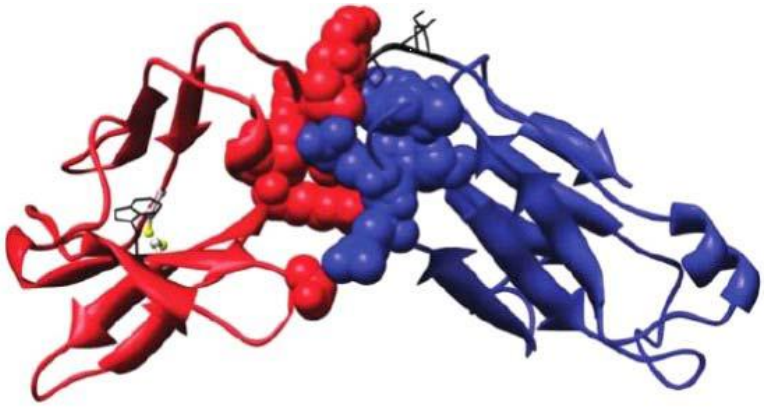

Fig 18. Computational representation of the VC1 domain model. The V domain(25-118) is red colored, the linker (119-121) in black and the C1 domain (122-222) in blue. The side chains of residues of the linker are shown in black, through "wire" representation. The side chains of the VresiduesandC1involved in the interaction between the two domains are represented in mode "fill space" using the respective colors of the belonging domains.

2.3.c. AGE-RAGE interaction.

The modular structure of sRAGE confirms that the three extracellular domains do not act independently (V, C1 and C2). Despite initial consideration, several lines of evidence have showed that during the course of evolution, the Ig-like protein superfamily has developed a scheme that includes the assembling of the domains. It follows that each domain cannot be considered as a single independent module, but as a multifunctional unit able to responding to a multiple ligands. RAGE, in fact, seems to adapt to this paradigm since the various ligands identifies so far appear to differently interact with the three individual components of the extracellular portion, although the most important link is regarded to be the V-domain[205].

The V domain is characterized by the presence of a large hydrophobic cavity between the loops L2, L3 and L4 and in addition, the molecular surface is entirely covered with positive charges. Within this area it is possible to distinguish an area in which these charges are condensed forming a cationic center. The residues involved are Lys39, Lys43, Lys44 e l' Arg48 on the loop L2, Lys52 on the C-strand, Arg98 on the strand F e Lys104, Arg107 and Lys110 on the loop L6[206].

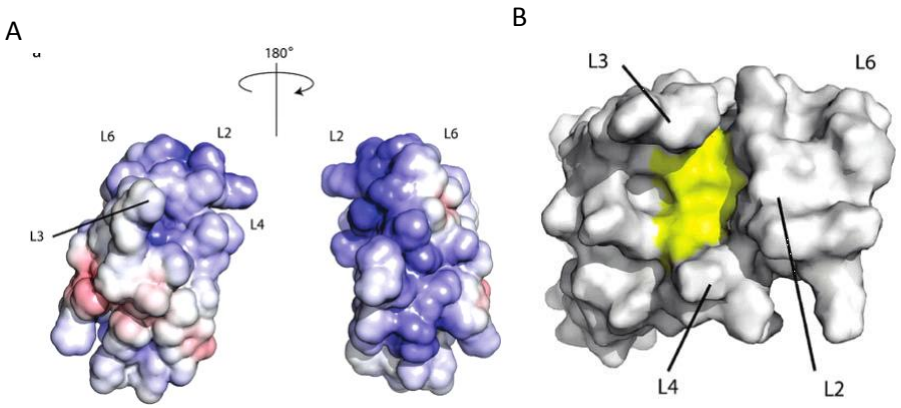

Fig 18. A Distribution of the electrostatic potential on the domain V surface(Blue color indicates a positive potential and red a negative one). .B Representation of the V domain molecular surface characterized by the hydrophobic cavity (yellow portion).

The positive charges located on the V-domain surface provide an essential support regarding the AGE-RAGE interactions. In fact, given that AGE are negatively charged due to the glycation of the positive residues of the protein, it can be deduced the essential role of the surface charges in the ligand-receptor interactions. Moreover, mutagenesis studies focused on the substitution of the nine basic amino acids forming the cationic center with the same number of alanines, allowed to classify these residues in two groups: the group 1 residues, in which the amino acids replacement brings

high reduction of the binding ability on AGE-RAGE axis (amino acids located around the hydrophobic cavity) and the group 2 in which the amino acids substitution (amino acids located on the opposite side with respect to the cavity) causes only a small effect on the binding capacity[206].

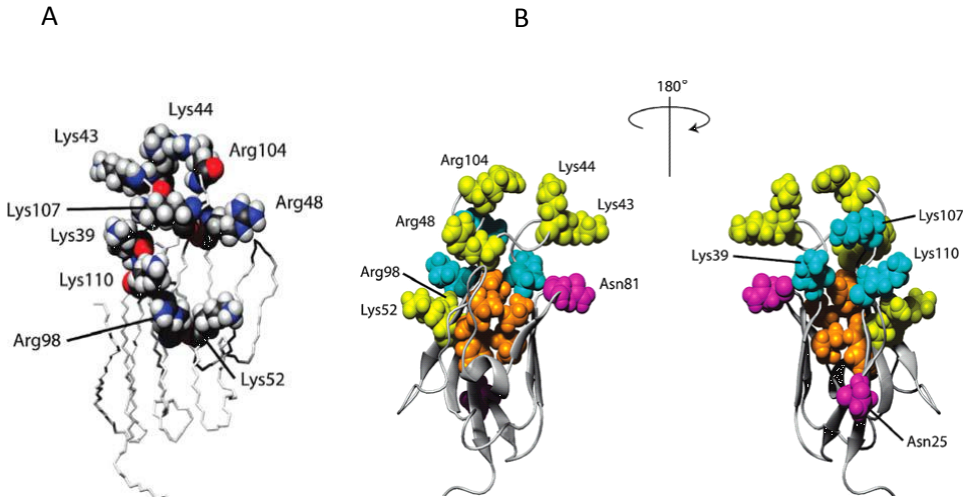

Fig 19. CPK representation of the replaced residues with alanine in site-specific mutagenesis studies. B Arrangement of the substituted residues with respect to the hydrophobic cavity. Residues belonging to the group 1 and2 are respectively yellow and blue colored. The side chain forming the hydrophobic cavity are showed in orange, while the two potential sites of N-glycosilation are pointed out in purple.

Moreover, considering the interaction BSA-AGE and Lys-AGE it has been observed that the complexes formed after receptor binding appear more stable with respect the AGE-RAGE interaction. Moreover, the complex between BSA-AGE and domain V requires the use of "extreme" condition, stronger in respect to those used to dissociate the Lys-AGE complex[206]. These results suggest AGEs bind to domain V not only through electrostatic interactions, but also through interactions of other types, including the hydrophobic ones. The hydrophobic cavity located closed to the basic residues (group 1) in the cationic center, forms a pocket essential in the AGE-RAGE interaction. The proposed mechanism consists of the following steps: as a first step, the ionic attraction between the positive charges of the receptor and the negative ones located on the ligands cause a narrowing of the pocket. Is the narrowing of the pocket (second step) that induces the formation of internal hydrophobic interactions which stabilize the complex[206]. This hypothesis supports the fact that the replacement of the basic residues belonging to the first group exhibit a drastic reduction in the formation of the complex. Thus, although several AGEs may have equal access to basic residues of the cationic center on the V domain, probably only those that interact with the amino acids of group 1 can easily move into the hydrophobic cavity, remaining trapped.

2.4. AGEs and ALEs: physiopathology and molecular strategies for their inhibition.

Considering the emerging deleterious role of aldehyde/protein adducts in several human diseases, as well as the complexity of reactions involved in ALEs, AGEs, and EAGLEs formation, the therapeutic approaches to inhibit and degrade AGEs and ALEs formation as well as RAGE activation should be mainly based on the efficient control of the sequence of events at the earliest possible stage.

By considering RCS,ALE/AGE-RAGE axis activation as drug-targets, different molecular strategies can be considered:

- Inhibition of the lipid-peroxidation chain-reaction (the primary source of RCS) by a direct (radical scavenging), indirect (metal-ion chelating) mechanism, or both. Regarding the radical-scavenging approach, different target radicals should be considered: 1) ROS, such as HO• and its radical precursor $O_2^{\bullet-}$ (through the formation of H_2O_2), which are responsible for initiating the lipid-peroxidation process, or 2) lipid radicals, which propagate the chain-reaction. The indirect antioxidant mechanism is based on targeting the pro-oxidant.

- Inactivation of the unstable intermediate products of sugar-degradation and lipid-peroxidation, whose breakdown leads to the formation of RCS.

- RCS entrapping and scavenging (forming nonreactive, non cytotoxic and with more hydrophilic characteristic reaction products).

- Induction of the enzymatic or non enzymatic degradation of accumulated ALEs and AGEs, and generally of undigested oxidation reaction products.

- Another therapeutic approach consist in inactivating RAGE . The receptor can be inactivated by high-molecular-weight substrates analogues, low-molecular-weight substrates analogues inhibitors, or anti-RAGE antibodies, neutralizing the receptor.

2.4.a. Antioxidants interventions.

The intervention strategy based on a direct radical-scavenging (antioxidant) approach that provides a first line of defence against free radicals, such as vitamin E and vitamin C, has failed to show beneficial effects in RCS-dependent diseases. There is limited evidence, from humans and animal models of atherosclerosis, that antioxidant therapy alone or given as diet supplementation can provide protection[207;208]. Several clinical trials have failed to provide a clear evidence for the efficacy of the antioxidant treatment in diabetic subjects[209] although a growing evidence shows that ROS and RCS production is increased in diabetes and that oxidative stress is associated with long-term complications. Some of these trials have been criticised in terms of insufficient dosing regimens or duration of antioxidant therapy, harmful interactions between the antioxidant compounds, or flaws in enrolling or excluding subjects.

Neurodegenerative disorders, including PD, AD, and ALS, clearly display increased indices of ROS and RCS (especially ACR and HNE) in affected brain regions. The antioxidant treatments have sorted different effects in these diseases: for example, whereas vitamin E has displayed some efficacy for the treatment of AD, it has not proved useful so far for the treatment of PD[210].

One possible limitation of the antioxidant therapy is that significant damage to macromolecules and tissue injury, which ultimately leads to cell death, will already have occurred by the time overt symptomatology of the disease is observed. Hence, antioxidant therapy, at best, can only rescue undamaged macromolecules and surviving cells, an effect that might not be sufficient to attenuate symptomatology[211].

2.4.a.1. Metal chelation intervention.

Several therapeutic approaches based on chelation of transition metals and in particular copper and iron have been recently proposed. It has been hypothesized that metal chelators could have dual inhibitory function on redox activity, restraining ROS generation as well as indirect inhibition of dialdeydes such as glyoxal. Furthermore, AGEs can be generated by oxidative and non-oxidative pathways, that appear to be accelerated by transition metals. Hence, chelation of transition metals inhibits several oxidative steps in glycoxidation.

This aspect results particularly important in neurodegenerative diseases where the dyshomeostasis of copper, iron and zinc has been detected, inducing for instance, metal hyper concentration, which can act as catalyst for detrimental oxidative reactions within the subtantia nigra in PD[212]. This might explain the growing interest in the development of metal chelation therapy as a potential promise for preventing or delaying disease progression in PD and other related neurodegenerative disorders.

2.4.b. RCS sequestering agents and AGEs detoxification compounds.

Among the molecular approaches up to now described, the most promising in terms of preventing or inhibiting carbonyl stress-related diseases is based on those compounds able to deactivate the intermediate products of lipid peroxidation or to scavenge RCS. Although several studies have already been conducted to develop AGE breakers, no study on compounds inducing enzymatic or non enzymatic degradation of ALEs has been reported, although this is an emerging field.

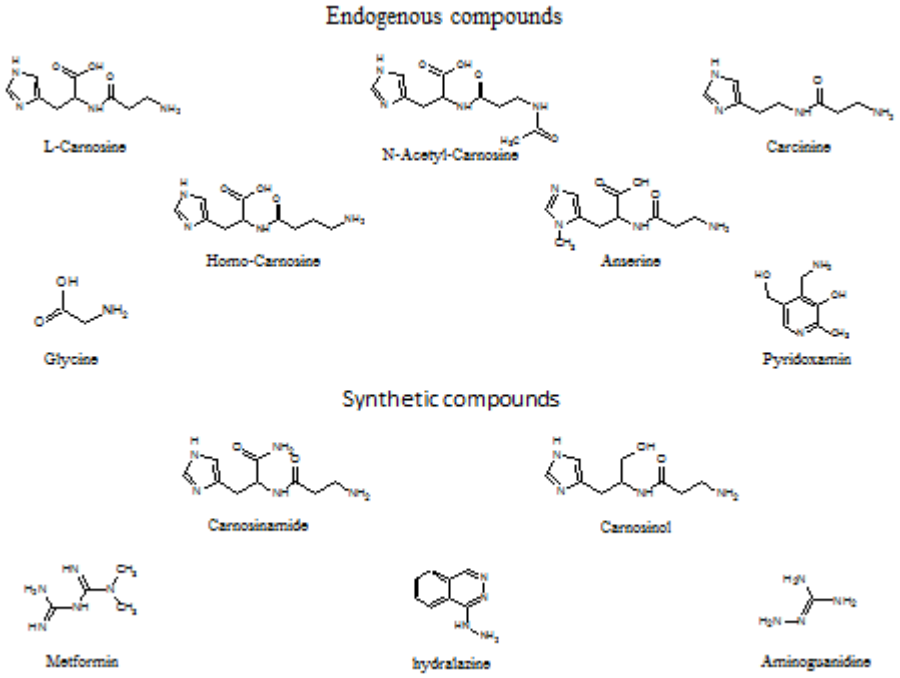

Fig 20. Endogenous and synthetic RCS sequestering agents.

Compounds described in the literature as RCS scavengers(small molecules able to detoxify RCS) can be divided into two groups:

Endogenous or naturally occurring compounds, such as the endogenous dipeptide L-carnosine (L-CAR) and derivatives such as N-acetil-carnosine (NA-CAR)and homocarnosine (H-CAR), anserine (ANS), the amino acid glycine (Gly), carcinine and finally the vitamer pyridoxamine (PYR).

Synthetic compounds initially described by their pharmacological or biological activities, such as the vasodilating antihypertensive drugs hydralazine (HYD), the iNOS inhibitor aminoguanidine (AG), and the oral hypoglycaemic agent metformin (MEF) , carnosinamide (CAR-NH2) and the carnosine derivative designed by us carnosinol (CAROH).

Originally, most of these compound were initially employed as pharmacological treatment for many diseases and only subsequently ware identified as RCS scavengers.

2.4.b.1. Pyridoxamin (PYR).

For instance PYR, which is a vitamer in the vitamin B_6 acting as an enzyme cofactor in a variety of metabolic processes[213], was initially employed as a novel and effective post-Amadori inhibitor. Then it was described as a RCS trapping agent able to inhibit the chemical modification of proteins acting mainly on Lys residues during lipid peroxidation reactions *in vitro* and during copper-catalysed oxidation of low-density lipoproteins[214].

2.4.b.2. Aminoguanidine (AG).

AG (hydrazinecarboximidamide) is considered to be a prototype scavenging agent of dicarbonyls, able to prevent the AGEs formation. In particular AG was found to detoxify α,β-dicarbonyls such as glyoxal (GO), methylglyoxal (MGO) and α,β-dicarbonyls, forming the corresponding 3-amino-1,2,4-triazine derivatives[215].

Moreover, AG is an efficient scavenger of α,β-unsaturated aldehydes when compared to nucleophilic amino acids (Cys, Lys, His). In particular AG react with HNE to yield a stable adduct through the well stabilized Schiff base[216]. AG was found to reduce tissue levels of AGEs in experimental models of diabetes as well as to retard the development of several pathologies including neuropathy, retinopathy, nephropathy and cataract[217;218;219]. However, due to its high reactivity , AG does not possess a suitable selectivity because it traps also physiological carbonyls[220] and physiological aldehydes. The lack of selectivity of aminoguanidine, causingvitamin B_6 deficiency, was the reason for its withdrawn form phase III clinical trials[221].

2.4.b.3. Hydralazine (HYD).

HYD (1-hydrazinylphthalazine) is a direct-acting smooth muscle relaxant characterizes by a nitrogen atom containing electron rich function represented by hydrazine group[222]. HyD was used to treat hypertension by acting as a vasodilator primarily in arteries and arterioles[223]. Furthermore HYD, was tested in the treatment of multiple sclerosis due tothe fact that this disease in characterized by an increase of acrolein that is effeciently quenched by HyD[224].

Up to now HYD is the lead compound of a series of hydrazine derivatives endowed by a marked scavenging ability toward both ALE and AGE precursors. However HYD as RCS scavenging compound is limited by two main issues: the lack of selectivity and the promiscuos activity.

Regarding the promiscuous activity HYD are well-known vasodilator agents which have been used for the treatment of essential hypertension since the 1950's.
As previously described for AG, also HYD, besides being characterizedby a promiscuos activity,it is also characterized by a lack of selectivity,since able to trapalso physiological carbonyls due to the hydrazine moietyable to form stable imine derivatives[220].

2.4.b.4. Metformin(MET).

MET (1,1-dimethylbiguadine) is an oral drug used as antidiabetic drug and belonging to the biguadine class. Nevertheless the adverse effects due to its use such as lactic acidosis and gastrointestinal complication, MET is considered the first-line drug of choice for the treatment of type 2 diabetes, in particular, in overweight and obese people and those with normal kidney function[225;226].
MET was also reported to decrease AGE formation in vitro, most likely by eliminating reactive carbonyl precursors[227;228]. In clinical studies, MET reduce levels of reactive dicarbonyls and AGEs[229] such an effect would contribute to the positive effects of MET beyond the benefits expected from the antihyperglycemic effect.

2.4.b.5. Carnosine (CAR) and the peptidomimetic derivative, Carnosinol (CAROH).

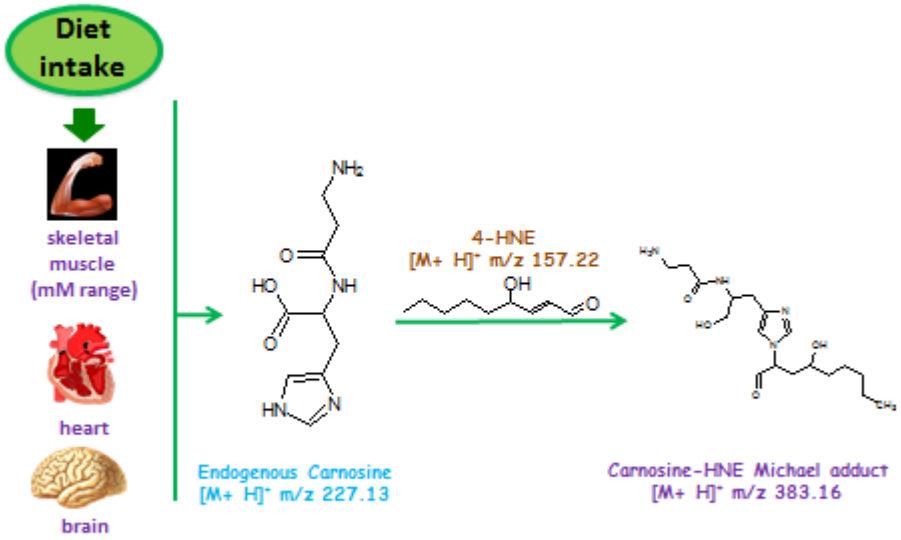

Fig 21. Chemical fate of suitable β-alanin-histidine CAR derived from dietary sources.

In humans, diet represent the main sources of carnosine (CAR) and histidine derivatives (HD), which are contained in significant amount in red and white meats. Dietary CAR is readily absorbed intact, primarily in the jejunum by a carrier-mediated transport system (hPEPT1) [230]. The enzymatic hydrolysis of the peptide bond represents the main metabolic fate of CAR, and in humans, it mainly occurs in the plasma by a specific serum hydrolase (carnosinase) that cleaves the b-alanine–histidine peptidic bond. The two hydrolyzed amino acids are then delivered to tissues and then again synthetized to carnosinein those tissues characterized by the presence of carnosine synthetase[231]. Hence CAR, which is also, an endogenous compound is present in millmolar concentration in some tissues as the skeletal muscle, heart and in some regions of the CNS and whose multi-step mechanism, mainly based on the ability of imidazole ring to yield Micheal addiction on the unsaturated imine intermediate, renders it markedly selective toward RCS[232;233].

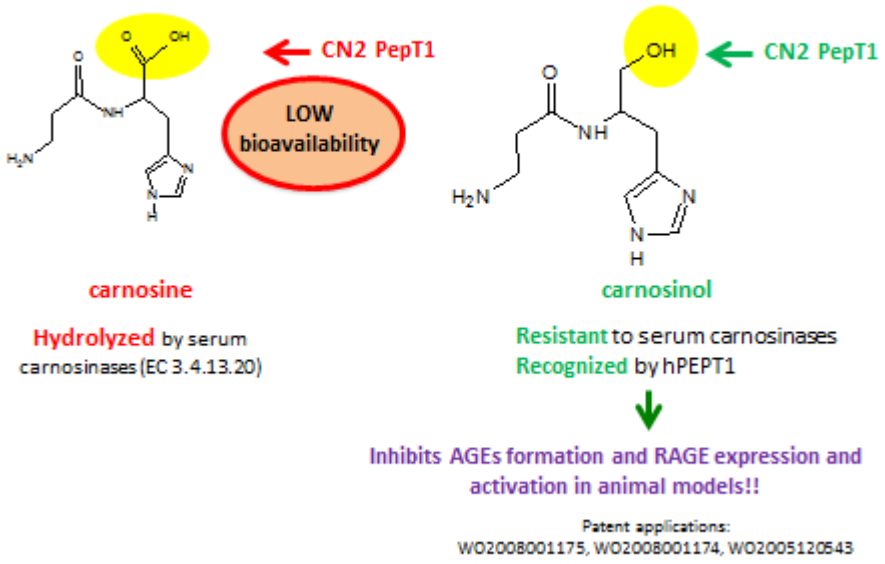

Fig. 22. Functional group of carnosine and carnosinol involved on endogenous recognition and serum carnosinases resistance.

Carnosine (β-Alanyl-L-histidine, L-CAR) is able to react with HNE through a two-step mechanism and based on the formation of a reversible Schiff base followed by an intra-molecular Michael adduction, leading to the formation of the Michael adduct stabilized in the hemiacetal form[234]. Such a concerted mechanism involving both the reactive centers of HNE to form a stable adduct makes the sequestering activity of L-CAR and derivatives more selective towards HNE and α,β-unsaturated aldehydes in respect to the other RCS. By using an HPLC method able to monitor the formation of HNE-quencher adducts together with a mass spectrometric approach able to measure the formation of covalent adducts of ubiquitin (protein target) induced by HNE incubation and its inhibition by the sequestering compounds, we recently compared the quenching activity of the known RCS scavengers which was as follows: carnosine>hydralazine>>aminoguandine>pyridoxamine.

By contrast when GO or MGO were used as carbonylating agent, L-CAR was the less efficient thus demonstrating that the RCS sequestering efficacy for this class of compounds is quite selective for α,β-unsaturated carbonyls[235].

Moreover, L-CAR was not found able to form stable adducts with the carbonyl function due to the fact its primary amino group is too basic (pK = 9.31) [236], since the stability of Schiff bases and the basicity of the primary amino group are inversely related. This lack of reactivity is very important because it avoids any reactivity towards endogenous and physiological carbonyl

compounds such as pyridoxal, so making carnosine a selective compound towards activated and cytotoxic RCS.

The HNE sequestering activity of L-CAR was then demonstrated in more complex biological matrices. Spiking HNE in rat skeletal muscle containing up to 5 mM of L-CAR and its methylated derivative (anserine) as endogenous components, resulted in the formation of the HNE Michael adducts of both the histidine compounds as determined by LC-ESI-MS/MS[234]. Moreover, the HNE Michael adducts of carnosine and anserine were both easily detected in the skeletal muscle undergoing a spontaneous oxidation and the amount of both the adducts significantly increased by depleting GSH thus demonstrating that carnosine participates in the endogenous detoxification of HNE together with GSH. Furthermore, carnosine-HNE Michal adduct and its metabolites, namely His-1,4-dihydroxynonane (His-DHN), His-4-hydroxynonanoic acid were identified by a mass spectrometric approach in the urine of obese Zucker rats and this is the first evidence of carnosine acting as a detoxifying agent of HNE in ex vivo conditions[237].

Very recently, the ability of L-CAR to act as an endogenous detoxifying agent of RCS was confirmed and extended in human samples. Conjugates of HNE with carnosine and metabolites such as His-HNE and His-DHN were detected by MS in human and mice urine although to a significantly lesser extent in respect to carnosine-acrolein conjugates[238].

However, the major limit of CAR and derivatives as RCS scavenger drug compound is the low bioavailability in humans due to the presence of human serum carnosinase that catalyses its hydrolysis. In order to overcome this limit our research group has designed a derivative in which the carboxylic group required for carnosinases recognition is replaced by an hydroxyl group . This compound, named carnosinol, was found to be bioavailable in rats thanks to the resistance to the endogenous carnosinases and to the fact that it is correctly recognised by carrier PEPT1. In addition, in animal models it has been found that carnosinol is able to inhibit AGEs formation and RAGE expression and activation nevertheless the reaction mechanisms through which these positive effects occur have not yet been elucidated.

2.4.c. Blocking AGEs-RAGE damaging axis.

RAGE is a pattern recognition receptor for many ligands such as AGEs, the s100 protein family, amyloid-β peptide. Several studies of the last decade have demonstrated that a significant part of cellular oxidative stress is due to the stimulation of this special receptor . The activation of RAGE by these compounds triggers an intracellular pathway resulting in a release of proinflammatory molecules. Hence, RAGE receptor has recently been identified as a possible drug target through its inactivation.

Different strategies has been developed in order block the AGEs-RAGE damaging axis. 1) Inactivating ligands, 2) low-molecular-weight antagonists of RAGE or 3) peptides and polysaccharides 4)downregulating RAGE expression 5) antibodies

2.4.c.1. Inactivating ligand.

The most abundant RAGE in blood and body fluids is represented by a population of shortened and soluble RAGE (sRAGE) which lacks the intracellular signalling domain. sRAGE competes with RAGE towards ligands since its affinity is maintained. However the sRAGE engagement with ligands does not trigger signal transduction an hence it does not evoke the inflammatory response. A possible molecular strategy is based on the protective role of sRAGE to block RAGE activation by competing with the ligands. sRAGE overexpression can be induced by small molecules. Interestingly, traditional cardiovascular drugs (statins, thiazolidinediones, ACE inhibitors) were found to be able to affect RAGE expression and circulating sRAGE levels in cardiovascular disease states characterized by enhanced RAGE activation, which may represent a novel mechanism of their action[239].

Introduction of recombinant sRAGE may be expected to become a new way of therapy to prevent the activation of RAGE by proinflammatory ligands. For instance, RAGE blockade by genetically engineered sRAGE was found to reduce vascular complications in a diabetic animal model[240].

2.4.c.2. Low-molecular-weight antagonists of RAGE.

Probably due to the complexity of the molecular interactions between AGEs-RAGE, only few studies on AGEs antagonists have so far been reported. Most of the studies on the rational design of RAGE antagonists have been carried out by considering amyloid β-peptide (Aβ) as a ligand [241]. Also in this case, the molecular interaction between Aβ and RAGE is not completely elucidated: by using fluorescence and MS it has been found that the major V-RAGE binding region of Aβ involves a highly hydrophobic stretch, $_{17}$LVFFAED$_{21}$ and a flanked negatively charged residue D$_{22}$E$_{23}$ at the C terminus. The interest of Aβ as RAGE ligand is due to the fact that the Aβ-RAGE axis is involved in the Alzheimer's disease and represents an emerging drug target. In particular, in brain endothelium, RAGE mediates the influx of circulating Aβ into the brain while in neurons, it mediates Aβ-induced oxidant stress and Aβ intraneuronal transport, causing mitochondrial dysfunction. Aβ-RAGE interaction also activates nuclear factor-κB (NF-κB) which plays a crucial role in various inflammatory responses.

Zlokovic et al. reported the structure of RAGE antagonist with a K_d in a nanomolar range. The lead compounds from the first screening shared common structural moieties such as a tertiary amide moiety substituted with a hydrophobic moiety and a monosubstitued aromatic group. A second-generation library of compounds was then synthesized on the basis of the chemical features retrieved from the first library. From the second library a compound coded as FPS-ZM1 was identified and characterized by a favorable inhibitory and dissociation constants (K_i/K_d= 0.66) as well as suitable pK and bioavailability properties. Structure-activity relationship studies revealed that the tertiary amide and aromatic rings are essential for activity and that the chlorine atom on the electron poor aromatic group may enhance its binding to the receptor [242]. Besides *in vitro* studies, FPS-ZM1 was also found effective in a mouse model of AD inhibiting the RAGE-mediated influx of circulating Aβ40 and Aβ42 into the brain, β-secretase activity, Aβ production and microglia activation and neuroinflammation, and normalizing cognitive performance and cerebral blood flow responses [241].

PF-04494700 (previously known as TTP488), an orally bioavailable low-molecular weight inhibitor of RAGE, which inhibits sRAGE from binding to RAGE ligands, S100B, amphoterin and CML has been developed as a potential treatment for AD (as well as diabetic nephropathy) and has reached a phase II clinical trial [243] but was discontinued in 2011 due to a poor efficacy. Feng et al. demonstrated that CM-1, a cell protecting agent able to prevent AGEs-induced endothelial dysfunction, blocks the interaction of MGH-1 with RAGE by acting as a competitive high-affinity antagonist, with IC_{50} values in the nanomolar range [244]. A screen of 50 compounds for their ability to prevent binding to RAGE of a fluorescent AGE-BSA derivative in RAGE-overexpressing

cells demonstrated that genistein inhibits this binding in a dose-dependent manner at nM concentrations [245]. Thiazolidinediones, calcium channel blockers, angiotensin-converting enzyme inhibitors, angiotensin II receptor blockers, and statins are reported to suppress RAGE expression [246].

There is no essential difference in the binding with RAGE between the macromolecular and monomeric AGE. Monomeric AGEs, which generally consist of an N-heterocyclic moiety and an amino acid moiety as a part of the AGE−protein linkage are thus attractive as a template for the design of novel small-molecule RAGE inhibitors. In particular, argpyrimidine 1, a monomeric AGE, was selected for design of the incipient RAGE inhibitors, because the key structure of argpyrimidine seems to provide more synthetic accessibility and more drug-like features compared with that of other monomeric AGEs. Using the approach of ligand-based drug design, the group of Suh discovered a novel series of 4,6-disubstituted 2-aminopyrimidines as RAGE inhibitors. In transgenic mouse models of AD, one of the 4,6-bis(4-chlorophenyl)pyrimidine analogs, significantly lowered the concentration of toxic soluble Aβ in the brain and improved cognitive function. Pyrimidine analogos binds directly to RAGE and thus inhibits the RAGE-Aβ interaction. A docking study predicted also the binding mode of the 4,6-bis(4-chlorophenyl)pyrimidine analogs to the RAGE V-domain [247].

2.4.c.3. Peptides and polysaccharides.

To date, Heparin and its derivatives are considered the most promising molecules acting as RAGE anatgonists. It was recently demonstrated that 2-O ,3-O -desulfated heparin (ODSH) is able to block the ligation of RAGE with a number of its important ligands, including CML-BSH, HMGB-1 and S100 protein family.
Heparin and derivatives compete with RAGE ligands due to the presence of electrostatic charges.
Low-molecular-weight heparin (LMWH) can also bind to RAGE and act as RAGE antagonists. LMWH treatment of mice showed preventive and therapeutic effects on albuminuria and increased glomerular cell number, mesangial expansion, and advanced glomerulosclerosis ina dose-dependent manner[248].

2.4.c.4. Downregulating RAGE expression.

Another important molecular strategy is based on downregulating RAGE expression. Drugs and natural substances have been found effective to downregulate RAGE expression as found for resveratrol[249].and for various plant extracts, of complex composition. Curcumin downregulated RAGE expression in rats with experimental diabetes[250]. Not only compounds derived from plants can downregulare RAGE expression, for instance alsoselenium supplementation in diet was found able to downregulated the expressions of both NFkB and RAGE is rats[251].

2.4.c.5. Antibodies.

The most common approach to prevent the deleterious outcomes of RAGE activation in in vitro system and animal models is the application of inactivating monoclonal or polyclonal antibodies against RAGE.One of the antibodies against RAGE, designated XT-M4, a rat-derived anti-mouse RAGE monoclonal antibody, binds the extracellular region of RAGE and inhibits the interaction of RAGE with multiple ligands. This antibody was found protective inthe mouse cecal ligation and puncture-induced (CLP) model of sepsis. As well the mouse derivative antibody, also the humanized XT-M4 antibody maintains all the inhibitory and binding properties[252].
The latest humanized anti-RAGE monoclonal antibody was found able to decrease mortality in mice and modulated expression of genes, especially those involved in the inflammatory response[253].

2.5 References.

[1] Schafer FQ, Buettner GR (2001). "Redox environment of the cell as viewed through the redox state of the glutathione disulfide/glutathione couple". *Free Radic. Biol. Med.*30 (11): 1191–212.).

[2] Lennon SV, Martin SJ, Cotter TG (1991). "Dose-dependent induction of apoptosis in human tumour cell lines by widely diverging stimuli". *Cell Prolif.*24 (2): 203–14).

[3] Patel VP, Chu CT. (2011). *"Nuclear transport, oxidative stress, and neurodegeneration.". Int J Clin Exp Pathol.*4 (3): 215–29.).

[4] Nunomura A, Castellani RJ, Zhu X, Moreira PI, Perry G, Smith MA. (2005). "Involvement of oxidative stress in Alzheimer disease". *J Neuropathol Exp Neurol.*65 (7): 631–41.

[5] Bošković M, Vovk T, Kores Plesničar B, Grabnar I. (2011). "Oxidative stress in schizophrenia". *Curr Neuropharmacol.*9 (2): 301–12.

[6] Ramalingam M, Kim SJ. (2012). "Reactive oxygen/nitrogen species and their functional correlations in neurodegenerative diseases". *Journal of Neural Transmission* 119.

[7] Vaziri ND. (2013). "Role of dyslipidemia in impairment of energy metabolism, oxidative stress, inflammation and cardiovascular disease in chronic kidney disease". *Clin Exp Nephrol*. [Epub ahead of print].

[8] Fukuda T, Kurano M, Fukumura K, Yasuda T, Iida H, Morita T, Yamamoto Y, Takano N, Komuro I, Nakajima T . (2013). "Cardiac rehabilitation increases exercise capacity with a reduction of oxidative stress". *Korean Circ J*.;43(7):481-7. doi: 10.4070/kcj.2013.43.7.481. [Epub ahead of print].

[9] Kotani K, Tsuzaki K, Taniguchi N, Sakane N. (2013 Apr). "Correlation between reactive oxygen metabolites & atherosclerotic risk factors in patients with type 2 diabetes mellitus". *Indian J Med* Res.;137(4):742-8.)

[10] Halliwell, Barry (2007). "Oxidative stress and cancer: have we moved forward?". *Biochem. J.*401 (1):
1–11).

[11] Thannickal VJ, Fanburg BL. (2000). "Reactive oxygen species in cell signaling. Am J Physiol Lung Cell". *Mol Physiol*;279:L1005-L1028.

[12] Beal MF. (2002). "Oxidatively modified proteins in aging and disease". *Free Radic Biol Med*;32:797-803.

[13] Finkel T. (1998). "Oxygen radicals and signaling". *Curr Opin Cell Biol;* **10**:248–253.

[14] Thannickal J, Fanburg L.,Am J. (2000). " Physiol Lung Cell Mol Physiol"; 279:L1005-L1028.

[15] Nathan C. (1992). "Nitric oxide as a secretory product of mammalian cells". *FASEB J***6**:3051–3064).

[16] Wilcox CS, Welch WJ, Murad F, Gross SS, Taylor G, Levi R, Schmidt HH. (1992). "Nitric oxide synthase in macula densa regulates glomerular capillary pressure". *Proc Natl Acad Sci USA***89**:11993–11997.

[17] Mac Micking JD, Nathan C, Hom G, Chartrain N, Fletcher DS, Trumbauer M, Stevens K, Xie QW, Sokol K, Hutchinson N, Chen H, Mudgett JS. (1995). "Altered responses to bacterial infection and endotoxic shock in mice lacking inducible nitric oxide synthase". *Cell***81**1995641650 (Corrigenda. *Cell* 81, following p. 1170.

[18] Thannickal J, Fanburg L. (2000). *Am J Physiol Lung Cell Mol Physiol*;279:L1005-L1028.

[19] Devasagayam, TPA; Tilak JC, Boloor KK, Sane Ketaki S, Ghaskadbi Saroj S, Lele RD (2004). "Free Radicals and Antioxidants in Human Health: Current Status and Future Prospects". *Journal of Association of Physicians of India (JAPI)***52**: 796.

[20] Han D, Williams E, Cadenas E. (2001). "Mitochondrial respiratory chain-dependent generation of superoxide anion and its release into the intermembrane space".*Free Radic Biol Med*;32:797-803.

[21] Li X, Fang P, Mai J, et al. (2013). "Targeting mitochondrial reactive oxygen species as novel therapy for inflammatory diseases and cancers". *J Hematol Oncol.***6** (19).

[22] Finkel T. (2004). "Oxygen free radicals and redox biology of organelles". *Histochem Cell Biol* 122:395-412.

[23] Valavanidis A, Vlachogianni T, Fiotakis K, Loridas S. (2013). "Pulmonary Oxidative Stress, Inflammation and Cancer: Respirable Particulate Matter, Fibrous Dusts and Ozone as Major Causes of Lung Carcinogenesis through Reactive Oxygen Species Mechanisms". *Int J Environ Res Public Health*;10(9):3886-907. doi: 10.3390/ijerph10093886.

[24] Dalle-Donne I, Giustarini D, Colombo R, Rossi R, Milzani A. (2003). "Protein carbonylation in human diseases". *Trends Mol Med*;9:169–176.

[25] Dalle-Donne I, Scaloni A, Butterfield DA. (2006). "Redox proteomics: From protein modifications to cellular dysfunction and disease". *New York: John Wiley & Sons*, Inc.;. p. 123–168.

[26] Aldini G, Dalle-Donne I, Facino RM, Milzani A, Carini M. (2007). "Intervention strategies to inhibit protein carbonylation by lipoxidation-derived reactive carbonyls!. *Med Res* Rev.Nov;27(6):817-68.

[27] Bartlett BS, Stadtman ER. (1997). "Protein oxidation in aging, disease, and oxidative stress". *J Biol Chem*;272: 20313–20316.13.

[28] Stadtman ER, Levine RL. (2003). "Free radical-mediated oxidation of free amino acids and amino acid residues in proteins". *Amino Acids*;25:207–218.

[29] Petersen DR, Doorn JA. (2004). “Reactions of 4-hydroxynonenal with proteins and cellular targets”. *Free Radic BiolMed*;37:937–945).

[30] Baynes JW. (1991). “The role of oxidative stress in the development of complications in diabetes”. *Diabetes*;40:405–412.

[31] Baynes JW, Thorpe SR. (1999). “Role of oxidative stress in diabetic complications: A new perspective on an old paradigm”. *Diabetes*;48:1–9.

[32] Ong WY, Lu XR, Hu CY, Halliwell B. (2000). “Distribution of hydroxynonenal-modified proteins in the kainatelesionedrat hippocampus: Evidence that hydroxynonenal formation precedes neuronal cell death”. *Free Radic Biol Med*;28:1214–1221. 19.

[33] Uchida K. (2000). “Role of reactive aldehyde in cardiovascular diseases”. *Free Radic BiolMed* ;28:1685–1696. 20.

[34] Poli G, Schaur J. (2000). “4-Hydroxynonenal in the pathomechanisms of oxidative stress”. *IUBMB Life*; 50:315–321. 21.

[35] Miyata T, vanYpersele de Strihou C, Kurokawa K, Baynes JW. (1999). “Alterations in nonenzymatic biochemistry in uremia: Origin and significance of ‘‘carbonyl stress’’ in long-term uremic complications”. *Kidney* Int;55:389–399.

[36] Baynes JW, Thorpe SR. (1999). “Role of oxidative stress in diabetic complications: A new perspective on an oldparadigm”. *Diabetes*;48:1–9.

[37] Uchida K. (2000). “Role of reactive aldehyde in cardiovascular diseases”. *Free Radic BiolMed* ;28:1685–1696.20.

[38] Carini M, Aldini G, Maffei Facino R. (2004). “Mass spectrometry for detection of 4-hydroxy-trans-2-nonenal(HNE) adducts with peptides and proteins”. *Mass Spectrom Rev*;23:281–305.

[39] Ong WY, Lu XR, Hu CY, Halliwell B. (2000). “Distribution of hydroxynonenal-modified proteins in the kainatelesionedrat hippocampus: Evidence that hydroxynonenal formation precedes neuronal cell death”. *FreeRadic Biol Med*;28:1214–1221.

[40] Pamplona R. (2011). “Advanced lipoxidation end-products” . *Chem Biol Interact*; 192: 14–20.

[41] Hermetter A , Kinnunen P , Spickett C . (2012). “Oxidized phospholipids. Their properties and interactions with proteins”. *Biochim Biophys Acta*; 1818 : 2373 – 2373.

[42] Bochkov VN, Oskolkova OV, Birukov KG, Levonen AL, Binder CJ, Stockl J. (2010). “Generation and biological activities of oxidized phospholipids”. *Antioxid Redox Signal*; 12 : 1009 – 1059.

[43] Hoff HF, O’Neil J, Wu ZP, Hoppe G, Salomon RL. (2003). “Phospholipid hydroxyalkenals - Biological and chemical properties of specific oxidized lipids present in atherosclerotic lesions”. . *Arterioscler Thromb Vasc Biol*; 23:275 – 282 .

[44] Shibata T, Kondo M, Osawa T, Shibata N, Kobayashi M, Uchida K . (2002). "15-deoxy-Delta(12,14)-prostaglandin J(2) – a prostaglandin D-2 metabolite generated during infl ammatory Processes". *J Biol Chem*;277:10459 – 10466 .

[45] Garzon B, Oeste CL, Diez-Dacal B, Perez-Sala D. (2011). "Proteomic studies on protein modifi cation by cyclopentenone prostaglandins: Expanding our view on electrophile actions". *J Proteomics* ;74:2243 – 2263.

[46] Schneider C, Porter NA, Brash AR. (2008). "Routes to 4-hydroxynonenal: fundamental issues in the mechanisms of lipid peroxidation". *J Biol Chem*;283:15539 – 15543.

[47] Long EK, Picklo MJ, Sr. (2010). "Trans-4-hydroxy-2-hexenal, a product of n-3 fatty acid peroxidation: Make some room HNE". *Free Radic Biol Med*; 49: 1– 8.

[48] Balogh LM, Atkins WM. (2011). " Interactions of glutathione transferases with 4-hydroxynonenal". *Drug Metab Rev*;43:165 – 178.

[49] Alary J, Gueraud F, Cravedi JP. (2003). "Fate of 4-hydroxynonenal *in vivo*: disposition and metabolic pathways". *Mol Aspects Med*;24:177 – 187.

[50] Esterbauer H, Schaur RJ, Zollner H. (1991). "Chemistry and biochemistry of 4-hydroxynonenal, malonaldehyde and related aldehydes". *Free Radic Biol Med*;1:81– 128.

[51] Zarkovic N. (2003). "4-hydroxynonenal as a bioactive marker of pathophysiological processes". *Mol Aspects Med*;24:281 – 291.

[52] Jaganjac M, Prah IO, Cipak A, Cindric M, Mrakovcic L,Tatzber F, et al . (2012). "Eff ects of bioreactive acrolein from automotive exhaust gases on human cells *in vitro*". *Environ Toxicol*;27:644 –
652.

[53] Abraham K, Andres S, Palavinskas R, Berg K , Appel KE, Lampen A. (2011). "Toxicology and risk assessment of acrolein in food". *Mol Nutr Food Res*;55:1277– 1290.

[54] Talhout R, Opperhuizen A, van Amsterdam JGC. (2006) " Sugars as tobacco ingredient: Effects on mainstream smoke composition". *Food Chem Toxicol*;44:1789– 1798.)

[55] Carmella SG, Chen M, Han S, Briggs A, Jensen J, Hatsukami DK, Hecht SS. (2009). "Eff ects of smoking cessation on eight urinary tobacco carcinogen and toxicant biomarkers". *Chem Res Toxicol*;22 : 734 – 741.

[56] Sengupta S, Chen H, Togawa T, DiBello PM, Majors AK, Büdy B, Ketterer ME, Jacobsen DW. (2001), *J Biol Chem*;276(32):30111-7.

[57] LoPachin RM, Gavin T, Petersen DR, Barber DS. (2009). "Molecular mechanisms of 4-hydroxy-2-nonenal and Acrolein Toxicity: Nucleophilic Targets and Adduct Formation". *Chem Res Toxicol*;22:1499 – 1508.

[58] Nadkarni DV, Sayre LM. (1995). "Structural defi nition of early lysine and histidine adduction chemistry of 4-hydroxynonenal". *Chem Res Toxicol*;8:284 – 291.

[59] Lin D, Lee HG, Liu Q, Perry G, Smith MA, Sayre LM. (2005). "4-oxo-2-nonenal is both more neurotoxic and more protein reactive than 4-hydroxy-2-nonenal". *Chem Res Toxicol*;18:1219 – 1231.

[60] Sayre LM, Lin D, Yuan Q, Zhu XC, Tang XX. (2006). "Protein adducts generated from products of lipid oxidation: Focus on HNE and ONE". *Drug Metab Rev*;38:651 – 675.

[61] Uchida K, Stadtman ER. (1993). "Covalent attachment of 4-hydroxynonenal to glyceraldehyde-3-phosphate dehydrogenase - a possible involvement of intramolecular and intermolecular cross-linking reaction". *J Biol Chem*;268:6388 – 6393.

[62] Lee SH, Blair IA. (2000). "Characterization of 4-oxo-2-nonenal as a novel product of lipid peroxidation". *Chem Res Toxicol*;13:698 – 702.

[63] Liu ZF, Minkler PE, Sayre LA. (2003). "Mass spectroscopic characterization of protein modifi cation by 4-Hydroxy-2-(E)-nonenal and 4-Oxo-2-(E)-nonenal". *Chem Res Toxicol*;16:901 – 91.

[64] Zhu XC, Sayre LM. (2007). "Mass spectrometric evidence for long lived protein adducts of 4-oxo-2-nonenal". *Redox Rep*;12:45 – 49.

[65] Aldini G, Dalle-Donne I, Facino RM, Milzani A, Carini M. (2007). "Intervention strategies to inhibit protein carbonylation by lipoxidation-derived reactive carbonyls". *Med Res Rev*;27:817 – 868.

[66] Uchida K. (1999). "Current status of acrolein as a lipid peroxidation product ". *Trends Cardiovasc Med*;9:109 – 113.

[67] Furuhata A, Ishii T, Kumazawa S, Yamada T, Nakayama T, Uchida K. (2003). "N-epsilon-(3-methylpyridinium) lysine, a major antigenic adduct generated in acrolein-modifi ed protein". *J Biol Chem*; 278:48658 – 48665.

[68] Maeshima T, Honda K, Chikazawa M, Shibata T, Kawai Y, Akagawa M, Uchida K. (2012). "Quantitative analysis of acrolein-specifi c adducts generated during lipid peroxidation-modifi cation of proteins *in vitro*: identifi cation of N-tau-(3-Propanal)histidine as the major adduct". *Chem Res Toxicol*;25:1384 – 1392.

[69] Del Rio D, Stewart AJ, Pellegrini N. (2005). "A review of recent studies on malondialdehyde as toxic molecule and biological marker of oxidative stress". *Nutr Metab Cardiovasc Dis*;15:316 – 328.

[70] Zhang M, Li W, Li T. (2011). "Generation and detection of levuglandins and isolevuglandins *in vitro* and *in vivo*". *Molecules*;16:5333 – 5348.

[71] Doureradjou P, Koner BC. (2008). "Effect of diff erent cooking vessels on heat induced lipid peroxidation of diff erent edible oils". *J Food Biochem*;32:740 – 751.

[72] Montuschi P, Barnes P, Jackson Roberts L. (2007). "Insights into oxidative stress: the isoprostanes". *Curr Med Chem*;14:703 – 717.

[73] Davies SS, Amarnath V, Roberts LJ. (2007). "Isoketals: highly reactive gamma-ketoaldehydes formed from the H-2-isoprostane pathway". *Chem Phys Lipids*;128:85 – 99.

[74] Esterbauer H, Schaur RJ, Zollner H. (1991). "Chemistry and biochemistry of 4-hydroxynonenal, malonaldehyde and related aldehydes". *Free Radic Biol Med*;11:81 – 128.

[75] Slatter DA, Bolton CH, Bailey AJ. (2000). "The importance of lipid derived malondialdehyde in diabetes mellitus". *Diabetologia*;43:550 – 557.

[76] Slatter DA, Murray M, Bailey AJ. (1998). "Formation of a dihydropyridine derivative as a potential cross-link derived from malondialdehyde in physiological systems". *Febs Lett*;421:180 – 184.

[77] Ishii T, Ito S, Kumazawa S, Sakurai T, Yamaguchi S, Mori T, et al . (2008). "Site-specific modification of positively-charged surfaces on human serum albumin by malondialdehyde". *Biochem Biophys Res Commun*;371:28 – 32.

[78] Ishii T, Kumazawa S, Sakurai T, Nakayama T, Uchida K. (2006). "Mass spectroscopic characterization of protein modification by malondialdehyde". *Chem Res Toxicol*;19:122 – 129.

[79] Slatter DA, Paul RG, Murray M, Bailey AJ. (1999). "Reactions of lipid-derived malondialdehyde with collagen". *J Biol Chem*;274:19661 – 19669.

[80] Slatter DA, Avery NC, Bailey AJ. (2004). "Identification of a new cross-link and unique histidine adduct from bovine serum albumin incubated with malondialdehyde". *J Biol Chem*;279:61 – 69.

[81] Maillard L. (1912). "Action des acides amine sur les sucres: formation des melano ̈ı dines par voie methodique". *CR Acad Sci*;154: 66 – 68.

[82] Hodge J. (1953). "Chemistry of browning reactions in model systems". *J Agric Food Chem*;1:928 – 943.

[83] Kunkel HG, Wallenius G. (1955). "New hemoglobin in normal adult blood". *Science*;122 - 288.

[84] Sell DR, Monnier VM. (2012). "Molecular basis of arterial stiffening: role of glycation- A mini-review". *Gerontology*;58:227 – 237.

[85] Del Turco S, Basta G. (2012). "An update on advanced glycation end products and atherosclerosis" . *Biofactors*;38:266 – 274.

[86] Goh S-Y, Cooper ME. (2008). "The role of advanced glycation end products in progression and complications of diabetes". *J Clin Endocrinol Metab*;93:1143 – 1152.

[87] Schalkwijk CG, Brouwers O, Stehouwer CDA. (2008). "Modulation of insulin action by advanced glycation endproducts: a new player in the field". *Horm Metab Res*;40:614 – 619.

[88] Hodge J. (1953). "Chemistry of browning reactions in model systems". *J Agric Food Chem*;1: 928 – 943.

[89] Amadori M . (1929). “The product of the condensation of glucose and p-phenetidine”. *Atti Reale Accad Nazl Lincei*;9:68 – 73.

[90] Isbell H, Frush H. (1958). “ Mutarotation, hydrolysis, and rearrangement reactions of glycosylamines”. J *Org Chem*;23:1309 – 1318.

[91] Morales FJ, Somoza V, Fogliano V. (2012). “Physiological relevance of dietary melanoidins”. *Amino Acids*;42:1097 – 1109.

[92] Zeitsch K. (2000). “The chemistry and technology of furfural and its many by-products”. *Amsterdam: Elsevier*; 48:227 – 237.

[93] Kurata T, Otsuka Y. (1998). “Amino-reductones. Formation mechanisms and structural characteristics”. *Adv Exp Med Biol*;434:269 – 276.

[94] Slaughter JC. (1999). “The naturally occurring furanones: formation and function from pheromone to food”. *Biol Rev Camb Philos Soc*;74:259 – 276.

[95] Davidek T, Robert F, Devaud S, Vera FA, Blank I. (2006). “Sugar fragmentation in the Maillard reaction cascade: Formation of short-chain carboxylic acids by a new oxidative alpha-dicarbonyl cleavage pathway. *J Agric Food Chem*;54:6677 – 6684.

[96] Cammerer B, Wedzicha BL, Kroh LW. (1999). “Nonenzymatic browning reactions of retro-aldol degradation products of carbohydrates”. *Eur Food Res Technol*;209:261– 265.

[97] Namiki M, Hayashi T. (1983). “A new mechanism of the Maillard reaction involving sugar fragmentation and free radical formation”. *Washington, DC: American Chemical Society*.

[98] Nursten H. (2005). “Maillard reaction: chemistry, biochemistry and implications. London: Royal Society of Chemistry.

[99] Bunn HF, Higgins PJ. (1981). “Reaction of monosaccharides with proteins: possible evolutionary significance”. Science;213:222 – 224.

[100] Laroque D, Inisan C, Berger C, Vouland E, Dufosse L, Guerard F. (2008). “Kinetic study on the Maillard reaction. Consideration of sugar reactivity”. *Food Chem*;111:1032 – 1042.

[101] Suarez G, Rajaram R, Oronsky AL, Gawinowicz MA. (1989). “Nonenzymatic glycation of bovine serum-albumin by fructose (fructation) - comparison with the maillard reaction initiated by glucose”. *J Biol Chem*;264:3674 – 3679.

[102] Dills WL. (1993). “Protein fructosylation – fructose and the maillard reaction”. *Am J Clin Nutr* ;58: S779 – S787.

[103] Rippe JM, Angelopoulos TJ. (2013). “Sucrose, high-fructose corn syrup, and fructose, their metabolism and potential health effects: what do we really know?”. *Adv Nutr*;4:236 – 245.

[104] Wang Y, Ho CT. (2008). “Formation of 2,5-dimethyl-4-hydroxy-3-(2H)-furanone through methylglyoxal: A Maillard reaction intermediate”. *J Agric Food Chem*;56:7405 – 7409.

[105] Noda Y, Peterson DG. (2007). "Structure-reactivity relationships of flavan-3-ols on product generation in aqueous glucose/glycine model systems". *J Agric Food Chem*;55:3686 – 3691.

[106] Nishibori S, Berhnard RA, Osawa T, Kawakishi S. (1998). "Volatile components formed from reaction of sugar and beta-alanine as a model system of cookie processing". *Adv Exp Med Biol*;434:255 – 267.

[107] Ota M, Kohmura M, Kawaguchi H. (2006). "Characterization of a new Maillard type reaction product generated by heating 1-deoxymaltulosyl-glycine in the presence of cysteine". *J Agric Food Chem*; 54:5127 – 513.

[108] Choudhary V, Mushrif SH, Ho C, Anderko A, Nikolakis V, Marinkovic NS, et al. (2013). "Insights into the interplay of Lewis and Bronsted acid catalysts in glucose and fructose conversion to 5-(hydroxymethyl)furfural and levulinic acid in aqueous media". *J Am Chem Soc*;135:3997 – 4006.

[109] Rabbani N, Thornalley PJ. (2012). "Glycation research in amino acids: a place to call home". *Amino Acids*;42:1087 – 1096.

[110] Luevano-Contreras C, Chapman-Novakofski K. (2010). "Dietary advanced glycation end products and aging". *Nutrients*;2:1247 – 1265.

[111] Van Lancker F, Adams A, De Kimpe N. (2011). "Chemical modifications of peptides and their impact on food properties". *Chem Rev*;111:7876 – 7903.

[112] Henle T. (2003). "AGEs in foods: do they play a role in uremia? ". *Kidney Int*;63:S145 – S147.

[113] Henle T, Schwarzenbolz U, Klostermeyer H. (1997). "Detection and quantification of pentosidine in foods". *Z Lebensm Unters Forsch*; 204: 95 – 98.

[114] Biemel KM, Buhler HP, Reihl O, Lederer MO. (2001). "Identification and quantitative evaluation of the lysine-arginine crosslinks GODIC, MODIC, DODIC, and glucosepan in foods". *Nahrung*;45:210 – 214.

[115] Erbersdobler HF, Somoza V. (2007). "Forty years of furosine – Forty years of using Maillard reaction products as indicators of the nutritional quality of foods". *Mol Nutr Food Res*;51:423 – 430.

[116] Wang Y, Ho CT. (2012). " Flavour chemistry of methylglyoxal and glyoxal". *Chem Soc Rev*;41: 4140 – 4149.

[117] Avzianova E, Brooks SD. (2013). "Raman spectroscopy of glyoxal oligomers in aqueous solutions". *Spectrochim Acta A MolBiomol Spectrosc*;101:40 – 48.

[118] Kielhorn J, Pohlenz-Michel C, Schmidt S. (2004). "Glyoxal. Concise international chemical assessment". Geneva, Switzerland: *World Health Organization*.

[119] Fu TM, Jacob DJ, Wittrock F, Burrows JP, Vrekoussis M, Henze DK. (2008). "Global budgets of atmospheric glyoxal and methylglyoxal, and implications for formation of secondary organic aerosols". *J Geophys Res Atmos*;113.

[120] O'Brien PJ, Siraki AG, Shangari N. (2005). "Aldehyde sources, metabolism, molecular toxicity mechanisms, and possible effects on human health". *Crit Rev Toxicol*;35:609 – 662.

[121] Manini P, La Pietra P, Panzella L, Napolitano A, d'Ischia M . (2006). "Glyoxal formation by Fenton-induced degradation of carbohydrates and related compounds". *Carbohydr Res*;34:1828 – 1833.

[122] Wellsknecht KJ, Zyzak DV, Litchfield JE, Thorpe SR, Baynes JW. (1995). "Mechanism of autoxidative glycosylation–identification of glyoxal and arabinose as intermediates in the autoxidative modification of proteins by glucose". *Biochemistry*;34:3702 – 3709.

[123] Yin HY, Porter NA. (2005). "New insights regarding the autoxidation of polyunsaturated fatty acids". *Antioxid Redox Signal*;7:170 – 184.

[124] Shangari N, O'Brien PJ. (2004). "The cytotoxic mechanism of glyoxal involves oxidative stress". *Biochem Pharmacol*;68:1433 – 1442.

[125] Mannervik B. (2008). "Molecular enzymology of the glyoxalase system". *Drug Metabol Drug Interact*;23:13 – 27.

[126] Shangari N, Bruce WR, Poon R, O ' Brien PJ. (2003). "Toxicity of glyoxals – role of oxidative stress, metabolic detoxification and thiamine deficiency". *Biochem Soc Trans*;31:1390 – 1393.

[127] Lange JN, Wood KD, Knight J, Assimos DG, Holmes RP. (2012). "Glyoxal formation and its role in endogenous oxalate synthesis". *Adv Urol*; 2012 : 819202.

[128] Thornalley PJ. (1995). "Advances in glyoxalase research. Glyoxalase expression in malignancy, anti-proliferative effects of methylglyoxal, glyoxalase I inhibitor diesters and S-Dlactoylglutathione, and methylglyoxal-modified protein binding and endocytosis by the advanced glycation end product receptor" *Crit Rev Oncol Hematol*;20: 99 – 128.

[129] Schwarzenbolz U, Henle T, Haebner R, Klostermeyer A. (1997). "On the reaction of glyoxal with proteins". *Z Lebensm Unters Forsch*;205:121 – 124.

[130] Zeng JM, Davies MJ. (2005). "Evidence for the formation of adducts and S-(carboxymethyl)cysteine on reaction of alpha-dicarbonyl compounds with thiol groups on amino acids, peptides, and proteins". *Chem Res Toxicol*;18:1232 – 1241.

[131] Mitchell SC, Steventon GB. (2012). "S-Carboxymethyl-L-cysteine". *Drug Metab Rev*; 44: 129 – 147.

[132] Glomb MA, Lang G. (2001). "Isolation and characterization of glyoxal-arginine modifications". *J Agric Food Chem*;49:1493 – 1501.

[133] Iijima K, Murata M, Takahara H, Irie S, Fujimoto D. (2000). "Identification of N(omega)-carboxymethylarginine as a novel acid-labile advanced glycation end product in collagen" . *Biochem J* ; 347 :23–27.

[134] Schwarzenbolz U, Mende S, Henle T. (2008). "Model studies on protein glycation: influence of cysteine on the reactivity of arginine and lysine residues toward glyoxal". *Ann N Y Acad Sci*;1126:248 – 252.

[135] Lederer MO, Klaiber RG. (1999). "Cross-linking of proteins by Maillard processes: characterization and detection of lysine arginine cross-links derived from glyoxal and methylglyoxal". *Bio org Med Chem*;
7:2499 – 2507.

[136] Adamiec J, Rossner J, Velisek J, Cejpek K, Savel J. (2001). "Minor Strecker degradation products of phenylalanine and phenylglycine". *Eur Food Res Technol*;212:135 – 140.

[137] Glomb MA , Pfahler C. (2001). "Amides are novel protein modifications formed by physiological sugars". *J Biol Chem*;276:41638 – 41647.

[138] Nemet I, Varga-Defterdarovic L. (2007). "Methylglyoxal-derived beta-carbolines formed from tryptophan and its derivates in the Maillard reaction". *Amino Acids*;32:291 – 293.

[139] Degen J, Hellwig M, Henle T. (2012). "1,2-dicarbonyl compounds invcommonly consumed foods". J *Agric Food Chem* 2012;60:7071 – 7079.

[140] HomokiFarkas P, Orsi F, Kroh LW. (1997). "Methylglyoxal determination from different carbohydrates during heat processing ". *Food Chem*;59:157 – 163.

[141] Hollnagel A, Kroh L. (1998). "Formation of α -dicarbonyl fragments from mono- and disaccharides under caramelization and Maillard reaction conditions". *Z Lebensm Unters Forsch*;207:50 – 54.)

[142] Kuntz S, Rudloff S, Ehl J, Bretzel RG, Kunz C. (2009). "Food derived carbonyl compounds affect basal and stimulated secretion of interleukin- 6 and -8 in Caco-2 cells". *Eur J Nutr*;48:499 – 503.

[143] Fujioka K, Shibamoto T. (2006). "Determination of toxic carbonyl compounds in cigarette smoke". *Environ Toxicol*;21:47 – 54.

[144] Beisswenger PJ, Howell SK, Nelson RG, Mauer M, Szwergold BS. (2003). "alpha-oxoaldehyde metabolism and diabetic complications". *Biochem Soc Trans*;31:1358 – 1363.

[145] Kalapos MP. (1999). " Methylglyoxal in living organisms – Chemistry, biochemistry, toxicology and biological implications". *Toxicol Lett*;110:145 – 175.

[146] Kalapos MP. (2008). "Methylglyoxal and glucose metabolism: a historical perspective and future avenues for research". *Drug Metabol Drug Interact*;23:69 – 91.

[147] Kalapos MP. (1999). "Methylglyoxal in living organisms – Chemistry, biochemistry, toxicology and biological implications". *Toxicol Lett*;110:145 – 175.

[148] Richard JP. (1993). "Mechanism for the formation of methylglyoxal from triosephosphates. Biochem Soc Trans";21:549 – 553.

[149] Dhar A, Desai K, Kazachmov M, Yu P , Wu LY. (2008). "Methylglyoxal production in vascular smooth muscle cells from different metabolic precursors". *Metabolism*;57:1211 – 1220.

[150] Bondoc FY, Bao ZP, Hu WY, Gonzalez FJ, Wang YY, Yang CS, Hong JY. (1999). "Acetone catabolism by cytochrome P450 2E1: studies with CYP2E1-null mice". *Biochem Pharmacol*;58: 461 – 463.

[151] Turk Z, Nemet I, Varga-Defteardarovic L, Car N. (2006). "Elevated level of methylglyoxal during diabetic ketoacidosis and its recovery phase". *Diabetes Metab*;32:176 – 180.

[152] Jung JY, Yun HS, Lee J, Oh MK. (2011). "Production of 1,2-Propanediol from Glycerol in Saccharomyces cerevisiae". *J Microbiol Biotechnol*;21:846 – 853.

[153] Bechara EJH, Dutra F, Cardoso VES, Sartori A, Olympio KPK, Penatti CAA, et al. (20079. 2The dual face of endogenous alpha-aminoketones: Pro-oxidizing metabolic weapons". *Comp Biochem Physiol C Toxicol Pharmacol*;146:88 – 110.

[154] Callingham BA, Crosbie AE, Rous BA. (1995). "Some aspects of the pathophysiology of semicarbazide-sensitive amine oxidase enzymes". *Prog Brain Res*;106:305 – 321.

[155] Lyles GA. (1996). " Mammalian plasma and tissue-bound semicarbazide-sensitive amine oxidases: Biochemical, pharmacological and toxicological aspects". *Int J Biochem Cell Biol*;28:259 – 274.

[156] Vander Jagt DL, Hunsaker LA. (2003). "Methylglyoxal metabolism and diabetic complications: roles of aldose reductase, glyoxalase-I, betaine aldehyde dehydrogenase and 2-oxoaldehyde dehydrogenase". *Chem Biol Interact*;143 – 144:341 – 351.

[157] Vander Jagt DL. (2008). "Methylglyoxal, diabetes mellitus and diabetic complications". *Drug Metabol Drug Interact*;23:93 – 124.

[158] Yang K, Qiang D, Delaney S, Mehta R, Bruce WR, O'Brien PJ. (2011). "Differences in glyoxal and methylglyoxal metabolism determine cellular susceptibility to protein carbonylation and cytotoxicity". *Chem Biol Interact*;191:322– 329.

[159] Vedantham S, Ananthakrishnan R, Schmidt AM, Ramasamy R. (2012). "Aldose reductase, oxidative stress and diabetic cardiovascular complications". *Cardiovasc Hematol Agents Med Chem*;10:234 – 240.

[160] Marchitti SA, Brocker C, Stagos D, Vasiliou V. (2008). "Non-P450 aldehyde oxidizing enzymes: the aldehyde dehydrogenase superfamily". *Expert Opin Drug Metab Toxicol*;4: 697 – 720.

[161] Munoz-Clares RA, Diaz-Sanchez AG, Gonzalez-Segura L, Montiel C. (2010). "Kinetic and structural features of betaine aldehyde dehydrogenases: Mechanistic and regulatory implications". *Arch Biochem Biophys*;493:71 – 81.

[162] Dunkerton J, James SP. (1975). "Purification of 2-oxoaldehyde dehydrogenase and its dependence on unusual amines". *Biochem J*;149:609 – 617.

[163] Degenhardt TP, Thorpe SR, Baynes JW. (1988). "Chemical modification of proteins by methylglyoxal". *Cell Mol Biol (Noisyle-grand)*;44:1139 – 1145.

[164] Westwood ME, Thornalley PJ. (1995). Molecular characteristics of methylglyoxal-modified bovine and human serum albumins–comparison with glucose-derived advanced glycation end product-modified serum albumins". *J Protein Chem*;14:359 – 372.

[165] Henle T, Walter AW, Haessner R, Klostermeyer H. (1994). "Detection and identification of a protein-bound imidazolone resulting from the reaction of arginine residues and methylglyoxal". *Z Lebensm Unters Forsch*;199:55 – 58.

[166] Lo TWC, Westwood ME, McLellan AC, Selwood T, Thornalley PJ. (1994). "Binding and modification of proteins by methylglyoxal under physiological conditions – a kinetic and mechanistic study with n-alpha-acetylarginine, n-alphaacetylcysteine, and n-alpha-acetyllysine, and bovine serum albumin". *J Biol Chem*;269:32299 – 32305.

[167] Klopfer A, Spanneberg R, Glomb MA. (2011). "Formation of arginine modifications in a model system of N-alpha-tert- Butoxycarbonyl (Boc)-Arginine with methylglyoxal". *J Agric Food Chem*;59:394 – 401.

[168] Oya T, Hattori N, Mizuno Y, Miyata S, Maeda S, Osawa T, Uchida K. (1999). "Methylglyoxal modification of protein – Chemical and immunochemical characterization of methylglyoxalarginine adducts. *J Biol Chem*;274:18492 – 18502.

[169] Shipanova IN, Glomb MA, Nagaraj RH. (1997). "Protein modification by methylglyoxal: Chemical nature and synthetic mechanism of a major fluorescent adduct". *Arch Biochem Biophys*;344:29 – 36.

[170] Ahmed MU, Brinkmann Frye E, Degenhardt TP, Thorpe SR, Baynes JW. (1997). "N-epsilon-(carboxyethyl)lysine, a product of the chemical modification of proteins by methylglyoxal, increases with age in human lens proteins". *Biochem J*;324:565 – 570.

[171] Lederer MO, Klaiber RG. (1999). "Cross-linking of proteins by Maillard processes: characterization and detection of lysinearginine cross-links derived from glyoxal and methylglyoxal". *Bioorg Med Chem*;7:2499 – 2507.

[172] Nasiri R, Field MJ, Zahedi M, Moosavi-Movahedi AA. (2011). "Cross-linking mechanisms of arginine and lysine with α, β-dicarbonyl compounds in aqueous solution". *J Phys Chem A*;115:13542 –13555.

[173] Nagaraj RH, Shipanova IN, Faust FM. (1996). "Protein cross-linking by the Maillard reaction – Isolation, characterization, and in vivo detection of a lysine-lysine cross-link derived from methylglyoxal". *J Biol Chem*;271:19338 – 19345.

[174] Meade SJ, Miller AG, Gerrard JA. (2003). "The role of dicarbonyl compounds in non-enzymatic crosslinking: a structureactivity study". *Bioorg Med Chem*;11:853 – 862.

[175] Nemet I, Varga-Defterdarovic L. (2007). "Methylglyoxal-derived beta-carbolines formed from tryptophan and its derivates in the Maillard reaction". *Amino Acids*;32:291 – 293.

[176] Nemet I, Varga-Defterdarovic L. (2008). "The role of methylglyoxal in the non-enzymatic conversion of tryptophan, its methyl ester and tryptamine to 1-acetyl-beta-carbolines". *Bioorg Med Chem*; 16:4551 – 4562.

[177] Park L. et al. (1998). " Suppression of accelerated diabetic atherosclerosis by the soluble receptor for advanced glycation endproducts". *Nat. Med*.;4,1025 – 1031.

[178] Bierhaus A and Nawroth PP. (2009). "Multiple levels of regulation determine the role of the receptor for AGE (RAGE) as common soil in inflammation, immune responses and diabetes mellitus and its complications". *Diabetologia*;52,2251 – 2263.

[179] Hofmann MA, et al. (1999). "RAGE mediates a novel proinflammatory axis: a central cell surface receptor for S100/calgranulin polypeptides". *Cell*;97,889 – 901.

[180] Taguchi A. et al. (2000). "Blockade of RAGE-amphoterin signalling suppresses tumour growth and metastases". *Nature*;405,354 – 360.

[181] Fritz G. (2012). "RAGE: a single receptor fits multiple ligands". *Trend in Biochimical Sciences*;36, 625 – 632.

[182] Ramasamy R, Yan SF, Schmidt AM. (2012). The diverse ligand repertoire of the receptor for advanced glycation end products and pathways to the complications of diabetes". *Vascul Pharmacol*;57: 160 – 167.

[183] Stogsdill JA, Stogsdill MP, Porter JL, Hancock JM, Robinson AB, Reynolds PR. (2012). "Embryonic overexpression of receptors for advanced glycation end-products by alveolar epithelium induces an imbalance between proliferation and apoptosis". *Am J Respir Cell Mol Biol*;47:60 – 66.

[184] Sorci G, Riuzzi F, Giambanco I, Donato R. (2013). "RAGE in tissue homeostasis, repair and regeneration". *Biochim Biophys Acta*;1833:101 – 109 .

[185] Han YT, Choi GI, Son D, Kim NJ, Yun H, Lee S, et al. (2012). "Ligand-based design, synthesis, and biological evaluation of 2-aminopyrimidines, a novel series of receptor for advanced glycation end products (RAGE) inhibitors". *J Med Chem*;55:9120 – 9135.

[186] Barlovic DP, Soro-Paavonen A, Jandeleit-Dahm KA . (2011). "RAGE biology, atherosclerosis and diabetes". *Clin Sci (Lond)*;121:43 – 55.

[187] Sparvero LJ, Asafu-Adjei D, Kang R, Tang D, Amin N, Im J, et al. (2009). "RAGE (Receptor for Advanced Glycation End products), RAGE ligands, and their role in cancer and inflammation". *J Transl Med*;7 : 17.

[188] Yamamoto Y, Kato I, Doi T, Yonekura H, Ohashi S, Takeuchi M, et al. (2001). "Development and prevention of advanced diabetic nephropathy in RAGE-overexpressing mice". *J Clin Invest*;108:261 – 268 .

[189] Chen CY, Abell AM, Moon YS , Kim KH. (2012). "An advanced glycation end product (AGE)-receptor for AGEs (RAGE) axis restores adipogenic potential of senescent preadipocytes through modulation of p53 protein function". *J Biol Chem*;287:44498 – 44507.

[190] Neeper M. et al. (1992). "Cloning and expression of a cell surface receptor for advanced glycosylation end products of proteins". *J. Biol. Chem*.267,14998 – 15004.

[191] Schmidt AM. et al. (1992). "Isolation and characterization of two binding proteins for advanced glycosylation end products from bovine lung which are present on the endothelial cell surface". *J. Biol. Chem.*,14987 – 14997.

[192] Ramasamy R, Yan SF, Schmidt AM. (2012). "The diverse ligand repertoire of the receptor for advanced glycation endproducts and pathways to the complications of diabetes". *Vascul Pharmacol*;57:160 – 167.

[193] Leclerc E. et al. (2009). "Binding of S100 proteins to RAGE: an update". *Biochim. Biophys. Acta* 1793,993 – 1007.

[194] Sturchler E. et al. (2008). "Site-specific blockade of RAGE-Vd prevents amyloid-beta oligomer". *neurotoxicity. J. Neurosci*.28,5149 – 5158.

[195] Fritz G . (2011). "RAGE: a single receptor fits multiple ligands". *Trends Biochem Sci*;36:625 – 632 .

[196] Xue J, Rai V, Singer D, Chabierski S, Xie J, Reverdatto S. et al. (2011). "Advanced glycation end product recognition by the receptor for AGEs". *Structure*;19:722 – 732.

[197] Neeper M. et al. (1992). "Cloning and expression of a cell surface receptor for advanced glycosylation end products of proteins". *J Biol Chem*;267(21):14998 - 15004.

[198] Kalea A, Schmidt A, Hudson B. (2012). "RAGE: a novel biological and genetic marker for vascular disease". *Division of Surgical Science, Department of Surgery, College of Physicians and Surgeons, Columbia University, New York,NY 10032, U.S.A.*

[199] Sakurai S, Yonekura H. (2012). "The AGE-RAGE System and Diabetic Nephropathy". *Department of Biochemistry and Molecular Vascular Biology*.

[200] Reverdatto S, Rai V, Xue J, Burz D, Schmidt AM. (2011). "Combinatorial Library of Improved Peptide Aptamers, CLIPs to Inhibit RAGE Signal Transduction in Mammalian Cells". *Department of Chemistry, Langone Medical Center, New York University, United States of America.*

[201] Dattilo BM. et al. (2007). "The extracellular region of the receptor for advanced glycation endproducts is composed of two independent structural units". *Biochemistry*;46(23):6957 - 70.

[202] Koch M. et al. (2012). “Structural Basis for Ligand Recognition and Activation of RAGE”. *Structure*;18(10):1342 – 1352.

[203] Singh R. et al. (2001). “Advanced glycation end-products: a review”. *Diabetologia*;44(2): 129-46.

[204] Koch M. et al. (2010). “Structural Basis for Ligand Recognition and Activation of RAGE”. *Structure*;18(10):1342-1352.

[205] Dattilo BM. et al. (2007). “The extracellular region of the receptor for advanced glycation endproducts is composed of two independent structural units”. *Biochemistry*;46(23):6957 - 70.

[206] Matsumoto S. et al. (2008). “Solution structure of the variable-type domain of the receptor for advanced glycation end products: new insight into AGE-RAGE interaction”. *Biochemistry*;47(47):12299 - 311.

[207] Shihabi A. Li WG, Miller J, Weintraub NL. (2002). *Am. J. Physiol. Heart Circ. Physiol*;282,797 – 802.

[208] Topol E, Lancet J. (2004). *Frei B.J. Nutr*;134, 3196S-3198S.

[209] Bonnefont-Rousselot D J. (2001). *Soc. Biol*;195,39 1 - 398.

[210] Andersen JK. (2004). *Nat. Rev. Neurosci*;5,S18-25.

[211] Dalle-Donne I, Giustarini D, Colombo R, Rossi R, Milzani A. (2003). *Trends Mol Med*;9,169 - 176.

[212] Jellinger KA, Kienzl E, Rumpelmaier G, Paulus W, Riederer P, Stachelberger H, Youdim MB, Ben- Shachar D. (1993). “Iron and ferritin in substantia nigra in Parkinson’s disease”. *Adv Neurol*;60:267 – 272.

[213] Roje S. (2007). "Vitamin B biosynthesis in plants". *Phytochemistry*;68(14):1904 – 21.

[214] Booth AA, Khalifah RG, Todd P, Hudson BGJ. (1997). *Biol. Chem*;272,5430 – 5437.

[215] Suzuki D, Miyata T. (1999). *Intern Med*;8, 309-314.

[216] Neely MD, Zimmerman L, Picklo MJ, Ou JJ, Morales CR, Montine KS, Amaranth V, Montine TJ. (2000) .”Congeners of N(alpha)-acetyl-L-cysteine but not aminoguanidine act as neuroprotectants from the lipid peroxidation product 4-hydroxy-2-nonenal”. *Free Radic Biol Med*;29:1028 – 1036.

[217] Cameron NE, Cotter MA. (1996). “Rapid reversal by aminoguanidine of the neurovascular effects of diabetes in rats: modulation by nitric oxide synthase inhibition”. *Metabolism*;45:1147 - 1152.

[218] Brownlee M, Vlassara H, Kooney A, Ulrich P, Cerami A. (1986). „Aminoguanidine prevents diabetes-induced arterial wall protein crosslinking“. *Science*;232:1629 - 1632.

[219] Soulis-Liparota T, Cooper M, Papazoglou D, Clarke B, Jerums G. (1991). „Retardation by aminoguanidine of development of albuminuria, mesangial expansion, and tissue fluorescence in streptozocin-induced diabetic rat“. *Diabetes*;40:1328 - 1334.

[220] Vistoli G, Orioli M, Pedretti A, Regazzoni L, Canevotti R, Negrisoli G, Carini M, Aldini G. (2009). "Design, synthesis, and evaluation of carnosine derivatives as selective and efficient sequestering agents of cytotoxic reactive carbonyl species". *ChemMedChem*;4:967 - 975.

[221] Freedman BI, Wuerth JP, Cartwright K, Bain RP, Dippe S, Hershon K, Mooradian AD, Spinowitz BS. (1999). "Design and baseline characteristics for the aminoguanidine Clinical Trial in Overt Type 2". *Diabetic Nephropathy (ACTIONII). Control Clin. Trials*;20:493 - 510.

[222] O'Donnell JP. (1982). "The reaction of amines with carbonyls: its significance in the nonenzymatic metabolism of xenobiotics". *Drug Metab. Rev*;13:123 - 159.

[223] Harvey, Richard A, Pamela A, Harvey, and Mark J. (2000). "Lippincott's Illustrated Reviews: Pharmacology". *2nd ed. Philadelphia: Lipincott, Williams & Wilkins*;190.

[224] Leung, G; Sun W, Zheng L, Brookes S, Tully M, Shi R. (2010). "Anti-acrolein treatment improves behavioral outcome and alleviates myelin damage in EAE mouse". *Neuroscience*;173:150 – 5.

[225] Clinical Guidelines Task Force, International Diabetes Federation. (2007). "Glucose control: oral therapy" In: Global Guideline for Type 2 Diabetes. Brussels: International Diabetes Federation, 35–8.

[226] National Collaborating Centre for Chronic Conditions. (2008). "Type 2 diabetes: national clinical guideline for management in primary and secondary care". London: Royal College of Physicians;ISBN 978-1-86016-333-3. 86.

[227] Rahbar S, Natarajan N, Yerneni K, Scott S, Gonzales N, Nadler J. (2000). "Evidence that pioglitazone, metformin and pentoxifylline are inhibitors of glycation". *Clin. Chim. Acta*;301:65 - 77.

[228] Ruggiero-Lopez D, Lecomte M, Moinet G, Patereau G, Lagarde M, Wiernsperger N. (1999). "Reaction of metformin with dicarbonyl compounds. Possible implication in the inhibition of advanced glycation end product formation". *Biochem. Pharmacol*;58:1765 - 1773.

[229] Beisswenger P, Ruggiero-Lopez D. (2003). "Metformin inhibition of glycation processes". *Diabetes Metab*;29:6S95 - 103.

[230] Bauchart C, Savary-Auzeloux I, Patureau Mirand P, Thomas E, Morzel M, Remond D. (2007). "Carnosine concentration of ingested meat affects carnosine net release into the portal vein of minipigs". *J Nutr*;137(3):589 – 593.

[231] Aldini G, Facino RM, Beretta G, Carini M. (2005). "Carnosine and related dipeptides as quenchers of reactive carbonyl species: from structural studies to therapeutic perspectives". *Biofactors*;24:77 – 87.

[232] Aldini G, Carini M, Beretta G, Bradamante S, Facino RM. (2002). "Carnosine is a quencher of 4-hydroxy-nonenal: through what mechanism of reaction?". *Biochem. Biophys. Res. Commun*.;298:699 - 706.

[233] Liu Y, Xu G, Sayre LM. (2003). "Carnosine inhibits (E)-4-hydroxy-2-nonenal-induced protein cross-linking: structural characterization of carnosine-HNE adducts". *Chem. Res. Toxicol.*;16:1589 - 1597.

[234] Aldini G. (2002) "Detoxification of cytotoxic alpha,beta-unsaturated aldehydes by carnosine: characterization of conjugated adducts by electrospray ionization tandem mass spectrometry and detection by liquid chromatography/mass spectrometry in rat skeletal muscle". *J Mass Spectrom.*;37(12):1219-28.

[235] Colzani A. et al. (2013). "A novel high resolution MS approach for the screening of 4-hydroxy-trans-2-nonenal sequestering agents". *Biochemistry*;32(26):5757 – 68.

[236] Vistoli G, Straniero V, Pedretti A, Fumagalli L, Bolchi C, Pallavicini M, Valoti E, Testa B. (2012). "Predicting the physicochemical profile of diastereoisomeric histidine-containing dipeptides by property space analysis". *Chirality*;.24(7):566-76.

[237] Orioli M, Aldini G, Beretta G, Facino RM, Carini M. (2005). "LC-ESI-MS/MS determination of 4-hydroxy-trans-2-nonenal Michael adducts with cysteine and histidine-containing peptides as early markers of oxidative stress in excitable tissues". *J Chromatogr B Analyt Technol Biomed Life Sci*. 2005 Nov 15;827(1):109-18.

[238] Baba SP, Hoetker JD, Merchant M, Klein JB, Cai J, Barski OA, Conklin DJ, Bhatnagar A., (2013). Role of aldose reductase in the metabolism and detoxification of carnosine-acrolein conjugates". *J Biol Chem.*;288(39):28163-79.

[239] Huebschmann AG, Regensteiner JG, Vlassara H, Reusch JE. (2006). "Diabetes and advanced glycoxidation end products". *Diabetes Care*;29:1420 – 1432.

[240] Wendt TM, Tanji N, Guo J, Kislinger TR, Qu W, Lu Y. et al. (2003). "RAGE drives the development of glomerulosclerosis and implicates podocyte activation in the pathogenesis of diabetic nephropathy". *Am J Pathol*;162:1123 – 1137.

[241] Deane R, Singh I, Sagare AP, Bell RD, Ross NT, LaRue B, Love R, Perry S, Paquette N, Deane RJ, Thiyagarajan M, Zarcone T, Fritz G, Friedman AE, Miller BL, Zlokovic BV. (2012). "A multimodal RAGE-specific inhibitor reduces amyloid β-mediated brain disorder in a mouse model of Alzheimer disease". *J. Clin. Invest.*;122:1377 - 1392.

[242] Zlokovic BV. (2008). " New therapeutic targets in the neurovascular pathway in Alzheimer's disease". Neurotherapeutics;5:409 - 414.

[243] Sabbagh MN, Agro A, Bell J, Aisen PS, Schweizer E, Galasko D. (2011). "PF-04494700, an oral inhibitor of receptor for advanced glycation end products (RAGE), in Alzheimer's disease". *Alzheimer Dis. Assoc. Disord.*;25:206-212.

[244] Feng L, Xu YH, Wang SS, Au-Yeung W, Zheng ZG, Zhu Q, Xiang P. (2012). "Competitive binding between 4,4'-diphenylmethane-bis(methyl) carbamate and RAGE ligand MG-H1 on human umbilical vein endothelial cell by cell membrane chromatography". *J. Chromatogr. B Analyt. Technol. Biomed. Life Sci.*;881 - 882:55 - 62.

[245] Jung DH, Kim YS, Kim JS. (2012). "Screening system of blocking agents of the receptor for advanced glycation endproducts in cells using fluorescence". *Biol. Pharm. Bull*.;35:1826 - 1830.

[246] Win MT, Yamamoto Y, Munesue S, Saito H, Han D, Motoyoshi S, Kamal T, Ohara T, Watanabe T, Yamamoto H. (2012). "Regulation of RAGE for attenuating progression of diabetic vascular complications". *Exp. Diabetes Res*.;2012:894605.

[247] Han YT, Choi GI, Son D, Kim NJ, Yun H, Lee S, Chang DJ, Hong HS, Kim H, Ha HJ, Kim YH, Park HJ, Lee J, Suh YG. (2012). "Ligand-based design, synthesis, and biological evaluation of 2-aminopyrimidines, a novel series of receptor for advanced glycation end products (RAGE) inhibitors". *J. Med. Chem*.;55:9120 - 9135.

[248] Rao NV, Argyle B, Xu X, Reynolds PR, Walenga JM, Prechel M. et al. (2010). "Low anticoagulant heparin targets multiplesites of inflammation, suppresses heparin-induced thrombocytopenia, and inhibits interaction of RAGE with its ligands". *Am J Physiol Cell Physiol*;299:C97 – C110.

[249] Jing YH, Chen KH, Yang SH, Kuo PC, Chen JK. (2010). "Resveratrol ameliorates vasculopathy in STZ-induced diabetic rats: role of AGE-RAGE signaling". *Diabetes Metab Res Rev*;26: 212 – 222.

[250] Yu W, Wu J, Cai F, Xiang J, Zha W, Fan D. et al. (2012). "Curcumin alleviates diabetic cardiomyopathy in experimental diabetic rats". *PLoS One*;7:e52013.

[251] Pillai SS, Sugathan JK, Indira M .(2012). "Selenium downregulates RAGE and NF κ B expression in diabetic rats". *Biol Trace Elem Res*;149:71 – 77.

[252] Vugmeyster Y, DeFranco D, Pittman DD, Xu X. (2010). "Pharmacokinetics and lung distribution of a humanized anti- RAGE antibody in wild-type and RAGE-/- mice". *MAbs*;2:571 – 575.

[253] Christaki E, Opal SM, Keith JCJ, Kessimian N, Palardy JE, Parejo NA. et al. (2011). "A monoclonal antibody against RAGE alters gene expression and is protective in experimental models of sepsis and pneumococcal pneumonia". *Shock*;35:492 – 498.

3. Set-up of novel analytical methods for testing. RCS trapping agents

3.1. A novel high resolution MS approach for the screening of 4-hydroxy-trans-2-nonenal sequestering agents.

3.1.a. Abstract.

An in vitro high resolution MS method was set-up to test the ability of compounds, mixtures and extracts to inhibit protein carbonylation induced by reactive carbonyl species (RCS). The method consists of incubating the protein target (ubiquitin) with 4-hydroxy-*trans*-2-nonenal (HNE) in the presence and absence of the tested compound. After 24 hours of incubation, the reaction is stopped and the protein is analyzed by high-resolution mass spectrometry (MS). The extent of protein carbonylation is determined by measuring the area of the +11 multicharged peak of the HNE adduct in respect to the native form. The method was validated by measuring the effect of well-known RCS sequestering agents, namely aminoguanidine, pyridoxamine, hydralazine and carnosine, yielding a good reproducibility and the possibility to be automatable. All the compounds were found to dose-dependently inhibit the protein carbonylation with the following order of potency carnosine ≈ hydralazine >> aminoguanidine > pyridoxamine, as determined by calculating the UC_{50} values, that is the concentration required to inhibit ubiquitin carbonylationby 50%. A good correlation was found with the results obtained by measuring HNE consumption using an HPLC method optimized by a mobile phase set at pH 7.4, in order to stabilize the eluted adducts. The MS approach was then applied to test the effect of two selected natural extracts on protein carbonylation, i.e. green coffee bean extract and procyanidins from *Vitisvinifera*. In summary, this paper reports a validated and highly reproducible MS method to test the ability of pure compounds as well as natural extracts to act as protein carbonylation inhibitors.

3.1.b. Introduction.

Reactive carbonyl species (RCS), generated by the non-enzymatic oxidation of lipids and sugars, are involved in several biological effects, most of them leading to a cell damage response[1]. From a chemical point of view, RCS can be grouped into three main classes: 1) α,β-unsaturated aldehydes such as 4-hydroxy-*trans*-2-nonenal (HNE) and acrolein; 2) cheto-aldehydes, such as methylglyoxal; 3) di-aldehdyes such as glyoxal and malondialdehdye[2].

The biological response of RCS is mainly due to their ability to covalently modify proteins, leading to adducts that are named AGEs, when the RCS are formed by sugars, and ALEs when formed from lipids. The damaging effect induced by covalent protein modification can be ascribed to different mechanisms, such as protein dysfunction, protein oligomerization, immunoresponce and RAGE (receptor for AGEs)activation [1;3]. AGEs and ALEs have been used for several years as biomarkers of oxidative stress and several analytical methods and immunological assays have been developed for their measurements in both ex vivo and in vitro samples[4; 5; 6]. More recently, due to their unequivocal involvement in the pathogenetic mechanisms of several oxidative based diseases, AGEs/ALEs are also considered as promising drug targets, and a substantial effort is now dedicated to delve into the molecular strategies aimed at preventing, reducing or removing these protein oxidation products[7; 8; 9]. Several approaches have so far been considered for AGEs and ALEs inhibition and they can be grouped by considering at which level of the damaging AGEs/ALEs cascade they are effective and in particular if they act by inhibiting AGEs/ALEs formation, accelerating their catabolism or blocking their biological effects. The first level of action, the inhibition of AGEs/ALEs formation, also consists of different approaches, and the most promising is that based on compounds able to detoxify the reactive carbonyl species (RCS) involved in AGEs/ALEs formation[7]. RCS sequestering agents have been demonstrated to be effective in several oxidative based animal models and some of them have also shown positive effects in clinical trials, thus prompting the interest towards this molecular approach. Pyridoxamine, aminoguanidine, hydralazine and carnosine are the main RCS sequestering agents so far reported in the literature[7; 10; 11]. Though on one hand their pharmacological activity is very promising, on the other hand the clinical applications of these compounds is limited for safety concerns and/or lack of selectivity and bioavailability, thus prompting the search of novel compounds effective as RCS quenchers. The search for novel effective sequestering compounds primarily requires a reliable and accurate *in vitro* method that can be adapted to a medium/high throughput screening in order to test large libraries, which is also able to screen complex mixtures such as natural extracts.

The analytical methods so far reported do not fulfill these requirements. Most of the assays measure the disappearance of the target aldehyde in the presence of the tested compound. The content of the aldehyde is determined by a direct spectrophotometric method when the RCS contains a

chromophore, such as in the case of α,β-unsaturated aldehydes, or upon a derivatization reaction, when the carbonyl moiety is not conjugated, as in the case of MDA, glyoxal or methylglyoxal[12]. Often, the direct UV analysis is integrated by an HPLC analysis in order to separate the RCS from possible interfering compounds that can be the tested compounds themselves[13;14]. However, such an assay is limited by several factors and in particular it cannot be applied to mixtures of compounds or extracts, it is not suitable for a high throughput screening and in most cases the experimental conditions required for the derivatization reaction or for the HPLC analysis can promote the dissociation of the adduct or catalyze its formation, thus under- or over-estimating the quenching effect. Another widely used assay is based on measuring the rate of AGEs/ALEs formation by incubating the RCS with a protein target, in the presence or absence of the tested compound. Such a method is more complete than the previous one, since it includes the protein which is the RCS target. AGEs and ALEs formation can then be determined due to an increased MW or by Western blot analysis[15;16]. Such a method suffers of several limitations and in particular it is quite time-consuming, expensive and is not adapted for the screening of several compounds or for accurate quantitative/semi-quantitative analyses.

Based on these limitations, the aim of the present paper is to set-up and validate a rapid and accurate method, based on high resolution MS, able to test the ability of compounds or extracts to inhibit protein carbonylation induced by RCS. To set-up the method, HNE, which is one of the most abundant and reactive lipid-derived RCS generated through the β-cleavage of hydroperoxides from PUFAs, was used as RCS and ubiquitin as a model of protein substrate. After the set-up process, the method was then applied to evaluate the ability of known RCS sequestering agents as well as of selected natural extracts to inhibit HNE induced protein carbonylation.

3.1.c. Experimental.

3.1.d. Reagents and materials.

Ammonium bicarbonate (NH_4HCO_3), formic acid (HCOOH), sodium dihydrogen phosphate ($NaH_2PO_4 \cdot H_2O$), sodium hydrogen phosphate ($Na_2HPO_4 \cdot 2H_2O$), lyophilized ubiquitin from bovine erythrocytes (BioUltra, ≥98%)and LC-MS grade solvents were purchased from Sigma-Aldrich (Milan, Italy). Sodium tetrahydridoborate ($NaBH_4$) was purchased from Fluka Analytical. LC-grade H_2O (18 MΩ·cm) was prepared with a Milli-Q H_2O purification system (Millipore, Bedford, MA, USA). All other reagents were of analytical grade. Sequence grade trypsin and Glu-C (protease V8) were obtained from Roche Diagnostics S.p.A. (Monza, Italy).

4-hydroxy-2-nonenal diethylacetal (HNE-DEA) was synthesized according to the literature [17] and stored at -20°C. For each experiment, fresh 4-hydroxy-2-nonenal (HNE) was prepared starting from stored HNE-DEA, which was evaporated under nitrogen stream and hydrolyzed with 1 mM HCl, pH 3 for 1 h at room temperature to obtain HNE. The concentration of HNE was estimated by measuring the absorbance at λ = 224 nm (molar extinction coefficient = 13750 M^{-1} x cm^{-1}).

3.1.d.1. Sample preparation.

3.1.d.1.1. In vitro carbonylation of ubiquitin with HNE.

Ubiquitin (10 µM final concentration) was incubated with increasing amounts of HNE (100 µM, 200 µM, 500 µM and 1 mM, corresponding to molar ratios between the protein and HNE equal to 1:10, 1:20, 1:50 and 1:100 at 37°C in 10 mM phosphate buffer ($Na_2HPO_4 \cdot 2H_2O$, pH adjusted to 7.4 with $NaH_2PO_4 \cdot H_2O$). Ubiquitin (10 µM) was incubated under the same conditions, but without HNE, as control sample.

The reactions were stopped after 3, 6, 24 or 48 h by centrifugation using Amicon YM3 filters (Millipore, Milan, Italy).To do so, 70 µl of solution was diluted with water, loaded on Amicon YM3 filters (Millipore, Milan, Italy) and centrifuged at 14000 g for 15 min. The eluates were discarded, while the ubiquitin solution remained on top of the filter (about 50 µl) was rinsed three times with 450 µl of H_2O to stop the reaction by diluting the excess reagents (HNE and inhibitors). The eluates were discarded and the washing procedure was repeated twice. After the last centrifugation step, the eluates were discarded and the filters were flipped to recover the ubiquitin solution (about 70 µl). If necessary, the sample was diluted to the initial volume (70 µl) with water. Ubiquitin was either enzymatically digested or directly injected into the mass spectrometer for intact protein analysis (see below).

3.1.d.1.2. In vitro inhibition of ubiquitin carbonylationusing small molecules.

Ubiquitin (10 µM final concentration) was incubated at 37° C in 10 mM phosphate buffer in presence of 500µM HNE, together with the known inhibitors of carbonylation hydralazine, aminoguanidine, pyridoxamine or carnosine at final concentration equal to 500 µM, 1 mM, 2.5 mM and 5 mM - corresponding to molar ratios between HNE and inhibitors equal to 1:1, 1:2, 1:5 and 1:10. Ubiquitin (10 µM) was incubated with HNE under the same conditions, but without inhibitors, as control sample. The reactions were stopped after 24 hours by centrifugation using Amicon YM3 filters, as described in paragraph 3.1.d.1.

3.1.d.1.3. In vitro inhibition of ubiquitin carbonylation using plant extracts.

Ubiquitin (10 µM final concentration) was incubated for 24 h at 37° C in 10 mM phosphate buffer in presence of 500µM HNE, together with commercial lplant extracts obtained from grape seed (Leucoselect, IndenaS.p.a., Milan, Italy) or green coffee (EPO S.r.l., Milan, Italy, catalogue number 3134845).The dried extracts were dissolved in phosphate buffer at final concentrations equal to 31 mg/ml. After vortexing, the solutions were centrifuged at 14000 g for 15 min; the supernatants were collected and loaded on Amicon YM3 filters. After 1 hour centrifugation at 14000 g, the filtered solutions - containing molecules smaller than 3 kDa - were incubated with ubiquitin and HNE at final concentrations equal to 1, 10 and 25 mg/ml. Ubiquitin (10 µM) was incubated with 500 µM HNE without extracts, as control sample. Additional control samples contained 10 µM ubiquitin together with grape seed or green coffee extract. For all samples, the reactions were stopped after 24 hours by centrifugation using Amicon YM3 filters, as described in paragraph 3.1.d.1.

3.1.d.1.4. Intact protein analysis: microflow automated loop injection ESI-MS.

40 µL aliquots of ubiquitin solution recovered from Amicon YM3 filters were mixed with 40 µl of denaturing solution ($H_2O/CH_3CN/HCOOH$; 40/60/0.2; v/v/v) to reach a final protein concentration of 5 µM. Aliquots of 5 µl of the diluted samples were then injected into a LTQ-Obitrap XL mass spectrometer using an ESI source (Thermo Scientific, Milan, Italy) equipped with a dynamic nanospray probe(Thermo Scientific, Milan, Italy).A fully automated method was used to load the sample using an Ultimate 3000 RSLCnano system set to pump an isocratic mobile phase ($H_2O/CH_3CN/HCOOH$; 70/30/0.1; v/v/v) at a constant flow-rate of 10 µl/min. Sample injection and spectra acquisition were fully automated and controlled by the software Xcalibur (version 2.0.7, Thermo Scientific) and Chromeleon Xpress (Dionex, version 6.80). Source parameters were set as follows: positive ion mode, spray voltage 1.5 kV, capillary temperature 200°C, capillary voltage 48 V, tube lens offset 100 V. Mass spectra were acquired at high resolution (FT analyzer)in profile mode using the following settings: scan range 110-2000 *m/z*, AGC target $5x10^5$, maximum inject time 500 ms, resolving power 100000 (FWHM at 400 m/z). A list of 20 identified background ions[18]was included in the lock mass feature for real time mass calibration. Spectra were acquired using a dedicate processing method for the detection and quantification of the multicharged peaks with a charge state of +11 localized in the *m/z* range 779.00-783.59 or 793.00-797.59, respectively for unmodified and HNE-modified ubiquitin. Peak areas were automatically detected and quantified post-acquisition using Xcalibur Quan browser.

3.1.d.1.5. Protein digestion.

12.5 µl of ubiquitin solution recovered from Amicon filters (see above) were incubated with 500 mM $NaBH_4$ (37°C, 1h) to stabilize carbonyl adducts. After 1 hour, the solution containing stabilized ubiquitin was mixed with LDS sample buffer (Bio-Rad) and load on a Mini-PROTEAN gel (TGX, any Kd, Bio-Rad) for SDS-PAGE. After 20 min run, the gel was stained for 1 hour using Coomassie (Bio-Safe G-250 Stain, Bio-Rad) and destained overnight with water. Gel band corresponding to ubiquitin (around 8 kDa) were cut, washed with ammonium bicarbonate 50 mM and digested with sequencing grade trypsin or Glu-C (both Roche Diagnostics, Monza, Italy). The enzymes were resuspended in 50 mM ammonium bicarbonate at 37°C overnight, using 0.4 µg of enzymes. The reaction was stopped using 2 µl of 50% trifluoroacetic acid (TFA). Peptides were collected by subsequent incubations with extraction solution (30% acetonitrile, 3% TFA, in water) and finally by incubation with 100% acetonitrile. For each sample, collected peptides were pooled and dried using a vacuum system (Christ, Germany). Peptides were resuspended in 20 µl of 0.1% formic acid.

3.1.d.1.6. NanoLC–ESI-MS/MS peptide analysis.

Chromatographic separation was performed by injecting 5 µL of digested peptides resuspended in 0.1% formic acid on a C18 HALO PicoFrit column (75 µm x 10 cm, 2.7 µm particle size, 100 Å, New Objective, USA). The sample was injected by an Ultimate 3000 RSLCnano system and electrosprayed using a nanoESI source (Thermo). Peptide separation was performed by a reverse phase linear gradient gradientfrom 1% acetonitrile, 0.1% formic acid to 40% acetonitrile, 0.1% formic acid over 60 minutes, at flow rate of 300 nl/min. The instrument operated in data-dependent mode to acquire both full MS and MS/MS spectra. Full MS spectra were acquired in profile mode by the FT analyzer in a scan range equal to 300-1500 *m/z*, using capillary temperature 220°C, AGC scan $5x10^5$ and resolution 60000 FWHM at m/z 400. Tandem mass spectra were acquired by the linear ion trap (LTQ) for the 2 most intense ions exceeding 1×10^4 counts. MS/Ms spectra acquisition was set as follows: centroid mode, resolution 15000, precursor ions isolation width of 2 *m/z*, AGC target 1×10^4 and normalized collision energy 30 eV. Dynamic exclusion was enabled to reduce redundant spectra acquisition as follows: 3 repeat counts, 30 s repeat duration, 45 s of exclusion duration. Monoisotopic precursor selection was enabled, and singly and unassigned charged ions were not fragmented. Instrument control and spectra analysis were provided by the software Xcalibur 2.0.7 and Chromeleon Xpress 6.80.

3.1.d.1.7. Mass spectral data elaboration and database searching.

The software Proteome Discoverer (Thermo) was used to extract peaks from spectra and to match them to the primary sequence of bovine ubiquitin (Uniprot entry sp|P0CG53|1-76). Accordingly to the enzyme used for the digestion, trypsin or Glu-C were selected as proteases, allowing a maximum of 2 missed cleavages. Peptide and fragment ions tolerance were set to 10 ppm and 0.5 Da, respectively. Allowed variable modifications were methionine oxidation and HNE-carbonylation on Lys, Arg and His to form the Michael or base Schiff adducts (respectively characterized by an isotopic delta mass equal to 158.13067 and 140.12011 in their reduced forms), as reported in the literature[3,4]. Low-confidence peptide matches were filtered out by selecting peptide confidence = high. The MS/MS spectra of modified peptides were requested to match the expected ions(*b* and/or *y*) neighboring the modified amino acid both at the N- and C-termini, to obtain a confident mapping of the modification site.

Semi-quantitative analysis was carried out by calculating the AUC (area under the curve) of the extracted ion chromatograms (XIC) for the adducted and native peptides, using m/z values corresponding to the either $[M+2H]^{2+}$ or $[M+3H]^{3+}$, accordingly to the charge state reported by Proteome Discoverer. The extent of peptide modification was expressed as percentage using the following formula:

$\%\text{modified peptide} = AUC_{\text{modified peptide}}/(AUC_{\text{modifiedpeptide}}+AUC_{\text{native peptide}})\ x100$

where$AUC_{\text{modified peptide}}$ and $AUC_{\text{native peptide}}$ correspond to the area of the modified and native peptide. When multiple peaks were present in the XIC, the AUC was calculated on the peak encompassing the retention time reported by Proteome Discoverer for the identified peptide.

3.1.d.1.8. HPLC analysis.

The reactivity of each tested compound toward HNE (quenching activity) was evaluated by measuring the HNE consumption by HPLC using a quaternary pump HPLC system and a PDA detector (Surveyor LC system, ThermoQuest, Milan, Italy) set at 224 nm. Separations were done by reversed-phase elution with a Phenomenex Synergy Fusion column (150 mm × 2 mm i.d., 4 μm) protected by a Synergy Fusion R–P guard column (CPSAnalitica, Milan Italy), thermostated at 37 °C, and using Na_2HPO_4 10 mM pH 7.4/CH_3CN, 40/60 (v/v) as mobile phase at a flow rate of 0.25 ml/min.

3.1.d.1.9. Quantification of inhibitors' efficacy.

In our analysis, the concentration of quencher able to inhibit adduct formation on ubiquitin by 50% was termed UC_{50}; this value refer to the quencher:HNE molar ratio and was computed as following. The percentage of modified ubiquitin obtained upon co-incubation with HNE and HNE-sequestering agents, based on quantification of the z11 peaks (see Paragraph 2.3), was normalized against the percentage of modified ubiquitin obtained in control samples, which were incubated with HNE without any quencher. Curves plotting the normalized percentages of modified ubiquitin versus the Log concentration of quencher (expressed as quencher:HNE molar ratio) were evaluated using the non-linear regression analysis tool in GraphPad Prism (version 6.02) to obtain IC_{50}values relative to the concentration-response curve.

A similar procedure was used to obtain Q_{50} values, referring to the concentration of HNE-sequestering agent necessary to quench by 50% the HNE signal in HPLC analyses. Data were normalized against the intensity of non-quenched HNE and analysed to obtain IC_{50} values by using the non-linear regression by GraphPad Prism, as described above.

3.1.d.1.10. Molecular modelling.

The resolved structure of human ubiquitin, retrieved from PDB (Id: 1UBQ), was completed by adding hydrogen atoms and to remain compatible with physiological pH, Asp, Glu, Lys and Arg residues were considered in their ionized form, while His and Cys were maintained neutral by default. The completed structure was then minimized until RMS = 0.01 kcal mol-1Å-1 keeping fixed the backbone atoms to preserve their experimental folding. The so optimized ubiquitin structure was then utilized to predict pose of HNE close to Lys 6 and His 68 by docking simulations using PLANTS [19] and focusing the search on a 10 Å radius sphere around the above mentioned residues. The simulation was performed by scoring the poses with the ChemPlp scoring functions using speed 1 and 20 poses were generated. The so generated best pose was then used to manually build the imino adduct on Lys6 and the obtained system was solvated by a 50 Å side cubic box of water molecules. After a preliminary minimization to optimize the relative position of solvent molecules the system underwent a 10 ns of equilibrating MD simulation with the following characteristics (a) Newton's equation was integrated every fs according to Verlet's algorithm; (b) the temperature was maintained at 300 ± 10 K by means of the Langevin's algorithm; (c) periodic boundary conditions were applied to stabilize the solvent clusters; (d) the electrostatic potential was treated by PME method. The simulation was carried out in two phases: an initial period of heating from 0 K to 300 K over 30000 iterations (30 ps, i.e. 10 K/ps), and the monitored phase of 10 ns. The MD run was carried out using Namd2.9 [20]with the force-field CHARMm v22 and Gasteiger's atomic charges.

3.1.e. Results.

3.1.e.1. Intact protein analysis: microflow automated loop injection ESI-MS.

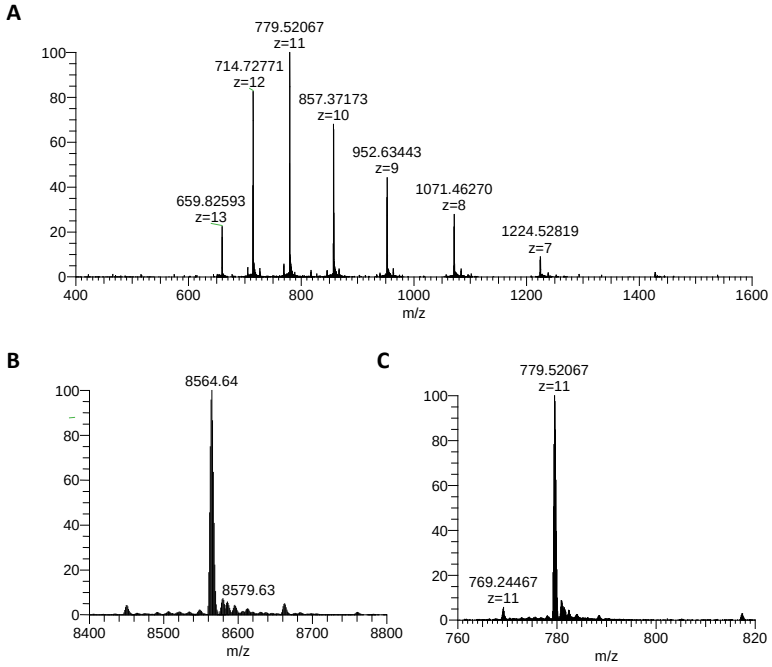

Fig 1. Ubiquitin detection by mass spectrometry analysis in denaturing, acidic conditions. A) Multi-charged spectrum of 5 µM ubiquitin. B) Deconvoluted ubiquitin spectrum.C) Zoom on the m/z region of the multi-charged spectrum, corresponding to the ubiquitin peak $[M+11H]^{11+}$.

Fig 1A shows the MS spectra of 5µM ubiquitin dissolved in denaturating conditions and characterized by the typical multi-charged ions pattern, where charge states span from +7 to +13, with the +11 peak representing the most abundant species. Fig. 1B shows the deconvoluted spectrum reporting the molecular weight of ubiquitin at 8564.64 Da, while Fig. 1C is a magnification of the *m/z* range 760-820, containing the +11 peak at *m/z* 779.52067. We set-up an automated method to estimate the area under the curve (AUC) of the multicharged peak +11; the method was tested by injecting different concentration of ubiquitin spanning the 0.1-10 µM range.

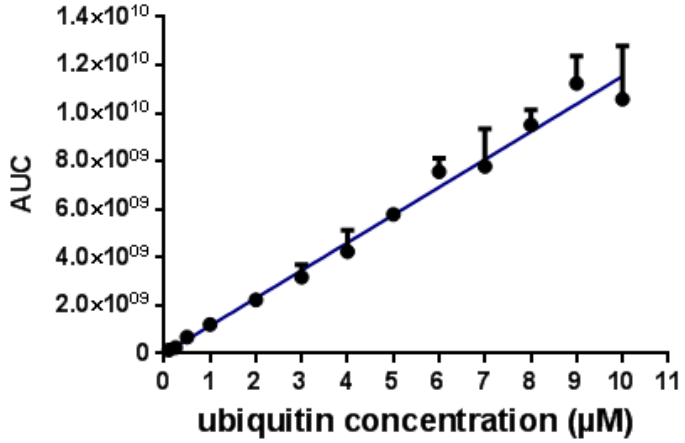

Fig 2. Quantification of the area under the curve (AUC) of the $[M+11H]^{11+}$ peak for three independent analyses at increasing ubiquitin concentration. The regression curve was calculated by the linear regression analysis. Squared correlation coefficient: 0.996.

The correlation between the AUC of the +11 multi-charge peak and ubiquitin concentration is reportedin Fig. 2, for three replicate experiments. The AUC estimated by the method well correlates with the concentration of ubiquitin; the response is linear in the range between 0.1 and 10 µM with a coefficient of determination (R^2) equal to 0.996, and average coefficient of variation (CV%) equal to 0.18.

3.1.e.2. Adduct formation on ubiquitin upon in vitro treatment with HNE.

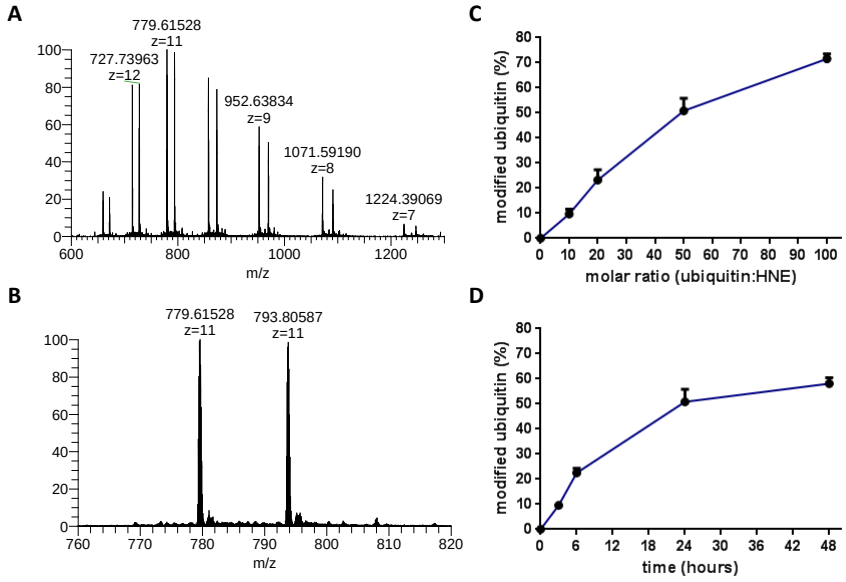

Fig 3. HNE-induced modification on ubiquitin: intact protein analysis. A) Multi-charged spectrum for HNE-modified ubiquitin, upon 24 h incubation with HNE (1:50 ubiquitin: HNE molar ratio). B)Zoom on the m/z region of the $[M+11H]^{11+}$ peaks corresponding to non-modified and HNE-modified ubiquitin. C)Quantification of the percentage of modified ubiquitin upon incubation with increasing concentration of HNE (equal to 0.1, 0.2, 0.5 and 1 mM, corresponding to 10, 20, 50, 100-fold excess over ubiquitin concentration, equal to 10 µM). D) Quantification of the percentage of modified ubiquitin upon incubation with HNE for 3, 6, 24 and 48 hours (1:50 ubiquitin:HNE molar ratio).

Upon ubiquitin incubation with HNE at 1:50 molar ratio, MS spectra present additional multi-charged ions (Fig. 3A), which are attributed to the formation of a covalent adduct, shifted by 156 Da in respect to the native protein and referred to the HNE Michal adduct. Fig. 3B shows the native +11 peak at *m/z* 779.51905 and the additional +11 peak observed at *m/z* 793.80129, attributed to the HNE adduct, characterized by a +156 Da increase in respect to the native protein, which corresponds to a*m/z* increase of ≈14 on the basis of the +11 charge state. At increasing concentrations of HNE (1:10, 1:20, 1:50 and 1:100 molar ratio as compared to ubiquitin concentration), the area of the modified +11 peak increased linearly, in respect to the area of the native +11 peak, as shown in Fig. 3C. We then monitored the kinetic of adduct formation at different incubation times (3, 6, 24 and 48hours) setting the protein: HNEmolar ratio equal to 1:50.

As shown in Fig. 3D, the increase of adduct formation is almost linear up to 24 hours and reaches a plateau thereafter.

The formation of the HNE-protein adducts as well as their detection was found to be highly reproducible with a CV%≤ 20%for all the measurements (average CV% equal to 11%).

Based on the data reported above, we decided to test the effect of carbonylation inhibitors using ubiquitin: HNE molar ratio equal to 1:50 -which is in the concentration-response linear range -and 24 hours as incubation time, since at this time the yield of ubiquitin modification is almost at the plateau level (about 50% modified protein).

3.1.e.3. Bottom-up approach: nanoLC–ESI-MS/MS.

To identify the sites of modification, ubiquitin was analyzed by mass spectrometry using a bottom-up approach. The HNE-modified protein was reduced to stabilize the adducts and digested using two different proteases, i.e. trypsin and Glu-C, in order to increase sequence coverage.

peptide sequence	modification	AA	charge	MH^+	enzyme
MQIFVK*TLTGK	K6(MA)	1-11	2	1423.860277	Trypsin
MQIFVK*TLTGKTITLE	K6(MA)	1-16	2	1981.169847	Glu-C
M*QIFVK*TLTGK	M1(Ox); K6(SB)	1-11	2	1421.843431	Trypsin
M*QIFVK*TLTGKTITLE	M1(Ox); K6(SB)	1-16	3	1979.152012	Glu-C
M*QIFVK*TLTGK	M1(Ox); K6(MA)	1-11	2	1439.855516	Trypsin
M*QIFVK*TLTGKTITLE	M1(Ox); K6(MA)	1-16	2	1997.161791	Glu-C
TLTGK*TITLEVEPSDTIENVK	K11(MA)	7-27	2	2446.357958	Trypsin
IQDK*EGIPPDQQR	K33(MA)	30-42	2	1681.913378	Trypsin
NVKAKIQDKEGIPPDQQRLIFAGK*QLE	K48(MA)	25-51	3	3221.829685	Glu-C
GIPPDQQRLIFAGK*QLE	K48(MA)	35-51	2	2068.18535	Glu-C
LIFAGK*QLEDGR	K48(MA)	43-54	2	1504.875536	Trypsin
DGRTLSDYNIQK*E	K63(MA)	52-64	2	1696.878099	Glu-C
TLSDYNIQK*ESTLH*LVLR	K63(MA); H68(MA)	55-72	2	2446.422411	Trypsin
ESTLH*LVLR	H68(MA)	64-72	2	1225.753221	Trypsin
STLH*LVLRLRGG	H68(MA)	65-76	3	1479.937015	Glu-C

Tab 1. HNE-modified peptides identified by bottom-up analysis of ubiquitin upon 24 hours incubation with 50-fold excess HNE. The reduced forms of Michael-adducts and Schiff base modified amino acids are respectively indicated as MA and SB, together with their localization in the ubiquitin sequence.

The peptides obtained from the digestion were analyzed by LC-MS/MS using a data-dependent method to fragment the most intense ions. Fragmentation spectra were searched against the ubiquitin sequence, setting the mass shift equal to +140 and +158 Da as variable modification, respectively corresponding to the reduced form of the HNE-deriving Schiff base and Michael adduct. Quality filter criteria were applied to obtain genuine peptide identification and to unambiguously map the modified residues. Overall, 15 peptides were found to be covalently modified by HNE; for each of them, it was possible to localize the site of modification by MS/MS spectra. Tab 1 shows the modified peptides and the sites of HNE modification. Different lysine residues were modified by HNE Michael adduct (K6, K11, K33, K48, K63), as well as histidine H68. Lysine 6 was also modified by HNE as Schiff base.

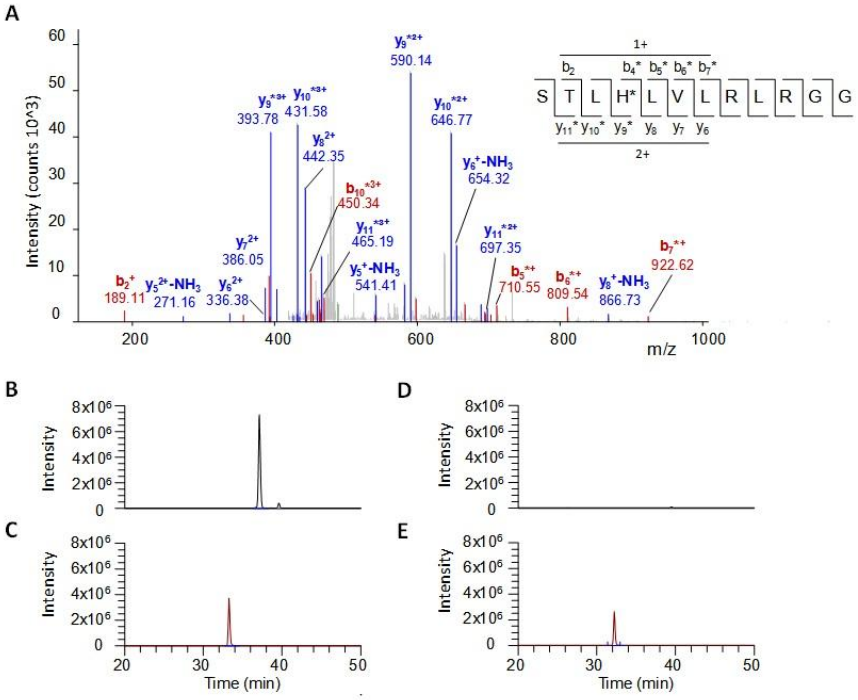

*Fig 4. Mapping of HNE-induced modification on ubiquitin sequence and relative quantification. A) MS/MS spectrum of the precursor ion isolated at m/z493.98 and attributed to the [M+3H]$^{3+}$ ion of the STLH*LVLRLRGG peptide. b and y fragment ions localize HNE-deriving Michael adduct on H68 residue. B-D) Extracted Ion Chromatograms (XICs) for relative quantification of HNE-modified vs. unmodified peptide. For the modified peptide, them/z493.98422 (± 10 ppm) relative to the HNE-modified STLH*LVLRLRGG peptide was extracted in the ubiquitin sample incubated with 50-fold excess HNE(B)and in control sample, where ubiquitin was not incubated with HNE (D).For the unmodified peptide, the m/z 441.27400 (± 10 ppm) relative to the HNE-modified STLH*LVLRLRGG peptide was extracted in the ubiquitin sample incubated with 50-fold excess HNE (C) and in control sample, where ubiquitin was not incubated with HNE (E).*

As an example, Fig. 4A shows the MS/MS spectrum relative to the C-terminal peptide STLH*LVLRLRGG (amino acids 65-76) modified on the histidine residue (H68). Its mass is shifted by 158 Da with respect to the native peptide form ($[M+H]^{1+}$ equal to 1479 Da instead of 1321 Da) due to the presence of a reduced HNE adducted formed by Michael addition. The MS/MS spectrum shows that b_2 and y_6, y_7 and y_8 are unmodified, while b_4, b_5, b_6, b_7, y_9, y_{10} and $y_{11}$are shifted by 158 Da, thus indicating H68 as the modification site (Fig. 4A).

The relative abundance of the modified peptides in respect to the native ones was computed by measuring the AUC in the extracted ion chromatograms (XIC) obtained for the native and modified forms of the peptides. The *m/z* values corresponding to the double charged $[M+2H]^{2+}$ or triple charged $[M+3H]^{3+}$ peptides were used, accordingly to the charge status reported for the identified peptides. As an example, the ion chromatograms extracted for the *m*/*z* value 493.98422 (±10 ppm), which corresponds to the $[M+3H]^{3+}$ ion of the HNE-modified peptide STLH*LVLRLRGG, is shown in Fig. 4B and Fig. 4D for the incubated and control sample, respectively. A well detectable peak with retention time of 37.12 min was present in the XIC of the ubiquitin sample incubated with 500 µM HNE (Fig. 4B), while the peak was absent in the control (Fig. 4D). Fig. 4C and Fig. 4E show the ion chromatograms extracted for the *m*/*z* value 441.27400 (±10 ppm), which corresponds to the $[M+3H]^{3+}$ ion of the native, non-modified peptide STLHLVLRLRGG, respectively for the incubated and control sample. Easily detectable peaks were present at 33.24 min in the XIC of both samples.

Peptide sequence	modification	Aa	charge	MH+	Enzyme	% modified peptide
MQIFVK*TLTGKTITLE	K6(MA)	1-16	2	1981.169847	Glu-C	3.7%
M*QIFVK*TLTGKTITLE	M1(Ox); K6(SB)	1-16	3	1979.152012	Glu-C	21.5%
M*QIFVK*TLTGKTITLE	M1(Ox); K6(MA)	1-16	2	1997.161791	Glu-C	4.7%
IQDK*EGIPPDQQR	K33(MA)	30-42	2	1681.913378	Trypsin	45.1%
GIPPDQQRLIFAGK*QLE	K48(MA)	35-51	2	2068.18535	Glu-C	5.1%
DGRTLSDYNIQK*E	K63(MA)	52-64	2	1696.878099	Glu-C	5.0%
STLH*LVLRLRGG	H68(MA)	65-76	3	1479.937015	Glu-C	69.1%

Tab 2. *Relative quantification of HNE-modified peptides vs. their unmodified, native forms. Peptide intensity was estimated by using the area under the curve (AUC) in the extracted ion chromatograms obtained for the m/z values corresponding to the double or triple-charged forms of the peptide, as indicated in the table.*

The XIC-based quantification returned the relative amount of modified peptide over the corresponding native peptide, reflecting the relative content of each modified residue, as summarized in Tab 2. Such quantification was preferentially performed on the peptides obtained by Glu-C digestion, since most native forms of HNE-modified peptides were not identified in the sample digested with trypsin (see Discussion paragraph).

3.1.e.4. Modelling study.

While detection of the ubiquitin adducts is not the primary objective of the study, a modeling analysis was undertaken with a view to rationalizing the remarkable reactivity of His68. Thus, the reactivity of the adducted lysine residues is clearly linked to their role in the polyubiquitylation mechanism and is in line with previous studies, where it was found to be related to the strength of polar interactions that lysines elicit with surrounding residues, the weaker the interaction the higher the lysine reactivity[21]. Hence, the modeling study was focused on the analysis of the molecular mechanism by which the reactivity of His68 is so significantly enhanced. As recently reviewed[22], the imidazole ring is indeed not nucleophilic enough to react as Michael donor group therefore, the histidine reactivity must be suitably improved by the surrounding residues acting as catalysts of the Michael addition. Such a mechanism might be based on the closeness (≅ 6 Å) between His68 and Lys6 whose capacity to yield Schiff bases was here experimentally confirmed.

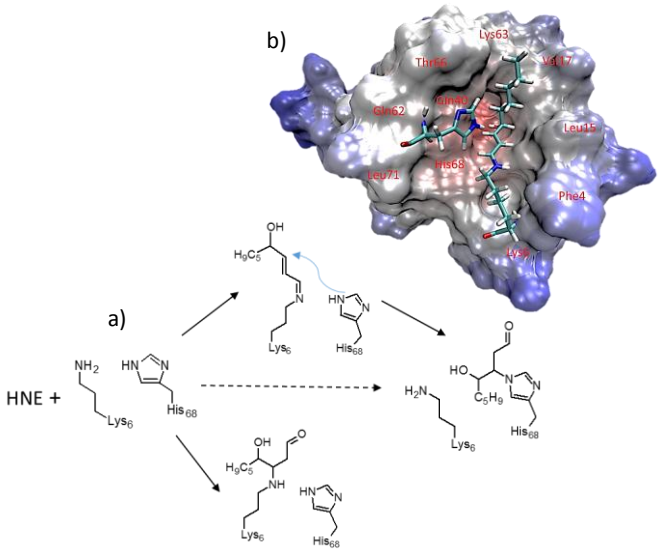

Fig 5. Putative multi-step mechanism explaining the marked reactivity of His68 with HNE, based on the closeness between Lys6 and His68 (5A). Such a mechanism involves an imino intermediate on Lys6 able to approach the α-carbon atom to His68 in a pose stably conducive to the Michael addition (5B).

As schematized in Fig 5A, it is possible to hypothesize that the Michael addition on His68 is preceded by the Schiff base intermediate on Lys6, which slightly enhances the electrophilicity of the β carbon atom and constrains it in a pose stably conducive to the addition. Once Michael adduct is formed, the Schiff base can hydrolyze thus restoring the Lys6 amino group. Interestingly, such a cross-talk mechanism between Lys6 and His68 has already been proposed to rationalize the abundance of acetylated adducts generated when treating ubiquitin with acetyl salicylate[23]. To further corroborate the hypothesized mechanism, the supposed imino intermediate was constructed by a procedure which combines a docking simulation of HNE focused on the region around Lys 6 and His68 with a short equilibrating MD run of the corresponding covalent imino adduct. Fig 5B shows the so obtained adduct and evidences how the region surrounding His68 can create a rather hydrophobic pocket where the HNE carbon skeleton is suitably accommodated. In this way, the imino adduct can assume a pose conducive to the Michael addition since the His68 imidazole ring conveniently approaches the reactive HNE α-carbon atom at a distance of about 3Å. Moreover, the adduct is also stabilized by a H-bond between the HNE hydroxyl group and Gln40 which further constrains HNE in a productive pose.

By considering that the adducted lysines are normally involved in polyubiquitination mechanisms as well as that the metal binding to His68 can alter the ubiquitin folding [24], one may suppose that also ubiquitin carbonylation might affect the biological activity of ubiquitin thus suggesting a pathogenic mechanism by which HNE can affect protein degradative pathways.

3.1.e.5. Validating the method by known RCS inhibitors.

The MS approach was applied to measure the HNE quenching ability of a set of known RCS inhibitors, namely pyridoxamine, hydralazine, aminoguanidine and carnosine. Ten µM ubiquitin was co-incubated for 24 hours with 500 µM HNE and increasing concentration HNE sequestering agents at the final concentration of 0.5, 1, 2.5 and 5 mM, corresponding to 1:1, 1:2, 1:5 and 1:10 molar ratios over HNE concentration. The samples were analyzed by mass spectrometry to quantify the percentage of HNE-modified ubiquitin, which was calculated by measuring the AUC of the +11 peaks corresponding to the native and modified forms of the protein. Data were normalized to the percentage of modified ubiquitin obtained upon protein incubation with 500 µM HNE without any inhibitor, which corresponded to 48% with a CV% equal to 15%.

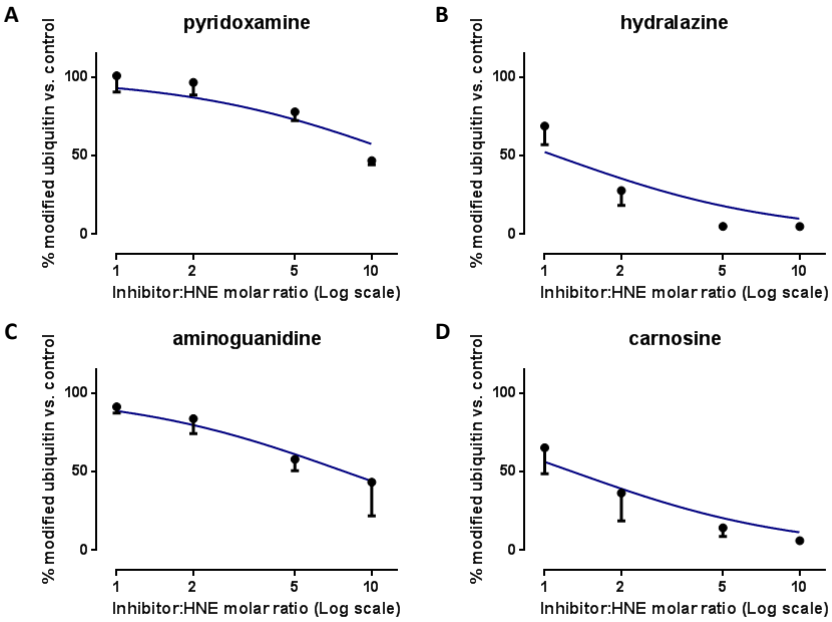

Fig 6. Inhibition of HNE-induced carbonylation by known RCS scavengers. The graphs report the percentage of HNE-modified ubiquitin upon co-incubation with 50-fold excess HNE and increasing concentration of: A)pyridoxamine, B) hydralazine, C) aminoguanidine and D)carnosine. Scavenger concentrations were equal to 0.5, 1, 2.5 and 5 mM, corresponding to HNE:scavenger molar ratio of 1, 2 5 and 10. The percentage of HNE-modified ubiquitin is expressed relative to the percentage of modified protein obtained by treatment with 50-fold excess HNE, without any scavenger.

Fig. 6 shows the normalized percentage of HNE-modified ubiquitin at increasing concentration of pyridoxamine (Fig. 6A), hydralazine (Fig. 6B), aminoguanidine (Fig. 6C) and carnosine (Fig. 6D) as HNE sequestering agents. All the inhibitors show dose-dependent effects over the HNE: quencher molar ratios ranging from 1:1 to 1:10. Hydralazine and carnosine were the most effective HNE quenchers, inhibiting at least by 80% the formation of HNE adducts at the inhibitor:HNE molar ratio 5:1 and showing a significant protective effect already at the molar ratio 1:1. Aminoguanidine was the next effective compound, followed by pyridoxamine.

3.1.e.6. Testing the HNE sequestering effect by an HPLC method.

The RCS quenching effect of the selected compounds was then determined by a more conventional method based on measuring the HNE disappearance. Most of the HPLC methods reported in the literature for measuring HNE are based on an acid mobile phase which though on one hand is suitable for the HNE separation, on the other hand can induce some artifactual reactions during the HPLC run, such as catalyzing the adduct's hydrolysis or its formation by changing the charge state of the quencher. For this reason, the method was optimized in order to maintain the mobile-phase at pH 7.4. For each sequestering agent a dose-dependent effect on the HNE content was determined and the results reported as Q_{50}, which is the concentration able to induce 50% HNE quenching.
Fig. 7 reports the Q_{50} values as calculated by using the HPLC method which are compared with the UC_{50} as determined by the MS method.

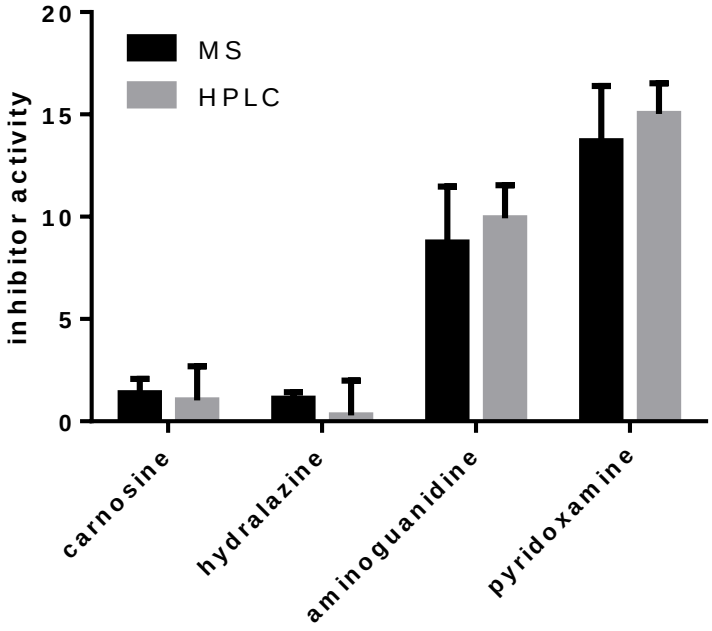

Fig 7. Comparison of Q_{50} and UC_{50} values obtained for the four tested HNE-sequestering agents by HPLC and mass spectrometry-based analyses, respectively. Q_{50} and UC_{50} values are generally indicated as inhibitor activity; theQ_{50} values refer to the concentration of the inhibitor necessary to quench by 50% the HNE chromatographic signal, while the UC_{50}values refer to the concentration of the inhibitor necessary to inhibit by 50% the formation of HNE-adduct on ubiquitin.

3.1.e.7. Testing the ability of natural extract on HNE induced protein carbonylation.

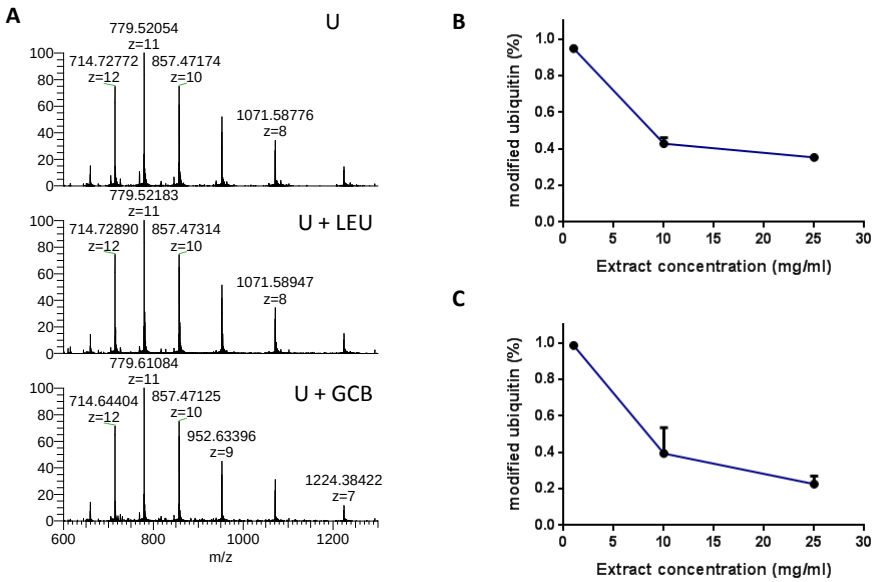

Fig 8. Inhibition of HNE-induced carbonylation by natural extracts. A) Multi-charged spectrum obtained by MS analysis of ubiquitin upon incubation with grape seed extract (LE) or green coffee been extract (GCB);multi-charged spectrum non-incubated ubiquitin (U) is reported as reference. B-C) The graph report the percentage of HNE-modified ubiquitin upon co-incubation with 50-fold excess HNE and increasing concentration of LE(B) or GCB (C). The concentration of the extracts in the ubiquitin sample was equal to 1, 10 or 25 mg/ml. The percentage of HNE-modified ubiquitin is expressed relative to the percentage of modified ubiquitin obtained by treatment with 50-fold excess HNE.

As a next step, we evaluated the HNE quenching ability of two natural extracts, namely procyanidins from *Vitisvinifera* (LE) and green coffee bean extract (GCB). It was not possible to test their quenching ability on HNE by using the HPLC method, since multiple peaks corresponding to different components of the extract co-eluted with the HNE peak (data not shown). For mass spectrometry analysis, 10 µM ubiquitin and 500 µM HNE were incubated with the natural extracts using a final concentrations equal to 1, 10 and 25 mg/ml. After the removal of excess reagent, the samples were analyzed to quantify the percentage of modified ubiquitin. As a first step, we evaluated whether incubating the target protein with the natural extracts for 24 hours had an effect on the MS spectrum of the protein, possibly deriving from formation of non-covalent adducts, protein degradation or oxidation. The results reported in Fig. 8A show that the MS spectra

of ubiquitin incubated in the absence or presence of LE and GCB are superimposable with control ubiquitin. The two extracts effectively inhibited dose-dependently the HNE induced ubiquitin carbonylation and GCB (Fig. 8C) was slightly more effective than LE (Fig. 8B). The precision of the method tested on the natural extracts was high, since the averaged coefficient of variation measured for the three replicate analyses was 11%.

3.1.f. Discussion.

Reactive carbonyl species are bioactive compounds generated by lipid and sugar oxidation, and since they are involved in the onset and propagation of several pathogenetic mechanisms, they represent a promising and quite novel drug target[2]. The RCS sequestering agents represent a class of quite heterogeneous compounds that are able to covalently react with the RCS, inactivating their biological response and producing un reactive products. Hydralazine, pyridoxamine, aminoguandine and carnosine represent the most studied RCS sequestering agents, whose trapping efficacy as well as protective effects have been demonstrated in *in vitro* and *in vivo* models[7;11]. However the clinical applications of the above mentioned compounds is limited by safety concerns and/or limited bioavailability. In detail, hydralazine and aminoguanidine have a promiscuous activity and an unsuitable selectivity[11]; carnosine is well absorbed by intestinal peptide transporters (hPepT1), but is immediately hydrolyzed in human plasma to its constituent amino acids by specific dipeptidases (e.g., serum carnosinase, CN1)[25]. Pyridoxamine has now reached clinical phase III due to its significant quenching activity combined with a satisfactory selectivity profile [26]but the potential concern with this agent is that it is related to the B vitamin family, which has demonstrated some serious adverse drug events such as stroke and myocardial infarction in diabetic kidney disease patients[27].

Although there is a great interest in the discovery of novel selective and efficient RCS scavengers, the number of truly effective carbonyl quenchers hitherto reported is rather limited and this is probably due to the lack of suitable screening approaches. The search of novel RCS-sequestering agents requires indeed an accurate, highly reproducible and automatable analytical method that can test not only pure compounds, but also mixtures and natural extracts. The methods so far reported in the literature do not fulfill these basic requirements, as pointed out in the introduction.

The present paper reports a novel method based on high resolution MS for evaluating the ability of compounds, mixtures or natural extracts to inhibit protein carbonylation. HNE was used as RCS since it is one of the most abundant and bioactive lipid-derived RCS, but it should be noted that the method can also be extended to other RCS able to covalently react with proteins, such as acrolein, methylglyoxal or glyoxal, thus permitting discriminationof the efficacy of a test compound towards the different RCS involved in protein carbonylation. Ubiquitin was selected as protein target since it is commercially available at high purity at a reasonable cost and because its molecular weight is suitable for intact protein analysis using a high resolution mass spectrometer such as the Orbitrap. Despite lacking cysteine residues, ubiquitin exposes a set of reactive lysines and a highly reactive histidine, which make this protein a suitable benchmark to test protein carbonylation and its inhibition. The method had a good reproducibility since the average CV% of three independent

experiments never exceeded20%, also when the extracts were used as inhibitors. Ubiquitin carbonylation by HNE was then fully characterized by MS in terms of stoichiometry and the sites of modification fully elucidated by a bottom-up approach and molecular modelling. The method was fully automated from the automatic injection of the sample to the quantitative analysis, with the final goal to apply the method for a medium throughput screening. Data analysis, consisting of calculating the AUC of the +11 multicharged peak relative to the native and HNE-adducted protein was automatically performed and the data were exported to an excel data-sheet to calculate the percentage of ubiquitin carbonylation. In one day triplicate analysis of a hundred samples can be easily processed by one operator.

Up to now, the RCS sequestering activity of compounds is conventionally evaluated by measuring the disappearance of the aldehyde by HPLC and in most cases they require acid conditions to derivatize the RCS or to obtain suitable chromatographic conditions. It is well known that acid conditions can greatly impact the stability of the RCS adducts, and in particular Schiff bases. Moreover, acid conditions can modify the ionization of the test compound - in particular of the amino group - thus changing its natural reactivity towards the RCS. The method here described overcomes these limits since the pH is maintained to physiological conditions (pH 7.4), until the reaction is stopped by removal of excess reagents. The sample is then acidified before mass spectrometry analysis, to denaturate and charge the protein, but at this stage the covalent adducts are already formed and are stable at this pH condition.

Another advantage of the method in respect of measuring the disappearance of the RCS by HPLC is the observation of the modified protein targeted by the RCS, thus making the analysis more reliable.

We mapped HNE-adducts in the protein sequence by bottom-up analyses. Different residues were modified at various degree of efficiency. Two enzymes (trypsin and Glu-C) were used to increase the sequence coverage, but also to allow the relative quantification of the modified peptides versus the non-modified ones. Such relative quantification was preferentially performed on peptides digested with Glu-C, instead of trypsin, since the latter enzyme specifically cleaves the peptide bond at the C-terminus of lysine and arginine amino acids, which are nucleophilic residues known to be targeted by HNE. Possibly due to the steric hindrance of the HNE Michael adducts, HNE-modified lysine residues caused trypsin missed cleavages, preventing the detection of the modified and unmodified forms of the same peptide. Therefore, relative quantification was performed on peptides digested with Glu-C, which preferentially cleave the peptide bond at the C-terminus of glutamic acid. The only exception is represented by the peptide IQDK*EGIPPDQQR that was detected only in the sample digested with trypsin. Since this peptide presents at the C-terminus an arginine residue (not modified by HNE), it was possible to detect both its modified and unmodified forms and to perform the relative quantification.

Once implemented, the method was applied to measure and compare the activity of well-known RCS scavengers towards protein carbonylation. The results are in good agreement with those obtained by measuring the HNE disappearance using an optimized HPLC method based on a neutral mobile phase, in order to maintain the stability of RCS adducts and to avoid artifactual modification of the natural reactivity of the RCS scavengers. In particular, by calculating the disappearance of HNE, the order of potency was as follows: hydralazine>carnosine>>aminoguandine>pyridoxamine. The order of potency determined by using the MS methods and based on the measurement of the protein carbonylation was carnosine≅hydralazine>>aminoguanidine>pyridoxamine. Overall, the results are quite superimposable except for the higher activity of hydralazine in respect to carnosine when the two compounds were tested by the HPLC method in respect to the MS assay. Such a difference can be easily explained by considering that the substrate protein was present only in the samples analyzed by the MS-based method. In detail, hydralazine forms reversible Schiff base with HNE, which cannot compete with the formation of Michael adducts on ubiquitin. By contrast, the carnosine-HNE adduct, that is an irreversible Michael adduct, is not shifted in the presence of ubiquitin; thus hydralazine was less efficient when tested in the MS method.

Currently, increasing interest resides in the detection of RCS sequestering agents present innatural extract of vegetable or animal origins. This is due to the fact that several natural components, such as polyphenols or peptides, have been reported to possess a quite interesting RCS trapping efficiency towards α,β-unsaturated aldehydes, cheto-aldehydes and di-aldehydes[28;29]. Hence, an analytical strategy for searching novel RCS sequestering agents is based on screening crude mixtures such as protein hydrolyzed, plant extracts and animal derivatives. HPLC based methods or methods based on RCS derivatization cannot be applied to such complex matrices, due to the presence of the different components that can co-elute with the HNE peak or interfere with the derivatizing agent. In the present paper, two selected natural extracts were evaluated as inhibitors of protein carbonylation. The measurement of HNE consumption by HPLC was confirmed that this strategy cannot be applied due to the simultaneous elution of the HNE peak with different components of the extract. The MS method was then tested and found suitable since the amount of native and carbonylated ubiquitin was easily determined, also in the presence of the extracts and no interfering peaks were observed. The two extracts reduced in a dose-dependent manner the percentage of protein carbonylation, the green coffee beans extract being slightly more effective.

3.1.g. References.

[1] Dalle-Donne I, Aldini A, Carini M, Colombo R, Rossi R, and Milzani A. (2006). "Protein carbonylation, cellular dysfunction, and disease progression". *Journal of Cellular and Molecular Medicine* 10:389 - 406.

[2] Vistoli G, De Maddis D, Cipak A, Zarkovic N, Carini M, and Aldini G. (2013). "Advanced glycoxidation and lipoxidation end products (AGEs and ALEs): an overview of their mechanisms of formation". *Free radical research* 47 Suppl 1: 3 - 27.

[3] Gaens KH, Stehouwer CD, and Schalkwijk CG. (2013). "Advanced glycation endproducts and its receptor for advanced glycation endproducts in obesity". *Curr Opin Lipidol* 24:4 - 11.

[4] Liang X, Chen Y, Zhuang Y, Zhang M, Xiong W, Guo H, Jiang F, Hu P, Guo D, and Shi D. (2012). "Advanced oxidation protein products as prognostic biomarkers for recovery from acute kidney injury after coronary artery bypass grafting". *Biomarkers* 17:507 - 12.

[5] Zhang Q, Ames JM, Smith RD, Baynes JW, and Metz TO. (2009). "A perspective on the Maillard reaction and the analysis of protein glycation by mass spectrometry: probing the pathogenesis of chronic disease". *J Proteome Res* 8:754 - 69.

[6] Colzani M, Aldini G, and Carini M. (2013). "Mass spectrometric approaches for the identification and quantification of reactive carbonyl species protein adducts". *J Proteomics*.

[7] Aldini G, Vistoli G, Stefek M, Chondrogianni N, Grune T, Sereikaite J, Sadowska-Bartosz I, and Bartosz G. (2013). "Molecular strategies to prevent, inhibit, and degrade advanced glycoxidation and advanced lipoxidation end products". *Free Radic Res* 47 Suppl 1:93 - 137.

[8] Aldini G, Dalle-Donne I, Colombo R, Facino RM, Milzani A, and Carini M. (2006). "Lipoxidation-derived reactive carbonyl species as potential drug targets in preventing protein carbonylation and related cellular dysfunction". *Chemmedchem* 1:1045-1052.

[9] Negre-Salvayre A, Coatrieux C, Ingueneau C, and Salvayre R. (2008). "Advanced lipid peroxidation end products in oxidative damage to proteins. Potential role in diseases and therapeutic prospects for the inhibitors". *British Journal of Pharmacology* 153:6-20.

[10] Burcham PC, Kaminskas LM, Tan D, and Pyke SM. (2008). "Carbonyl-scavenging drugs & protection against carbonyl stress-associated cell injury". *Mini Rev Med Chem* 8:319-30.

[11] Aldini G, Dalle-Donne I, Facino RM, Milzani A, and Carini M. (2007). "Intervention strategies to inhibit protein carbonylation by lipoxidation-derived reactive carbonyls". *Medicinal Research Reviews* 27:817 - 868.

[12] Mitchel RE, and Birnboim HC. (1977). "The use of Girard-T reagent in a rapid and sensitive methods for measuring glyoxal and certain other alpha-dicarbonyl compounds". *Anal Biochem* 81:47 - 56.

[13] Sang S, Shao X, Bai N, Lo CY, Yang CS, and Ho CT. (2007). "Tea polyphenol (-)-epigallocatechin-3-gallate: a new trapping agent of reactive dicarbonyl species". *Chem Res Toxicol* 20:1862 - 70.

[14] Vistoli G, De Maddis D, Straniero V, Pedretti A, Pallavicini M, Valoti E, Carini M, Testa B, and Aldini G. (2013). "Exploring the space of histidine containing dipeptides in search of novel efficient RCS sequestering agents". *Eur J Med Chem* 66:153 - 60.

[15] Sasaki NA, Garcia-Alvarez MC, Wang Q, Ermolenko L, Franck G, Nhiri N, Martin MT, Audic N, and Potier P. (2009). " N-Terminal 2,3-diaminopropionic acid (Dap) peptides as efficient methylglyoxal scavengers to inhibit advanced glycation endproduct (AGE) formation". *Bioorg Med Chem* 17:2310 - 20.

[16] Liu Y, Xu G, and Sayre LM. (2003). "Carnosine inhibits (E)-4-hydroxy-2-nonenal-induced protein cross-linking: structural characterization of carnosine-HNE adducts". *Chem Res Toxicol* 16:1589 - 97.

[17] Rees M, Vankuijk F, Siakotos A, and Mundy B, (1995). "Improved synthesis of various isotope labeled 4-hydroxyalkenals and peroxidation intermediates". *Synthetic Communications* 25:3225 - 3236.

[18] Keller BO, Sui J, Young AB, and Whittal RM. (2008). "Interferences and contaminants encountered in modern mass spectrometry". *Anal Chim Acta* 627:71 – 81.

[19] Korb O, Stutzle T, and Exner T. (2009). "Empirical Scoring Functions for Advanced Protein-Ligand Docking with PLANTS". *Journal of Chemical Information and Modeling* 49;84 - 96.

[20] Phillips J, Braun R, Wang W, Gumbart J, Tajkhorshid E, Villa E, Chipot C, Skeel R, Kale L, and Schulten K. (2005). "Scalable molecular dynamics with NAMD". *Journal of Computational Chemistry* 26:1781 - 1802.

[21] Novak P, Kruppa G,Young M, and Schoeniger J. (2004). "A top-down method for the determination of residue-specific solvent accessibility in proteins". *Journal of Mass Spectrometry* 39; 322 - 328.

[22] Bhatnagar A, Sharma P, and Kumar N. (2011). "Review on Imidazoles: Their Chemistry and Pharmacological Potentials". *Int. J. Pharm Tech. Res.* 3:268 - 282.

[23] Macdonald JM, Haas AL, and London RE. (2000). "Novel mechanism of surface catalysis of protein adduct formation. NMR studies of the acetylation of ubiquitin". *J Biol Chem* 275:31908 - 13.

[24] Arena G, Bellia F, Frasca G, Grasso G, Lanza V, Rizzarelli E, Tabbì G, Zito V, and Milardi D. (2013). "Inorganic stressors of ubiquitin". *Inorg Chem* 52:9567 - 73.

[25] Boldyrev AA, Aldini G, and Derave W. (2013). " Physiology and pathophysiology of carnosine". *Physiol Rev* 93:1803 - 45.

[26] Lewis EJ, Greene T, Spitalewiz S, Blumenthal S, Berl T, Hunsicker LG, Pohl MA, Rohde RD, Raz I, Yerushalmy Y, Yagil Y, Herskovits T, Atkins RC, Reutens AT, Packham DK, Lewis JB, and Group CS. (2012). "Pyridorin in type 2 diabetic nephropathy". *J Am Soc Nephrol* 23:131-6.

[27] Shepler B, Nash C, Smith C, DiMarco A, Petty J, and Szewciw S. (2012). "Update on Potential Drugs for the Treatment of Diabetic Kidney Disease". *Clinical Therapeutics* 34:1237 - 1246.

[28] Zhu Q, Zheng ZP, Cheng KW, Wu JJ, Zhang S, Tang JS, Sze KH, Chen J, Chen M, and Wang M. (2009). "Natural polyphenols as direct trapping agents of lipid peroxidation-derived acrolein and 4-hydroxy-trans-2-nonenal". *Chem Res Toxicol* 22:1721 - 7.

[29] Zhao J, Chen J, Zhu H, and Xiong YL. (2012). "Mass spectrometric evidence of malonaldehyde and 4-hydroxynonenal adductions to radical-scavenging soy peptides". *J Agric Food Chem* 60:9727 - 36.

4. Searching novel and efficient RCS sequestering agents.

4.1. Exploring the RCS scavenging activities of the naturally occurring histidine containing dipeptides: a comprehensive comparative study.

4.1.a. Introduction.

Among the oxidative processes affecting protein structures, carbonylation is a well-characterized post-translational modification, involving condensation reactions between electrophilic reactive carbonyl species (RCS) and protein nucleophilic residues. The generated covalent adducts can be essentially grouped into advanced glycation (AGEs) or lipid-oxidation end products (ALEs), depending on the biochemical source of the electrophilic species[1].

AGEs and ALEs structures can markedly vary depending on:

A) the chemical nature of the reactive carbonyls [namely, di-carbonyl derivatives, such as glyoxal (GO), methylglyoxal (MGO) and malondialdehyde (MDA) or α,β-unsaturated carbonyls, such as 4-hydroxy-2-nonenal (HNE), 4-oxo-2-nonenal (ONE), acrolein (ACR)],
B) thenucleophilicaminoacids undergoing the chemical modification [mostly, Cys, Lys, His and Arg side chains]
C) the involved mechanisms of condensation,

Besides usually inducing protein dysfunction, AGEs and ALEs can also activate signaling pathways involved in cellular homeostasis as exemplified by their interaction with the receptor for AGEs (RAGE) which is a type I transmembrane glycoprotein belonging to the immunoglobulin superfamily of cell surface receptors[2].

Although the cell possesses a variety of phase I and phase II enzymes able to detoxify the reactive carbonyl species and/or their corresponding adducts, several conditions of oxidative stress can compromise such antioxidant defenses thus resulting in an accumulation of protein carbonyls.

Besides being widely accepted biomarkers to monitor the course of oxidative based diseases, a substantial amount of literature is now available reporting the molecular and cellular pathogenic mechanisms by which AGEs/ALEs accumulation acts as a causative in the onset and progression of different diseases including neurodegeneration, atherosclerosis, muscle wasting, insulin resistance, diabetic nephropathies and aging. Therefore, AGEs and ALEs can be seen as promising targets for therapeutic intervention as confirmed by several studies showing that compounds effective as inhibitors of AGEs/ALEs or able to block their biological effects can significantly ameliorate

different oxidative based diseases. Among the possible molecular strategies, direct carbonyl quenching appears to be truly effective since it allows RCS to be covalently trapped and converted into nontoxic and easily excreted derivatives so inhibiting protein carbonylation and all downstream pathways[3].

Some known carbonyl quenchers have reached clinical studies: for example, aminoguanidine was found to be very effective in scavenging RCS but the clinical trials were discontinued because of its promiscuous activity (it is a NO-synthase inhibitor) and unselective quenching profile since it traps and depletes also physiological carbonyls. Whereas, pyridoxamine has now reached clinical phase III due to its significant quenching activity combined with a satisfactory selectivity profile. Among the marketed drugs, hydralazine, the well-known antihypertensive agent, showed a promising carbonyl quenching activity but its use is hampered by its promiscuous activity and an unsuitable selectivity. Lastly, metformin (and its biguanide analogues), the first-line antidiabetic drug, was found to directly quench RCS in several in vitro and in vivo models thus suggesting that, besides its known antihyperglycemic effect, it may also decrease
carbonyl stress with beneficial effects for the prevention of diabetic complications[4]. Among the naturally occurring carbonyl quenchers, carnosine (βAla-His) and other related histidine containing dipeptides (e.g., anserine, homocarnosine, Gly-His, carnosinamide, carcinine, see Fig 1) have attracted considerable interest for their protective effects against ALEs formation as evidenced by several in vivo models for oxidative based disorders[5].
Although such a protective activity can involve different molecular mechanisms, there is enough evidence to indicate that carnosine acts by a direct quenching mechanism, at least for α,β-unsaturated carbonyls. Nevertheless, the beneficial activity of carnosine is limited in humans by its unfavorable pharmacokinetic profile, since it is actively absorbed by intestinal peptide transporters (hPepT1) but immediately hydrolyzed in human plasma to its constituent amino acids by specific dipeptidases (e.g., serum carnosinase, CN1). Considering its potential therapeutic applications as recently reviewed, it is not surprising that many synthetic carnosine analogues have been reported in the last few years[6].

While considering the remarkable interest for carnosine (and its natural derivatives) as well as the promising results obtained in several animal models, the specific quenching profiles of these molecules against RCS have been sporadically examined and most reported studies had the objective of investigating the quenching molecular mechanism of only a few molecules without a broad comparative character. Moreover, the quenching activities were often determined by utilizing different approaches and/or different protocols without allowing an easy comparison of the obtained data. In this way, there is not an accepted wealth of fully comparable quenching activities

although such data might deepen our understanding of the quenching mechanisms thus supporting the rational design of improved derivatives. As an aside, the same limitation also affects the quenching activities for the mentioned marketed drugs and so it is impossible to compare them with other carbonyl quenchers such as the histidine containing dipeptides.

On these grounds, the present study was undertaken with the aim of acquiring truly comparable quenching activities for carnosine and its naturally occurring derivatives as well as for the mentioned known scavengers that can be seen as reference compounds. In detail, this comparative analysis was focused on 4-hydroxy-2-nonenal (HNE) as it is the most important example of α,β-unsaturated carbonyls. Since an unselective quenching profile has been one of the most impeding limitation in the development of new carbonyl quenchers, the selectivity of the examined molecules was also assessed by monitoring their quenching activity against pyridoxal, which was chosen as a well-known example of physiological carbonyl compound. These quenching analyses involved firstly a quantitative study based on well standardized chromatographic techniques and then the so obtained quenching activities were compared with the ability of these quenchers to competitively inhibit the protein carbonylation using a recently approach proposed by us. Moreover, the adducts formed by the active compounds were determined by mass spectrometry thus also allowing a fruitful comparison of the involved quenching mechanisms.

4.1.b. Materials and methods.

4.1.b.1. Reagents and materials.

All chemicals and reagents were of analytical grade and purchased from Sigma–Aldrich Chemical (Milan, Italy). LC-MS grade solvents were purchased from Sigma-Aldrich from Sigma–Aldrich Chemical (Milan, Italy). LC-grade H_2O (18 mW) was prepared with a Milli-Q H_2O purification system (Millipore, Bedford, MA, USA). 4-hydroxy-2-nonenal diethylacetal (HNE-DEA) was synthesized according to the literature[7] and stored at -20^{0}C. For each experiment, fresh 4-hydroxy-2-nonenal (HNE) was prepared starting from stored HNE-DEA, which was evaporated under nitrogen stream and hydrolyzed with 1 mM HCl, pH 3 for 1 h at room temperature to obtain HNE. L-Carnosine, D-carnosine (β-alanyl-L-histidine), N-acetyl-carnosine and carnosinol and methylglyoxal, HNE were gifts from Flamma S.p.A. (Chignolo d'Isola, Bergamo, Italy).
L-Histidine, β-alanine, homocarnosine, anserine, carnosinamide, glycine-histidine, carcinine, pyridoxamine, hydralazine, amminoguanidine, and metformin and pyridoxal were from Sigma-Aldrich Chemical (Milan, Italy).

4.1.b.2. HNE incubation and HPLC analysis.

The reactivity of each tested compound toward HNE and pyridoxal (quenching activity) was directly evaluated by measuring the HNE consumption byHPLC system(Surveyor, ThermoFinnigan Italia, Milan, Italy), equipped with a quaternary pump, a Surveyor UV-vis diode array programmable detector 6000 LP set at 224 nm, a vacuum degasser, a thermostated column compartment, and a Surveyor autosampler (200 vials capacity),was used for solvent and sample delivery. Separations were done by reversed-phase elution with a Phenomenex Synergy Fusion column (150 mm × 2 mm i.d., 4 μm) protected by a Synergy Fusion R–P guard column (CPSAnalitica, Milan Italy), thermostated at 37 °C, and using Na_2HPO_4 10 mM pH 7.4/CH_3CN, 40/60 (v/v) as mobile phase at a flow rate of 0.25 mL/min.

HNE and pyridoxal (100μM in phosphate buffer, pH 7.4, 10mM) were incubated with each compound considering several quencher/RCS ratios ranging from 1/10 to 10/1 in 10mM phosphate buffer (pH 7.4) for 3 and 24 h at 37 C°.

The reactivity of each tested compound toward MGO (quenching activity) was than directly evaluated by measuring the MGO consumption by the sameHPLC system(Surveyor, ThermoFinnigan Italia, Milan, Italy) in which the Surveyor UV-vis diode array programmable detector 6000 LP was set at 285 nm. Separations were done by reversed-phase elution with a Thermo scientific Hypercarb column (100 mm × 2.1 mm i.d., 3μm)) protected by a MAX-RP guard column(4 _ 2 mm; 4 μm) thermostated at 37 °C in the following conditions: gradient elution was performed, afterwards 6 min of conditioning phase [95% A (H_2O) , 5% B (MeOH)] after 5 min from95% solvent A, 5% solvent B to50% solvent A, 50% solvent B, and the composition of the eluent was then restored to 100% A within 5 min, and the system was re-equilibrated for 6 min.; flow rate 0.3 mL/min.

MGO (1mM in phosphate buffer, pH 7.4, 10mM) was incubated with each compound considering several quencher/RCS ratios ranging from 1/10 to 10/1 in 10mM phosphate buffer (pH 7.4) for 3 and 24 h at 37 C°.

4.1.b.3. Quantification of aldehydes efficacy and selectivity.

In our analysis, the quenching activities towards HNE, MGO and pyridoxal as derived by both HPLC and competitive studies (the latter only for HNE and MGO). They were obtained by monitoring the consumption percentages (Q% ± SD) of the carbonyl species after 3 and 24 h (the first only for HNE) and considering several quencher/RCS ratios ranging from 1/10 to 10/1. Besides, have been evaluated the consumption percentage averages as monitored by using an indicative 1/1 ratio ($Q_{1/1}$), the extrapolated ratio (R_{50}) with which the quencher consumes the 50% of the tested carbonyl compound and taking a cue from the Stern-Volmer constant (K_{SV}), commonly used to parameterize fluorescence quenching, a quenching constant (K_Q) is here proposed corresponding to the slope of the plot of $Q\%_0/Q\%$ versus the quencher/RCS ratio. The plots used to calculate the K_Q values were evaluated using analysis tool in GraphPad Prism (version 6.02).

4.1.b.4. ESI-MS instrument analysis for reaction products identification and characterization.

HNE and pyridoxal (800 µM in phosphate buffer, pH 7.4, 1-10mM) were incubated both alone and with each compound considering several quencher/RCS ratios ranging from 1/10-1/1-10/1 from 1mM to 10mM phosphate buffer (pH 7.4)in order to maintain compounds in the undissociated form for 24 h at 37 C°.

MGO (8mM in phosphate buffer, pH 7.4, 10mM) was incubated both alone and with each compound considering several quencher/RCS ratios ranging from 1/10-1/1-10/1 from 10mM to 100mM phosphate buffer (pH 7.4) in order to maintain compounds in the undissociated form for 24 h at 37 C°.

The reaction mixtures, containing each compound above listed, were diluted at a final concentration of 50µM (HNE, MGO and PL are not detectable by mass spectrometry) in 100% Milli-Q H_2O and then infused into the mass spectrometer using an Hamilton syringe at a flow rate of 10 µL/min.

ESI/MS and ESI-MS/MS analyses were done on a Thermo FinniganLCQ Advantage (Thermoquest, Milan, Italy) ion trap mass spectrometer was equipped with an electrospray interface (ESI), which was operated in the positive-ion mode, and controlled by Xcalibur software (version 1.4). Spectra were acquired in positive-ion modes, with a scan range m=z100–1000 (scan rate 0.5 scans/s). ESI interface parameters (positive-ion mode) were set as follows: middle position; capillary temperature 270 °C; spray voltage 4.0 kV. Nitrogen was used as the nebulizing gas at the following pressure: sheath gas 30 psi; auxiliary gas 5 a.u. The samples rack was maintained at 37 °C. MS conditions and tuning were optimized for each compound. The intensity of the $[M+H]^+$ ions of the test compounds were monitored and adjusted to the maximum by using the Quantum Tune Master® software.

4.1.b.5. Competitive studies.

Competitive studies were reported as described in the chapter 3.1. Briefly, ubiquitin (10 µM final concentration) was incubated at 37° C in 10 mM phosphate buffer in presence of 500 µM HNE or MGO, together with the inhibitors at final concentration equal to 500 µM, 1 mM, 2.5 mM and 5 mM - corresponding to molar ratios between HNE and inhibitors equal to 1:1, 1:2, 1:5 and 1:10. Ubiquitin (10 µM) was incubated with HNE or MGO under the same conditions, but without inhibitors, as control sample. The reactions were stopped after 24 hours by centrifugation using Amicon YM3 filters.

40 µL aliquots of ubiquitin solution recovered from Amicon YM3 filters were mixed with 40 µl of denaturing solution ($H_2O/CH_3CN/HCOOH$; 40/60/0.2; v/v/v) to reach a final protein concentration of 5 µM. Aliquots of 5 µl of the diluted samples were then injected into a LTQ-Obitrap XL mass spectrometer using an ESI source (Thermo Scientific, Milan, Italy) equipped with a dynamic nanospray probe (Thermo Scientific, Milan, Italy). A fully automated method was used to load the sample using an Ultimate 3000 RSLCnano system set to pump an isocratic mobile phase ($H_2O/CH_3CN/HCOOH$; 70/30/0.1; v/v/v) at a constant flow-rate of 10 µl/min. Sample injection and spectra acquisition were fully automated and controlled by the software Xcalibur (version 2.0.7, Thermo Scientific) and Chromeleon Xpress (Dionex, version 6.80). Source parameters were set as follows: positive ion mode, spray voltage 1.5 kV, capillary temperature 200°C, capillary voltage 48 V, tube lens offset 100 V. Mass spectra were acquired at high resolution (FT analyzer) in profile mode using the following settings: scan range 110-2000 m/z, AGC target 5x105, maximum inject time 500 ms, resolving power 100000 (FWHM at 400 m/z). A list of 20 identified background ions was included in the lock mass feature for real time mass calibration. Spectra were acquired using a dedicate processing method for the detection and quantification of the multicharged peaks with a charge state of +11 localized in the m/z range 779.00-783.59 or 793.00-797.59, respectively for unmodified and HNE-modified ubiquitin. Peak areas were automatically detected and quantified post-acquisition using XcaliburQuan browser.

4.1.c. Results.

4.1.c.1. Overview.

Fig 1 collects the analyzed quenchers and shows that, as mentioned in the introduction, they can be subdivided into two groups: the first includes natural carnosine derivatives, while the second comprises well-known quenchers although quite promiscuous.

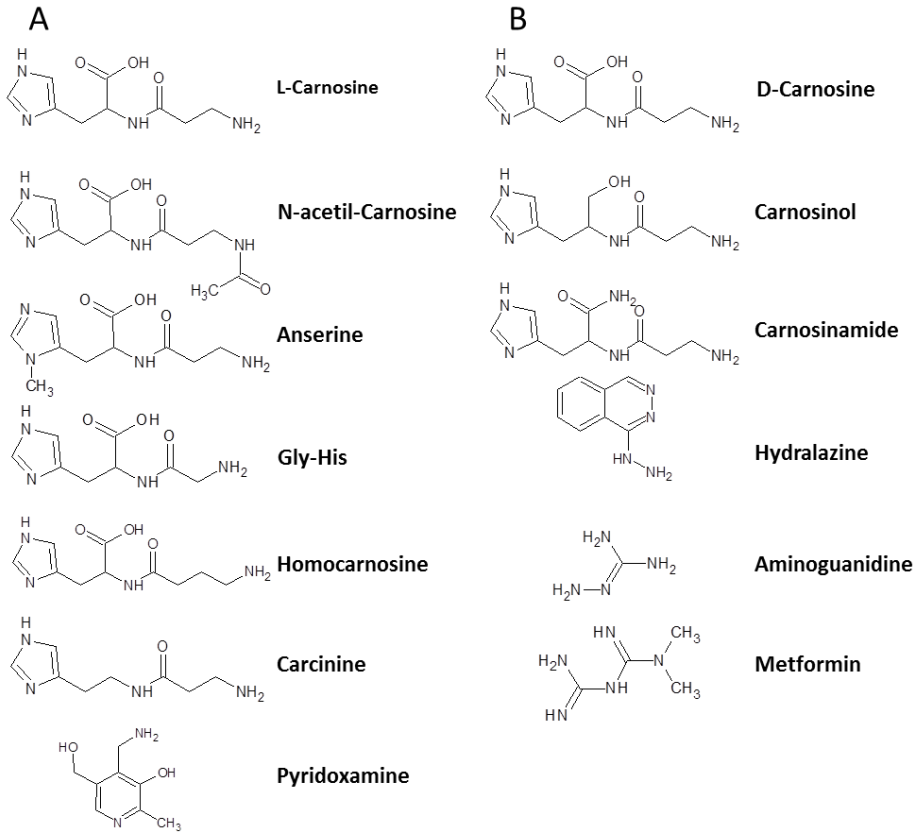

Fig 1. Structures of the RCS scavenger compounds tested in this dissertation. Column A) Natural RCS scavenger compounds. Column B) Synthetic RCS scavenger compounds.

Taken together, the examined carnosine analogues allow the investigation of how the quenching activity is influenced by (1) the length of the N-terminus residue (by comparing homocarnosine, carnosine and Gly-His); (2) the modification of the carboxyl group (by comparing carnosine, carnosinamide, carcinine and carnosinol); (3) the modification of the histidine imidazole ring (by considering anserine). Again, the comparison of carnosine, histidine, β-alanine and their physical mixture reveals the specific role of carnosine constituents as well as the synergic effect exerted when they are fused in a dipeptide. Lastly, N-acetyl carnosine can be seen as a negative control to verify the pivotal role of the terminal amino group.

All reference compounds are characterized by a nucleophilic nitrogen-containing function which should play a key role in quenching activity and is largely in its neutral form at physiological pH. As detailed below, they can be grouped depending on their whole ionization state, since hydralazine and pyridoxamine mostly exist in their unionized form at physiological pH, while aminoguanidine and metformin exist as hydrophilic cationic species due to the strong basicity of their guanidine function.

Compound	***pK_1***	***pK_2***	***pK_3***
L-carnosine	2.76	9.33	6.72
D-carnosine[a]	n.d	n.d	n.d
Carnosinol	3.61	9.78	6.55
Histidine[b]	1.77	9.18	6.10
β-Alanine[b]	3.60	10.19	---
Homocarnosine	2.75	9.89	6.79
Anserine	2.70	9.37	7.08
N-acetylcarnosine	2.83	---	6.85
Carnosinamide	---	9.31	6.28
Gly-His	2.39	8.05	6.73
Carcinine	---	---	---
Pyridoxamine	10.24	7.97	3.39
Hydralazine	---	7.18	1.52
Aminoguanidine	---	11.08	---
Metformin[b]	---	11.80	2.50

Tab 1. Ionization constants of the RCS scavenger compounds tested in this dissertation. a) the pK values for D-carnosine were not determined since they are identical to those of its isomer. b) pK values taken from literature since they are somewhat out of the ranges of the used apparatus.

To better analyse the behavior of the ionizable groups, Tab 1 collects the ionization constants of the considered quenchers. Concerning the carnosine derivatives, one may note that the acidity of the carboxyl group (pK_1 values) is minimally influenced by the remaining part of the molecule and only the single residues (His and β-Ala) show rather different pK_1 values.

The basicity of the imidazole ring (pK_3 values) appears to be rather constant, anserine showing the most basic imidazole due to its N-methylation. Differently, the basicity of the amino groups (pK_2 values) shows a marked variability spanning about two logarithmic units. It mainly depends on the distance from the peptide bond which decreases the amine's basicity due to its electron-drawing effect.

With regard to the examined reference compounds, both hydralazine and pyridoxamine possess a weakly basic function which is mostly responsible for their reactivity (pK_2, see below), while the protonation of their hetero aromatic rings cannot occur at physiological pH (pK_3 values). Notably, pyridoxamine also possesses a weakly acid phenolic group (pK_1) which it is suggested plays an ancillary role in determining reactivity towards RCS. Finally, the ionization state of aminoguanidine and metformin is evenly influenced by the strong basicity of the guanidine function the protonated state of which is the most probable at physiological pH.

4.1.c.2. Quenching activity towards HNE and MGO.

Compound	*HNE*			*MGO*			*Pyridoxal*	
	$Q\%_{1/1}$	R_{50}	K_Q	$Q\%_{1/1}$	R_{50}	K_Q	$Q\%_{10/1}$	K_Q
L-carnosine	37.28 ± 2.29	1.52	1.28	12.82 ± 1.62	3.96	0.028	0.01 ± 0.98	0.0001
D-carnosine	36.33 ± 1.92	2.06	0.62	1.26 ± 0.88	7.29	0.0026	0.22 ± 0.09	0.0002
Carnosinol	61.52 ± 1.88	1.48	0.89	36.39± 1.65	1.23	1.256	0.03 ± 0.09	0.0003
Histidine	18.27 ± 0.30	5.99	0.13	8.92 ± 0.38	n.d.	0.014	2.90 ± 0.36	0.0015
β-Alanine	2.33 ± 0.51	n.d.	0.0091	0.67 ± 0.76	n.d.	0.0074	1.01 ± 0.33	0.0005
β-Ala + His	30.01 ± 3.19	2.09	0.39	1.28 ± 0.61	12.12	0.041	4.48 ± 0.48	0.0025
Homocarnosine	5.47 ± 1.28	n.d.	0.015	0.28 ± 0.08	7.36	0.0067	1.58 ± 1.11	0.0003
Anserine	16.60 ± 0.16	2.14	0.54	2.68 ± 1.11	n.d.	0.0022	5.80 ± 0.23	0.0038
N-acetylcarnosine	0.33 ± 0.14	n.d.	0.0029	0.13 ± 1.73	n.d.	0.004	5.44 ± 0.82	0.0042
Carnosinamide	35.75 ± 4.70	1.44	1.77	48.78 ± 2.32	0.78	1.48	8.46 ± 2.37	0.0078
Gly-His	38.70 ± 3.44	1.66	0.97	19.30 ± 3.21	4.68	0.26	9.72 ± 3.23	0.0099
Carcinine	2.23 ± 0.78	9.53	0.11	0.69 ± 0.01	12.02	0.013	2.66 ± 0.27	0.0021
Pyridoxamine	2.11 ± 0.47	11.78	0.074	2.47 ± 1.38	9.31	0.081	2.15 ± 0.08	0.0017
Hydralazine	87.21 ± 3.16	0.33	10.29	48.65 ± 4.19	0.85	2.58	100.0	9.44
Aminoguanidine	2.27 ± 0.69	8.40	0.16	34.72 ± 2.67	1.67	0.96	12.79 ± 0.09	0.011
Metformin	0.47 ± 0.52	n.d.	0.0039	2.79 ± 0.94	13.66	0.058	3.05 ± 0.84	0.0019

Tab 2. Quenching activities of the RCS scavenger compounds tested towards HNE, MGO and PYR expressed as percentages of aldehyde reacted in the presence of the test compounds, after 24 h and reporting 1) consumption percentage averages monitored by using an indicative 1/1 ratio ($Q_{1/1}$), 2 the extrapolated ratio (R_{50}), 3 quenching constant (K_Q) corresponding to the slope of the plot of $Q\%_0/Q\%$ versus the quencher/RCS ratio.

Compound	*HNE*						*Pyridoxal*	
	HPLC studies			*MS competitive studies*			*HPLC studies*	
	$Q\%_{1/1}$	R_{50}	K_Q	$Q\%_{1/1}$	R_{50}	K_Q	$Q\%_{10/1}$	K_Q
L-carnosine	37.28 ± 2.29	1.52	1.28	25.42 ± 3.73	1.34	4.11	0.01 ± 0.98	0.0001
D-carnosine	36.33 ± 1.92	2.06	0.62	23.36 ± 3.06	1.41	4.44	0.22 ± 0.09	0.0002
Carnosinol	61.52 ± 1.88	1.48	0.89	38.12± 4.01	1.21	3.81	0.22 ± 0.09	0.0002
Histidine	18.27 ± 0.30	5.99	0.13	0.08 ± 3.33	6.55	0.29	2.90 ± 0.36	0.0015
β-Alanine	2.33 ± 0.51	n.d.	0.0091	0.65 ± 2.80	7.89	0.23	1.01 ± 0.33	0.0005
β-Ala + His	30.01 ± 3.19	2.09	0.39	4.15 ± 2.11	6.72	0.32	4.48 ± 0.48	0.0025
Homocarnosine	5.47 ± 1.28	7.36.	0.015	15.61 ± 3.20	2.03	2.99	1.58 ± 1.11	0.0003
Anserine	16.60 ± 0.16	2.14	0.54	12.00 ± 2.09	2.61	0.81	5.80 ± 0.23	0.0038
N-acetylcarnosine	0.33 ± 0.14	n.d.	0.0029	5.78 ± 0.43	7.47	0.15	5.44 ± 0.82	0.0042
Carnosinamide	35.75 ± 4.70	1.44	1.77	15.52 ± 3.80	1.85	1.09	8.46 ± 2.37	0.0078
Gly-His	38.70 ± 3.44	1.66	0.97	4.81 ± 2.97	3.52	0.65	9.72 ± 3.23	0.0099
Carcinine	2.23 ± 0.78	9.53	0.11	0.91 ± 0.70	4.89	0.33	2.66 ± 0.27	0.0021
Pyridoxamine	2.11 ± 0.47	11.78	0.074	0.04 ± 3.41	10.1	0.12	2.15 ± 0.08	0.0017
Hydralazine	87.21 ± 3.16	0.33	10.29	15.22 ± 3.29	1.74	2.15	100.0	9.44
Aminoguanidine	2.27 ± 0.69	8.40	0.16	3.94 ± 3.19	8.15	0.15	12.79 ± 0.09	0.011
Metformin	0.47 ± 0.52	n.d.	0.0039	2.34 ± 1.69	6.95	0.15	3.05 ± 0.84	0.0019

Tab 3. Quenching activities of the RCS scavenger compounds tested towards HNE and pyridoxal as derived by both HPLC and competitive studies (MS).

Compound	*MGO*						*Pyridoxal*	
	HPLC studies			*MS competitive studies*			*HPLC studies*	
	$Q\%_{1/1}$	R_{50}	K_Q	$Q\%_{1/1}$	R_{50}	K_Q	$Q\%_{10/1}$	K_Q
L-carnosine	12.82 ± 1.62	3.96	0.028	4.12 ± 0.58	8.42	0.0085	0.01 ± 0.98	0.0001
D-carnosine	1.26 ± 0.88	7.89	0.0026	2.21 ± 0.99	n.d	0.0120	0.22 ± 0.09	0.0002
Carnosinol	36.39 ± 1.65	1.23	1.256	13.56 ± 2.12	3.56	0.0036	0.22 ± 0.09	0.0002
Histidine	8.92 ± 0.38	n.d.	0.014	2.14 ± 1.15	n.d	0.042	2.90 ± 0.36	0.0015
β-Alanine	0.67 ± 0.76	n.d.	0.0074	0.21 ± 0.30	n.d	0.057	1.01 ± 0.33	0.0005
β-Ala + His	1.28 ± 0.61	12.12	0.041	0.85 ± 0.33	9.58	0.036	4.48 ± 0.48	0.0025
Homocarnosine	0.28 ± 0.08	7.36	0.0067	0.30 ± 0.27	n.d	0.027	1.58 ± 1.11	0.0003
Anserine	2.68 ± 1.11	n.d.	0.0022	0.85 ± 0.09	n.d	0.081	5.80 ± 0.23	0.0038
N-acetyl carnosine	0.13 ± 1.73	n.d.	0.0004	0.11 ± 0.43	n.d	0.0084	5.44 ± 0.82	0.0042
Carnosinamide	48.78 ± 2.32	0.78	1.48	15.21 ± 2.86	2.15	0.055	8.46 ± 2.37	0.0078
Gly-His	19.30 ± 3.21	4.68	0.26	4.52 ± 1.09	6.96	0.072	9.72 ± 3.23	0.0099
Carcinine	0.69 ± 0.01	12.02	0.013	0.10 ± 0.03	n.d	0.0035	2.66 ± 0.27	0.0021
Pyridoxamine	2.47 ± 1.38	9.31	0.081	0.12 ± 0.12	10.78	0.063	2.15 ± 0.08	0.0017
Hydralazine	48.65 ± 4.19	0.85	2.58	14.21 ± 2.04	3.12	0.028	100.0	9.44
Aminoguanidine	34.72 ± 2.67	1.67	0.96	11.27 ± 1.99	4.21	0.063	12.79 ± 0.09	0.011
Metformin	2.79 ± 0.94	13.66	0.058	0.57 ± 0.17	9.05	0.086	3.05 ± 0.84	0.0019

Tab 4. Quenching activities of the RCS scavenger compounds tested towards MGO and pyridoxal as derived by both HPLC and competitive studies (MS).

4.1.c.3. Quenching activity towards HNE.

Tables 3,4 collect the quenching activities towards HNE and pyridoxal as derived by both HPLC and competitive studies (the latter only for HNE). They were obtained by monitoring the consumption percentages (Q% ± SD) of the carbonyl species after 3 and 24 h and considering several quencher/RCS ratios ranging from 1/10 to 10/1. For easy comparison, Table 2 summarizes these data focusing on the consumption percentages after 24 h and reporting (1) the consumption percentage averages as monitored by using an indicative 1/1 ratio ($Q_{1/1}$), (2) the extrapolated ratio (R_{50}) with which the quencher consumes the 50% of the tested carbonyl compound and (3) taking a cue from the Stern-Volmer constant (K_{SV}), commonly used to parameterize fluorescence quenching, a quenching constant (K_Q) is here proposed corresponding to the slope of the plot of $Q\%_0/Q\%$ versus the quencher/RCS ratio.

4.1.c.4. HNE Quenching by HPLC analyses.

As a preamble, it should be remembered that carnosine derivatives react with α,β-unsaturated aldehydes through a multi-step mechanism involving an initial reversible unsaturated imino intermediate followed by the key intramolecular Michael addition between the histidine imidazole ring and the acceptor β-carbon atom (Fig. 2) [8].

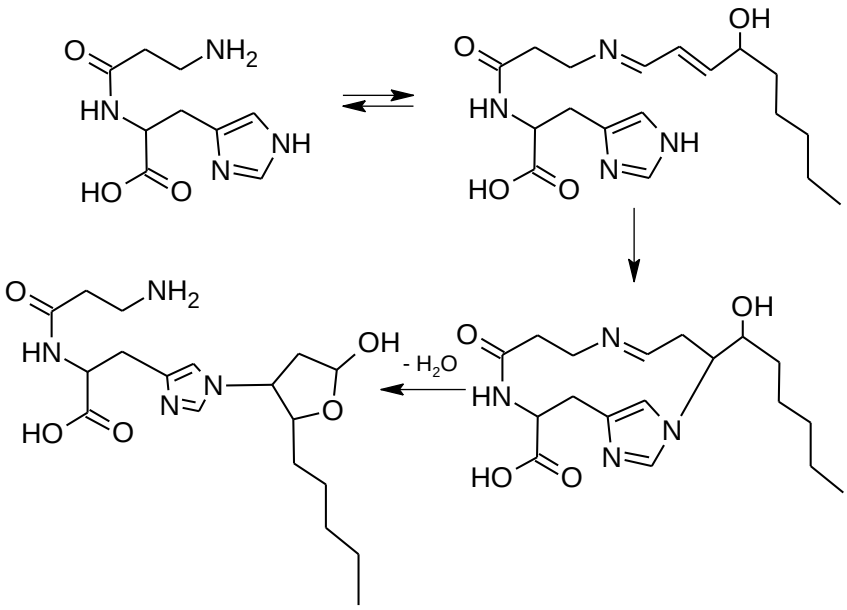

Fig 2. Reaction mechanism of the carnosine incubated with HNE

Several hitherto reported quenching activities have been obtained by HPLC analyses using an acidified mobile phase which hydrolyses the imino intermediates and so the monitored activities were ascribable only to the quencher's ability to yield the final Michael adduct[9].

To remain fully compatible to physiological conditions, the here reported activities (see Tab 2) are obtained using a mobile phase buffered at pH = 7.4. Hence, one may expect that the here reported activity is somewhat higher especially for those quenchers which easily form imino adducts regardless of their ability to transform them in stable Michael adducts. Albeit indirectly, the role of Schiff base formation at the equilibrium could be evaluated by considering the quenching of pyridoxal (Tab 2)

A bird's eye view of Table 2suggests that the $Q_{1/1}$ values are rather homogeneous and allow the tested quenchers to be roughly grouped into active ($Q_{1/1}$> 30), intermediate ($Q_{1/1}$ around 20) and inactive compounds ($Q_{1/1}$< 10), most derivatives belonging to the two extreme groups. Whereas, the R_{50} values and, even more so, the K_Q constants, accounting for more tested ratios, appear to be broadly distributed allowing a better differentiation of the examined quenchers. A clear example of these different distributions is offered by the physical mixture His + β-Ala, which shows a $Q_{1/1}$ value which is comparable to that of L-carnosine, but a K_Q constant which is about one fourth of that of L-carnosine. In this case, the difference evidenced by the K_Q values appears to be more reasonable and confirms the synergic effect of the two amino acids when fused in a dipeptide as extensively discussed in previous studies.

Regarding the length of the N-terminal residue, the reported data suggest that its extension (as seen in homocarnosine) is particularly detrimental, a result which can be explained by considering the stronger basicity (see Tab 1) of its amino group which prevents the imine formation. Conversely, shortening the N-terminal residue does not influence the quenching activity since Gly-His reports a reactivity comparable with that of L-carnosine. This result might be affected by the lower basicity of Gly-His, which promotes the imino formation regardless of the following Michael addition. Such a hypothesis is confirmed by the remarkable activity of gly-his towards pyridoxal (see Tab 3) as well as by the recently reported modest HNE quenching (about one half of L-carnosine) as obtained by gly-his in acidic condition.

A similar behaviour is shown by carnosinamide, the remarkable activity of which might be due to the sum of both the Michael adduct and the imine formation, the latter playing a predominant role as suggested by its significant activity towards pyridoxal (see Tab 3) and confirmed by the reported poor HNE quenching activity as monitored in acidic conditions. The formation of both the imine and Michael adduct between carnosinammide and HNE was then confirmed by the MS analysis of the reaction mixture after 24 hours of incubation. As shown in Fig. 2 the imine and Michael adducts were easily identified at m/z 365 and m/z 383, respectively, and the structures fully characterized by MS/MS analysis.

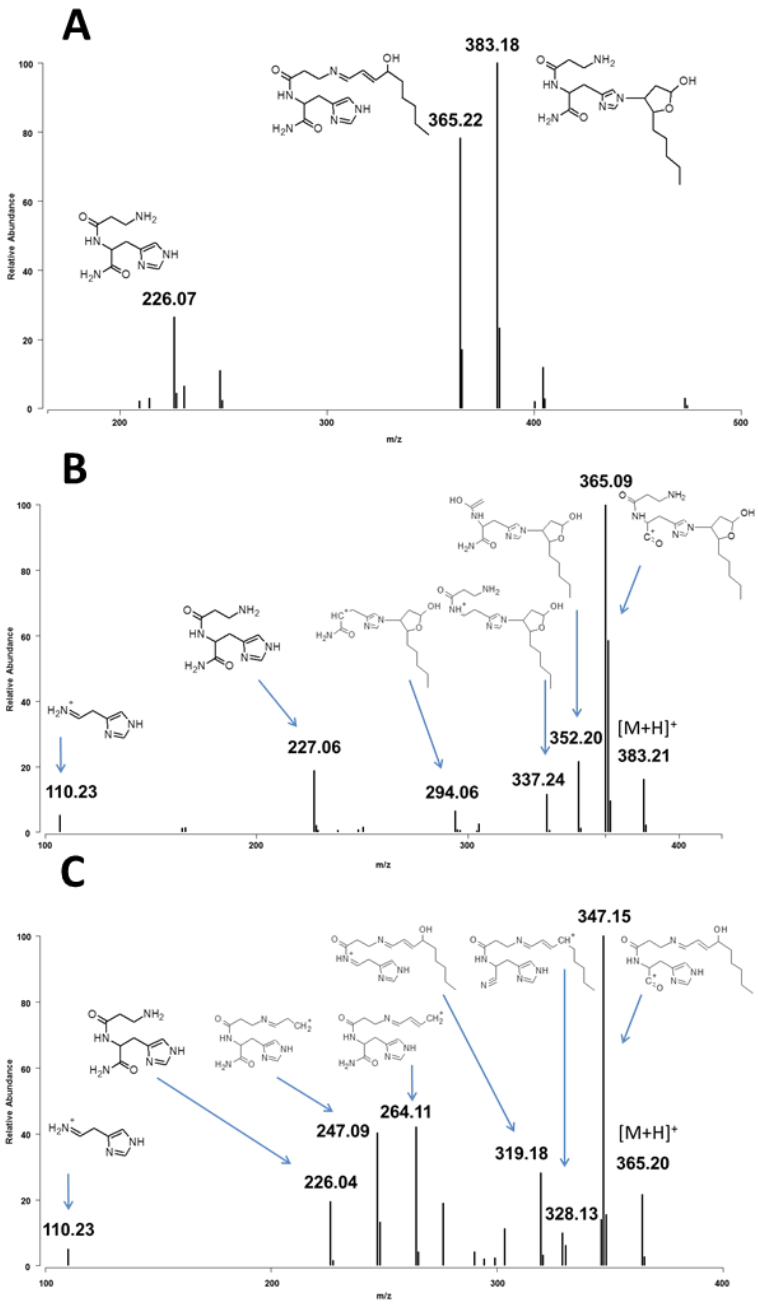

Fig 3. Mass spectra of the reaction mixture of carnosinamide-HNE after 24h of incubation at 37°C. A) mass spectrum of the reaction Mixture of carnosinamide-HNE characterized by the peaks m/z 226 attributed to the carnosinamide, m/z 365 attributed to the Schiff Base and m/z 393 attributed to the Michael Adduct. B) MS/MS spectrum of the Michael Adduct with am/z 393 (collision energy 30V) C) MS/MS spectrum of the Schiff Base with am/z 365 (collision energy 20V).

Taken together, the analyzed compounds confirm that the carboxylic function is not required for activity, a result which brings to mind the marked HNE quenching observed for the D-carnosine methyl ester. Nevertheless, the scarce activity of carcinine suggests that the carboxylic function cannot be completely removed, while it can be conveniently replaced by different H-bonding groups.

Such considerations led to the design of carnosinol, a carnosinase resistant peptidomimetic where the hydroxyl group replaces the carboxylic function of carnosine. Carnosinol was found significantly more reactive in respect to carnosine and this can be clearly addressed to the ability of the hydroxyl group to form an hemiacetal intermediate with HNE which catalyzes the Michael adduct formation.

Hence, regarding the HNE quenching mechanism of carnosinol we can propose one reaction mechanism similar to that already clarified for carnosine and based on the formation of an imine derivative that catalyse the Michael adduct as reported in the fig 4.

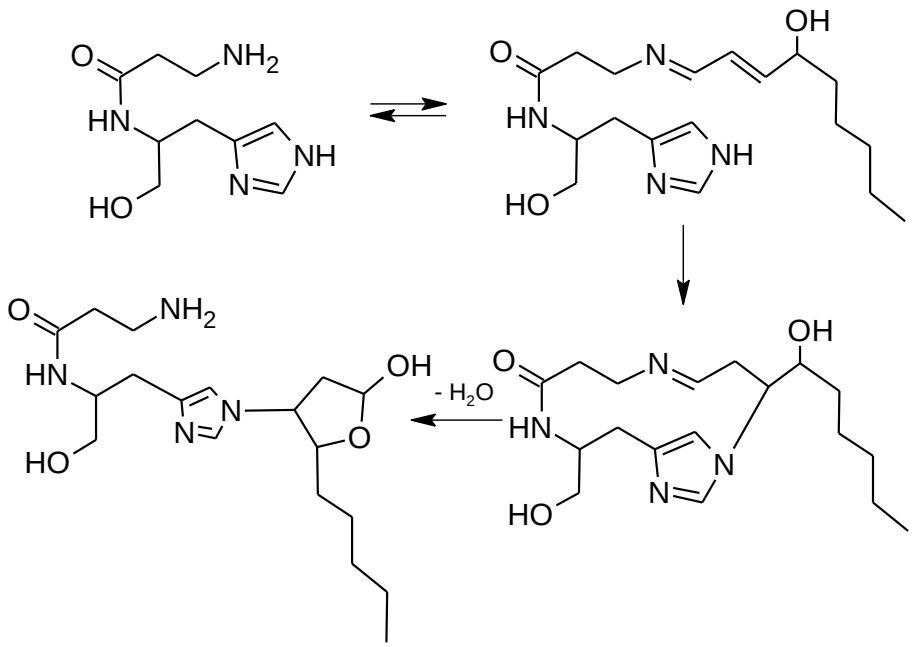

Fig 4. Reaction mechanism 1 of the carnosinol incubated with HNE through imino formation.

The higher quenching activity of carnosinol in respect to carnosine is explained by considering the ability of the hydroxyl group to form an unsaturated hemiacetal that catalyzes the Michael adduction through a mechanism proposed in fig. 4. In particular the hemiacetal intermediate dehydrates giving an unsaturated enol which is in equilibrium with the corresponding a,β unsaturated keto adduct which in turn condenses with the imidazole ring yielding the final Michael Adduct.

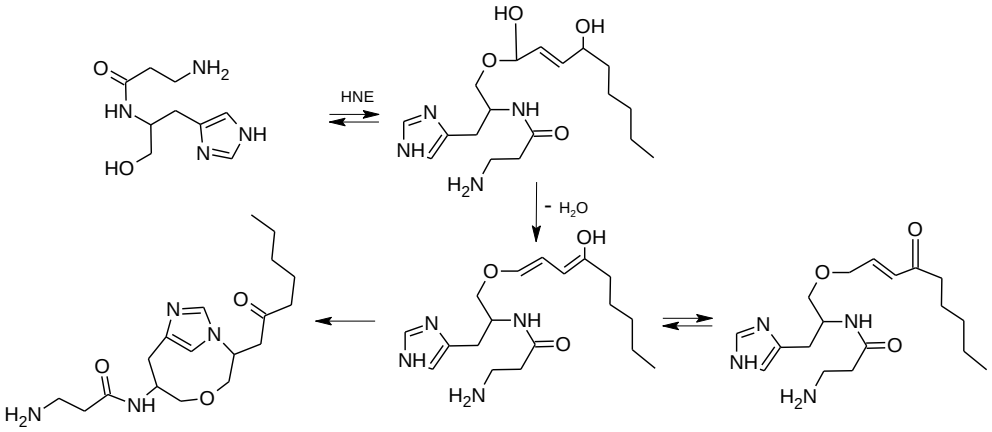

Fig .5 Reaction mechanisms 2 of the carnosinol incubated with HNE through hemiacetal formation.

Fig 5 shows the MS spectrum of the reaction mixture containing carnosinol and HNE. Besides the peak ion at *m/z* 213 referred to the unreacted carnosinol, two peaks are well detected at *m/z* 369 and 351 which can be attributed to the Schiff base and to the Michael adduct, respectively. Moreover, on the basis of the additional mechanism involving the hydroxyl group, The two peaks can also be attributed to the enol/keto-adduct at *m/z* 351 and to the unsaturated hemiacetal adduct at *m/z* 369 which are isobaric to the Schiff base and to Michael adduct, respectively. The structure of the four proposed reaction products were then confirmed on the basis of the MS/MS fragment ions and the attributed fragment ions are reported in Fig. 6.

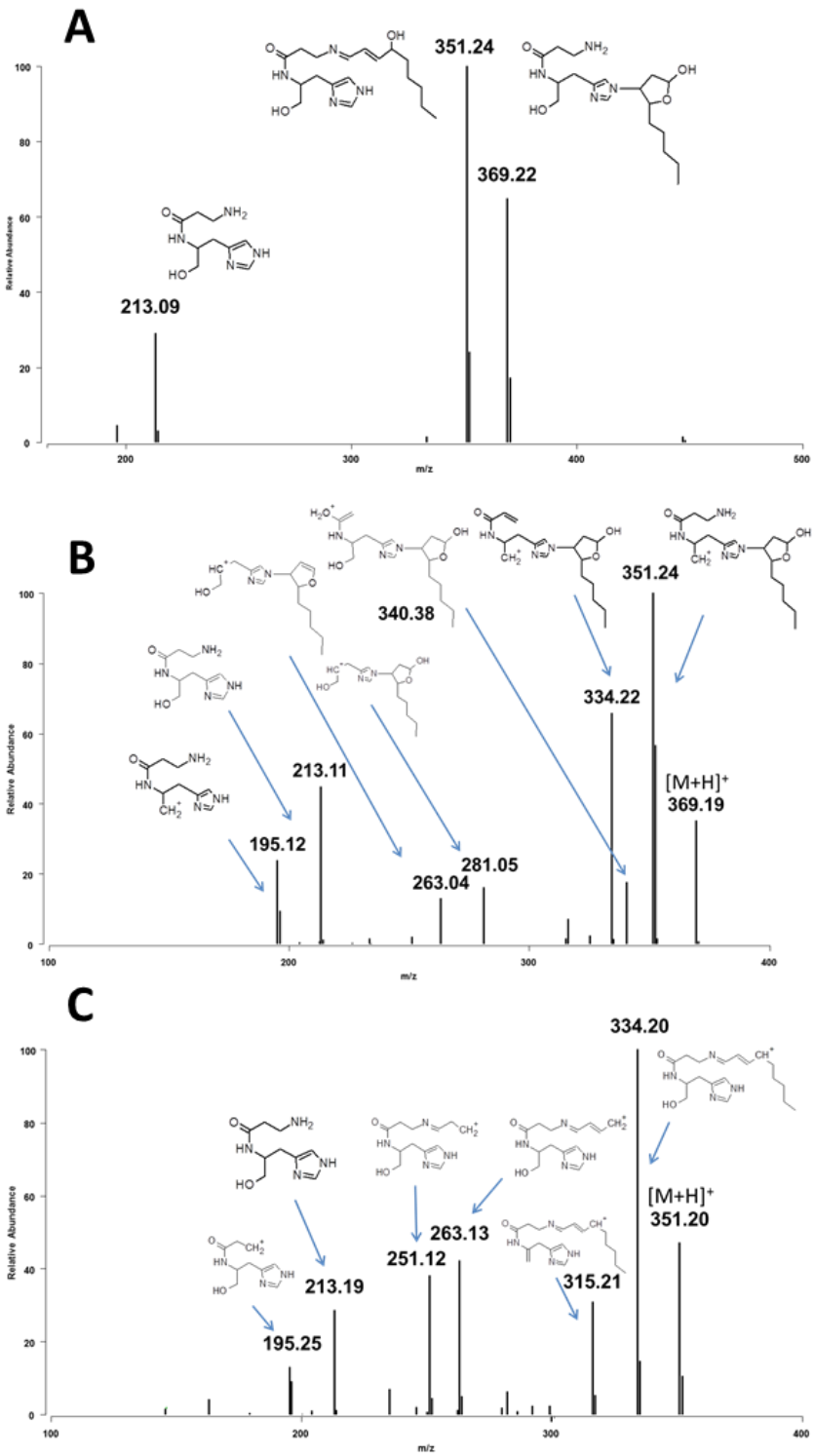

Fig 6. Mass spectra of the reaction mixture of carnosinol-HNE after 24h of incubation at 37°C. A) mass spectrum of the reaction Mixture of carnosinol-HNE characterized by the peaks at m/z 213 attributed to the carnosinol, m/z 351 attributed to the Schiff Base and m/z 369 attributed to the Michael Adduct. B) MS/MS spectrum of the Michael Adduct at m/z 369 (collision energy 35V) C) MS/MS spectrum of the Schiff Base at m/z 351 (collision energy 25V).

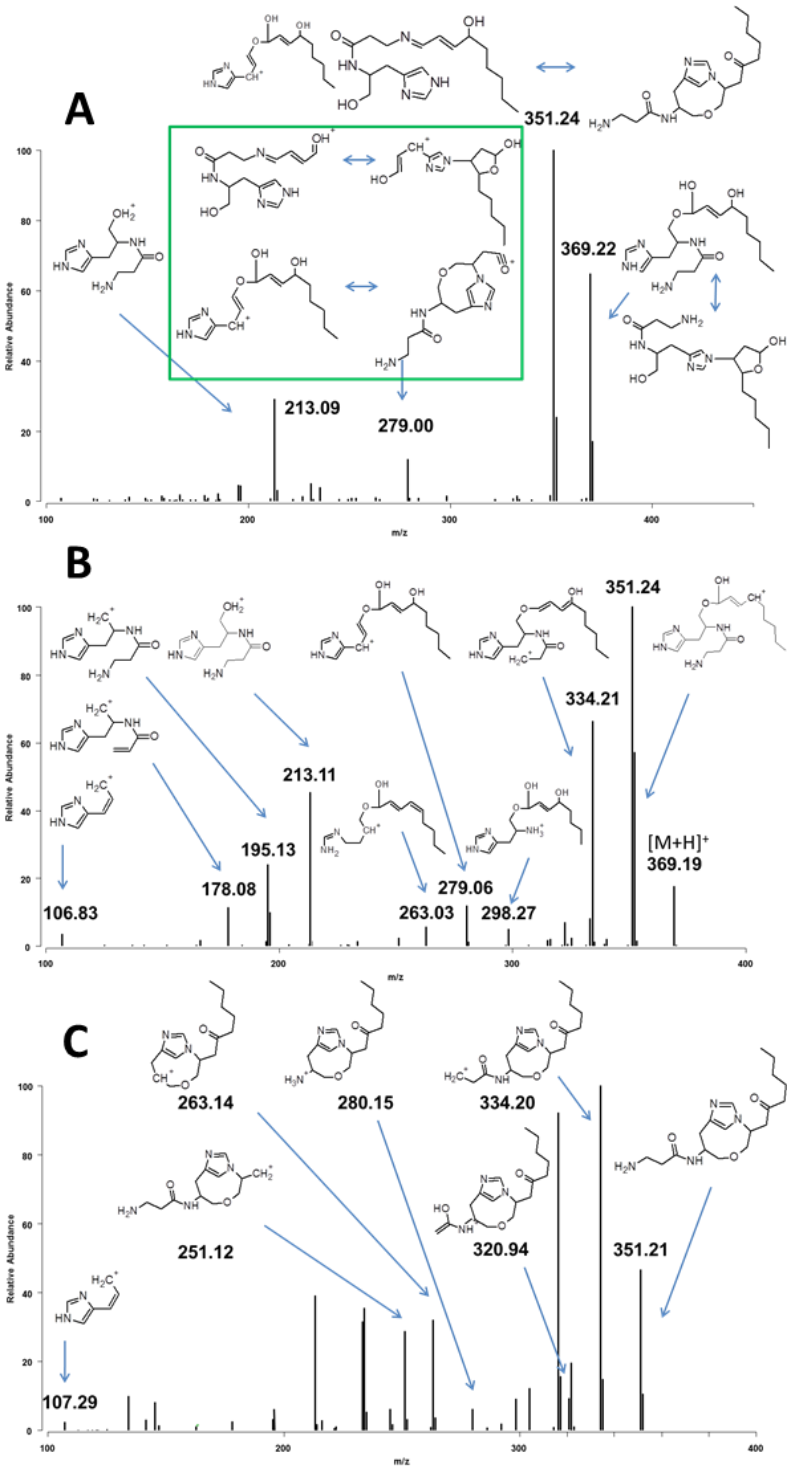

Fig 7. Mass spectra relative to the reaction mixture containing carnosinol and HNE incubated for24h at 37°C. A)mass spectrum of the reaction Mixture of carnosinol-HNE characterized by the peaks at m/z 213 attributed to the carnosinol, m/z 351 attributed to both the Schiff Base and enol/keto-adduct, m/z 369 attributed to both the Michael Adduct and the unsaturated hemiacetal adduct. B)MS/MS spectrum of hemiacetal with am/z 369 (collision energy 25V) C)MS/MS spectrum of the Michael Adduct derived from the unsaturated keto/enol with am/z 351 (collision energy 30V).

As mentioned above commenting on the activity of the physical mixture, the obtained results confirm the synergic effect of carnosine since the two amino acids alone show modest activity. Finally, the reported quenching activities confirm that L-carnosine and D-carnosine show a similar activity towards HNE, although fig 2 evidences a greater activity of L-carnosine at the highest ratios. This unexpected result suggests that the diasteroisomeric intermediates which form during the quenching mechanism may differ in their reactivity.

With regard to the reference compounds, hydralazine shows an impressive reactivity since it quenches almost all HNE in the reported 1/1 ratio even though such a reactivity can be due to the marked ability of the hydrazine function to give stable imino adducts as suggested by its marked quenching towards pyridoxal. Conversely, the other three compounds are substantially inactive thus indicating that their nucleophilic groups are able to yield neither stable imines nor Michael adducts.

4.1.c.5. HNE Quenching by MS competitive studies.

As we recently proposed, a more realistic picture of the quenching ability of the tested compounds can be given by competitive studies by which the activity of a given compound is evaluated by monitoring its capacity to inhibit the formation of the HNE induced adducts on a target protein, the human ubiquitin, whose carbonylation specifically involves Lys6 and His68, as recently investigated (see chapter 3.a.1.). These competitive data should be more realistic for two major reasons. First, the so obtained quenching activities account also for kinetic factors since slow reacting quenchers cannot compete with HNE thus providing lower quenching activity, regardless of their intrinsic reactivity which was already monitored by HPLC studies. Second and despite being measured at physiological pH, the reversible adducts (e.g. the Schiff bases) cannot compete at the equilibrium with protein carbonylation and thus these competitive activities should account only for the formation of stable and irreversible adducts (e.g. the Michael adducts).

Moreover, it should be noted that these results can be affected by nonspecific non-covalent interactions between protein and quencher. Such interactions can overestimate the quenching ability when they shield protein regions around the adducted residue(s), or they can underestimate activity when they involve unreactive protein regions by which they remain trapped. An illustrative example of this biasing protein-quencher interaction is provided by N-acetyl carnosine, which shows a modest albeit detectable activity even though its masked amino group should prevent the formation of the key imino intermediate. This result may be justified by considering that N-acetyl carnosine, due to its anionic state, stably interacts with the cationic residues on the protein surface, and thus the reactive Lys6 residue remains masked and less inaccessible to HNE.

Fig 3 and Tab 2 summarize the obtained data showing a broad distribution of the quenching activities thus allowing a clear differentiation of the tested compounds. As expected, the reported data are, on average, lower than the corresponding activities as derived by HPLC analyses. However, Tab 2 shows a remarkable correlation between the R_{50} values obtained by the two utilized approaches and the fact that these two parameters correlate despite their different nature can be seen as a mutual validation of the respective methods used to derive them.

The first consideration involves the two carnosine enantiomers which show the highest quenching activity even considering the reference compounds. This result can be easily explained considering that the impressive activity of hydralazine as observed by HPLC studies is largely influenced by its ability to yield stable but reversible imino adducts, while quenching of the carnosine enantiomers involves preferentially the irreversible Michael adducts.

With regard to the length of the N-terminal residue, the competitive data appear to be significantly different compared to those obtained by HPLC analyses. Indeed, both extension and shortening are here found to be detrimental even though the extension appears to possess a less negative effect

since homocarnosine retains a quenching activity which is about one half that of carnosine, while Gly-His shows a more marked drop in activity. This different result suggests that homocarnosine, although its greater basicity hampers the initial imino formation, can conveniently yield the final Michael adducts. Whereas, Gly-His, although its lower basicity promotes the initial imino formation, cannot easily give the final Michael adducts due to the instability of the constrained macrocyclic intermediates, a drawback affecting all carnosine derivatives in which β-Ala is replaced by an α-amino acid.

Similarly, carnosinamide appears to be less reactive in these competitive studies compared to the HPLC results. As recently reported, such a decrease in activity can be explained considering that the terminal amido group can stabilize π-π stacking contacts with the imidazole ring thus hampering its interaction with the acceptor β-carbon atom. The very poor activity of carcinine confirms that the carboxyl group can be modified but not completely removed.

Though showing some modest differences compared to HPLC data, these competitive results confirm the substantial inactivity of the single amino acids as well as of their physical mixture and reveal a group of carnosine derivatives (namely, anserine, homocarnosine and carnosinamide) which, while showing lower activity compared to that of carnosine, conserve a significant quenching activity which render them potential alternatives to carnosine itself. Carnosinol was confirmed the most reactive and efficient tested compound.

4.1.c.6. Pyridoxal Quenching by HPLC analyses and ligand selectivity.

Fig 4 and Tab 2 collect the obtained data concerning the consumption of pyidoxal at different ratios after 24 h. Since this quenching is an undesired feature, Tab 2 reports the consumption percentage averages as monitored by using the most challenging 10/1 ratio ($Q_{1/10}$ instead of $Q_{1/1}$ data) plus the corresponding K_Q constants. The corresponding R_{50} values are not reported since most compounds are too poorly reactive towards pyridoxal to extrapolate such a parameter.

Tab 2 reveals indeed that most of the tested compounds possess a very low quenching activity towards pyridoxal and only two quenchers, hydralazine and aminoguanidine, show a $Q_{10/1}$ value greater than 10%. Specifically, hydralazine shows a remarkable quenching activity towards pyridoxal, which is comparable to that towards HNE, as seen in their K_Q values, and renders the quencher unsafely unselective, a well-known problem first observed by Rumsby and Shepherd in 1979[10].

Similarly, the significant pyridoxal quenching exhibited by aminoguanidine can easily explain why its clinical trials were discontinued, even though the corresponding pyridoxal-aminoguanidine adduct was found to maintain a significant capacity to prevent neuropathy and cataract in diabetic rats which is ascribable to the pyridoxal's antioxidant activity. Finally, the obtained results confirm the satisfactory selectivity of both pyridoxamine and metformin thus explaining why pyridoxamine, while considering the cardiovascular adverse drug events typically related to compounds belonging to the vitamin B family, is under investigation in a trial involving 300 patients to further test the effects of pyridoxamine on the serum creatinine level[11].

All carnosine derivatives show very modest quenching activity towards pyridoxal even though one may note two compounds, namely Gly-His and carnosinamide, the $Q_{10/1}$ values of which approach the threshold of 10% thus representing the less selective carnosine derivatives. Interestingly, these two analogues show marked differences in HNE quenching between HPLC and competitive data further emphasizing their remarkable propensity to yield stable (but reversible) imino adducts. Nevertheless, their reactivity suggests different explanations. For Gly-His, it is ascribable to the lower basicity of its amino group which increases the relative abundance of its neutral and reactive form. Whereas, the reactivity of carnosinamide may be explained by supposing that its amino group, not involved in intramolecular ion-pairs, is more accessible regardless of its basicity.

The correlations between pyridoxal quenching and HPLC data for HNE quenching are documented by Tab 2 which shows a fair correlation between the corresponding $Q_{1/1}$ and $Q_{1/10}$ percentages (r^2 = 0.58) while there is no correlation between the corresponding parameters of pyridoxal quenching and MS competitive analyses (r^2 = 0.02). Overall, these results bring to mind the similarly poor correlations obtained by analysing proteinogenich istidine containing dipeptides and emphasize that

pyridoxal and HNE quenching occur through two completely distinct mechanisms since the former is a single step process not involving the irreversible Michael addition. Nonetheless, the HPLC data, when acquired at pH = 7.4, unavoidably account also for the reversible imino formation thus justifying the greater correlation as discussed above.

4.1.c.7. MGO Quenching by HPLC and MS competitive studies.

As ascribable in the case of HNE analysis, Tab 2 and 4 summarize the obtained data showing a broad distribution of the quenching activities thus allowing a clear differentiation of the tested compounds. As expected, the reported data are, on average, lower than the corresponding activities as derived by HPLC analyses. However, a remarkable correlation between the R_{50} values obtained by the two utilized approaches and the fact that these two parameters correlate despite their different nature can be seen as a mutual validation of the respective methods used to derive them.

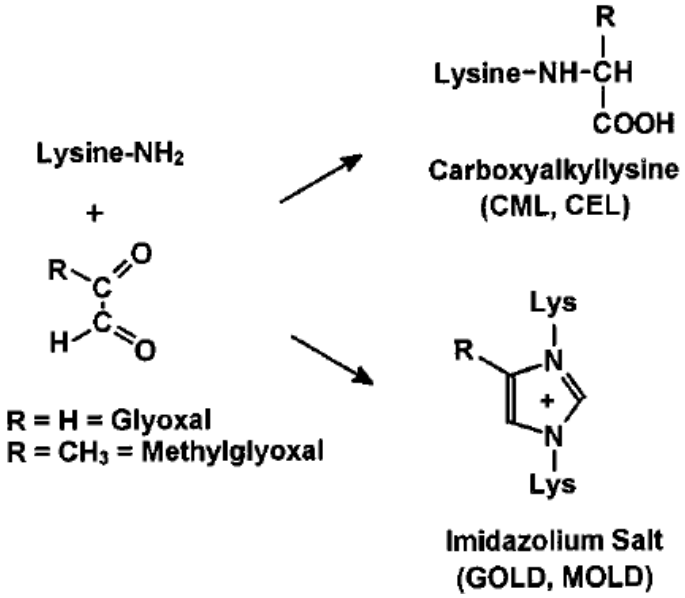

Fig 8. General scheme of the reaction products formation of glyoxal and gethylglyoxal with Lysine residues in protein.

As reported in Tab 4, contrary to what observed for HNE, L-car shows only a slight higher activity in respect to the mixture His + βAla, thus suggesting that the quenching activity towards MGO strongly depends on the amino group. The higher activity of β-Alain respect to His as MGO scavenger can be addressed to the large difference in the amino group basicity. The key effect of the amino group basicity on MGO quenching is clear shown by considering the following compounds: homocarnosine, L-carnosine, Gly-His where the quenching activity well correlates with the amino group basicity.

The high reactivity of carnosinamide further confirms the key role of the amino group. In particular the high reactivity of the carnosinamide can be ascribed to the fact that here the amino group is not involved in intramolecular salt bridge and thus is more susceptible to the reaction with MGO.

Other groups can clearly affect the reactivity of the sequestering agent towards MGO, such as the

imidazolic ring as highlighted by anserine.

The involvement of the amino group in the chemical reaction is well confirmed by the characterization of the adducts by MS. Most of the considered sequestering agents form a MOLD like reaction products that is generated by the reaction of the amino groups of two sequestering agents with two MGO, leading to an imidazolium cross-link.

As an example here below is the MS spectra of the reaction mixture (24 hrs incubation) of Gly-His with MGO which is characterized by the ion referred to the MOLD like adduct at m/z 461.89 and the di-imine-GOLD derivative formed by ring opening.

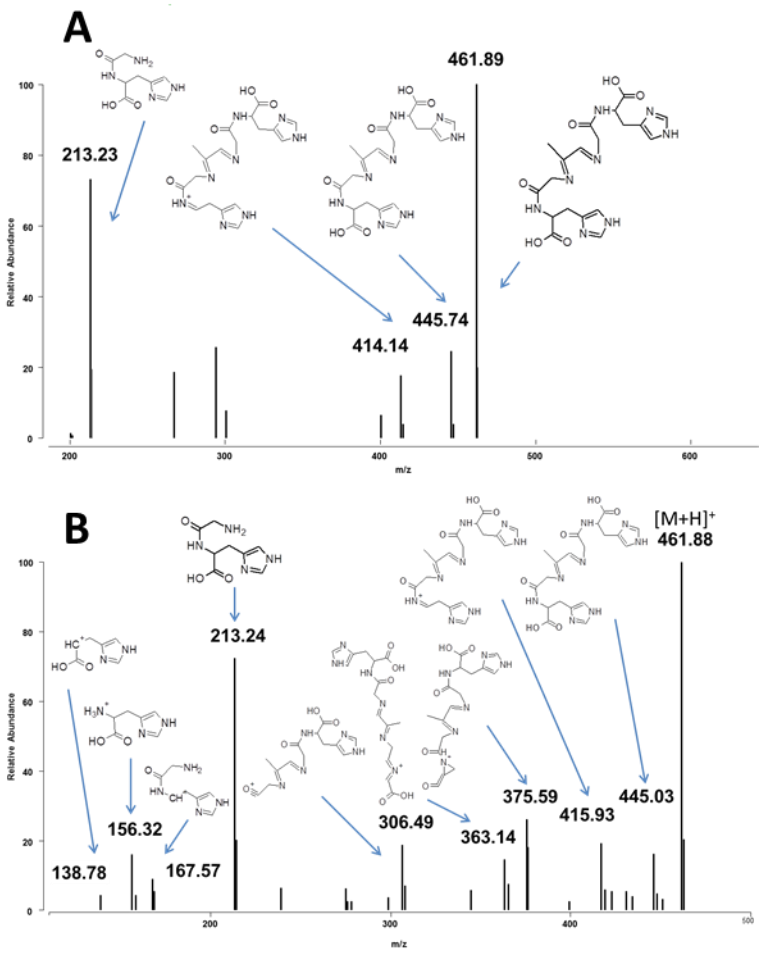

Fig 9. Mass spectra of the reaction mixture of Gly-His with MGO after 24h of incubation at 37°C. A) mass spectrum of the reaction mixture of Gly-His-MGO characterized by the peaks m/z 213 attributed to the Gly-His- m/z,461 attributed to the MOLD (Methylglyoxal-derived Lysine Dimer.) B) MS/MS spectrum of the MOLD adduct with am/z 461 (collision energy 30V).

The reaction mechanism is summarized in fig 10.

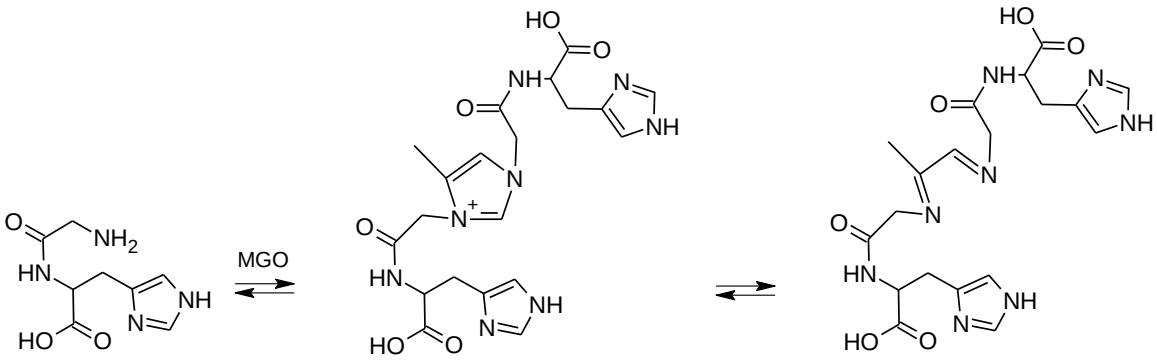

Fig 10. Reaction mechanism of the Gly-His incubated with MGO. The first reaction step leads to the MOLD like adduct (Methylglyoxal-derived Lysine Dimer) arising from the reaction between two molecules of Gly-His with two molecules of MGO, followed by the ring opening and the concomitant diimine-GOLD derivative formation.

The characterized adducts confirm the key role of the amino basicity which influences also the addition mechanisms. A similar reaction mechanism was also observed for carnosine although in this case the MOLD like adduct at *m/z* 501 was identified as the unique detectable adduct while the imino adducts was undetected to the higher basicity of carnosine that make the immine derivative less stable.

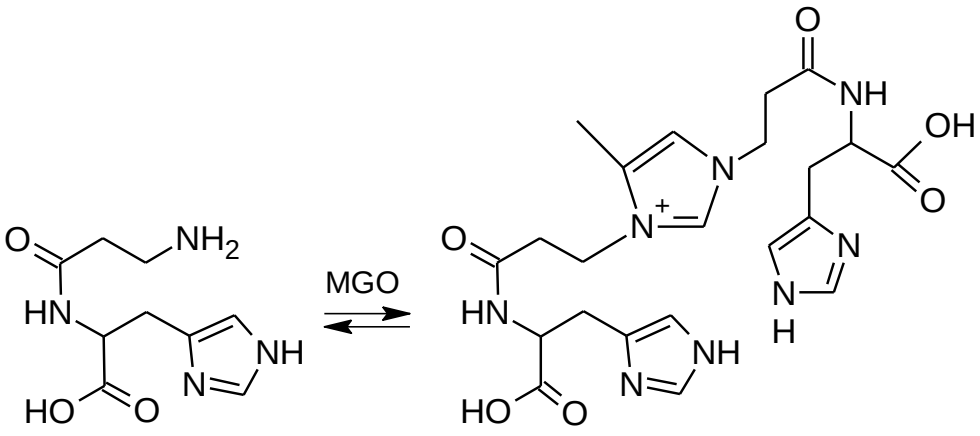

Fig 11. Reaction mechanism of carnosine with MGO forming the MOLD like adduct (Methylglyoxal-derived Lysine Dimer) adduct which is generated by the reaction between two molecules of carnosine with two molecules of MGO.

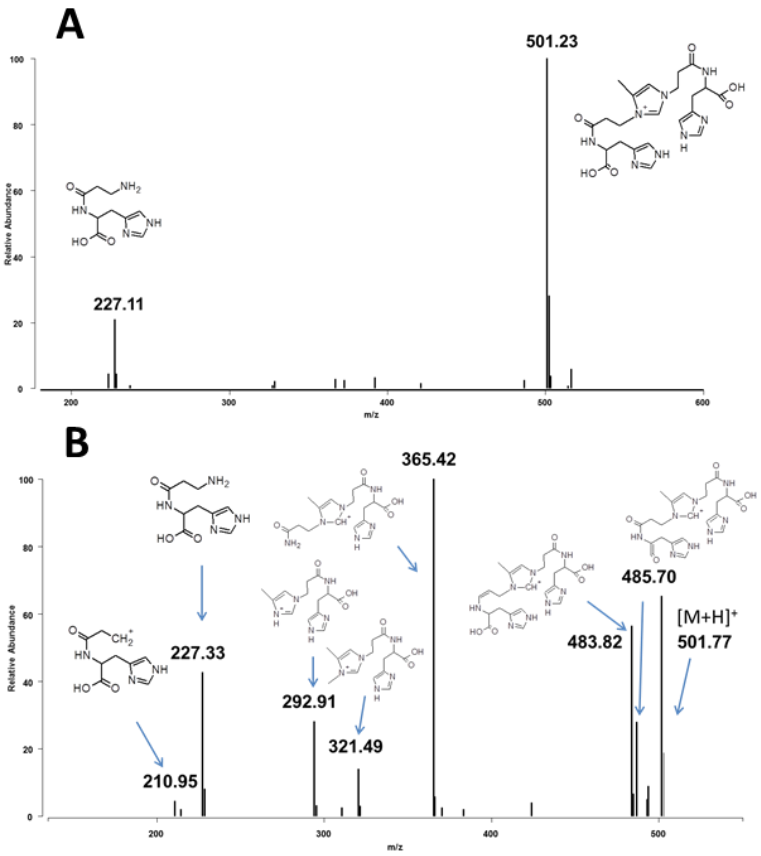

Fig 12. Mass spectra of the reaction mixture of carnosine-MGO after 24h of incubation at 37°C. A) mass spectrum of the reaction mixture of carnosine-MGO characterized by the peaks m/z 227 attributed to the carnosine, m/z 501 attributed to the MOLD (Methylglyoxal-derived Lysine Dimer.)B) MS/MS spectrum of the MOLD adduct with am/z 501 (collision energy 35V) .

Although the quenching mechanism for MGO appears to be strictly related to its condensation with the quencher's amino group, the marked difference between L-car and D-car suggest a more complex adducts which involve diastereoisomeric intermediates which render the quenching mechanism enantioselective.

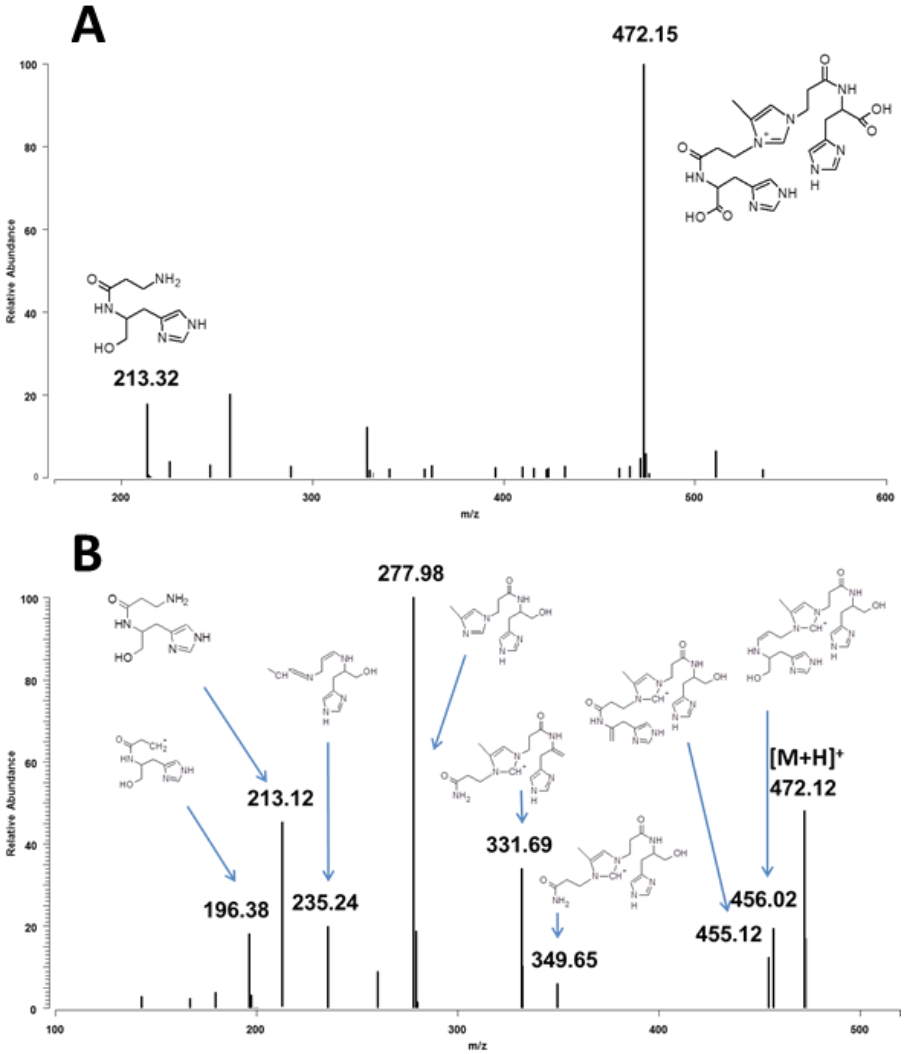

Fig 13. Mass spectra of the reaction mixture of carnosinol-MGO after 24h of incubation at 37°C. A) mass spectrum of the reaction mixture of carnosinol-MGO characterized by the peaks m/z 213 attributed to the carnosinol, m/z 472 attributed to the MOLD (Methylglyoxal-derived Lysine Dimer.)B) MS/MS spectrum of the MOLD adduct with am/z 472 (collision energy 35V).

Similalry to carnosine, also carnosinol reacts with MGO forming a MOLD like adduct at m/z 472.15 as shown in Fig 13 The higher quenching activity of carnsoinol in respect to carnosine could be explained by considering the presence of the hydroxyl function which can contribute to the MGO quenching through the formation of an hemiacetal adduct.

4.1.d. References.

[1] Vistoli G, De Maddis D, Cipak A, Zarkovic N, Carini M, Aldini G. (2013). "Advanced glycoxidation and lipoxidation end products (AGEs and ALEs): an overview of their mechanisms of formation". *Free Radic Res.*:47Suppl 1:3 - 27.

[2] Kierdorf K, Fritz G. (2013). "RAGE regulation and signaling in inflammation and beyond". *J Leukoc Biol.*;94(1):55 - 68.

[3] Aldini G, Vistoli G, Stefek M, Chondrogianni N, Grune T, Sereikaite J, Sadowska-Bartosz I, Bartosz G. (2013). "Molecular strategies to prevent, inhibit, and degrade advanced glycoxidation and advanced lipoxidation end products". *Free Radic Res.*;47 Suppl 1:93 - 137.

[4] Aldini G, Dalle-Donne I, Facino RM, Milzani A, Carini M. (2007). "Intervention strategies to inhibit protein carbonylation by lipoxidation-derived reactive carbonyls". *Med Res Rev.*;27(6):817 - 68.

[5] Boldyrev AA, Aldini G, Derave W. (2013). "Physiology and pathophysiology of carnosine". *Physiol Rev.*; 93(4):1803 - 45.

[6] Vistoli G, Carini M, Aldini G. (2012). "Transforming dietary peptides in promising lead compounds: the case of bioavailable carnosine analogs". *Amino Acids.*; 43(1):111-26

[7] Rees M, Vankuijk F, Siakotos A, and Mundy B. (1995). "Improved synthesis of various isotope labelled4-HYDROXYALKENALS and peroxidation intermediates". *Synthetic Communications*;25 :3225 - 3236.

[8] Aldini G, Carini M, Beretta G, Bradamante S, Facino RM. (2002). "Carnosine is a quencher of 4-hydroxy-nonenal: through what mechanism of reaction?". *Bioche Biophys Res Commun*. 15 ;298(5):699 - 706.

[9] Vistoli G, Orioli M, Pedretti A, Regazzoni L, Canevotti R, Negrisoli G, Carini M, Aldini G. (2009). "Design, synthesis, and evaluation of carnosine derivatives as selective and efficient sequestering agents of cytotoxic reactive carbonyl species". *ChemMedChem.*;4(6):967 - 75.

[10] Rumsby PC, Shepherd DM. (1979). "Effect of penicillamine, hydrallazine and phenelzine on the function of pyridoxal-5'-phosphate [proceedings]". *Br J Pharmacol.*;67(3):453 -454.

[11] Tanios BY, Ziyadeh FN. (2012). "Emerging therapies for diabetic nephropathy patients: beyond blockade of the Renin-Angiotensin system". *Nephron Extra.*;2(1):278 - 82.

4.2. Exploring the space of histidine containing dipeptides in search of novel efficient RCS sequestering agents.

4.2.a. Abstract.

The study reports a set of forty proteinogenic histidine-containing dipeptides as potential carbonyl quenchers. The peptides were chosen to cover as exhaustively as possible the accessible chemical space, and their quenching activities towards 4-hydroxy-2-nonenal (HNE) and pyridoxal were evaluated by HPLC analyses. The peptides were capped at the C-terminus as methyl esters or amides to favor their resistance to proteolysis and diastereoisomeric pairs were considered to reveal the influence of configuration on quenching. On average, the examined dipeptides are less active than carnosine (βAla + His) thus emphasizing the unfavorable effect of the shortening of the βAla residue as confirmed by the control dipeptide Gly-His. Nevertheless, some peptides show promising activities towards HNE combined with a remarkable selectivity. The results emphasize the beneficial role of aromatic and positively charged residues, while negatively charged and H-bonding side chains show a detrimental effect on quenching. As a trend, ester derivatives are slightly more active than amides while heterochiral peptides are more active than their homochiral diastereoisomer. Overall, the results emphasize that quenching activity strongly depends on conformational effects and vicinal residues (as evidenced by the reported QSAR analysis), offering insightful clues for the design of improved carbonyl quenchers and to rationalize the specific reactivity of histidine residues.

4.2.b. Introduction.

Reactive carbonyl species (RCSs) are electrophilic molecules which react with nucleophilic groups in proteins yielding oxidative-based non-enzymatic protein adducts[1-3]. These covalent adducts can be subdivided into two major classes depending on the source of the reactive species. Advanced glycation end products (AGEs) are generated by sugars or sugar derivatives including di-carbonyl derivatives such as glyoxal (GO), methylglyoxal (MGO), and 3-desoxyglucosone (3-DG), while lipid-oxidation end products (ALEs) are formed by the oxidative reactions of lipids comprisingα,β-unsaturated carbonyls such as 4-hydroxy-2-nonenal (HNE),4-oxo-2-nonenal (ONE) and acrolein (ACR)[4, 5]. AGEs and ALEs are involved in oxidative cellular damage through different mechanisms[6] including protein dysfunction, protein oligomerization and fibrillogenesis[7], altered signal transduction, immune response[8] and activation of the receptor for AGEs (RAGE)which is a type I transmembrane glycoprotein of the immunoglobulin superfamily of cell surface receptors[9]. AGEs and ALEs have been widely accepted as biomarkers for oxidative-based diseases[10]. Moreover, taking into account the most recent studies reporting that AGEs and ALEs are involved in the pathogenesis of several diseases, including diabetes and arteriosclerosis, they are now also considered as promising targets for therapeutic intervention. This is promoting the design of carbonyl scavengers able to trap RCSs converting them into nontoxic and easily excretable derivatives so inhibiting protein carbonylation and all downstream pathways [11,12].

Although clinical investigations are still very limited, several *in vitro* and *in vivo* animal studies demonstrated that carnosine (βAla-His), an endogenous dipeptide found in millimolar concentrations in some tissues such as brain, heart and skeletal muscles[13, 14], is able to detoxify RCS, inhibiting AGEs and ALEs formation and restraining oxidative-based diseases. The mechanism by which carnosine prevents AGEs and ALEs formation is still under investigation and the involvement of multiple molecular mechanisms should be considered, given that the formation of AGEs and ALEs can involve different reactions and several catalysts including transition metals [15, 16]. Nevertheless, there is enough evidence to indicate that carnosine acts by a direct quenching mechanism, at least for α,β-unsaturated aldehydes as clearly demonstrated by two independent groups[17, 18].

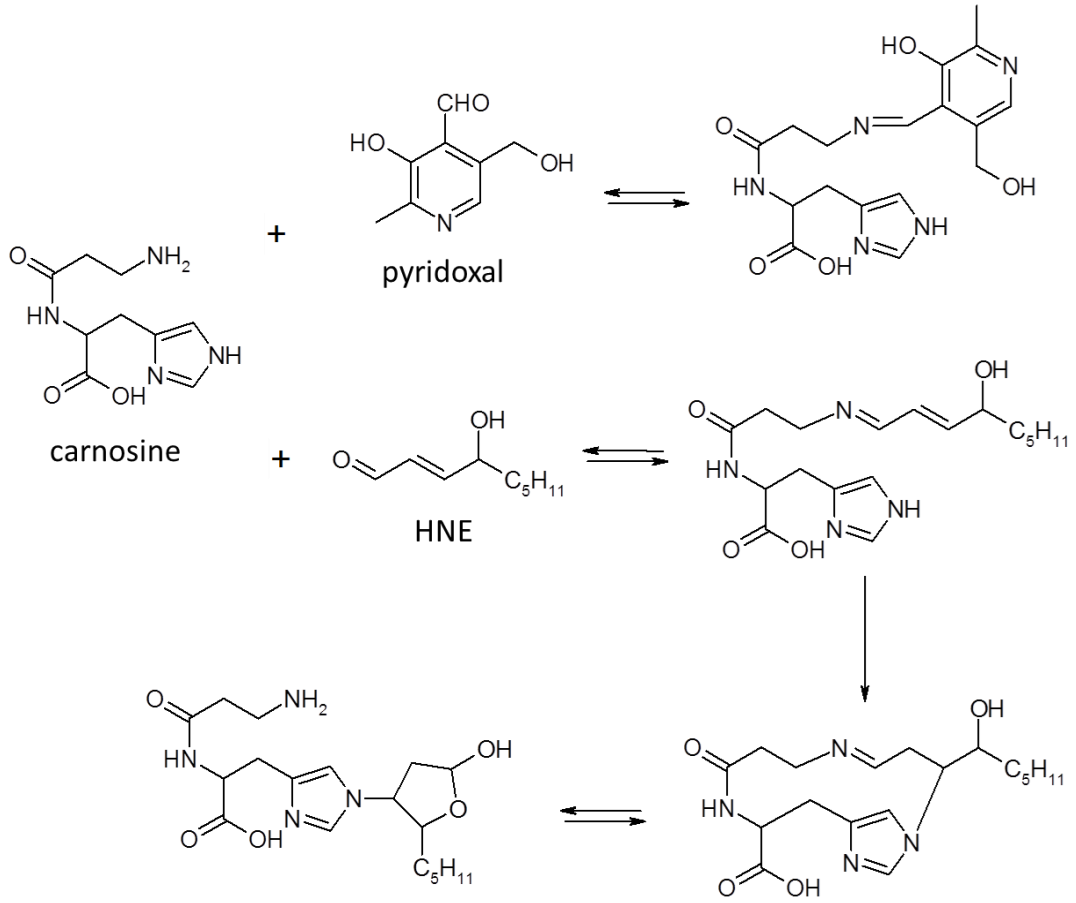

Fig 1. Quenching mechanisms of carnosine with HNE and pyridoxal. One may note that quenching of pyridoxal involves a reversible condensation which yields the corresponding imine adduct, whereas HNE quenching occurs through a multi-step mechanism involving firstly the reversible imine intermediate, then the key intramolecular Michael addiction and lastly the hydrolysis of imine group to give the final hemiacetal adduct.

As shown by Fig 1, carnosine reacts with α,β-unsaturated aldehydes through a multi-step mechanism involving the initial formation of a reversible unsaturated imino intermediate followed by the key intramolecular Michael addition between the histidine imidazole ring and the acceptor β-carbon atom. The imino intermediate acts as an intramolecular catalyst promoting a stable approach between the two reacting centers, thus explaining why a mixture of the two separate amino acids (βAla + His) does not possess a significant quenching activity. Similarly, the reversible nature of the imino intermediate can explain why carnosine selectively quenches reactive α,β-unsaturated carbonyls without stably trapping physiological carbonyl compounds[19].

Despite these promising results, the beneficial activity of carnosine is limited in humans due to its unfavorable pharmacokinetic profile. Indeed, carnosine is actively absorbed by peptide transporters

(hPepT1) [20] but immediately hydrolyzed in human plasma to its constituent amino acids by specific dipeptidases such as serum carnosinase (CN1) [21]. Considering the therapeutic interest of carnosine, it comes as no surprise that many analogues have been reported in the last few years. As recently reviewed[22], these derivatives have been designed with a view to A) increasing quenching activity, B) maintaining the mentioned selectivity, and C) ensuring a satisfactory oral bioavailability by preventing carnosinase-catalyzed hydrolysis while preserving active absorption by hPepT1. A critical analysis of all reported carnosine analogues[22], combined with computational studies involving serum carnosinase and peptide transporters[23-25], revealed that the carboxyl terminus and the β-alanine carbon skeleton can be largely modified to improve pharmacokinetic profile without detrimentally affecting quenching activity. Notably, C-terminus capping is a well-known strategy to enhance plasma stability by hampering peptide recognition by all hydrolases, thus suggesting that such a modification should prevent the hydrolytic effects of both specific carnosinases and nonspecific peptidases[26]. Conversely, the primary amino group and the imidazole ring are mandatory for quenching activity and cannot be modified without markedly altering efficiency and/or selectivity. However, it is worth observing that all proposed derivatives modified at the β-alanine residue were produced by replacing it with other β-amino acids, while the possibility of replacing β-alanine with proteinogenic α-amino acids has never been examined comprehensively.

On these bases, the present study was undertaken to investigate the quenching activity of proteinogenic histidine-containing dipeptides exploring as exhaustively as possible their accessible chemical space. Since the carnosine carboxyl group is not required for carbonyl scavenging and its modifications can improve the resulting pharmacokinetic profile (see above), the dipeptides were prepared with the C-terminus capped by a methyl ester or a primary amido group so as to study dipeptides which should be still recognized by peptide transporters and resistant to proteolysis. Moreover, the study considered diastereoisomeric pairs of dipeptides produced by alternating the absolute configuration of the histidine residue with a view to revealing the effect of configuration on quenching activity. Indeed, while the two carnosine enantiomers have the same quenching activity[27], a result easily explainable since two enantiomers must possess the same chemical reactivity, the introduction of a second chiral center should allow diastereoisomeric differences useful for a better understanding of the precise scavenging mechanism.

The results obtained in this work should provide new clues to design carnosine analogues which, while maintaining the same reactive moieties, are structurally quite different compared to the parent compound. Finally, the quenching activity of these proteinogenic dipeptides could improve our understanding of the factors influencing protein carbonylation, showing in particular whether dietary or endogenous proteins can become detoxifying agents after partial digestion.

4.2.c. Experimental.

4.2.c.1. Reagent and materials.

4.2.c.1.1. Chemicals.

The forty analyzed dipeptides (twenty diastereoisomeric pairs) are listed in Tab 1. The twenty methyl esters (Tab 1A, of general formula NH_2-*L*-X-(*L* or *D*)-His-OMe) were synthesized as described in a previous study [39], while the twenty amides (Tab 1B, of general formula NH_2-*L*-X-(*L* or *D*)-His-NH_2) were purchased from EZBiolab (EZBiolab Inc, Carmel, IN, USA)with a purity greater than 95%. Lastly, Gly-His was purchased by Sigma-Aldrich (St Louis, MO, USA). HNE was prepared from synthesized 4-hydroxy-non-2-enal diethylacetal as previously described [36] and quantitated by UV spectroscopy (λ max 224 nm; ε= 13.75 x 10^4 cm^{-1} M^{-1}).

4.2.c.1.2. Quenching activity and selectivity by HPLC studies.

The reactivity of each dipeptide toward 4-hydroxy-2-nonenal (HNE, quenching activity) was evaluated by measuring the HNE consumption (50 µM in 10 mmol PBS, pH 7.4) in the presence of the tested compound (1 mM) during a fixed incubation time (180 min, T = 37 ° C). HNE consumption was determined by HPLC using a quaternary pump HPLC system and a PDA detector (Surveyor LC system, ThermoQuest, Milan, Italy) set at 224 nm. Separations were done by reversed-phase elution with a Phenomenex Synergy Fusion column (150 mm x 2 mm i.d.,4 µm) protected by a Synergy Fusion R-P guard column (CPS Analitica, Milan Italy), thermostated at 37°C, and using H_2O/CH_3CN/ HCOOH, 40/60/0.1 (v/v/v) as mobile phase at a flow rate of 0.25 ml/min. Selectivity was determined after the same incubation time and using pyridoxal (PYR) as the target aldehyde (as represented in Fig 1). Pyridoxal consumption was determined by HPLC using a fluorimetric detector as previously reported[40]. All results are reported as percentages of aldehyde consumption with respect to a blank incubated in the absence of the tested compound.

4.2.c.1.3. Serum stability.

Serum stability was evaluated by incubating the target peptide (50 µm final concentration) in human serum from healthy donors (30–40 years). After incubation for 30 min at 37°C, the incubation mixture was chilled in ice, spiked with Tyr-His as internal standard (50 µM final concentration), deprotonated by perchloric acid (PCA, 700 mM final concentration), and centrifuged at 18000 rpm (30000 g) for 10 min. The supernatants were then diluted 1:1 (v/v) with mobile phase A (CH_3CN/H_2O/heptafluorobutyric acid 90:10:0.1 v/v/v), filtered through 0.2 µm filters, and then injected into the LC–MS system. Analyses were performed using a ThermoFinnigan Surveyor LC system equipped with a quaternary pump, a Surveyor autosampler, a vacuum degasser, and connected to a TSQ Quantum Triple Quadrupole Mass Spectrometer (ThermoFinnigan Italia, Milan, Italy). Chromatographic separations were done by reverse phase elution with a Phenomenex Sinergy polar-RP column (150mm×2mm i.d.; particle size 4µm) (Chemtek Analytica, Anzola Emilia, Italy) protected by a polar-RP guard column (4mm×2mm i.d.; 4µm) kept at 25 °C and by a gradient elution from 100% phase A to 80% phase B (CH_3CN) in 12 min at a flow rate of 0.2 ml min^{-1} (injection volume 10 µl); the composition of the eluent was then restored to 100% A within 1 min, and the system was re-equilibrated for 6 min. The mass spectrometer was equipped with an electrospray interface (ESI), which was operated in the positive-ion mode, and controlled by Xcalibur software (version 1.4).The samples rack was maintained at 4 °C. ESI interface parameters (positive-ion mode) were set as follows: middle position; capillary temperature 270 °C; spray voltage 4.0 kV. Nitrogen was used as the nebulizing gas at the following pressure: sheath gas 30 psi; auxiliary gas 5 a.u. MS conditions and tuning were optimized for each peptide by mixing through a T-connection the water-diluted stock solutions of analytes (flow rate 10 µl/min), with the mobile phase A maintained at a flow rate of 0.2 ml/min: the intensity of the $[M+H]^+$ ions of the target peptide were monitored and adjusted to the maximum by using the Quantum Tune Master® software. The serum content of each peptide was determined by recording the single ion traces (SICs) relative to the $[M+H]^+$ in positive ion mode and using Tyr-His as internal standard. The results are reported as percentage remaining of the tested compound with respect to a blank incubated in the absence of serum.

4.2.c.1.4. Computational studies.

The amide derivatives were analyzed by the same computational procedures as carried out for the methyl esters in the previous study[39]. In detail, they underwent MD simulations in vacuo, in water and in chloroform to investigate their dynamic behavior in media of different polarity. The MD runs lasted for 10 ns and the computational details can be found elsewhere[39].
The reported predictive equations were developed by using the property averages and ranges as obtained by above mentioned MD simulations as well as a set of well-known 2D/3D descriptors as computed by the VEGA suite of programs[47]. Moreover and since all tested peptides underwent MD runs, all considered conformer-dependent 3D descriptors were calculated by averaging the corresponding values for all frames memorized during MD simulations in vacuo. As evidenced by previous analyses[48], such averages should be indeed more informative than a single property value albeit computed for the lowest energy conformation.

As indicated above, the equations were iteratively generated by multiple linear regression analysis as implemented in the Analyse-it program (Analyse-it Software, Ltd., Leeds, UK). The equations included at most four non-interrelated (i.e. variance inflation factor, VIF, greater than 5) independent variables automatically selected from among the 35 molecular descriptors as described above.

4.2.d. Results.

4.2.d.1. Overview.

The forty dipeptides were protected either as methyl esters (Tab S1A) or as primary amides (Tab S1B). These protecting groups were chosen following a recent study on D-carnosine prodrugs which evidenced that D-carnosine methyl ester is completely stable in human plasma and possesses a quenching activity almost identical to that of unmodified D-carnosine[28]. Similarly, Bertinaria and co-workers reported a set of amide analogues generated by coupling the carnosine carboxyl group with bulky primary amines[29]; these compounds were found to be stable but to have a quenching activity somewhat weaker than that of carnosine. Collectively, these results confirm that C-terminus modification is a suitable strategy to ensure plasma stability (as experimentally confirmed for some dipeptides, see below) and suggest that the smaller the protecting group the greater the quenching activity thus rationalizing the modifications exploited here.

Table S1A. Methyl esters					
Dipeptide	**HNE**		**PYR**		**HNE/PYR**
	quenching	**Dev. Std**	**quenching**	**Dev. Std**	
Carnosine	48.20	---	5.57	---	8.65
Gly-His	9.11	0.75	3.77	0.55	2.42
L-Asn-*L*-His-OMe	9.59	3.08	1.00	0.44	9.59
L-Asn-*D*-His-OMe	9.50	3.27	1.14	0.64	8.33
Δ (Asn-His-OMe)	+0.09	p > 0.05	-0.14	p > 0.05	+1.26
L-Cys-*L*-His-OMe	100.00	---	25.26	1.56	3.96
L-Cys-*D*-His-OMe	100.00	---	40.78	0.73	2.45
Δ (Cys-His-OMe)	0.00	ND	-15.52	**p < 0.05**	+1.51
L-Glu-*L*-His-OMe	12.21	4.37	0.76	0.78	16.07
L-Glu-*D*-His-OMe	13.12	2.15	0.73	1.19	17.97
Δ (Glu-His-OMe)	-0.91	p > 0.05	+0.03	p > 0.05	-1.91
L-His-*L*-His-OMe	6.00	1.75	1.82	1.14	3.30
L-His-*D*-His-OMe	8.86	2.13	7.70	0.78	1.15
Δ (His-His-OMe)	-2.86	p > 0.05	-5.88	**p < 0.05**	+2.15
L-Lys-*L*-His-OMe	31.27	1.06	1.87	0.54	16.72
L-Lys-*D*-His-OMe	10.20	0.98	0.35	0.11	29.14
Δ (Lys-His-OMe)	+21.07	**p < 0.05**	+1.52	**p < 0.05**	-12.42
L-Met-*L*-His-OMe	0.17	0.80	2.61	0.17	0.07
L-Met-*D*-His-OMe	1.81	1.49	3.11	0.29	0.58
Δ (Met-His-OMe)	-1.64	p > 0.05	-0.50	**p < 0.05**	-0.52
L-Ser-*L*-His-OMe	5.18	0.14	0.10	0.65	51.80
L-Ser-*D*-His-OMe	5.91	0.37	2.08	1.55	2.84
Δ (Ser-His-OMe)	-0.73	p > 0.05	-1.98	p > 0.05	+48.96
L-Trp-*L*-His-OMe	11.71	2.51	4.20	0.23	2.79
L-Trp-*D*-His-OMe	18.83	3.75	5.81	0.55	3.24
Δ (Trp-His-OMe)	-7.12	**p < 0.05**	-1.61	**p < 0.05**	-0.45
L-Tyr-*L*-His-OMe	12.53	0.78	4.02	0.29	3.12
L-Tyr-*D*-His-OMe	27.44	1.08	1.29	1.08	21.27
Δ (Tyr-His-OMe)	-14.91	**p < 0.05**	+2.73	**p < 0.05**	-18.15
L-Val-*L*-His-OMe	4.97	2.46	0.87	0.42	5.71
L-Val-*D*-His-OMe	16.92	1.27	3.62	4.27	4.67
Δ (Val-His-OMe)	-11.95	**p < 0.05**	-2.75	p > 0.05	+1.04
Means	20.31± 28.31		5.46 ± 9.94		10.24 ± 12.64
(*L*, *L*) Means	19.36 ± 29.53		4.25 ± 7.51		11.31 ± 15.32
(*L*, *D*) Means	21.26 ± 28.59		6.66 ± 12.22		9.17 ± 10.01
Δ Mean	-1.90 ± 9.64		-2.41 ± 5.18		+2.15 ± 17.79

Table S1B. Amides					
Dipeptide	**HNE**		**PYR**		**HNE/PYR**
	quenching	**Dev. Std**	**quenching**	**Dev. Std**	
L-Gln-*L*-His-NH2	9.37	0.56	2.65	0.64	3.54
L-Gln-*D*-His-NH2	14.76	0.68	1.57	1.44	9.40
Δ (Gln-His-NH2)	-5.39	**p < 0.05**	1.08	p > 0.05	-5.87
L-Cys-*L*-His-NH2	100	---	27.7	0.96	3.61
L-Cys-*D*-His-NH2	100	---	37.2	0.84	2.69
Δ (Cys-His-NH2)	0.00	ND	-9.50	**p < 0.05**	+0.92
L-Asp-*L*-His-NH2	5.99	0.92	1.49	0.97	5.16
L-Asp-*D*-His-NH2	5.98	0.58	1.16	1.31	4.02
Δ (Asp-His-NH2)	0.01	p > 0.05	0.33	p > 0.05	+1.14
L-His-*L*-His-NH2	9.81	0.21	7.86	0.32	1.35
L-His-*D*-His-NH2	9.16	0.6	7.28	0.66	1.26
Δ (His-His-NH2)	0.65	p > 0.05	0.58	p > 0.05	+0.01
L-Lys-*L*-His-NH2	15.72	0.27	0.41	0.56	38.34
L-Lys-*D*-His-NH2	4.16	0.45	0.75	0.41	5.55
Δ (Lys-His-NH2)	11.56	**p < 0.05**	+0.34	p > 0.05	-32.79
L-Trp-*L*-His-NH2	8.62	0.12	1.86	0.74	6.01
L-Trp-*D*-His-NH2	11.17	0.72	0.13	0.05	86.20
Δ (Trp-His-NH2)	-2.55	**p < 0.05**	1.76	**p < 0.05**	-80.19
L-Thr-*D*-His-NH2	12.12	0.81	6.62	0.33	1.83
L-Thr-*L*-His-NH2	3.90	0.58	1.42	0.83	2.75
Δ (Thr-His-NH2)	-8.22	**p < 0.05**	-5.20	**p < 0.05**	+0.92
L-Arg-*L*-His-NH2	7.79	0.72	0.26	0.12	29.96
L-Arg-*D*-His-NH2	12.0	0.63	0.43	0.2	27.91
Δ (Arg-His-NH2)	-4.21	**p < 0.05**	-0.17	p > 0.05	-2.05
L-Phe-*L*-His-NH2	9.79	0.47	1.22	0.6	8.02
L-Phe-*D*-His-NH2	6.7	0.46	0.7	0.08	9.57
Δ (Phe-His-NH2)	-3.09	**p < 0.05**	-0.52	p > 0.05	+1.55
L-Ile-*L*-His-NH2	7.09	0.79	2.02	0.73	3.51
L-Ile-*D*-His-NH2	5.13	0.15	0.59	0.34	8.69
Δ (Ile-His-NH2)	1.96	**p < 0.05**	1.43	**p < 0.05**	-5.19
Means	17.96 ± 28.24		5.17 ± 9.74		13.25 ± 20.13
(*L*, *L*) Means	18.63 ± 28.72		5.21 ± 8.30		10.13 ± 12.95
(*L*, *D*) Means	17.29 ± 29.28		5.12 ± 11.45		15.81 ± 25.89
Δ Mean	-0.93 ± 5.37		-0.99 ± 3.57		-12.15 ± 26.03

Table S1C. Overall means			
Dipeptide	**HNE**	**PYR**	**HNE/PYR**
Overall mean	19.14 ± 27.93	5.31 ± 9.72	11.74 ± 16.61
Overall means of esters	20.31 ± 28.31	5.46 ± 19.89	10.24 ± 12.64
Overall means of amides	17.96 ± 28.24	5.17 ± 9.74	13.25 ± 20.13
Overall (*L*, *L*) means	18.99 ± 28.36	4.73 ± 7.72	10.72 ± 13.81
Overall (*L*, *D*) means	19.27 ± 28.24	5.89 ± 11.55	12.48 ± 19.40
Overall Δ mean	-2.41 ± 7.34	-1.25 ± 4.55	4.03 ± 23.11

Tab S1. Quenching activities of the forty analyzed dipeptides expressed as percentages of aldehyde reacted in the presence of the tested compound (Tab S1A for esters and Tab S1B for amides), plus the corresponding diastereoisomeric differences expressed as (L, L) – (L, D). Data for carnosine were taken from [36]. Tab S1C reports overall means (± SDs) combining Tab S1A and S1B.

For each dipeptide, Tab S1 and Fig 2(Tab S1A, Fig 2A ester derivatives as well as Tab S1B and Fig 2B for amides) report quenching activities toward 4-hydroxy-2-nonenal (HNE, chosen as representative of α,β-unsaturated aldehydes), and pyridoxal (PYR, chosen as representative of physiological carbonyl compounds). These quenching activities are expressed as percentages of quenched carbonyl compound after a fixed incubation time of 180 min. Tab S1 and Fig 2 report also the corresponding standard deviations as well as the dipeptide selectivity calculated as the ratio between the quenching activities toward HNE and PYR. For each diastereoisomeric pair, Tab S1 and Fig 2C show the resulting differences, their statistical significance (as computed by a t-test) plus some overall means (Tab S1C).

Fig 2A.

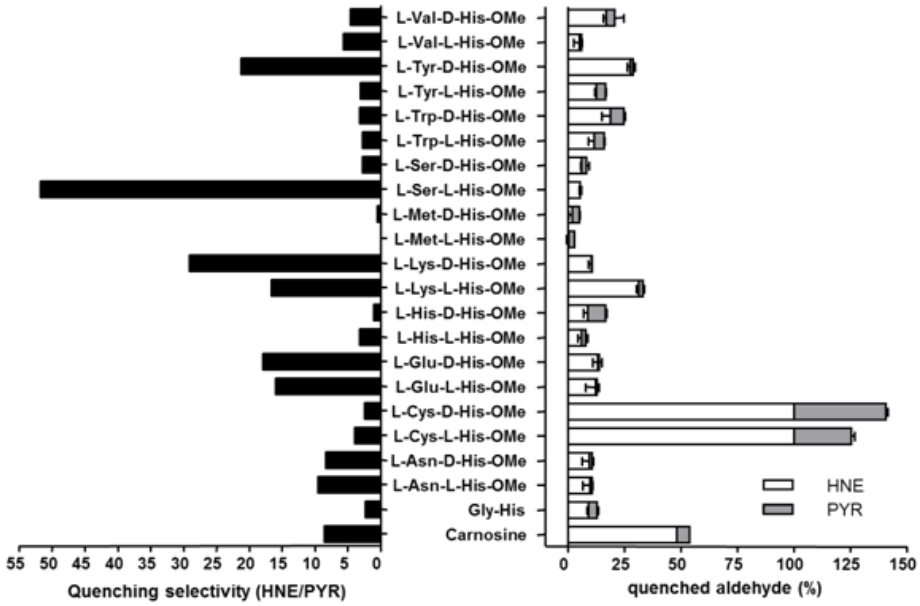
L-Val-D-His-OMe
L-Val-L-His-OMe
L-Tyr-D-His-OMe
L-Tyr-L-His-OMe
L-Trp-D-His-OMe
L-Trp-L-His-OMe
L-Ser-D-His-OMe
L-Ser-L-His-OMe
L-Met-D-His-OMe
L-Met-L-His-OMe
L-Lys-D-His-OMe
L-Lys-L-His-OMe
L-His-D-His-OMe
L-His-L-His-OMe
L-Glu-D-His-OMe
L-Glu-L-His-OMe
L-Cys-D-His-OMe
L-Cys-L-His-OMe
L-Asn-D-His-OMe
L-Asn-L-His-OMe
Gly-His
Carnosine
HNE
PYR
55 50 45 40 35 30 25 20 15 10 5 0
Quenching selectivity (HNE/PYR)
0 25 50 75 100 125 150
quenched aldehyde (%)

Fig 2B.

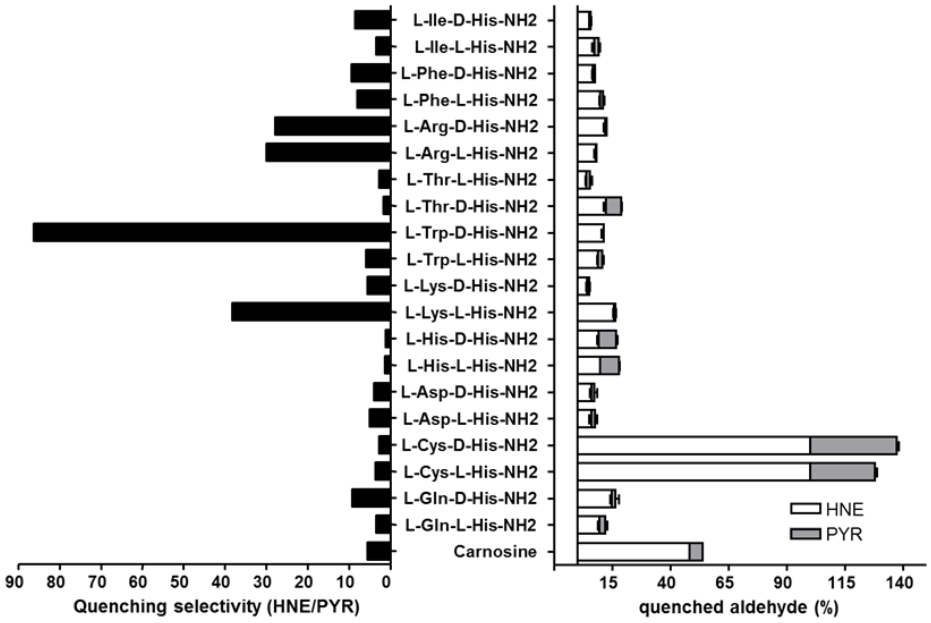
L-Ile-D-His-NH2
L-Ile-L-His-NH2
L-Phe-D-His-NH2
L-Phe-L-His-NH2
L-Arg-D-His-NH2
L-Arg-L-His-NH2
L-Thr-L-His-NH2
L-Thr-D-His-NH2
L-Trp-D-His-NH2
L-Trp-L-His-NH2
L-Lys-D-His-NH2
L-Lys-L-His-NH2
L-His-D-His-NH2
L-His-L-His-NH2
L-Asp-D-His-NH2
L-Asp-L-His-NH2
L-Cys-D-His-NH2
L-Cys-L-His-NH2
L-Gln-D-His-NH2
L-Gln-L-His-NH2
Carnosine
HNE
PYR
90 80 70 60 50 40 30 20 10 0
Quenching selectivity (HNE/PYR)
15 40 65 90 115 140
quenched aldehyde (%)

Fig 2C.

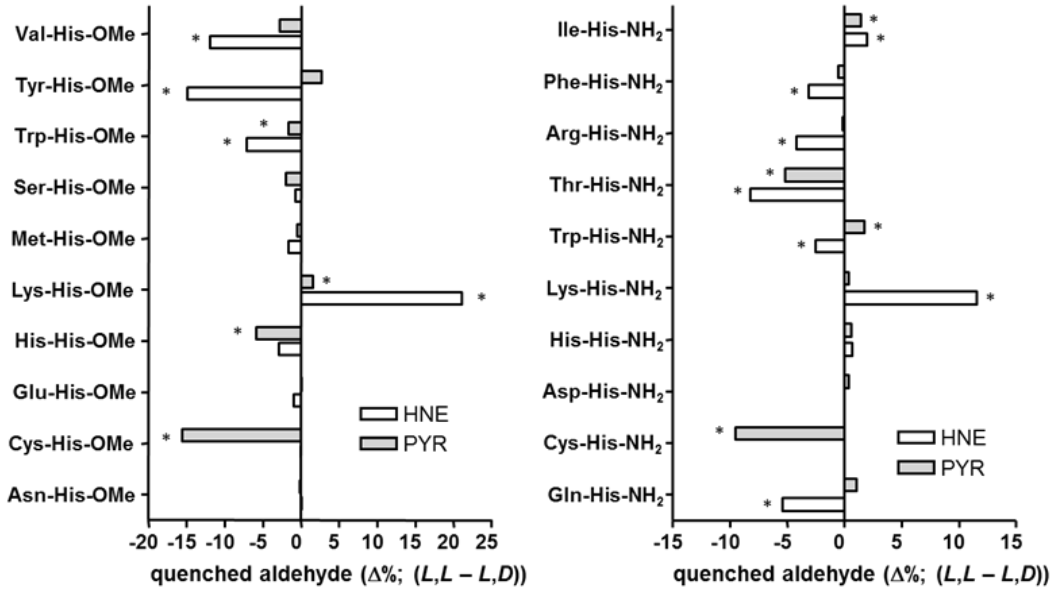

Fig 2. Bar plots for the quenching activities of the forty analyzed dipeptides expressed as percentages of aldehyde reacted in the presence of the tested compound (white bars for HNE and gray bars for pyridoxal). The black bars show the selectivity values expressed as the ratio HNE/pyridoxal Fig 2A: quenching activities of twenty ester dipeptides; Fig 2B: quenching activities of twenty ester dipeptides towards pyridoxal; Fig 2C:comparison of the diastereoisomeric pairs expressed as percentage differences of the quenching activities towards HNE (white bars) and pyridoxal (gray bars). The asterisks indicate the pairs showing statistically significant differences (i.e. $p < 0.05$).

4.2.e. Discussion.

4.2.e.1. HNE quenching.

Tab S1 and Fig 2 clearly show that cysteine-containing dipeptides possess an impressive scavenging activity since they completely quenched HNE during the incubation time regardless of their capping and configuration. These data suggest that cysteine-containing dipeptides do not follow the multistep mechanism involving the amino and imidazolyl moieties as seen for carnosine, while their high reactivity seems to be due almost exclusively to the marked nucleophilicity of the thiol group. Such a mechanism is indirectly confirmed by the virtually undetectable activity of the methionine-containing dipeptides. Although their favorable reactivity, the Cys containing dipeptides cannot be considered as promising scaffolds in the design of improved carbonyl quenchers because the remarkable thiol nucleophilicity makes them prone to reacting unsafely via nonspecific mechanisms. The toxicity of thiol-containing drugs is mostly ascribable to their ability to react with cysteinyl residues to form protein-drug mixed disulfides[30]. Such adducts can impair the physiological functions of the modified proteins[31] and, more importantly, can behave as haptens triggering immune responses which can culminate in idiosyncratic reactions (IDRs) [32].

Apart from the cysteine-containing dipeptides, all other derivatives are less active than carnosine whose quenching activity is reported in Tab S1 for easy comparison. In order to allow a more appropriate comparison, the quenching activity of the corresponding nor-analogue of carnosine (i.e. Gly-His, Tab S1) was also determined revealing that the shortening of the C-terminus induces a marked decrease of the activity toward HNE. Interestingly, Gly-His has been extensively studied for its ability to chelate transition metals[33] and for its oxidative reactions [34], but its quenching activity was never determined. The results reported here confirm the poor activity of the proteinogenic peptides, as already seen in GHK tripeptides[35]. This finding can be rationalized by their greater rigidity as reflected in weaker interactions between the frontier molecular orbitals of the imidazolyl ring and the unsaturated imino group, as well as in a greater instability of the resulting macrocyclic intermediates due to their hindered and constrained geometry[35].

Nevertheless, some of the present dipeptides show remarkable quenching activities which deserve specific considerations. The significant activity of the NH_2-*L*-Lys-*L*-His-X peptides can be explained considering that they possess two primary amino groups which favor the formation of the imino intermediate regardless of which amino group is the more reactive one. In general, dipeptides containing aromatic residues show marked quenching activities probably because the aromatic rings facilitate interactions between the imidazole ring and the acceptor β-carbon atom through π-π

stacking, with a beneficial effect already seen with β-aryl amino acids[36]. However, all NH_2-*L*-His-(*L* or *D*)-His-X dipeptides show modest activities suggesting that the interference between the two imidazolyl rings has a prevalently negative effect on scavenging activity. Finally, the poor quenching activity of the dipeptides containing hydroxyl functions (Ser- and Thr-containing peptides) indicates that the possibility to yield hemiacetal intermediates does not enhance scavenging activity, a result which resembles those reported by Guiotto et al. for dihydroxy carnosine derivatives[37].

Tab S1 and Fig 2 indicate that the amide derivatives (17.96 ± 28.24) are less active than the methyl esters (20.31 ± 28.31) (Tab 1C), but the difference is a mere trend devoid of statistical significance. Nevertheless, the trend gains credibility when comparing the derivatives for which both esters and amides have been analyzed, as in the case of NH_2-*L*-Lys-(*L* or *D)*-His-X and NH_2-*L*-Trp-(*L* or *D)*-His-X. As revealed by molecular modeling simulations, the trend is compatible with the interference of the terminal amido group which tends to interpose itself between the imidazolyl ring and the unsaturated imino group, thus stabilizing interactions and preventing their mutual approach. This observation is in line with recent studies emphasizing the strength of amide stacking and its heavy influence on the conformational profile of small peptides[38].

As illustrated by Tab S1 and Fig 2C, the pairs of diastereoisomers show only marginal quenching differences since the heterochiral isomers (19.7 ± 28.1) are nearly equiactive with their respective homochiral diastereoisomer (18.6 ± 28.5), a result explainable by the heterogeneity of the examined dipeptides which prevents general trends to be uncovered. Nevertheless, several pairs of diastereoisomers exhibit statistically significant differences which may reflect the already investigated physicochemical differences (see below). As reported by Tab S1 and Fig 2C and , 11 diastereoisomeric pairs out of 20 show statistically significant differences (i.e. $p < 0.05$) and for 7 pairs out of 11 the heterochiral dipeptide is more active than the homochiral one thus substantiating the trend observed in the overall means.

This result can be explained by the conformational differences between diastereoisomers evidenced by previous studies[39] which suggest that the favored conformations of the homochiral isomers are mainly characterized by intramolecular interactions between the side chains, while those of the heterochiral isomers show stabilizing contacts between the terminal groups. Consequently, the greater activity of heterochiral dipeptides is easily interpretable in terms of increased accessibility of the histidine side chain. This renders the imidazole ring more prone to Michael addition, while the intramolecular interactions which characterize the homochiral isomers shield the imidazolyl ring preventing its approach to the unsaturated imino group.

For both lysine-containing pairs of diastereoisomers, the homochiral isomers are conversely more active than the corresponding heterochiral ones. This finding may suggest that here the imino intermediate is mostly derived not from the N-terminus but from the lysine's ε-amino group which

is stably closer to the imidazolyl ring in the homochiral dipeptides, a proximity that favors the key Michael addition.

By supposing that C-terminal capping induces negligible effects on quenching activities, a consideration indirectly confirmed by the above-mentioned marginal differences between esters and amides, the comparison between the reported dipeptides and the corresponding unsubstituted Gly-His reference derivative allows the specific contribution of each N-terminal side-chain to be revealed. In detail (and excluding cysteine-containing dipeptides due to their different mechanism), Tab S1 and Fig 2 indicate that 11 dipeptides out of 36 have a significantly greater quenching activity compared to Gly-His. Furthermore, the N-terminal side-chain does not induce significant activity changes in 11 cases and 14 dipeptides possess lower activities than Gly-His, thus suggesting that the influence of the N-terminal side-chain on the scavenging activity strongly depends on its physicochemical properties.

A closer analysis confirms that aromatic and positively charged side-chains have generally a significantly beneficial effect; aromatic residues promote contacts between the imidazolyl ring and the carbon atom as discussed above, while positively charged residues may promote the initial imino formation. In contrast, negatively charged and H-bonding side-chains show an overall negative effect on quenching activity: the former can stabilize ion-pairs with a primary amino group thus hampering imino formation, while H-bonding residues may engage the imidazolyl ring and the imino function in intramolecular H-bonds which shield their nucleophilicity or preclude their contacts. In general, hydrophobic residues have a modest effect on quenching activity when slightly hampering the approach of the reactive groups by steric hindrance.

4.2.e.2. Pyridoxal quenching and peptide selectivity.

A bird's eye view of Tab S1 and Fig 2 show that all considered derivatives possess very modest quenching activities toward pyridoxal. Specifically, Tab S1 and Fig 2 reveal that cysteine-containing dipeptides show the greatest quenching activity, a fact explainable by the marked nucleophilicity of their thiol group. As for the detectable activity of some hydroxy-containing dipeptides, it can be explained by their capacity to form hemiacetal adducts.

Overall, the very poor activity toward PYR of the examined dipeptides confirms that they are unable to yield stable imino derivatives with physiological carbonyls. A similar result was already seen for carnosine, indicating that the basicity of the N-terminus of the present dipeptides, despite being on average weaker than that of carnosine (as experimentally determined, see ref. 39), is still too strong to yield stable imines. On average, all peptides show the same poor activity regardless of their capping and absolute configuration, which indeed have a limited impact on the reactivity of

the amino group. Similarly, all peptides show an activity roughly comparable with that of the reference compound Gly-His, thus suggesting that the N-terminal side chain has a marginal effect on the reactivity of the primary amine.

As observed for HNE quenching, the pairs of diastereoisomers show, on average, only marginal quenching differences which are mostly ascribable to the markedly greater activity of the cysteine-containing heterochiral dipeptide, probably due to a greater accessibility of its thiol group. When considering diastereoisomeric pairs individually (as illustrated by Fig 2C), their difference is statistically significant for 10 pairs out of 20. However, these statistically significant differences are equally distributed since in 5 cases the homochiral dipeptides are the more active ones, thus cancelling any overall significance.

Concerning the HNE/PYR selectivity (as reported in Fig 2), all tested dipeptides show a marked selectivity for HNE given their very weak quenching activity toward pyridoxal. More importantly, such a remarkable selectivity emphasizes that the HNE quenching of these dipeptides cannot be restricted to the formation of a mere imino function but may also involve a crucial Michael addition.

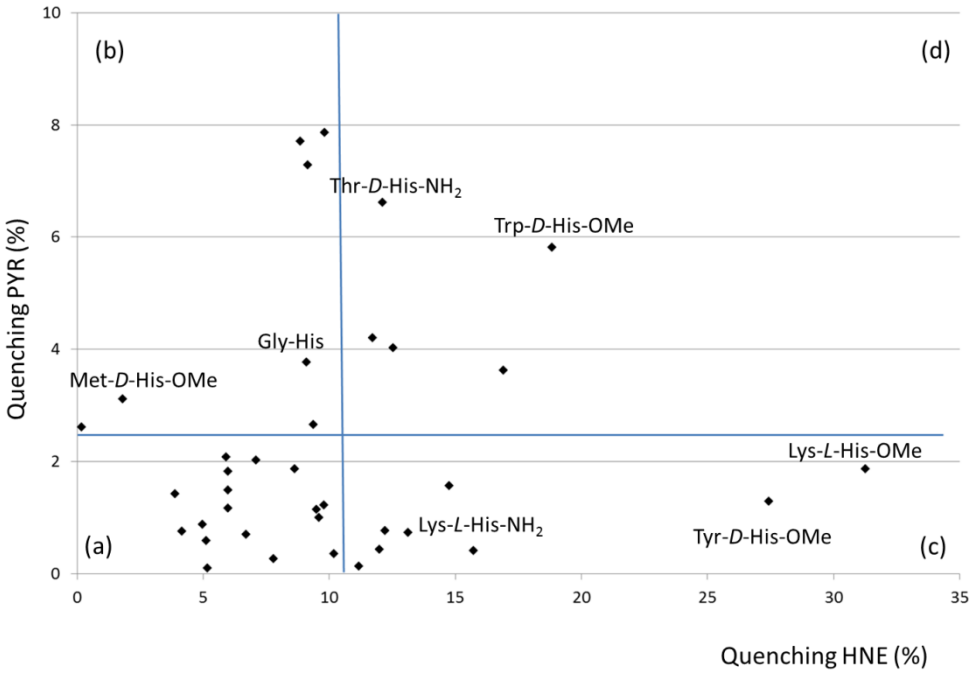

Fig 3. Distribution of HNE quenching activities versus PYR quenching activities showing that there is no correlation between them. Due to their different mechanism, cysteine-containing dipeptides are not included. The straight lines passing through the average activities subdivide the plot into four fuzzy regions: (a) inactive dipeptides; (b) inactive and unselective dipeptides; (c) active and selective dipeptides; and (d) active but unselective dipeptides.

Fig 3 compares quenching activities toward HNE and PYR showing that there is no correlation at all between them. This result confirms the aforementioned selectivity of the tested compounds. It also emphasizes that, excluding the Cys-containing peptides, HNE and PYR are quenched through substantially different mechanisms. When subdividing the obtained plot by straight lines passing through the average values of the quenching activities (average HNE = 12.2; average PYR = 3.89), it is possible to recognize four fuzzy regions. Among these, the (c) region includes the most promising dipeptides, namely those endowed with both a high HNE quenching activity and a significant selectivity, while the other three regions comprise less interesting peptides which show either low quenching activities toward HNE [(a) and (b) regions] or unsatisfactory selectivity ratios [(d) region] even though this last region contains some remarkable peptides such as the tryptophan-containing derivatives.

4.2.e.3. Peptide Stability.

Dipeptides	Residual Amount (%) after 30 min.
L-Lys-L-His-OMe	87.5 ± 2.6
L-Lys-D-His-OMe	90.5± 1.3
L-Tyr-D-His-OMe	40.5 ± 3.1
L-Lys-L-His-NH_2	67.7± 3.2
L-Lys-D-His-NH_2	68.0 ± 1.4
L-Gln-D-His-NH_2	81.3 ± 2.5

Tab 1. Plasma stability for some selected dipeptides.

Although the considered dipeptides were capped at the C-terminus to reduce the effect of hydrolases and so improve their pharmacokinetic profile, the stability of selected representative dipeptides was experimentally investigated in human plasma. As reported in Table 1, the study involved the four lysine-containing dipeptides since they allow the role of capping and configuration to be comprehensively analyzed. Besides lysine-containing dipeptides, the study also involved two very active quenchers (namely L-Tyr-L-His-OMe and D-Gln-L-His-NH_2). Overall, the measured residual amounts reveal that the reported dipeptides are significantly stable (mean residual amount is 72.6%) and only L-Tyr-L-His-OMe shows a residual amount smaller than 50%. More importantly, all the tested dipeptides are much more stable than L-carnosine which is totally consumed after 30 min of incubation[28]. A more in-depth analysis of the stability data suggest that the ester derivatives are on average more stable than the amides, the capping of which could be hydrolyzed by non-specific peptidases. As expected, heterochiral peptides are slightly more stable than homochiral ones even though the reported differences are very modest, suggesting their stability to be mostly influenced by capping. Finally, the instability of the L-Tyr-L-His-OMe could be ascribed to its lipophilicity which may make it a good substrate for serum esterases, thus confirming that stability of ester derivatives strongly depends on their polarity.

4.2.e.4. Molecular modeling.

As discussed in the Supplementary Material, a preliminary computational study analyzed the property space of the amide dipeptides, representing the extension of a previous study focused on the ester derivatives[39]. Such an analysis involved MD simulations in isotropic solvents of different polarity to investigate how the conformational profile of the dipeptides is influenced by their environment. The solvent's effect was examined by computing the property space of few representative physicochemical descriptors (namely, radius of gyration[40], logP_MLP[41] and polar surface area[42]) and parameterized by the corresponding property range values as proposed by us in previous studies.

Afterward, the computed property space ranges plus some well-known 2D/3D molecular descriptors were utilized to derive relationships able to rationalize quenching activities as later discussed. Specifically, the correlations were iteratively developed by maximizing their r^2 value and including at most four independent non-interrelated variables. The molecular descriptors included in the presented equations are collected in Table S2.

Dipeptide	Rotors	HBtot	Ovality	Rings	Volume (Å^3)	logP range	PSA range (Å^2)
L-Asn-D-His-OMe	8	12	1.70	1	251.7	1.34	25.5
L-Asn-L-His-OMe	8	12	1.67	1	253.0	1.31	20.8
L-Cys-D-His-OMe	7	9	1.58	1	236.2	1.22	24.5
L-Cys-L-His-OMe	7	9	1.58	1	238.4	1.07	28.1
L-Glu-D-His-OMe	8	11	1.71	1	261.4	1.18	24.5
L-Glu-L-His-OMe	8	11	1.71	1	263.8	1.09	26.5
L-His-D-His-OMe	8	11	1.75	2	277.1	1.4	23.6
L-His-L-His-OMe	8	11	1.73	2	275.1	1.48	23.9
L-Lys-D-His-OMe	10	12	1.79	1	286.0	1.62	25.6
L-Lys-L-His-OMe	10	12	1.80	1	286.9	1.65	28.7
L-Met-D-His-OMe	8	10	1.73	1	254.8	1.42	16.5
L-Met-L-His-OMe	8	10	1.75	1	255.0	1.46	16.2
L-Ser-D-His-OMe	7	11	1.63	1	228.8	1.31	20.1
L-Ser-L-His-OMe	7	11	1.65	1	228.6	1.07	19.6
L-Trp-D-His-OMe	8	10	1.76	3	324.9	1.21	23.1
L-Trp-L-His-OMe	8	10	1.79	3	327.3	1.48	22.9
L-Tyr-D-His-OMe	8	11	1.72	2	299.9	1.37	22.3
L-Tyr-L-His-OMe	8	11	1.63	2	289.9	1.55	21.6
L-Val-D-His-OMe	6	9	1.69	1	260.6	1.2	28.5
L-Val-L-His-OMe	6	9	1.72	1	255.8	1.46	24.6
L-Gln-*D*-His-NH2	7	13	1.62	1	234.5	1.27	30.2
L-Gln-*L*-His-NH2	7	13	1.60	1	233.5	1.35	28.5
L-Cys-*D*-His-NH2	6	10	1.45	1	225.3	1.39	28.2
L-Cys-*L*-His-NH2	6	10	1.45	1	221.7	1.65	27.8
L-Asp-*D*-His-NH2	6	12	1.58	1	227.7	1.28	27.8
L-Asp-*L*-His-NH2	6	12	1.60	1	225.2	1.2	33.2
L-His-*D*-His-NH2	7	12	1.66	2	253.5	1.23	29.6
L-His-*L*-His-NH2	7	12	1.62	2	253.0	1.1	21
L-Lys-*D*-His-NH2	9	13	1.65	1	264.9	1.82	24
L-Lys-*L*-His-NH2	9	13	1.70	1	266.2	1.9	22.8
L-Trp-*D*-His-NH2	7	10	1.68	3	308.6	1.15	20.5
L-Trp-*L*-His-NH2	7	10	1.69	3	308.9	1.36	19.1
L-Thr-*D*-His-NH2	6	12	1.64	1	232.7	1.24	27.4
L-Thr-*L*-His-NH2	6	12	1.58	1	231.6	1.4	29.2
L-Arg-*D*-His-NH2	10	15	1.73	1	285.8	1.21	30.7
L-Arg-*L*-His-NH2	10	15	1.72	1	282.2	1.73	26.4
L-Phe-*D*-His-NH2	7	10	1.64	2	275.2	1.52	17.4
L-Phe-*L*-His-NH2	7	10	1.67	2	277.0	1.03	16.4
L-Ile-*D*-His-NH2	5	10	1.62	1	255.5	1.32	25.2
L-Ile-*L*-His-NH2	5	10	1.69	1	259.6	1.34	25

Tab S2. Molecular descriptors included in the reported equations.

N	**Equation**	**Statistics**
1[a]	Quenching HNE = 5.61 + 0.206 Rotors – 3.40 Ovality – 0.174 HB_{Tot} + 0.0275 PSA_Range	n = 40; r^2 = 0.85; r^2_{cv} = 0.83; SE = 0.12; F = 44.4; p< 0.0001
2[b]	Quenching HNE = 5.52 + 0.221 Rotors – 3.49 Ovality – 0.174 HB_{Tot} + 0.0304 PSA_Range	n = 25; r^2 = 0.79; r^2_{cv} = 0.73; SE = 0.13; F = 17.1; p< 0.0001
3[b]	Quenching HNE = 0.911 Quenching HNEpred + 0.034	n = 15; r^2 = 0.83; r^2_{cv} = 0.77 SE = 0.11; F = 16.8; p< 0.0001
4	Quenching PYR = 6.67 + 0.461 Rings – 3.97 Ovality – 0.0152 HB_{Tot} + 0.00559 PSA_Range	n = 40; r^2 = 0.66; r^2_{cv} = 0.62; SE = 0.19; F = 13.8; p< 0.0001
5	Selectivity ratio HNE/PYR = – 43.3 + 2.01 Rotors + 0.156 Volume – 10.2 Rings + 9.71 log P_Range	n = 40; r^2 = 0.70; r^2_{cv} = 0.65; SE = 5.69; F = 19.6; p< 0.0001

Tab 2. Main predictive equations developed in the study. All included property space descriptors were obtained from MD runs in vacuo.

Tab 2 reports the best relationship (Eq. 1) which correlates quenching activities with a set of computed descriptors. Specifically, Eq. 1 indicates that HNE quenching is favorably influenced by flexibility as encoded by both structural and property variability (namely, number of rotors and PSA range, respectively), whereas it is negatively affected by strong intramolecular interactions (as reflected by the number of H-bonding groups, HBTot) which shield the reactive groups and stabilize folded conformations (as parameterized by molecular ovality). These results imply that both flexibility and intramolecular contacts influence the ability of a given molecule to assume the conformations most suitable to the formation of the imino intermediate followed by the reaction of Michael addition. In other words, a too rigid molecule cannot undergo the necessary conformational transitions to bring in close vicinity the imidazole ring and the acceptor β-carbon atom.

To assess the predictive power of Eq. 1, the set of forty dipeptides was randomly subdivided into a training (n = 25) and a test (n = 15) set. The correlation as computed for the training set only confirms the robustness of Eq. 1 since these two equations (Eqs. 1 and 2) have very similar coefficients. Eq. 1 thus appears to be reasonably independent of the number of ligands considered. The relation between experimental and predicted pKm values (Eq. 3, Table 4), as computed by Eq. 2 for the external test set, affords an encouraging validation for the predictive power of Eq. 1. Equation 3 is indeed a satisfactory one given its statistics, its slope being close to 45° (= 42.3°)

and the intercept close to zero. The analysis of residuals (results not shown) indicates that there is no correlation with quenching activities thus suggesting that Eq. 1 applies equally to good and poor HNE quenchers.

Similarly, Tab 2 reports an interesting correlation (Eq. 4, somewhat poorer than the previous one) to predict the quenching of pyridoxal. The equation includes parameters which are related to the ability to expose the amino group (HB_{Tot}, ovality, and PSA_Range, already present in Eq. 1), as well as to stabilize the resulting imino adducts since aromatic rings can contribute to their formation by (1) attracting protonated amines; (2) stabilizing charged intermediates; and (3) shielding the imines from the water environment. Comparing Eqs. 1 and 4 reveals the disappearance in the latter of the flexibility descriptor (i.e. number of rotors), thus emphasizing that PYR quenching obeys a one-step mechanism and does not require significant conformational adaptation as previously discussed for HNE quenching.

These considerations find confirmation when analyzing Eq. 5(Tab 2) meant to predict HNE/PYR selectivity ratios. Indeed, the number of rotatable bonds and the log P range (both of which describe molecular flexibility) favor selectivity, which in turn is influenced negatively by aromatic rings due to their stabilizing effect on imine formation. Taken together, these correlations emphasize the critical role played by flexibility in HNE quenching, presumably because it accounts for the ability of a given molecule to assume a conformation able to promote the crucial Michael addition. Such a consideration is in line with what was previously investigated for some aryl derivatives of carnosine [36], the quenching activity of which was linearly related to their ability to assume folded and reactive conformations.

4.2.e.5. Conclusions.

As a rule, the hitherto published carnosine derivatives are structurally quite similar to the parent compound[39]. Consequently, they are devoid of enough structural variability to deepen our understanding of the major molecular factors influencing quenching activity, except for straightforward deductions derived from a knowledge of the quenching mechanism (e.g., the nucleophilicity of the Michael donor moiety or the basicity of the primary amino group). As documented by the QSAR equations in Tab 2, the derivatives presented in this work, while having the same reactive groups and being, on average, less active than carnosine, possess a structural and configurational variability compatible with a broader structure-activity analysis. The latter concerns non only factors characterizing the reactive centers but also factors which pertain to a given molecule as a whole and contribute indirectly to the quenching activity (e.g., H-bonding capacity versus HNE quenching, and the presence of aromatic rings versus PYR quenching).

Such a detailed analysis provides a more precise picture of the entire quenching mechanism and could support the design of novel carbonyl quenchers featuring all the key properties able to maximize both activity and selectivity. In other words, an in-depth understanding of all relevant factors could permit to improve the quenching activity of a given compound without necessarily increasing the nucleophilicity of its reactive moieties, thus avoiding compounds of dangerously low selectivity.

By considering the key contribution of both the N-terminal side-chains and configuration for the investigated dipeptides, the obtained results emphasize how reactivity of the imidazolyl ring heavily depends on both conformational properties and vicinal residues. This finding can explain the remarkable specificity with which histidine residues form covalent adducts with reactive carbonyl species and might provide useful clues to rationalize the different reactivity of histidine residues for a given protein.

Finally, the present study reports some dipeptides (namely *L*-Lys-*L*-His-OMe and *L*-Tyr-*D*-His-OMe, see Fig 1) which show a quenching activity slightly weaker than that of carnosine, but are endowed by a markedly greater selectivity and can represent truly promising candidates for the design of improved carnosine derivatives. Also, the good quenching activity of tryptophan-containing dipeptides deserves specific attention. Indeed, considering that (a) Trp-His is a vasodilating dipeptide which inhibits extracellular Ca^{2+} entry by blocking dihydropyridine-like L-type channels[44], and (b) some carnosine derivatives show antihypertensive effects in animal models[45], Trp-His derivatives could become useful agents to treat dyslipidemia-induced hypertension.

4.2.f. References.

[1] Cho SJ, Roman G, Yeboah F, Konishi Y. (2007). "The road to advanced glycation end products: a mechanistic perspective". *Curr Med Chem.* 2007, 14, 1653-71.

[2] Niki E.(2009). "Lipid peroxidation: physiological levels and dual biological effects". *Free Radic Biol Med.*;,47,469 - 84.

[3] Madian AG, Regnier FE. (2010). "Proteomic identification of carbonylated proteins and their oxidation sites". *J Proteome Res*.;9,3766 - 80.

[4] Pamplona R. (2011). "Advanced lipoxidation end-products". *Chem Biol Interact*.;192,14 - 20.

[5] Thomas MC. (2011)."Advanced glycation end products". *Contrib Nephrol.*;170,66 – 74.

[6] Dalle-Donne I, Aldini G, Carini M, Colombo R, Rossi R, Milzani A. (2006). "Protein carbonylation, cellular dysfunction, and disease progression". *J Cell Mol Med*.;10,389 – 406.

[7] Näsström T, Fagerqvist T, Barbu M, Karlsson M, Nikolajeff F, Kasrayan A, Ekberg M, Lannfelt L, Ingelsson M, Bergström J. (2011). "The lipid peroxidation products 4-oxo-2-nonenal and 4-hydroxy-2-nonenal promote the formation of α-synuclein oligomers with distinct biochemical, morphological, and functional properties". *Free Radic Biol Med*.;50,428 - 37.

[8] Virella G, Thorpe SR, Alderson NL, Stephan EM, Atchley D, Wagner F, Lopes-Virella MF; DCCT/EDIC Research Group. (2003). "Autoimmune response to advanced glycosylation end-products of human LDL". *J Lipid Res.*;44,487 - 93.

[9] Barlovic DP, Soro-Paavonen A, Jandeleit-Dahm KA. (2011). "RAGE biology, atherosclerosis and diabetes". *Clin Sci (Lond).*;121, 43 - 55.

[10] Dalle-Donne I, Giustarini D, Colombo R, Rossi R, Milzani A. (2003). "Protein carbonylation in human diseases". *Trends Mol Med.*;9,169 – 76.

[11] Aldini G, Dalle-Donne I, Colombo R, Maffei Facino R, Milzani A, Carini M. (2006). "Lipoxidation-derived reactive carbonyl species as potential drug targets in preventing protein carbonylation and related cellular dysfunction". *ChemMedChem.*;1,1045 - 58.

[12] Aldini G, Dalle-Donne I, Facino RM, Milzani A, Carini M. (2007). "Intervention strategies to inhibit protein carbonylation by lipoxidation-derived reactive carbonyls". *Med Res Rev*.;27,817 - 68.

[13] Aldini G, Facino RM, Beretta G, Carini M. (2005). "Carnosine and related dipeptides as quenchers of reactive carbonyl species: from structural studies to therapeutic perspectives". *Biofactors.*;24,77 - 87.

[14] Hipkiss AR. (2009). "Carnosine and its possible roles in nutrition and health". *Adv Food Nutr Res*.;57,87 - 154.

[15] Pepper ED, Farrell MJ, Nord G, Finkel SE. (2010). "Antiglycation effects of carnosine and other compounds on the long-term survival of Escherichia coli". *Appl Environ Microbiol*.;76, 7925 - 30.

[16] Pietkiewicz J, Bronowicka-Szydełko A, Dzierzba K, Danielewicz R, Gamian A. (2011). "Glycation of the muscle-specific enolase by reactive carbonyls: effect of temperature and the protection role of carnosine, pyridoxamine and phosphatidylserine". *Protein J*.;30,149 - 58.

[17] Aldini G, Carini M, Beretta G, Bradamante S, Facino RM. (2002). "Carnosine is a quencher of 4-hydroxy-nonenal: through what mechanism of reaction?". *Biochem Biophys Res Commun.* 298,699 - 706.

[18] Liu Y, Xu G, Sayre LM. (2003). « Carnosine inhibits (E)-4-hydroxy-2-nonenal-induced protein cross-linking: structural characterization of carnosine-HNE adducts". *Chem Res Toxicol*.;16,1589 - 97.

[19] Aldini G, Orioli M, Carini M, Maffei Facino R. (2004). "Profiling histidine-containing dipeptides in rat tissues by liquid chromatography/electrospray ionization tandem mass spectrometry". *J Mass Spectrom.*,39,1417 - 28

[20] Geissler S, Zwarg M, Knütter I, Markwardt F, Brandsch M. (2010). "The bioactive dipeptide anserine is transported by human proton-coupled peptide transporters". *FEBS J*.;277,790 - 5.

[21] Pegova A, Abe H, Boldyrev A. (2010). "Hydrolysis of carnosine and related compounds by mammalian carnosinases". *Comp Biochem Physiol B Biochem Mol Biol*;127,443 – 6.

[22] Vistoli G, Carini M, Aldini G., (2012). "Transforming dietary peptides in promising lead compounds: the case of bioavailable carnosine analogues", *Amino acids,*;1:7,549 - 60.

[23] Vistoli G, Pedretti A, Cattaneo M, Aldini G, Testa B. (2006). "Homology modeling of human serum carnosinase, a potential medicinal target, and MD simulations of its allosteric activation by citrate." *J Med Chem.*;49,3269 - 77.

[24] Pedretti A, De Luca L, Marconi C, Negrisoli G, Aldini G, Vistoli G. (2008). "Modeling of the intestinal peptide transporter hPepT1 and analysis of its transport capacities by docking and pharmacophore mapping". *ChemMedChem.* ;3,1913 - 21.

[25] Pedretti A, De Luca L, Marconi C, Regazzoni L, Aldini G, Vistoli G. (2011). "Fragmental modeling of hPepT2 and analysis of its binding features by docking studies and pharmacophore mapping". *Bioorg Med Chem.*;19,4544 - 51.

[26] Werle M, Bernkop-Schnürch A. (2006). "Strategies to improve plasma half life time of peptide and protein drugs". *Amino Acids*.;,30,351 - 67.

[27] Aldini G, Orioli M, Rossoni G, Savi F, Braidotti P, Vistoli G, Yeum KJ, Negrisoli G, Carini M. (2011). "The carbonyl scavenger carnosine ameliorates dyslipidaemia and renal function in Zucker obese rats". *J Cell Mol Med.*;15,1339 - 54.

[28] Orioli M, Vistoli G, Regazzoni L, Pedretti A, Lapolla A, Rossoni G, Canevotti R, Gamberoni L, Previtali M, Carini M, Aldini G. (2011). "Design, synthesis, ADME properties, and pharmacological activities of β-alanyl-*D*-histidine (*D*-carnosine) prodrugs with improved bioavailability". *ChemMedChem.*;6,1269 - 82.

[29] Bertinaria M, Rolando B, Giorgis M, Montanaro G, Guglielmo S, Buonsanti MF, Carabelli V, Gavello D, Daniele PG, Fruttero R, Gasco A. (2011). "Synthesis, physicochemical characterization, and biological activities of new carnosine derivatives stable in human serum as potential neuroprotective agents". *J Med Chem.*;54,611 - 21.

[30] Zuniga FI, Loi D, Ling KH, Tang-Liu DD. (2012). "Idiosyncratic reactions and metabolism of sulfur-containing drugs". *Expert Opin Drug Metab Toxicol.*;8,467 - 85.

[31] Di Simplicio P, Frosali S, Priora R, Summa D, Cherubini Di Simplicio F, Di Giuseppe D, Di Stefano A. (2005). "Biochemical and biological aspects of protein thiolation in cells and plasma". *Antioxid Redox Signal.*;7,951 - 63.

[32] Elsheikh A, Lavergne SN, Castrejon JL, Farrell J, Wang H, Sathish J, Pichler WJ, Park BK, Naisbitt DJ. (2010). "Drug antigenicity, immunogenicity, and costimulatory signaling: evidence for formation of a functional antigen through immune cell metabolism". *J Immunol.*;185,6448 - 60.

[33] Rychlewska U, Warzajtis B, Glisić BD, Zivković MD, Rajković S, Djuran MI. (2010). "Monocationic gold(III) Gly-L-His and L-Ala-L-His dipeptide complexes: crystal structures arising from solvent free and solvent-containing crystal formation and structural modifications tuned by counter-anions". *Dalton Trans.*;39,8906-13.

[34] Reis A, Fonseca C, Maciel E, Domingues P, Domingues MR. (2011). "Influence of amino acid relative position on the oxidative modification of histidine and glycine peptides". *Anal Bioanal Chem.*;399,2779 - 94.

[35] Beretta G, Artali R, Regazzoni L, Panigati M, Facino RM. (2007). "Glycyl-histidyl-lysine (GHK) is a quencher of alpha,beta-4-hydroxy-trans-2-nonenal: a comparison with carnosine. insights into the mechanism of reaction by electrospray ionization mass spectrometry, 1H NMR, and computational techniques". *Chem Res Toxicol.;*20,1309 - 14.

[36] Vistoli G, Orioli M, Pedretti A, Regazzoni L, Canevotti R, Negrisoli G, Carini M, Aldini G., (2009). "Design, synthesis, and evaluation of carnosine derivatives as selective and efficient sequestering agents of cytotoxic reactive carbonyl species". *ChemMedChem.*;4,967 - 75.

[37] Guiotto A, Calderan A, Ruzza P, Osler A, Rubini C, Jo DG, Mattson MP, Borin G. (2005). "Synthesis and evaluation of neuroprotective alpha,beta-unsaturated aldehyde scavenger histidyl-containing analogues of carnosine". *J Med Chem.*;48,6156 - 61.

[38] James WH 3rd, Müller CW, Buchanan EG, Nix MG, Guo L, Roskop L, Gordon MS, Slipchenko LV, Gellman SH, Zwier TS. (2009). "Intramolecular amide stacking and its competition with hydrogen bonding in a small foldamer". *J Am Chem Soc.*;131,14243 - 5.

[39] Vistoli G, Straniero V, Pedretti P, Fumagalli L, Bolchi C, Pallavicini M, Valoti E, Testa B. (2012). "Predicting the physicochemical profile of diastereoisomeric histidine-containing dipeptides by property space analysis". *Chirality,*;24,566 - 76.

[40] Zyrianov Y. (2006). "Distribution-based descriptors of the molecular shape". *J Chem Inf Model.*;45,657 - 72.

[41] Clark DE. (2011). "What has polar surface area ever done for drug discovery?". *Future Med Chem.*;3,469 - 84.

[42] Gaillard P, Carrupt PA, Testa B, Boudon A. (1994). "Molecular lipophilicity potential, a tool in 3D-QSAR. Method and applications". *J Comput Aided Mol Des.*;8,83 - 96.

[43] Vistoli G, Pedretti A, Testa B. (2011). "Chemodiversity and molecular plasticity: recognition processes as explored by property spaces". *Future Med Chem.*;3,995 - 1010.

[44] Wang Z, Watanabe S, Kobayashi Y, Tanaka M, Matsui T. (2010). "Trp-His, a vasorelaxant di-peptide, can inhibit extracellular Ca2+ entry to rat vascular smooth muscle cells through blockade of dihydropyridine-like L-type Ca2+ channels". *Peptides.*;31,2060 - 6.

[45] Menini S, Iacobini C, Ricci C, Scipioni A, Fantauzzi CB, Giaccari A, Salomone E, Canevotti R, Lapolla A, Orioli M, Aldini G, Pugliese G, (2012). "D-carnosine-octylester attenuates atherosclerosis and renal disease in ApoE null mice fed a Western diet through reduction of carbonyl stress and inflammation". *Br J Pharmacol.*;166,1344 – 56.

[46] Taguchi T, Sugiura M, Hamada Y, Miwa I. (1999). "Inhibition of advanced protein glycation by a Schiff base between aminoguanidine and pyridoxal". *Eur J Pharmacol*.;378,283 - 9.

[47] Pedretti A., Villa L., Vistoli G. (2002). "VEGA: a versatile program to convert, handle and visualize molecular structure on windows-based PCs". *J. Mol. Graph.;*21,47 - 49.

[48] Vistoli G, Pedretti A, Testa B. (2009). "Partition coefficient and molecular flexibility: the concept of lipophilicity space". *Chem Biodivers.*;6,1152 - 69.

5. A new high resolution mass spectrometry application for the comprehensive analysis of the ligand-binding properties of RAGE.

5.1. Introduction.

The receptor for advanced glycation end products (RAGE) is a type I transmembrane glycoprotein of the immunoglobulin superfamily of cell surface receptors[1]. The engagement of RAGE by ligands triggers key signalling pathways resulting in oxidative damage and release of pro-inflammatory and pro-fibrotic molecules[2]. RAGE is able to bind a class of heterogeneous compounds such as advanced glycation end products (AGEs) formed as a result of nonenzymatic biochemical reactions involving glucose and oxidative derived cheto-aldehydes.
AGEs are involved in the onset and progression of different oxidative based diseases, including diabetic vascular complications and atherosclerosis. Hence, the inhibition of AGEs formation as well as the blockade of AGEs-RAGE interaction represents a promising drug target.
The receptor can be inactivated by high-molecular substrate analogs, low-molecular weight inhibitors or by anti-RAGE antibodies, neutralizing the receptor. A set of compounds has been proposed as RAGE inhibitors and tested in animal models.

Probably due to the complexity of the molecular interactions between AGEs-RAGE, only few studies on AGEs antagonists have so far been reported. A main limit in the discovery program of AGEs antagonists is the lack of reliable methods for studying AGEs-RAGE interaction.

In order to exploit RAGE as a therapeutic target, a comprehensive analysis of the structure and ligand-binding properties of RAGE is required. For this purpose, aim of the present work was to set-up a MS method able to study the non covalent interactions between ligands and recombinant sRAGE (V1-C1), which represents the ligand binding domain of RAGE. The V1-C1 protein target was expressed in E. coli and the ligand-protein binding properties (stoichiometry and Kd values) were determined by a high resolution mass spectrometric (orbitrap) approach carried out in non denaturating conditions.

5.2. Materials and methods.

5.2.a. Sterilization methods.

In order to avoid contaminations by undesirable microorganism, sterilization has an important role for the microorganisms manipulation. Each equipment was sterilized on dry heat flow in an oven at a temperature of 150 °C for a minimum of 3 hours. Overall medium, solutions, buffers and other materials were sterilized at 110 °C at a pressure of 0.8 atmospheres for 30 minutes.
Solutions containing heat-labile substances were sterilized by filtration through Millipore filters with a pore diameter of 0.22 µM or with Stericap (Millipore).

5.2.b. Strains preservation and *E.coli strains* growth conditions.

With a view to preserve the strains for several months, the strains were propagated at 4 °C in solid medium. The long-term storage was performed in glycerinate solution: *E.coli* cells were placed in a sterile solution of water mq/glycerol 50/50 (v/v) and store at -80 °C.

***E.coli strains* and growth conditions:**

The strains of *E.coli* used are listed in Tab 1.
Strains ORIGAMI B (DE3)-pET-15b-sRAGE and ORIGAMI B (DE3)-pET-15b-VC1
were kindly provided by Dr. G. Fritz [Department of Neuropathology Albert-Ludwigs University of Freiburg (Germany)].

Strain	Genotype	Provenance
ORIGAMI B (DE3)-pET-15b-sRAGE	F$^-$ *ompThsd*S_B($r_B^-m_B^-$) *gal dcm lacY1 ahpC* (DE3) *gor522::*Tn*10trxB* (Kan^R, Tet^R)	Dattilo, B.M., et al.
ORIGAMI B (DE3)-pET-15b-VC1	F$^-$ *ompThsd*S_B($r_B^-m_B^-$) *gal dcm lacY1 ahpC* (DE3) *gor522::*Tn*10trxB* (Kan^R, Tet^R)	Dattilo, B.M., et al.
ORIGAMI 2 (DE3)	Δ(*ara-leu*)*7697* Δ*lacX74*Δ*phoAPvu*II*phoR araD139 ahpCgalEgalKrpsL* F [*lac*$^+$*lacI*^{q} *pro*] (DE3) *gor522*:: Tn *10 trxB* (Str^R, Tet^R)	Novagen
ORIGAMI 2 (DE3)-pET-15b-V	F$^-$ *ompThsd*S_B($r_B^-m_B^-$) *gal dcm lacY1 ahpC* (DE3) *gor522::*Tn*10trxB* (Str^R, Tet^R)	Collection from Professor Popolo
DH5α	F$^-$ φ80*lacZ*ΔM15 Δ(*lac*ZYA-*arg*F) U169 *rec*A1 *end*A1 *hsd*R17(r_k^-, m_k^+) *pho*A*sup*E44 *thi*-1 *gyr*A96 *rel*A1 *ton*A	Invitrogen
DH5α-pET-15b-V	F$^-$ φ80*lacZ*ΔM15 Δ(*lac*ZYA-*arg*F) U169 *rec*A1 *end*A1 *hsd*R17(r_k^-, m_k^+) *pho*A*sup*E44 *thi*-1 *gyr*A96 *rel*A1 *ton*A	Collection from Professor Popolo

Tab 1. E.coli strains used in this work.

The media for the growth of *E.coli* are listed in Tab 2.

Medium	**Composition**	**Usage**
LB	1% triptone, 0,5% yeast estract, 0,5% NaCl (2% agar for solid medium).	*E. coli* growth
LB-BUFFERED	1% triptone, 0,5% yeast estract, 0,5% NaCl, 0,2 M NaH_2PO_4, 0,2 M Na_2HPO_4.	Induction of transformed *E. coli* clones
LB 1% NaCl	1% triptone, 0,5% yeast estract, 1% NaCl.	Induction of transformed *E. coli* clones
DYT	0,6% triptone, 1% yeast estract, 0,5% NaCl, 50 Mm Na_2HPO_4, 0,2% glucose.	Induction of transformed *E. coli* clones
AM	0,5% triptone, 0,25% yeastestract, 25 mMNaH_2PO_4, 25 mM KH_2PO_4, 50 mM NH_4Cl, 5 mM Na_2SO_4, 50 µM $FeCl_3$, 20 µM $CaCl_2$, 10 µM $MnCl_2$, 10 µM $ZnSO_4$, 2 µM $CoCl_2$, 2 µM $CuCl_2$, 2 µM $NiCl_2$, 2 µM Na_2MoO_4, 2 µM Na_2SeO_3, 2 µM H_3BO_3, 1 M $MgCl_2$, 0,5% glycerol, 0,05% glucose, 0,2% lactose.	Induction through the autoinduction method of transformed clones of *E. coli*

Tab 2. Media for E.coli growth.

The media were added with 100 µg/ml of ampicillin (from 1000X stock solution in ethanol, filtered and stored at -20 °C), or with 15 µg/ml of kanamycin (from 1000X stock solution in H_2O, filtered and stored at 4 °C) or 12.5 µg/ml(from 1000X stock solution in ethanol, filtered and stored at -20 °C), according to the experimental needs.

5.2.c. Molecular biology techniques.

5.2.c.1. Plasmids and oligonucleotides.

The expression of the V-C1 was performed by the vector pET-15b which includes ampicillin resistance as selective marker (fig. x). The employment of this vector in the presence of lactose or IPTG guarantees high levels of expression of recombinant proteins. In addiction the vector pET-15b allows an easy purification step by affinity chromatography due to the pET-15b sequence encoding for an oligopeptide containing six histidine residues linked to the N-terminal portion of the recombinant protein. The high affinity of the histidine tag for divalent metals based affinity column allows the purification of the protein of interest.

A

pET-15b sequence landmarks	
T7 promoter	453-469
T7 transcription start	452
His•Tag coding sequence	362-380
Multiple cloning sites	
(*Nde* I - *Bam*H I)	319-335
T7 terminator	213-259
lacI coding sequence	(866-1945)
pBR322 origin	3882
bla coding sequence	4643-5500

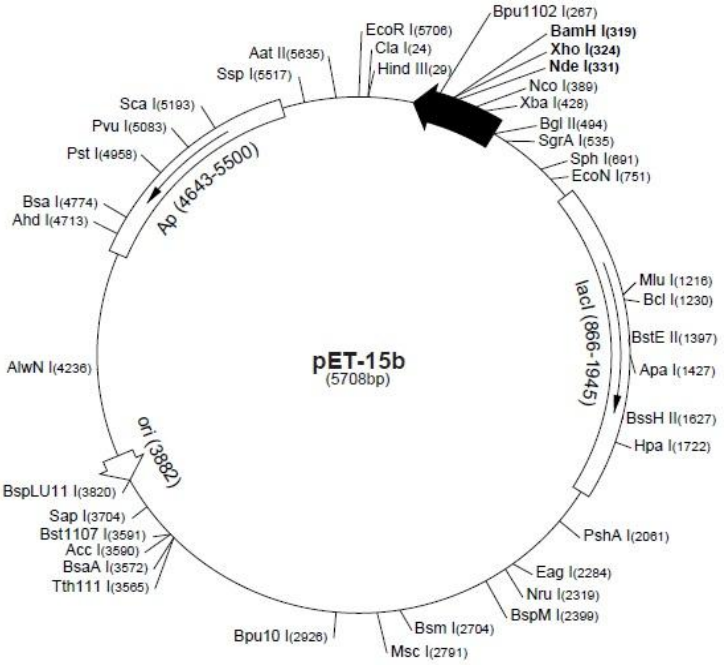

B

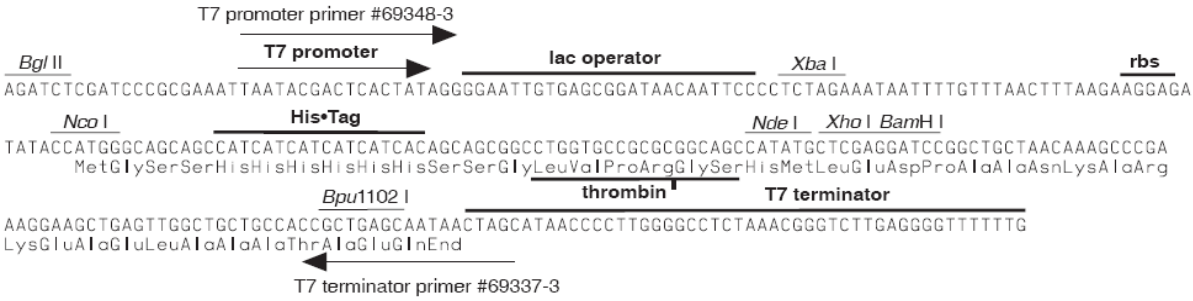

Fig 1. A) pET15b vector map with highlighted the polylinker region. B) Cloning/expression pET15b vector sequence.

The oligonucleotides used in this work are listed in Tab 3.

Name	Sequence 5'-3'	Use
VNdeI-For	AGCATATTCGACTGACATATGGCTCAAAACATCACAGCCCG	Amplification sequence encoding for V domain of RAGE to cloning into pET-15b (in red: complementary region of the sequence encoding the V domain; stressed: sequence recognized by NdeI restriction enzyme).
V223Xho-Rev	ATCGTCGGGCTCACTCGAG*CTA*AGGAATCTGGTAGACACGGA	Amplification sequence encoding for V-C1 domain of RAGE to cloning into pET-15b (in red: complementary region of the sequence encoding the V-C1 domain; stressed: sequence recognized by Xhol restriction enzyme; italics: STOP codon).
T7 promoter	TAATACGACTCACTATAGGG	PCR performed on *E. coli* colony for the transformed clones verification. DNA sequencing.
T7 terminator	GCTAGTTATTGCTCAGCGG	PCR performed on *E. coli* colony for the transformed clones verification. DNA sequencing.
5' AOX1	GACTGGTTCCAATTGACAAGC	PCR performed on *E. coli* colony for the transformed clones verification. DNA sequencing.
3' AOX1	GCAAATGGCATTCTGACATCC	PCR performed on *E. coli* colony for the transformed clones verification. DNA sequencing.

Tab 3. List of oligonucleotides used to revise pET15b vector and characterize E. coli .

The reaction was performed at 37 °C for one hour followed by an inactivation step at 65 °C for 20 minutes. The dephosphorylation was carried out on agarose gel and the band corresponding to the dephosphorylated vector pHIL-S1 was eluted from the gel by using the QIAquick® Gel Extraction Kit (QIAGEN).

After the vector quantification, it was set up the ligation reaction between the pET15b/XhoI vector and the two V-C1 inserts amplified by OCR and digested by Xhol enzyme.

The ligation reaction consisted to incubate 12.47 ng of vector (for V-C1 domain), 10 µl of buffer, 1 µl of NEB and Milli Q water to reach the final volume of 21µl. The reaction was incubated at 25 °C for 10 minutes.

The ligation mixture was used to transform DH5α *E. coli* cells, designed for the plasmid replication containing a high number of copies per cell and made competent by adding $CaCl_2$.

The correct inserts integration into the pHIL-S1 vector has been checked through screening; the protocol provided the screening of 10 clones for each construct, by PCR performed on E. coli colony using 5'AOX1 as primer (which appears on the vector pHIL-S1) and V223XHis -Rev for the domain V-C1 (Tab 3).

The amplifications have required, in a final volume of 20 µl, primers in a final concentration of 5 µM, dNTPs in a final concentration of 2.5 mM, $MgCl_2$ in a final concentration of 50 mM and 1.25 U of INVITROGEN Taq polymerase.

The PCR program was the following:

Temperature	**Time**	**Cycles**
94 °C	4 min	X1
94 °C	1 min	
58 °C	1 min	X35
72 °C	45 sec	
72 °C	10 min	X1
Hold8 °C		

10 µl of the PCR mixture was uploaded on 0.9% agarose gel to check the sequence amplification of the target sequence in the vector pET-15b. From the positive colonies tested by PCR (2/10 for V-C1 domain) recombinant plasmids were extracted using QIAprep ® Spin Miniprep Kit (QIAGEN) . In order to confirm the correct insertion of the target sequences encoding for V-C1 a control digestion was performed on the plasmids sequence through the restriction enzyme Xhol.

The reactions were carried out as well:

Plasmidic DNA	300 ng
BSA 1 mg/ml	2 µl
Buffer 10x	2 µl
XhoI (20 U/µl)	20 U
Milli Q water	4 µl
Final volume	20 µl

In order to verify the absence of mutations, the recombinant plasmids resulted positive for the control digestion were sequenced at the BMR Genomics laboratories (University of Padua) by the Sanger method (1975).

Achievement of the recombinant plasmid pET-15b-V for the expression of V-C1 domain (23-233) in *E. coli* as host.

The gene encoding the V-C1 domain of RAGE was amplified by PCR by using the oligonucleotides VNdeI-For e V223Xho-Rev (Tab.4) which contains the restriction sites for the enzymes NdeI and XhoI. The recombinant plasmid pET-15b-V-C1 (23-243) kindly provided by Dr. G. Fritzwas used as template for the PCR reaction

The reaction was carried out by mixing 10 µl of template (pET-15b-VC1), 0.5µM (final concentration) of VNdeI-For e V223Xho-Revprimers, dNTPs (final concentration) 0.25 mM, $MgCl_2$ (final concentration) 1mM and 1 U of Phusion High-Fidelity supplied by Finnzymes.

The PCR reactions were the following:

Temperature	Time	Cycles
98 °C	2 min	X1
98 °C	30 sec	
58 °C	30 sec	X30
72 °C	30 sec	
72 °C	10 min	X1
Hold8 °C		

The PCR products were analyzed by electrophoresis in 1% agarose gel.

GeneClean Turbo for PCR Kit (supplied by Q-Biogene) was applied for the PCR product purification.

The PCR product was digested using the restriction enzyme and XhoI, both supplied by New England Biolabs, NEB.

The digestion reaction was so prepared:

PCR product	~480 ng
BSA 1 mg/ml	4 µl
Buffer 10x	4 µl
XhoI (20 U/µl)	20 U
Final volume	40 µl

The reaction was incubated at 37 °C for one hour and, at the end of this step the reaction was inactivated at 65 °C for 20 minutes. Also the vector pET-15b-V-C1, utilized for the cloning of the target sequence was digested by Xhol through the following reaction conditions:

pET-15b-VC1	~1,2 µg
BSA 1 mg/ml	6 µl
Buffer 10x	6 µl
XhoI (20 U/µl)	60 U
Final volume	60 µl

The reaction was incubated at 37 °C for 45 minutes (the milli Q water was added to get a final volume of 70 µl):

BSA 1 mg/ml	1 µl
Buffer 10x	1 µl
XhoI (20 U/µl)	10 U
Milli Q water	7 µl

The reaction was re-incubated at 37 °C for one hour and, at the end of this step, the reaction was inactivated at 65 °C for 20 minutes. With the purpose to evaluate the occurred protein digestion, 10 µl of digestion reaction were run by gel electrophoresis on agarose gel. 0.7%.
The remaining digestion reaction was loaded on a 0.6% agarose gel. In order to allow the DNA purification from salts and other digestion components that might inhibit the ligase enzyme, the band corresponding to the digested vector with XhoI was eluted from the gel by using the QIAquick ® Gel Extraction Kit (QIAGEN).
This process allows to purify DNA from salts or other components undigested of the digestion reaction which can inhibit the ligase and eliminate Moreover, any molecules of undigested vector.
The commercial kits are based on the DNA adsorption by silica membranes with the presence of high salt concentrations. Hence, after multiple final washing to remove the residual impurities the DNA was eluted by dH2O or by 10 mM Tris, pH 8.
The eluted vector from gel was then quantified.

The ligation reaction was up in a final volume of 21 µl. The protocol involved the addition of 50ng of pET-15b/NdeI/XhoI vector, 8.98 ng of insert, 10 µl of buffer, 4.91 µl of Milli Q water and 1 µl of NEB ligase. The reaction was incubated at 25 °C for 10 minutes.

The ligation mixture was used to transform cells of *E.coli* DH5α, designed for the plasmids replication allow a high number of copies per cell and made them competent by treatment with $CaCl_2$.

Colony PCR screening of 17 clones was applied to check the correct integration into the vector pET-15b of the target insert. As reported in figure x the gene amplification of the target region has been allowed by using 0.7 µM of T7 promoter and T7 terminator primers.

For the reaction in a final volume of 20µl were used, T7 promoter and T7 terminator primers 0.5µM (final concentration), dNTPs (final concentration) 0.25 mM, $MgCl_2$ (final concentration) 2.5mM and 0.5 U of INVITROGEN TAQ Polymerase.

The PCR program was the following:

Temperature	Time	Cycles
94 °C	4 min	X1
94 °C	1 min	
52 °C	1 min	X35
72 °C	45 sec	
72 °C	10 min	X1
Hold 8° C		

10 µl of the PCR mixture was uploaded on 0.9% agarose gel to check the sequence amplification of the target sequence in the vector pET-15b. From the positive colonies tested by PCR (6/17 for V-C1 domain) recombinant plasmids were extracted using QIAprep ® Spin Miniprep Kit (QIAGEN) . In order to confirm the correct insertion of the target sequences encoding for V-C1 a control digestion was performed on the plasmids sequence through the restriction by Xhol enzyme.

The reactions were carried out as well:

DNA plasmidic	300 µg
BSA 1 mg/ml	2 µl
Buffer 10x	2 µl
XhoI (20 U/µl)	20 U
Milli Q water	4 µl
Final volume	20 µl

In order to verify the absence of mutations, the recombinant plasmids resulted positive for the control digestion were sequenced at the BMR Genomics laboratories (University of Padua) by the Sanger method (1975).

5.2.c.2. *E. coli* transformation.

With the purpose of transforming *E. coli* were exploited DH5α cells. For the expression strain was preferred to use ORIGAMI B (DE3), mutated in trxB/gor genes that consent to encode for thio redox in reductase and glutathione oxidoreductase that promotes the formation of disulfide bridges.

The protocol to make competent E. coli cells is the following:

- Inoculate 5 ml of LB medium (Tab. 2) with an unspecified number of *E. coli* cells;
- incubate at 37 °C, overnight stirring;
- dilute 0.5 ml of pre inoculum in 20 ml of fresh medium, place at 37 °C on stirring;
- stopped the cells growth until an OD600 value in a range between 0.3-0.5;
- collect the cells and centrifuge for 5 minutes at 4000 rpm in a 50 ml tube;
- discarded the supernatant and suspend the cell pellet in 1 ml of sterile solution A (10 mM MOPS pH 6,5, 10 mM RbCl);
- make up to 10 ml with sterile solution A spin at 4000 rpm for 5 minutes;
- discard the supernatant and suspend the cell pellet in 1 ml of sterile solution B(10 mM MOPS ph 6,5, 50 mM $CaCl_2$, 10 mM RbCl);
- make up to 10 ml with sterile solution B;
- place the cells for 30 minutes on ice. Collect the cells by centrifugation and suspended them gently in 2 ml of solution B;
- prepare 200 µm aliquots for further transformation.

The DNA contained in the ligation buffer was spiked with 200 µl of competent cells for the transformation, while for internal control it was employed a cells line not loaded of DNA.
After keeping the mixture on ice for 30 minutes, the cells were subjected to a thermic shock at 42 °C for 2 minutes in order to promote the DNA incorporation. Each aliquot was spiked with 1 ml of LB medium and after at least one hour of incubation, the cells were collected by centrifugation, suspended in 100 µl of LB medium and then plated on selective medium. The last step was to incubate for 12-14 hours at 37 °C.

5.2.c.3. Expression and purification from *E. coli.*

5.2.c.3.1. *E. coli* transformed clones induction.

E. coli growth and induction were promoted using different media and two different methods of induction:

1) Induction by IPTG: the transformed cells were grown in LB medium 1% NaCl (Tab 2), implemented with 50 µg/ml of ampicillin, 15 µg/ml of tetracycline and 12.5 µg/ml of kanamycin, O.N. at 37 ° C.At the end of incubation, the sample was centrifuged and resuspended in LB medium buffered (Tab 2), and the cells growth at 25 °C. When the optical density at 600 nm was between 0.4 and 0.6, the cells were induced by adding IPTG (0.5 mM, 0.75mM, 1mM) and kept growing O.N. at the same temperature.

2) Self-induction: the transformed cells were grown by the implementation of DYT medium (Tab. 2) and by supplementing ampicillin, O.N. at 37 °C.

At the end of incubation, the sample was centrifuged and resuspended in AM medium (Tab 2) and then the cells were growth at 37 °C. When the optical density at 600 nm was between 0.4 and 0.6, the flasks were transferred and kept growing O.N. at 21 °C.

In both the methods above reported, the cells were kept on ice and stirred for 10 minutes to avoid the proteases, afterwards they were collected by centrifugation using a Sorvall centrifuge at 8000 rpm for 30 minutes at 4 ° C. The pellet was weighed (wet weight), frozen in liquid nitrogen and stored at -80 ° C.

5.2.c.3.2. Total extracts of *E. coli* protein preparation.

The E. coli cells were broken down through two physical mechanisms.

1) Sonication: This method, based on mechanical breakage, because develops a high heat stress, was carried out maintaining the cells on ice. The cells were subjected to 5 rupture cycles, each cycle consisting of 30 seconds of sonication and 30 seconds on ice.

2) Liquid extrusion: Also this method is based on mechanical breakage, and involves the use of a steel cell fitted with a piston closed by a valve (French Press) in which the cell suspension is inserted.

At the end of the slow thawing of the bacterial pellet, the cells were resuspended in a lysis buffer

solution (about 2-3 ml of buffer per grams of cell) containing complete protease inhibitor cocktail (EDTA-free Roche Applied Science), DNasi I, 0,5 mM MgCl2, 20 mM HEPES, 300 mM NaCl, pH 7,4.

The liquid extrusion proceeds with the breaking of the cells by the application of a pressure of 1000 psi. Isolation of the soluble fraction from the cellular debris was carried out by apply in an ultra centrifuge cycle at 4 ° C for one hour at 100,000 rpm and then the supernatant was collected.

5.2.c.3.3. Scale-up purification of V-C1 domain from *E. coli* cells.

The soluble fraction obtained from ultracentrifugation was loaded on Ni-Sepharose column (26 mm of diameter, loading volume 50 ml, GE healthcare) previously equilibrated with Lysis buffer (50 mM NaH_2PO_4, 300 mM NaCl) and uploaded with imidazole 30mMuntil the signal was stable at A280 (baseline).

The elution was performed by using a buffer containing 50 mM NaH_2PO_4, 300 mM NaCl and 500 mM imidazole. The different elution fractions were collected in separate tubes.

The second step consisted in the removal of the His-tag fusion proteins which was carried out by incubating the purified proteins for 3 hours at 25 °C with thrombin enzyme (GE Healthcare), in the presence of $CaCl_2$ as cofactor.

In order to remove the protein precipitate the incubation mixture was centrifuged in a Sorvall centrifuge at 10000 rpm for 4 °C.

A further passage on Ni-Sepharose column allowed the separation of the V-C1 portion from the VC-1-His-tag moiety not correctly digested.

At the end of the separation the Flow-through was collected, containing the not bound proteins.

The last of the purification protocol consisted in a Size Exclusion Chromatography using Superdex 75 (26/60) previously equilibrated with 20 mM Na acetate, 150 mM NaCl, pH 5.2.

5.2.d. Biochemical techniques.

5.2.d.1. SDS-PAGE.

SDS-PAGE technique allows the individual protein separation in function of the molecular weight from a complex mixture of proteins. The separating gel is composed of two different parts that allow the simultaneously separation in based on porosity and the buffer pH. The high porosity STAKING GEL permit the protein concentration on the surface of the low porosity RUNNING GEL, that allows the effective protein separation; and going into detail the system resolution can be increased in case of excessive protein concentration by varying the acrylamide concentration.
Both minigels (9x7 cm) and slab gels (14x13 cm) at 16% of polyacrylamide were used in the present work

Running Gel 16%

Lower gel buffer (1.5 M Tris-HCl pH 8.8, 0.4% SDS)	0.250 vol
Acrilammide stock II 30%	0.215 vol
H_2O	0.532 vol
Ammoniumpersulfate 10%	0.003 vol
TEMED	0.001 vol

Stacking Gel

Upper gel buffer (0.5 M Tris-HCl pH 6.8, 0.4% SDS)	0.250 vol
Acrylamide stock II 30%	0.150 vol
H2O	0.600 vol
Ammoniumpersulfate 10%	0.003 vol
TEMED	0.001 vol

The composition of the electrophoresis buffer was as follows: 0.025 M Tris-HCl, 0.192 M glycine, 0.1% SDS, pH 8.3.

5.2.d.1.1. Coomassie and Silver staining assays.

Staining was performed by incubating the gel with the Coomassie brilliant blue R-250 for 30 minutes at room temperature on mild stirring. The solution was then removed and the gel washed up with the destaining solution (40% ethanol,55% H2O, 5% acetic acid) to allow the removal of the stain in excess.
Silver staining was carried out using the commercial kit ProteoSilver ™ Silver Stain (SIGMA) and following the protocol of the supplier.

5.2.d.1.2. Immunoblotting.

The immunoblotting consists of the proteins transfer from the gel to a nitrocellulose membrane by the direct contact through the two surfaces.
The transfer buffer composition was as follows: 0.025 M Tris-HCl, 0.192 M glycine, 20% methanol, pH 8.3. The protein transfer was carried out by applying an electric current of 500 mA for two hours or 250 mA O.N. After the protein transfer, the membrane was stained for 1 minute ina red Ponceau S (Sigma) solution in order to check the electrophoretic run, the separation, uploads and also to identify the known molecular weight markers. Before the next step consisting in the immuno-decoration, the red Ponceau was removed by washing the membrane for 5 minutes in TBS(0.01 M Tris-HCl pH 7.4, 0.166 M NaCl). The protocol for the immuno-decoration provides one hour gel saturation by milk in TBS-5% w / v, 0.1% Tween20 at room temperature. Alternatively, the saturation was performed over night at 4 ° C. After 5 minutes of washing by using TBS-0.3% Tween 20, the membrane was incubated for 2 hours with the primary antibody [mouse anti-polyHIS (ROCHE)] on mild stirring followed by 4 washes in TBS-Tween 20 0.3% of 15 minutes each. Membranes were then incubated with the secondary antibody at least for one hour (anti-mouse antibody provided by Jackson Laboratories and diluted 1:10000)and after 3 washes of three minutes each in TBS-Tween 20 0.3%, the membrane was covered by ECL (luminol, Thermo Scientific) for 1 min. As a last step, the membrane was placed between two sheets of tracing paper and exposed, in dark boxes, to autoradiographic plate.

5.2.d.2.3. Mass spectrometry analysis.

Direct infusion of VC1 by ESI-MS spectrometer in denaturing and native conditions.

V-C1 protein was stored at -80 °C in 20 mM sodium acetate pH 5.2 150 mM NaCl until the MS analysis. In order to desalt and concentrate the protein, allowing mass spectrometric analysis, the sample was centrifuged by Amicon Ultra-0,5 ml Filter (Millipore). This step also enables the buffer exchange with a volatile buffer for a suitable mass spectrometry analysis. For the denaturing analysis conditions the proteins were mixed (in a of 1:1 ratio) with a denaturaing buffer composed by ammonium acetate, acetonitrile, formic acid (25/30/0.1 v/v/v). MS analysis in native conditions were carried out using the following conditions: proteins at 10µM concentration in 1 mM ammonium acetate pH 7.4.

Mass spectra were acquired by direct infusion (10 µl/min) by usingan LTQ XL-Orbitrap mass spectrometer (Thermo Scientific, Milan, Italy) equipped with a ESI source (Thermo Scientific, Milan, Italy) set as follows: spray voltage 4.0 kV; capillary temperature 150 °C, capillary voltage 41 V; tube lens offset 100 V, no sheath gas flow, 20 arbitrary units auxiliary gas flow. The Orbitrap mass spectrometer continuously performed scan cycles at high-resolution (resolving power 60,000,FWHM at m/z 400) in full scan (500–3500*m/z*) and in profile mode.

Protonated phthlates [dibutylphthlate (plasticizer), m/z 279.159086; bis(2-ethylhexyl)phthalate, m/z391.284286] and polydimethylcyclosiloxaneions ([(Si(CH3)2O)6+H]+, m/z 445.120025) were used for real time internal mass calibration.

For the acquisition has been used Xcalibur software (Thermo).

5.3. Results.

5.3.a. Expression and purification of V, V-C1 human s-RAGE by *E. coli.*

5.3.a.1. Cloning of the V-domain in *E. coli.*

The V-domain of RAGE receptor was produced exploiting the *E. coli* Origami B (DE3) strain as intracellular recombinant protein by using the bacterial expression vector pET-15b.

With the aim to develop the recombinant vector, the DNA fragment encoding the V domain was amplified by PCR and then cloned into the target vector. To do this the DNA fragment encoding for the V domain was amplified by PCR and cloned in frame into the vector pET-15b containing the sequence coding for the tag of 6 histidines (His-Tag) and the site cutting for Thrombin (LVPRGS), located on the N-terminus. The protein expression is controlled by the lac promoter.

The recombinant vector pET-15b-V was used to transform the strain of *E. coli* Origami B (DE3).

The strain *E. coli* Origami B (DE3) represents one of the most used expression host strains to synthesize recombinant proteins in which disulfide bridges are present due too the fatc that mutations in the trxB/gor genes create an oxidant microenvironment leading the formation of disulfide bridges.

The expression of the V-domain has been tested together with that of the domains V-C1 and sRAGE (V-C1-C2).The strains of *E. coli* Origami B (DE3) employed in this work and transformed with vectors pET-15b and pET-15b-VC1-sRAGE were kindly provided by Dr. G. Fritz.

Here below is shown a schematic representation of the constructs used for the recombinant proteins production.

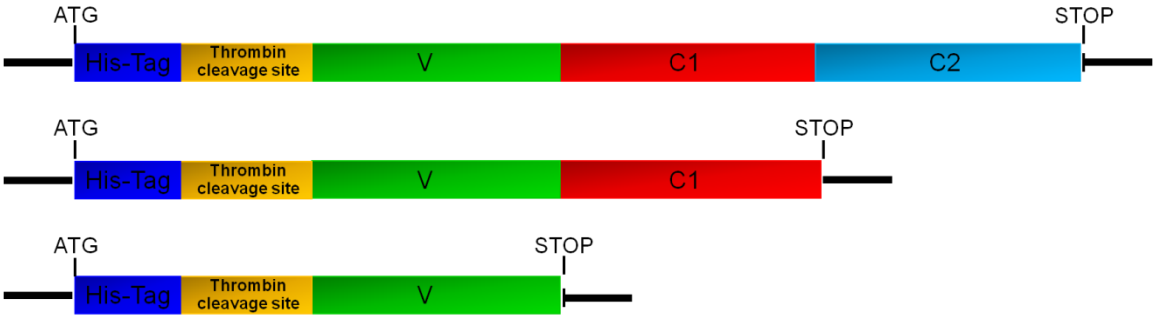

Fig 2. Schematic representation of the fusion proteins constructs sRAGE, V-C1 and V obtained from the recombinant vectors.

5.3.a.2. Small-scale V-C1 expression and purification from *E. Coli.*

E. coli cells were grown at 37 °C O.N. in LB 1% NaCl medium (Tab 2) and the following day the exhausted medium was replaced with LB-BUFFERED (Tab 2) and the temperature lowered at 25 °C. When the optical density at 600 nm reached a value of 0.6 a.u., the protein expression was induced by adding IPTG to the medium culture at a final concentration of 0.5 mM. After 16 hours from the induction, the cells where broken down by ultrasonication and the protein purified. In order to obtain a soluble fraction containing all the soluble proteins of the *E. coli*, the total extract was centrifuged at 100.000 g for one hour at 4 °C. The purification was performed by using the protocol previous reported in the section "Materials and Methods".

The purification of V-C1 was found very difficult to achieve due to the ability of the protein to bind DNA fragments as reported by the UV spectrum of the protein where the characteristic peak at 280 nm referred to proteins was masked by a much wider peak with a maximum of absorption at 260 nm representing the characteristic peak of nucleic acids. This feature, combined with the considerable degree of protein precipitation, make the purification of the V-C1-His domain very difficult to be achieve.

The Fig 3 displays the SDS-PAGE analysis performed to verify the V-C1 expression. The protein expression was verified and compared with the total extract sample of *E. coli* cells.

The SDS-PAGE analysis carried out by a 16% polyacrylamide gel shows that the addiction of IPTG has effectively favored the protein expression. In fact, while the lane 2 doesn't display any visible band at the molecular weight relative to the V-C1 domain, lane3 which is relative to the cells added with IPTG shows the expected band. A further confirmation of the protein expression is the presence of the protein in the soluble fraction from the total extract (lane 4).

Purification of the protein by Ni-NTA resin was found effective as shown by the lanes in the SDS

PAGE which show the purified protein and the removal of cell proteins.

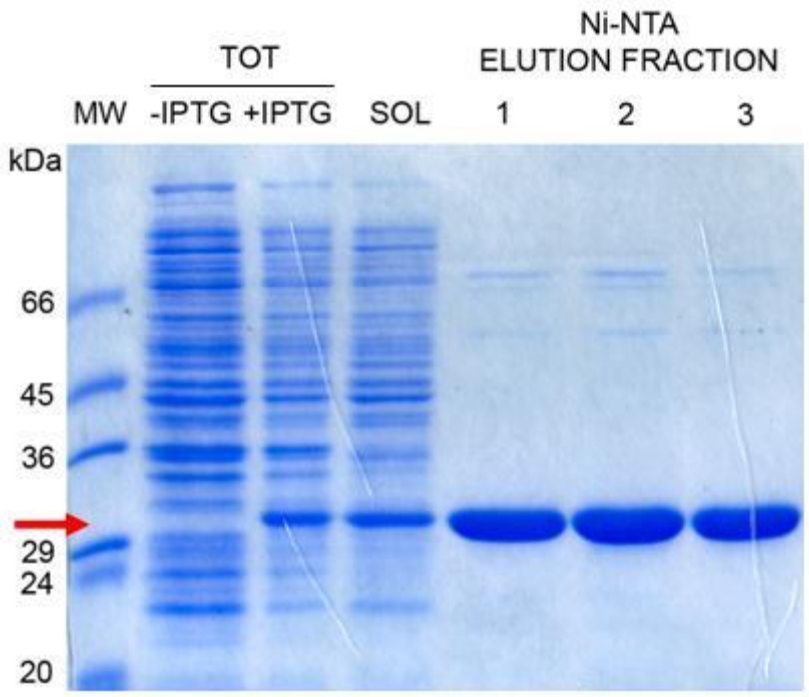

Fig 3. SDS-PAGE stained with Coomassie to verify V-C1-his domain from E. Coli expression and purification. The arrow indicates the VC1-His (26 kDa) position. -IPTG and + IPTG indicate the absence or presence of the inductor IPTG, SOL: soluble fraction, Ni-NTA ELUTION FRACTION: fractions eluting from the resin by adding imidazole 250 mM.

The data of V-C1-His yield after column passage showing high levels of purification, are reported in Tab 4.

	OD_{600}	ml culture	OD total	Mg protein	Mg protein/OD_{600}
VC1-HIS	1,4	500	700	3,9	**0,0055**

Tab 4. V-C1-His protein purification yield.

The second part of the protein purification process was focused on the His-Tag removal from V-C1 fusion protein. The protein purified by the Ni-NTA resin underwent a thrombin treatment at 25 °C for 3 hours. At the end of this step, with the purpose of verify the correct protease cut, an Immunoblotting analysis was performed by using an Anti-polyHis monoclonal antibody which is selective towards the 6 polyhistidines tag linked to the fusion protein.
Fig 4 shows a direct comparison between the protein before and after the treatment with thrombin. The Ponceau staining shows the protein in both the lanes while the Western blot analysis reveals the spot only in the lane relative to the His tag protein but not after trombin treatment thus confirming the enzymatic cut of the polyhistidin moiety

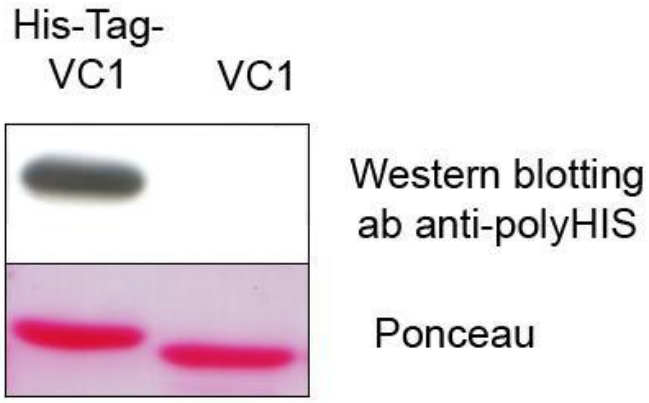

Fig 4. VC1 and VC1-His Western blot analysis performed to verify the thrombin photolytic cut.
The staining with Ponceau, in the bottom panel, confirms the presence of the VC1 protein characterize by a lower molecular weight in respect with the corresponding His-Tag fusion protein.

The protein fraction resulting from the enzymatic cut of the polyhistidin moiety was reloaded on a Ni-NTA resin for a second step in batch purification in order to separate the V-C1 fraction from the VC1-His-Tag fraction not properly digested.

5.3.a.3. Large-scale V-C1 expression and purification from *E. Coli.*

E. coli cells were inoculated into DYT medium (Tab 2) at 37 °C O.N. and the following morning the exhausted medium replaced with AM (Tab 2) lowering the temperature at 21 °C. After about 16 hours of medium exchange, the cells were broken in the presence of DNase I. In order to obtain the soluble fraction containing all the soluble protein of the *E. coli*, the total extract was centrifuged at 100.000 g for one hour at 4 °C. The purification was performed by using the protocol previous reported in the section "Materials and Methods".

The pellet (insoluble fraction) and the supernatant (soluble fraction) were analyzed by SDS-PAGE (data not shown). The first part of the protein purification process was focused on the His-Tag removal from V-C1 fusion protein soluble fraction. Hence, after having joined the purified proteins collected from the Ni-NTA (about 70 mg) resin column, the fractions underwent to the thrombin treatment at 25 °C for 3 hours and reloaded on the nickel column to a collect the HIs-Tag protein free.

A final purification using a a size exclusion chromatography was then performed.

The yield of the process is quite low due to the abundant protein precipitation. Starting from an amount of purified VC1-His of almost 70 mg of fusion protein, 5 mg of purified protein was obtained in the last purification step.

5.3.b. Mass spectrometry analysis focused on RAGE-ligand interactions.

5.3.b.1. V-C1 domain and known ligands ESI-MS analysis.

The first step of the MS analysis of the recombinant RAGE was addreesed to determine the MW and the primary sequence of the protein. The MW of the protein was determined in top-down mode and in denaturating conditions. Fig 6 shows the typical multicharged ion spectrum of RAGE and Fig 5 the deconvoluted spectrum. The MW of 24580 Da as well as the isotopic pattern well match the simulated ones thus confirming the identity of the protein.

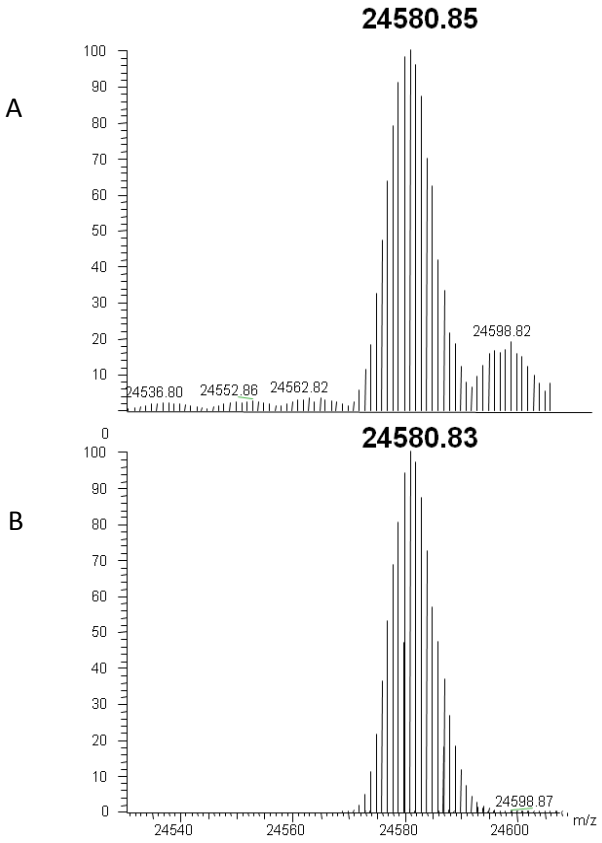

Fig 5. A) Deconvoluted spectrum of V-C1 from experimental analysis. B) Theoretical deconvoluted spectrum of V-C1 calculated from the amino acidic structure.

The sequence of the protein was then determined by a bottom-up approach which consists in the enzymatic digestion of the protein following by the separation of the resulting peptides through a reverse phase chromatography. The eluted peptides were sequenced by a nano LC-ESI MS/MS. The primary sequence of VC1 was in agreement with the nucleotide sequence of the protein with a coverage of the sequence higher than 85%.

A

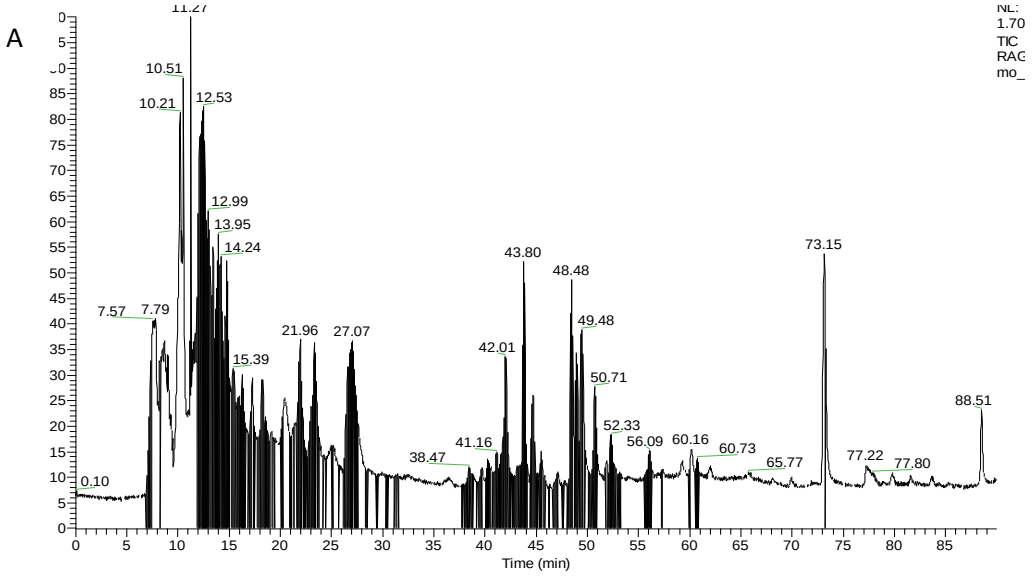

B

GSHMAQNITARIGEPLVLKCKGAPKKPPQRLEWKLNTGRTEAWKVLSPQGGGPWDSVARVLPNG
SLFLPAVGIQDEGIFRCQAMNRNGKETKSNYRVRVYQIPGKPEIVDSASELTAGVPNKVGTCVS
EGSYPAGTLSWHLDGKPLVPNEKGVSVKEQTRRHPETGLFTLQSELMVTPARGGDPRPTFSCSF
SPGLPRHRALRTAPIQPRVWEPVPLEEVQLVVE

Fig 6. A) LC-MS/MS chromatogram trace of V-C1 protein. B)V-C1 amino acids sequence. In red are reported the peptides mapped on the amino acids sequence deduced from the V-C1 nucleotide sequence.

5.3.b.2. RAGE-ligand interaction study by native ESI-MS: set-up of the method.

MS analysis in native conditions was used to study the protein–ligand interaction. The first step was to optimize the experimental conditions and the mass spectrometer source parameters in order to maintain the protein in the native state during the ESI source ionization, a condition that is required in order to maintain the protein in a proper conformation state required for the ligand engagement and to maintain stable the protein-ligand complex.

Besides MS and ESI optimization, a further key factor for obtaining a suitable mass spectrum characterized by a suitable signal/noise ratio regards the buffer selection, the desalting step and the protein concentration.

Unfortunately, most of the common buffers used for protein purification and storage are not compatible with ESI-MS techniques due to the presence of not-volatile salts; in particular the salts represent the major problem in mass spectrometry, causing instrument sedimentation, that occur during the sample desolvation which is require for the entire molecule transfer to the gas phase.

Furthermore, the proteins tend to form electrostatic complexes with several cations derived from alkali metals, causing the appearance of high molecular weight cluster larger than the free protein, thereby reducing the intensity of signal. Moreover, the presence of salts and impurities can lead to the ion suppression and thus to a further signal reduction.

Hence, to allow the data acquisition the buffer exchange was required as initial step and therefore, the protein was exchanged in ammonium acetate which is a volatile buffer very common in ESI-MS experiments. Ammonium acetate permits that the adduct formed between protein and ions such as sodium and potassium are readily exchanged by ammonium ions, which evaporate during the ESI process leaving the protein without saline adducts. The buffer exchange allowed obtaining not only a more intense signal, but also a more simplified mass spectrum which is therefore better interpretable. Nevertheless, the ammonium acetate buffer concentration was required to be carefully balanced according to the target protein.

In this respect different ammonium acetate concentrations were tested and in particular: 100 mM, 75 mM, 50 mM, 25 mM and 10 mM. The effects of buffer concentration on the mass spectra of VC1 domains are in figure x shown.

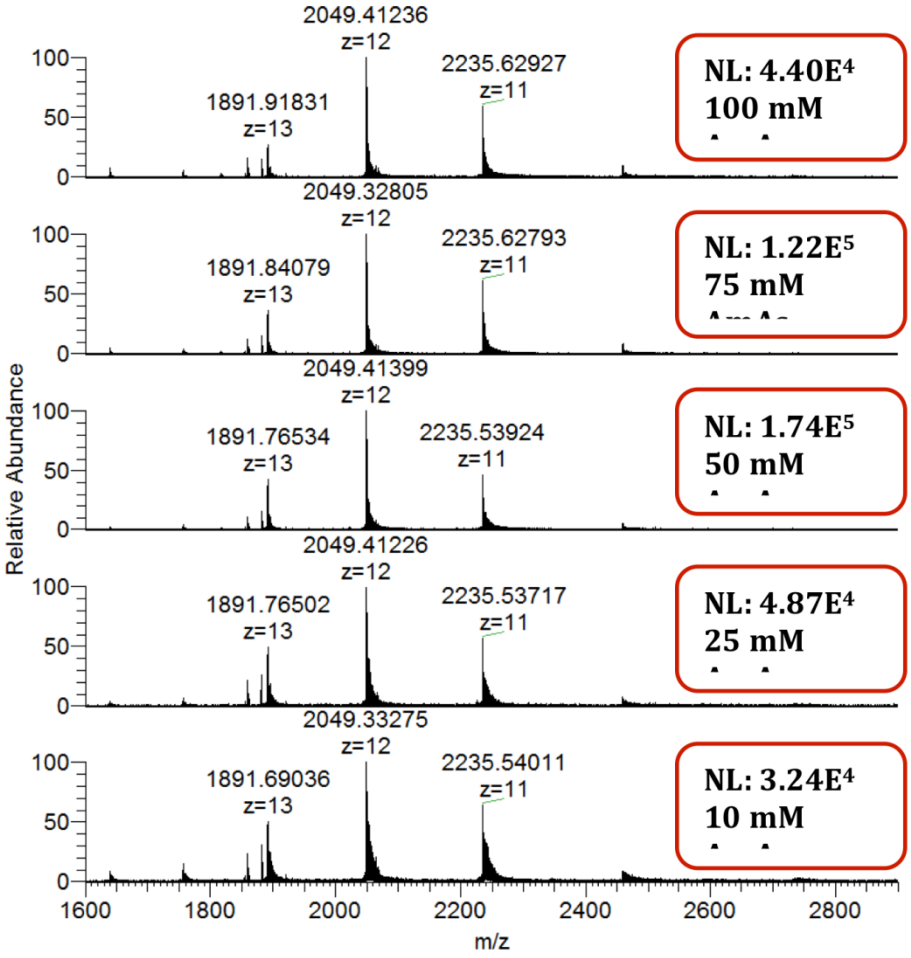

Fig 7. Effects of ammonium acetate concentrations on the VC1 mass spectra. The protein concentration was maintained constant and equal to10uM..

As shown by the ESI-MS spectra reported in Fig 7, the buffer concentration affected both the signal intensity and the peaks broadening and the ammonium acetate concentration of 50 mM was found the most suitable concentration in regards to both the two parameters.

The second step consisted to optimize the protein concentration and the effect of this parameter on the signal intensity is shown in Fig 8.

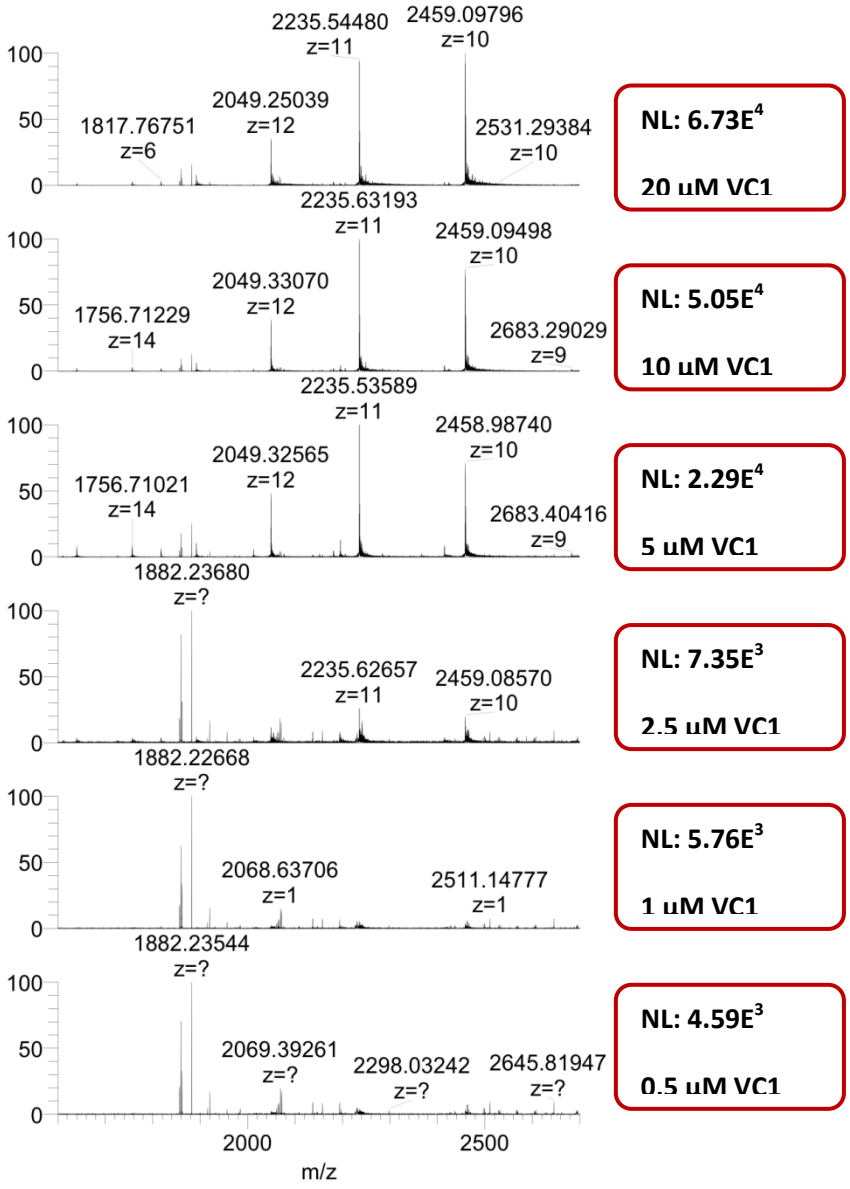

Fig 8. Effect of protein concentration on the signal intensity of V-C1.

A quite linear correlation was found between the protein concentration and the signal intensity and the concentration of 10 µM was found a good choice in order to get a suitable signal/noise ratio with the lowest protein consumption.

The next step was to optimize the ESI parameters and in particular the temperature and the ionization voltage. Fig 9 shows the effect of the temperature on VC1 spectra.

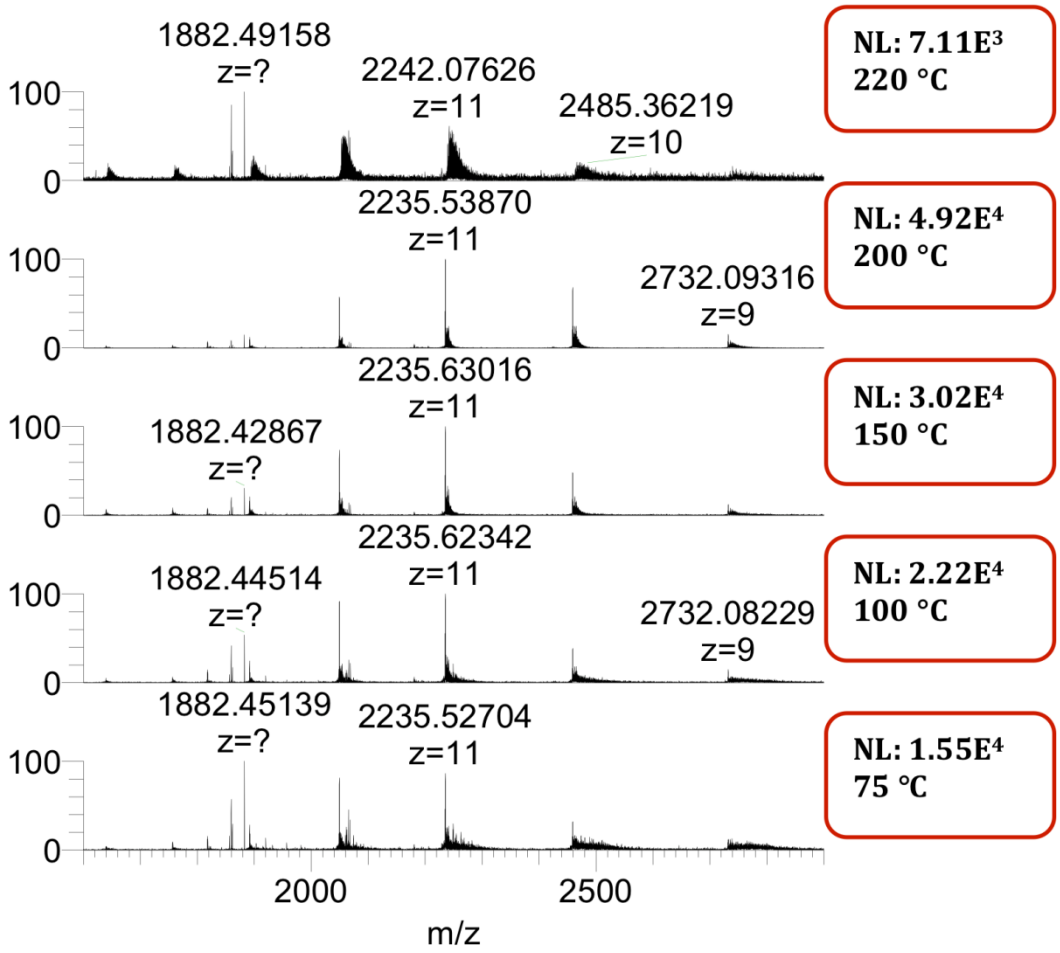

Fig 9. Effect of ESI source temperature on the V-C1 spectra acquisition..

As a general aspect the optimization of the temperature represents a critical step in native ESI-MS experiments since it should remain as low as possible in order to maintain the protein in a native condition but at the same time it should be able to suitable desolve the protein. As shown in Fig 9, at low temperatures, below 100 ° C, the peak ions resulted particularly broad, due to the fact that the molecules are in a solvated form. A satisfactory desolvation was reached setting the ESI temperature at 150 ° C.

Fig 10 shows the ESI-MS spectra of RAGE recorded in denaturating and non-denaturating conditions. It is quite clear that in denaturating conditions, the peak ions are characterized by lower m/z values and hence by a higher charges state in respect to the peak ions recorded in non-denaturating conditions. This is due to the fact that in denaturating conditions the protein is in a unfolded state and hence the basic residues, which are more exposed to the solvents, are easily protonated, leading the formation of high charge state ions. By contrast, when the protein is in a native state it is folded and the basic residues are not exposed to the solvents and this leads to less charge state ions.

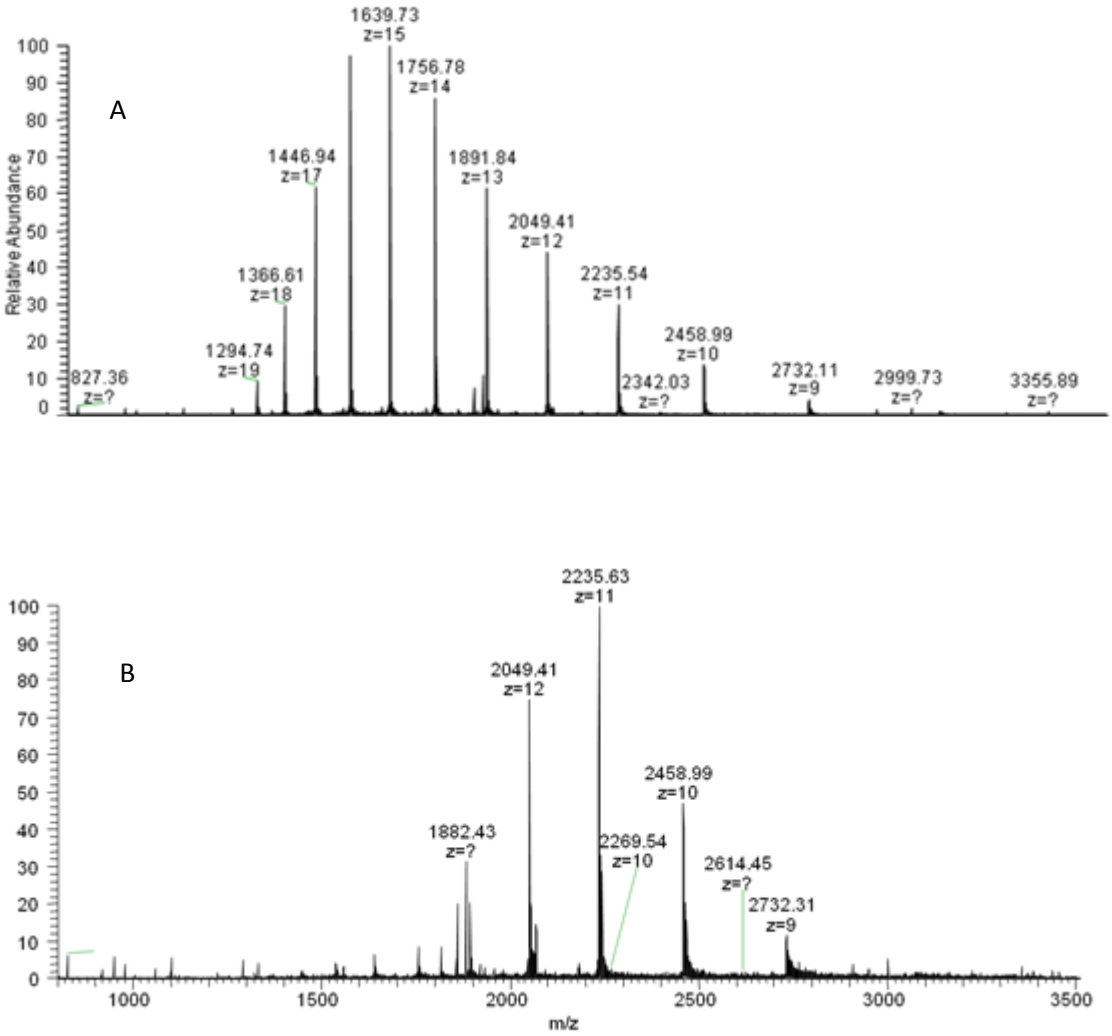

Fig 10. A) V-C1 ESI-MS spectrum recorded in denaturing conditions. B) V-C1 ESI-MS spectrum recorded in native conditions after the parameters set-up.

5.3.b.3. Set-up of an automated output screening ESI-MS method for V-C1-ligand binding.

The next step was to set-up and validate an ESI-MS method for studying the VC-1 ligand interaction and to calculate the dissociation constant.

The carboxymethylated and carboxyethylated derivatives of the peptides DEFKADE and FKDLGEE, in which the lysine residues are modified by the addition of carboxymethyl and carboxyethyl moiety, previously reported to act as RAGE ligands,were used as known ligands for the binding studies and to validate the approach. The amino acid sequence of the peptides was derived from the primary glycation sites of human serum albumin (HSA).

The peptides with the same amino acid sequence but containing the lysine residue is unmodified state were used as negative control.

The spectra of the two series of modified peptides recorded in denaturing experimental conditions are reported here below.

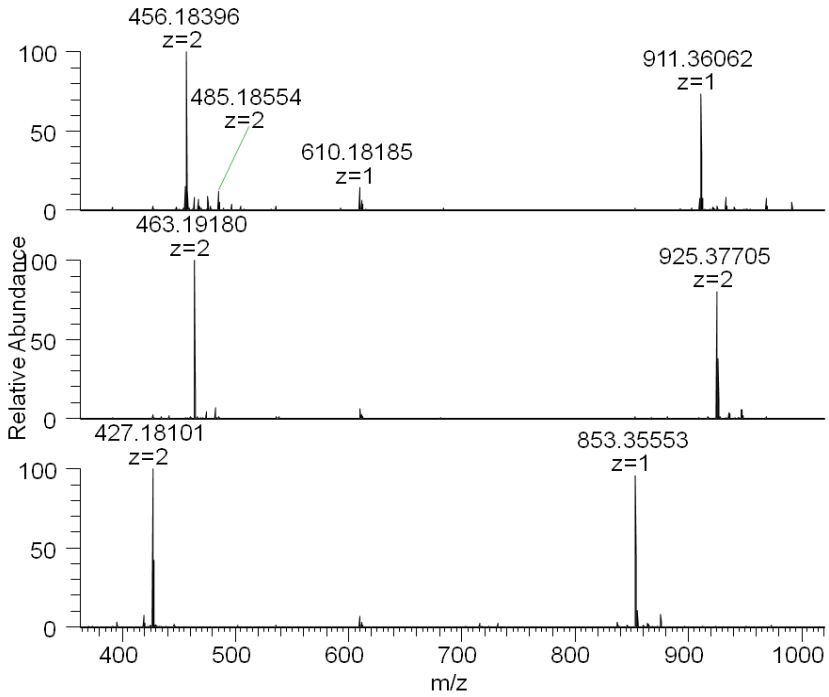

Fig 11. MS Spectra of DEFKADE series recorded in denaturating conditions: the upper spectrum is relative to theCML-modified peptide, below that relative to the CEL-modified peptide and in the bottom the spectrum relative to the unmodified peptide.

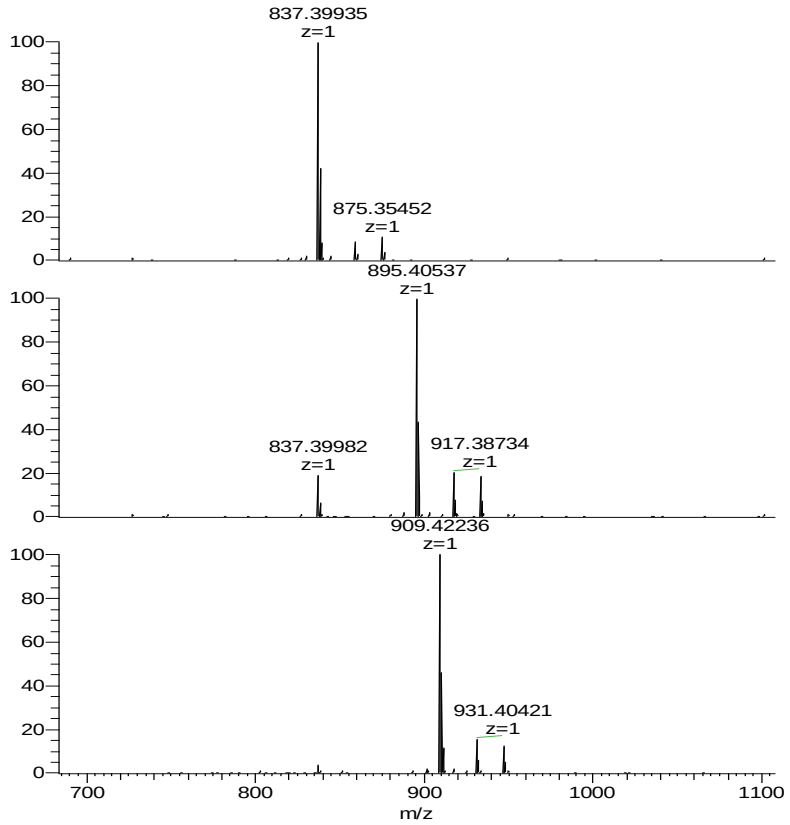

Fig 12. Spectra of FKDLGEE series in denaturation conditions: the upper spectrum is relative to the CML-modified peptide, below that relative to the CEL-modified peptide and in the bottom the spectrum relative to the unmodified peptide.

The complete automation of the method for the sample injection associated with the mass spectra acquisition was needed to allow in a short time a quick spectra acquisition. To get this goal it was, therefore, set up a 96-well plate in which, after having been allocated the same amount of VC1 (10 mM) in each well, were added the different peptides species by keeping different stoichiometric ratios with respect to VC1. The experimental procedure just described allowed to calculate the Kd values derived from the V-C1-ligands binding.

After the sample incubation, performed at 25 °C and directly managed into the thermostated autosampler, 10 µl of each reaction was withdrawn from each well at established time by the operator with a gap of 6 minutes and injected into the mass spectrometer to be analyzed.

The mass spectra related to the V-C1 incubation with the DEFKADE series peptides in a 1:10 ratio are here below reported (Fig 13, 14, 15).

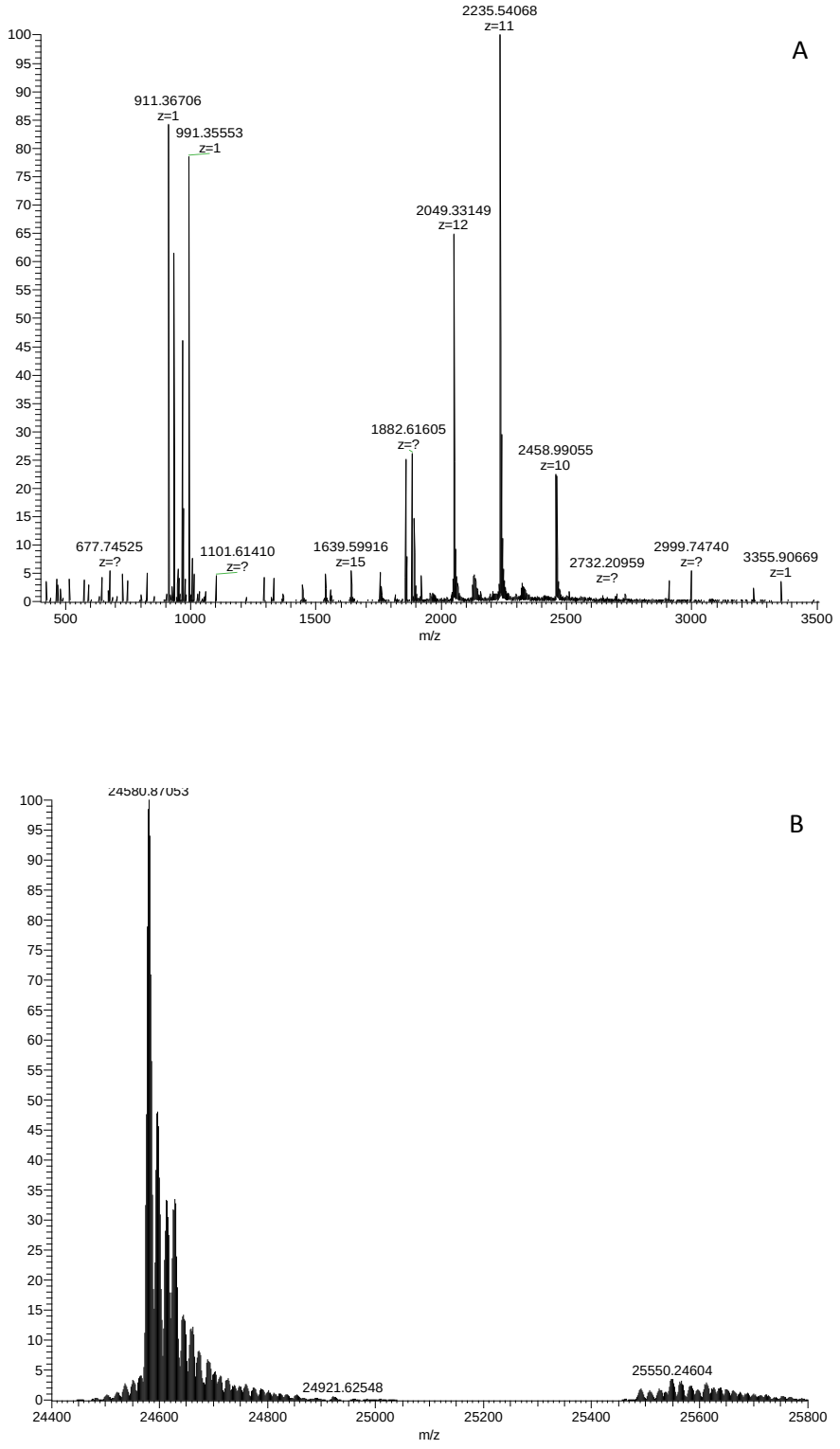

Fig 13. A) Multicharged spectrum relative to the V-C1-DEFKADE CML-modified bond incubated at t=0. B) Deconvoluted zoom spectrum of A (calculated by the Xtract software).

Fig 13 panel A shows the MS spectrum of the reaction mixture containing VC-1 incubated in the presence of *DEFKADE CML-modified* peptide at a 10:1 molar ratio. The peak ion series relative to the VC-1 and to the peptide are well evident. Fig. 13 panel b shows the deconvoluted spectrum reporting a peak cluster relative to the free VC-1 as well as a cluster at higher MW and shifted by almost 910 Da which can be attributed to the non-covalent complex between VC-1 and the modified peptide. The MS spectrum was acquired immediately after mixing the protein with the ligand indicating that the complex forms immediately and did not increase in respect to time.

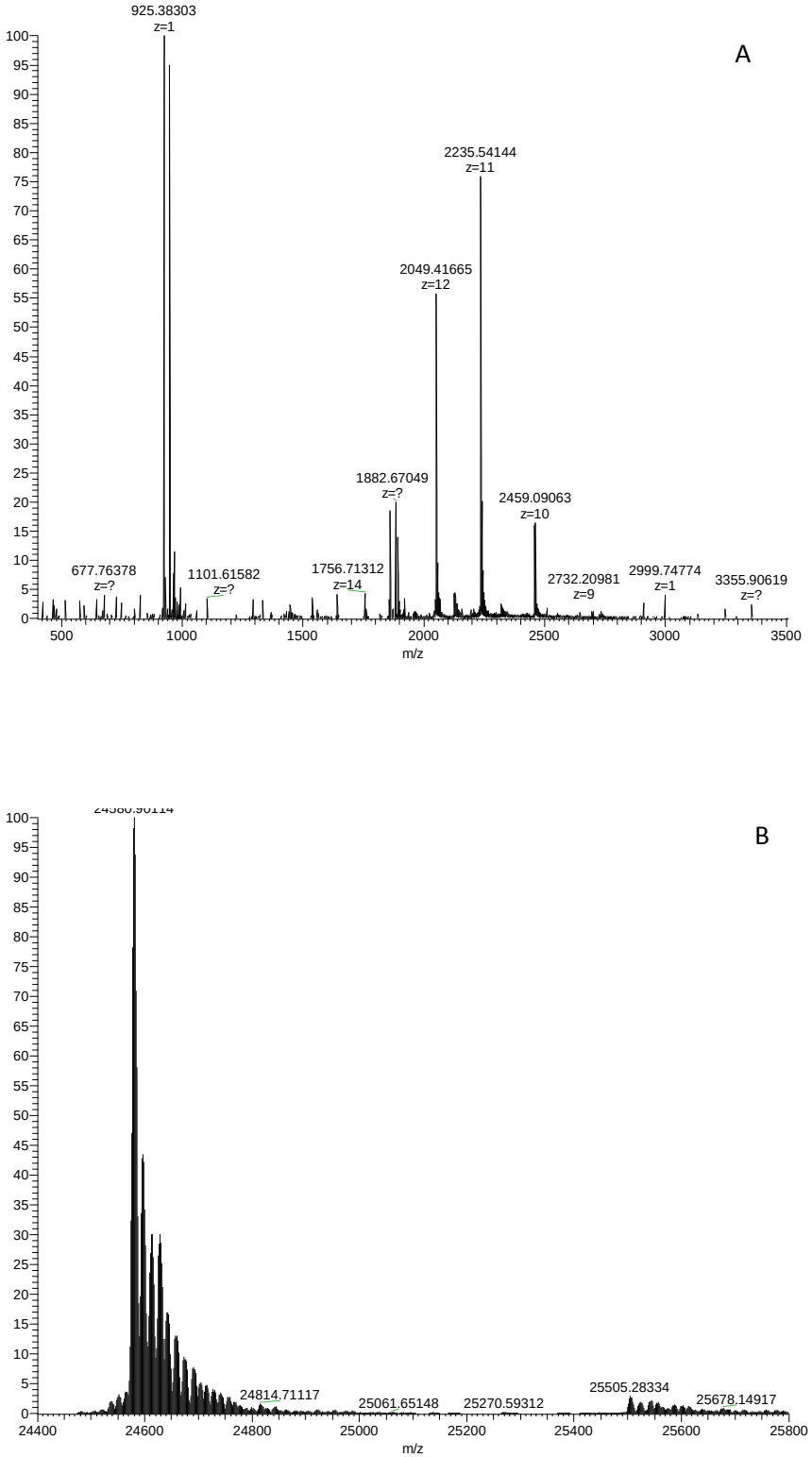

Fig 14. A) Multicharged spectrum relative to the V-C1-DEFKADE CEL-modified bond incubated at t=0. B) Deconvoluted zoom spectrum of A (calculated by the Xtract software).

Also in the case of the MS spectrum relative to the mixture containing V-C1 and DEFKADE CEL- the clusters relative to the protein and peptide in free form can be observed. The deconvoluted spectrum shows the peak ion relative to the free protein as well as that attributed to the non-covalent complex and with a relative intensity below 5%.

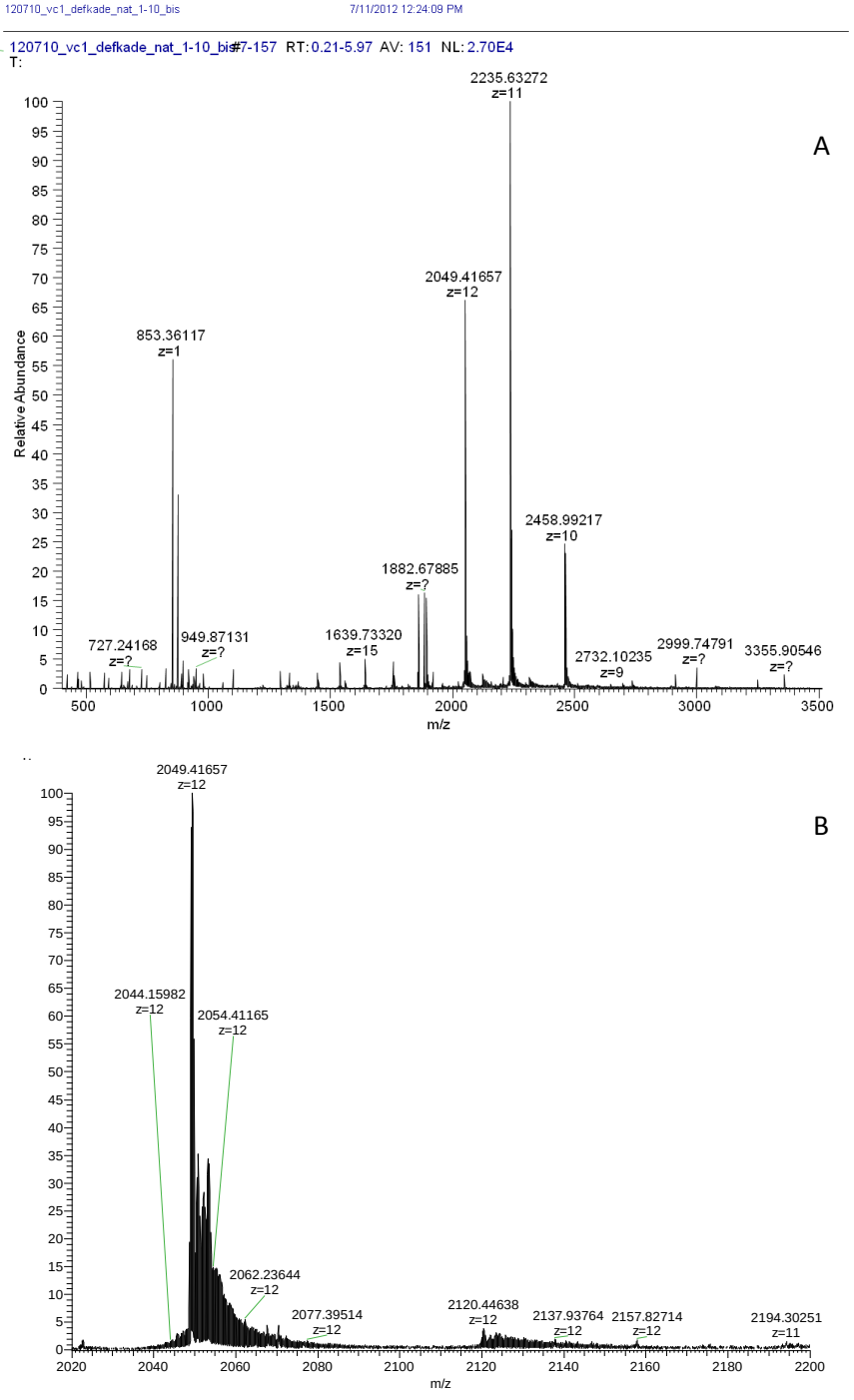

Fig 15. A)Multicharged spectrum relative to the V-C1-DEFKADE unmodified bond incubated at t=0 B) Zoomed spectrum of A relative to the ion z= 12 (calculated by the Xtract software).

Fig. 15 shows the MS spectrum of VC-1 incubated in the presence of the native peptide. Besides the clusters relative to the protein and peptide, also in this case the deconvoluted spectrum shows a cluster ion attributed to the non covalent complex but characterized by a lower relative intensity in respect to that observed when the CEL or CML peptides were used. The data indicate that the peptide as such binds to the VC-1 and that the CML and CEL modification significant increases the affinity.

Dissociation constant (Kd) of the complexes were then determined by titration experiments, consisting to calculate the relative abundance of the complex in respect to the different concentrations of the ligands and maintaining the concentration of the protein at a constant level.
The following equations were used for the Kd calculation:

k_d:

$$[P] = [P]_0 \times I_{(P)} / \left(I_{(P)} + I_{(PL)} \right)$$

$$[PL] = [P]_0 \times I_{(PL)} / I_{(P)} + I_{(PL)}$$

$$L_{free} = I_0 - I_{bound}$$

$$K_d = [P]_0 \times L_{free} / [PL]$$

As an example Fig 16 shows the titration experiments of the peptide DEFKADE-CEL incubated with the protein at the following molar ratio (protein:peptide):1:1, 1:5, 1:50, 1:100 (Fig 16).

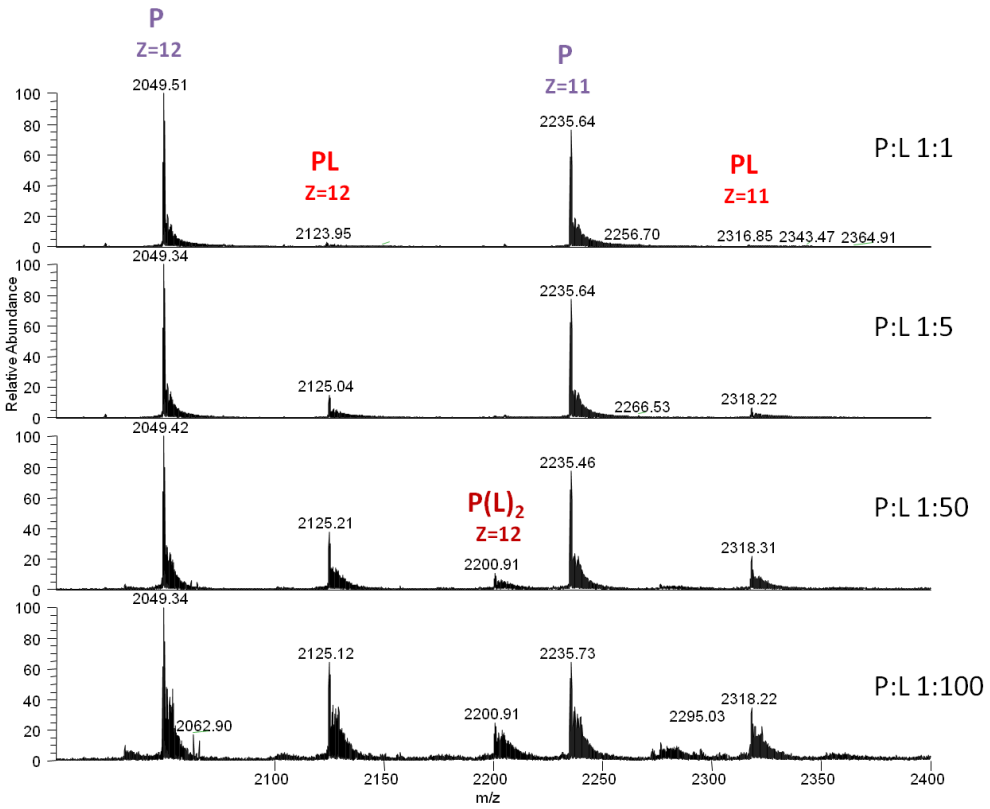

Fig 16. Monocharged deconvoluted spectra relative to the V-C1 incubated with DEFKADE-CEL modified peptide incubated at different stoichiometric ratios.

It is well evident a dose-dependent increase of the relative concentration of the non-covalent complex.

The values of Kd obtained by using the titration experiments are shown in table 17 and well indicate that for both the peptides, those characterized by the CML and CEL moiety have greater affinity in respect to the native ones. Moreover the Kd were found not significantly different in respect to those determined by quenching fluorescence experiments thus indicating that the MS method is a reliable approach for studying RAGE-AGEs interaction.

Method validation by determining the Kd of known ligands

Binding affinities of the **CML/CEL** peptides for the **wild type** and **mutants** of V domain.

Peptide sequence	V domain K_d, μM^1
DEF(CML)ADE	97 ± 3
DEF(CEL)ADE	104 ± 5
DEFKADE	617 ± 24
F(CML)DLGEE	87 ± 5
F(CEL)DLGEE	93 ± 6
FKDLGEE	673 ± 38

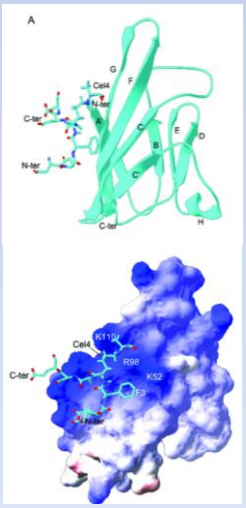

Dissociation constant was obtained by fitting **fluorescence titration** data with a single site binding isotherm.

Xie et al. Structure 2011

Tab 17. Kd values related to the binding activity of V-C1 incubated in the presence of DEFKADE and FDKLGEE series.

5.4. Conclusion.

In conclusion the high resolution ESI-MS method here reported is suitable to detect V1-C1 RAGE portion-ligand complexes and to determine accurate Kd. The method we set up is suitable to test a library of peptides bearing a variety of AGEs modifications including imidazolinone, methyl-imidazolinone, and the Michael adducts with alfa,beta-unsaturated aldehydes, in order to understand the structure requirements for RAGE recognition.

Furthermore, in view to a drug discovery approach aimed to identify RAGE antagonist, the method here proposed is suitable to screen libraries in order to identify RAGE ligands.

5.5. References.

[1] Dattilo BM, Fritz G, Leclerc E. et al. (2007). *Biochemistry* ;46, 6957 - 6970.

[2] Barlovic DP, Soro-Paavonen A, Jandeleit-Dahm KA. (2011). *ClinSci (Lond).*;121,43 - 55.